Simplified seismic design methods for low-ductile steel multi-tiered concentrically braced frames

by

Eshagh Derakhshan Houreh

A thesis submitted in partial fulfillment of the requirements for the degree of

Master of Science

in

STRUCTURAL ENGINEERING

Department of Civil and Environmental Engineering

University of Alberta

Abstract

Multi-Tiered Concentrically Braced Frames (MT-CBFs) represent a bracing configuration where two or more concentric braced panels are stacked between the storey levels in multi-storey buildings or between the ground and roof levels in single-storey buildings such as sports facilities, airplane hangers, or industrial buildings. This configuration is commonly used in tall storeys when it is impractical or uneconomical to employ one braced panel along the frame height. The multi-tiered configuration is preferable to avoid the use of large brace sections and impractical brace connections in design. A large proportion of MT-CBFs in Canada is located in low-to-moderate seismicity regions where low-ductile frames, such as Limited Ductility (Type LD) or Conventional Construction (Type CC) category, are often preferred to avoid relatively complicated seismic design and detailing requirements. Limited research studies have focused on the seismic stability and design of such low-ductile MT-CBFs. The current special seismic design provisions for Type LD MT-CBFs in the current Canadian steel design standard (CSA S16), which often requires performing multiple tedious analyses, particularly for tall frames, lack sufficient background research. For Type CC MT-CBFs, the Canadian steel design standard does not provide specific seismic design requirements. This research aims to investigate the seismic behaviour of Type LD and Type CC steel MT-CBFs with the focus on the stability of their columns, assess the current seismic design provisions, and propose enhanced and yet simplified design guidelines for the design of such frames in low-to-moderate seismicity regions.

An industrial building located in Montreal, QC, Canada representing a moderate seismicity region, was selected. A parametric study matrix consisting of 64 low-ductile steel MT-CBFs was developed by varying various parameters, including the frame ductility level, frame height, tier height ratio, brace and column cross-sections. The selected frames were then designed to CSA

S16-14 provisions, excluding the key design requirements for MT-CBF columns of Type LD and Type CC. The nonlinear numerical models of the frames were then developed using fibre-based elements in *OpenSees*, including the connection effects. The models were then used to perform nonlinear response history analyses under 30 ground motion records.

Results of the NLRH analyses showed multiple column buckling cases in both Type LD and Type CC frames. It was confirmed that the inelastic response in the selected frames was limited. No tension yielding has occurred in the tension-acting braces of the majority of the selected frames. Although the majority of compression-acting braces knuckled in compression, none of them entered the post-buckling zone. Storey drifts in all frames were significantly lower than the 2015 NBCC limit. Similarly, tier drifts were found to be noticeably lesser than the drift that can cause low-cycle fatigue fracture in braces. For Type LD frames, the axial compression forces did not exceed the design forces obtained using the capacity design principle. Additionally, in-plane and out-of-plane moments induced in the columns of Type LD frames were found to be lower than 6% and 8% of the respective column plastic moments in the plane and out of the plane of the frame. The columns of Type CC MT-CBFs experienced larger compression forces than their design forces. Column in-plane and out-of-plane moments observed in the columns of Type CC frames were lower than 8% and 28% of the respective column plastic moments in the plane and out of the plane of the frame. Improved and simplified seismic analysis and design methods were proposed for the design of Type LD and Type CC MT-CBFs with the emphasis on their columns. The adequacy of the proposed methods was examined for six case study frames, which confirmed that the proposed methods lead to a satisfactory seismic performance without column instability. The column size remained unchanged in Type LD frames and reduced in Type CC frames when compared to the columns designed to CSA S16-14.

Dedication

To the victims of the 2020 Flight PS752 tragedy

and

to my family for their unwavering affection and support for my success.

Acknowledgements

Table of Contents

List of Tables

List of Figures

List of Symbols

A, A_g Gross cross-sectional area

b_f Width of flange of wide-flange section

C_f Axial compression demand (CSA S16)

C_r Design axial compressive resistance (CSA S16)

$C_{r,\phi=1}$ Column axial compressive resistance with resistance factor equal to 1.0

F_y Yielding stress of steel

h   Total Frame Height

h_i Height of Tier i

I_E Importance factor for seismic load calculation (NBCC)

I_W Importance factor for wind load calculation (NBCC)

K   Effective length factor

Kl   Effective length

Kl/r   Effective slenderness ratio

M_{fx} Column design out-of-plane moment demand

M_{fy} Column design in-plane moment demand

M_p Plastic moment of section

M_{px} Plastic moment of section about its strong-axis

M_{py} Plastic moment of section about its weak-axis

M_v Higher mode effect factor

r   Radius of gyration

R_d Ductility related force modification factor (NBCC)

R_o Overstrength-related force modification factor (NBCC)

$S(T)$ Design response spectral acceleration (NBCC)

T Fundamental period of the frame

T_f Axial tension demand (CSA S16)

t_f Thickness of the flange of wide-flange section

t_w Thickness of the web of wide-flange section

V Design base shear

$V_{E/Frame}$ Seismic Design base shear per braced frame

$V_{W/Frame}$ Wind Design base shear per braced frame

β Coefficient for bending in beam-columns

λ Slenderness parameter

ϕ Resistance factor

δ_{St} Storey displacement obtained from NLRH

δ_i Tier i displacement obtained from NLRH

δ_e Elastic storey displacement

T_u Brace probable tensile resistance

C_u Brace probable compressive resistance

C'_u Brace probable buckled resistance

V_u Storey shear capacity corresponding to the probable resistance of braces

T_{Design} Brace design tension force

C_{Design} Brace design compression force

NL   Notional Load

List of Abbreviations

AISC	American Institute of Steel Construction
CBF	Concentrically Braced Frame
CC	Conventional Construction
CC-HSS-2L	Type CC frames with Square HSS columns and tension-only double-angle braces
CC-HSS-L	Type CC frames with Square HSS columns and tension-only single-angle braces
CC-W-HSS	Type CC frames with W-shape columns and tension-compression HSS braces
CSA S16	Canadian steel design standard
DCF	Drift Concentration Factor
ESFP	Equivalent Static Force Procedure
HSS	Hollow Square Shape
IOS	Initial Out-of-Straightness
ISPD	Initial Stiffness-Proportional Damping
LD	Limited Ductility
LHS	Left-Hand-Side
LLBB	Long-Leg-Back-to-Back
MD	Moderately Ductile
OCBF	Ordinary Concentrically Braced Frames
MPa	Mega Pascal
MPD	Mass-Proportional Damping
MT-CBF	Multi-Tiered Concentrically Braced Frame
NBCC	National Building Code of Canada

NEES   Network for Earthquake Engineering Simulation

NLRH   Nonlinear Response History

OpenSees   Open System for Earthquake Engineering Simulation

RHS   Right-Hand-Side

SCBF   Special Concentrically Braced Frame

SFRS   Seismic Force-Resisting System

T/C   Tension-Compression

T/O   Tension-Only

TSPD   Tangent Stiffness-Proportional Damping

W-shape   Wide-Flange

3D   Three-dimensional

Chapter 1: Introduction

1.1   Background

Steel Concentrically Braced Frames (CBFs) are widely used as Seismic Force-Resisting Systems (SFRSs) in construction of steel buildings in Canada. CBFs comprise columns, beams, and diagonal bracing members, creating a vertical truss to transfer horizontal loads such as the wind or earthquake. In CBFs, bracing members meet each other at the beam-to-column connection or intersect with each other on the beam. Various configurations of CBFs are shown in Figure 1.1.
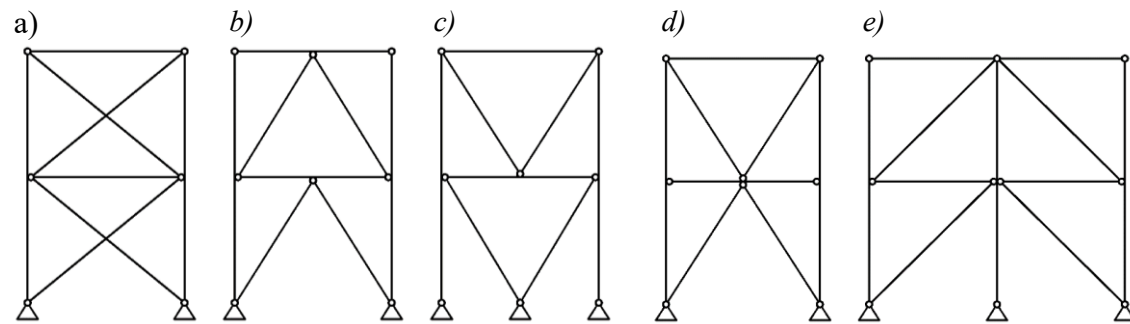
Figure 1.1. CBF configurations: a) X-bracing; b) Inverted V-bracing or Chevron; c) V-bracing;
d) Split-X-bracing; e) Diagonal bracing.

Multi-Tiered Concentrically Braced Frames (MT-CBFs) consist of multiple concentric bracing panels that are stacked between two adjacent floor levels. MT-CBFs are commonly used in North America in tall storeys of multi-storey or single-storey buildings such as industrial buildings, warehouses, airplane warehouses, or sports facilities when it is impractical or uneconomical to employ only a single braced panel along the storey height. Four examples of MT-CBFs in structures are illustrated in Figure 1.2. Design engineers in such buildings often prefer to divide

the storey height into multiple bracing tiers with a tier height typically ranging from 4 m – 6 m because using a single bracing panel would lead to long and, in turn, large braces.
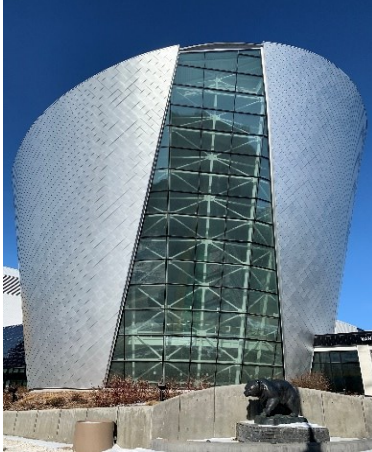
Figure 1.2. a) an MT-CBF in a sports facility; b) a two-tiered CBF in a single-storey shopping centre; c) a four-tiered CBF in a single-storey industrial building; d) a two-tiered CBF in the second storey of a two-storey commercial building.

The application of a single-panel braced frame would result in unrealistically large connections, which also precludes the choice of such bracing configuration. Finally, multi-tiered arrangements can efficiently reduce the column in-plane unbraced length for the stability check by providing lateral bracing between braced panels by means of horizontal intermediate struts. The in-plane

unbraced length of the columns in MT-CBFs is therefore reduced to the distance between the intermediate struts, while the unbraced length of the column for out-of-plane buckling is equal to the full frame height. Figure 1.3a and Figure 1.3b schematically demonstrate the difference between a single-storey building with a single X-braced frame and a multi-tiered X-braced frame, respectively. MT-CBFs (Figure 1.3b) can be compared to multi-storey CBFs (Figure 1.3c) as they share some similarities, such as nearly similar brace length and size, connection size, or column unbraced length in the plane of the frame; however, lack of floor slab at strut levels and long out-of-plane unbraced length of the column are the unique features of MT-CBFs. Multi-tiered configurations may also be used in multi-storey structures with long storey heights (Figure 1.2d and Figure 1.3d).
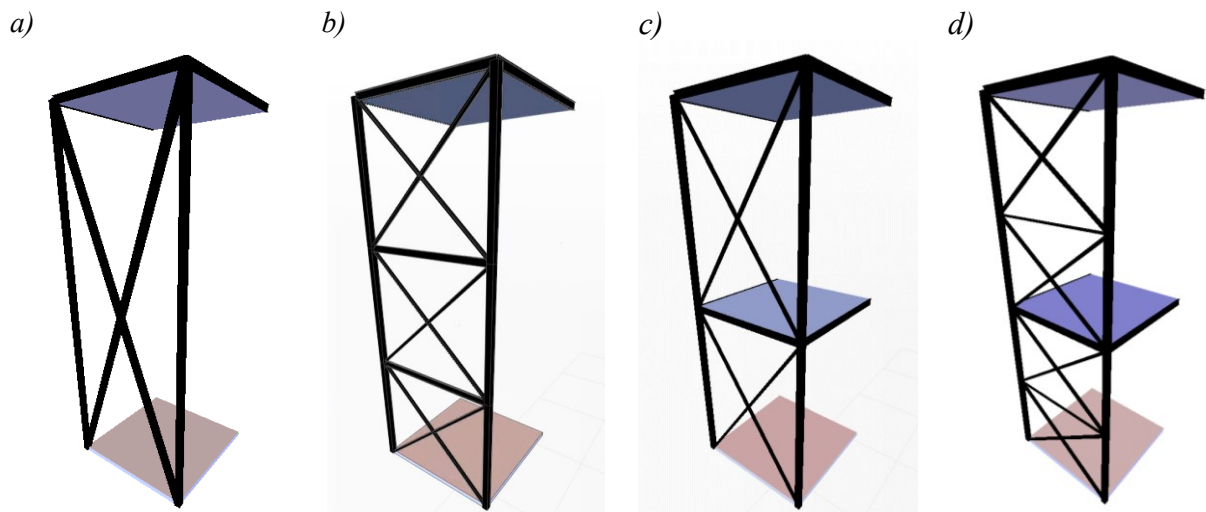
Figure 1.3. a) A single-storey single-panel CBF, b) a single-storey three-tiered CBF, c) a two-storey single-panel CBF, and d) a two-storey two-tiered CBF.

When designing under seismic loads, shorter braces, as expected in multi-tiered configurations, can effortlessly meet stringent seismic design requirements, including global slenderness and width-to-thickness ratio limits. Moreover, capacity-induced forces in columns, beams, adjacent connections, and footing are expected to reduce in such bracing configuration because of smaller

brace sizes. Various combinations of structural shapes are used in the design of MT-CBFs. The braces are typically made of Hollow Structural Shapes (HSS), Wide-flanges (W-shape), and single or double-angles. Wide-flange sections or HSSs are often used for columns. The combination of both column sections can also be used where W-shaped columns are used in exterior columns to resist lateral wind and seismic loads, and interior columns are made of HSSs to resist gravity loads (e.g. shopping centres). The struts can be designed using HSSs or wide-flange sections. The choice of sections depends on the building type, seismicity level, ductility level selected, availability of the sections in the market, and connection details.

A large portion of steel MT-CBF structures is located in regions of low-to-moderate seismicity of North America. In such buildings, design engineers often prefer to use low-ductile systems to avoid using intricate structural details and prohibitively expensive strengthening requirements primarily developed for highly ductile systems, which are often used in high seismic regions.

In Canada, two types of low-ductile braced frame systems have been introduced in the 2014 edition of the Canadian steel design standard, CSA S16 (CSA 2014):

1) Limited-ductility (Type LD) Concentrically Braced Frames with a ductility-related force modification factor, $R_d = 2.0$ and over-strength related modification factor $R_d = 1.3$, and

2) Conventional Construction (Type CC) frames, which can apply to any SFRS category (i.e. braced frames, plate shear walls, or moment-resisting frames), with a ductility-related force modification factor, $R_d = 1.5$ and over-strength related modification factor $R_d = 1.3$.

According to CSA S16, Type LD CBFs are expected to dissipate limited amounts of energy through the yielding of their bracing members. The standard requires Type LD braced frames to be designed using the capacity design principal. Whereas, the capacity design methodology is not

required to consider when designing lower ductility Type CC braced frames. Instead, all of the components of such braced frames are designed to carry the factored seismic forces except that the design forces in frames taller than 15 m located in moderate and high seismic regions are amplified. Two amplification factors are introduced:

1) The factored seismic forces must be amplified linearly by 2% per meter of the fraction of the frame height above 15 m to account for additional shear in upper storeys under dynamic loading;

2) The factored seismic forces of the columns must be amplified by another amplification factor equal to 1.3 to protect them when limited yielding takes place in braces or their connections resulting in probable resistances.

CSA S16-14 specifies special design requirements for Type LD braced frames with multi-tiered configuration under "Columns with braces intersecting between horizontal diaphragms." These guidelines aim to protect the columns of MT-CBFs against yielding and instability while reducing ductility demand on braces to avoid brace fracture. The special requirements for Type LD MT-CBFs are as follows:

1) The number of tiers is limited to five;

2) Horizontal struts must be provided to attain a load path over the height of the frame after the load-carrying capacity of compression braces are reduced due to global buckling; and

1) The columns must be designed for forces as follows:

   a) All applicable gravity loads.

   b) Axial force, shear force, and bending moments induced by yielding and buckling of the braces at the design storey drift as determined by performing a set of nonlinear incremental analyses assuming that for each analysis the tension-acting brace of one of

the tiers yields, tension braces of other braced panels remain elastic, and compression braces of all tiers buckle. (For a two-tiered braced frame shown in Figure 1.4a, the brace loading condition mentioned above is illustrated in Figure 1.4b and Figure 1.4c, respectively, when brace tensile yielding takes place in Tier 1 and Tier 2.)

c) An out-of-plane transverse force at each brace-to-column joint equal to 2% of the factored axial load of the column below the joint (Figure 1.4b).
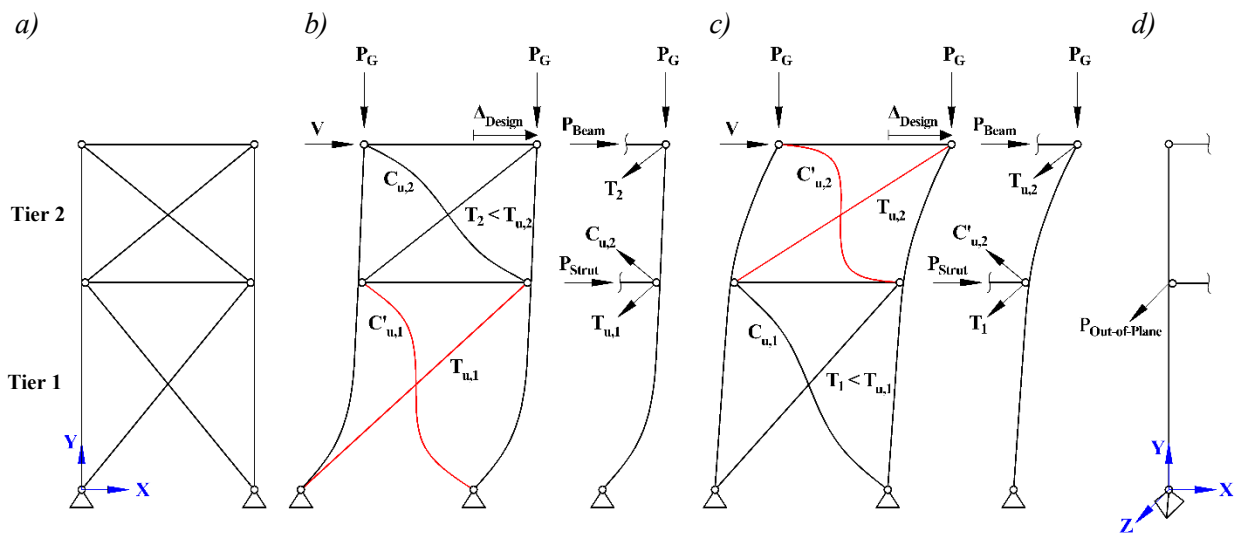
Figure 1.4. Column design forces for a Type LD two-tiered CBF: a) two-tiered CBF; b) in-plane demands for brace tensile yielding in Tier 1; c) in-plane demands for brace tensile yielding in Tier 2; d) out-of-plane demands.

In Type CC MT-CBFs, structural elements must be designed to resist factored seismic forces, including the force amplifications (if applied) described earlier (Figure 1.5a). For members that are intersected by bracing members at an unbraced location (e.g. column in multi-tiered braced frames), an additional out-of-plane bending moment due to out-of-plane transverse force equal to 10% of the axial load carried by the column at each brace-to-column intersection point must be considered in the design (Figure 1.5b).

6
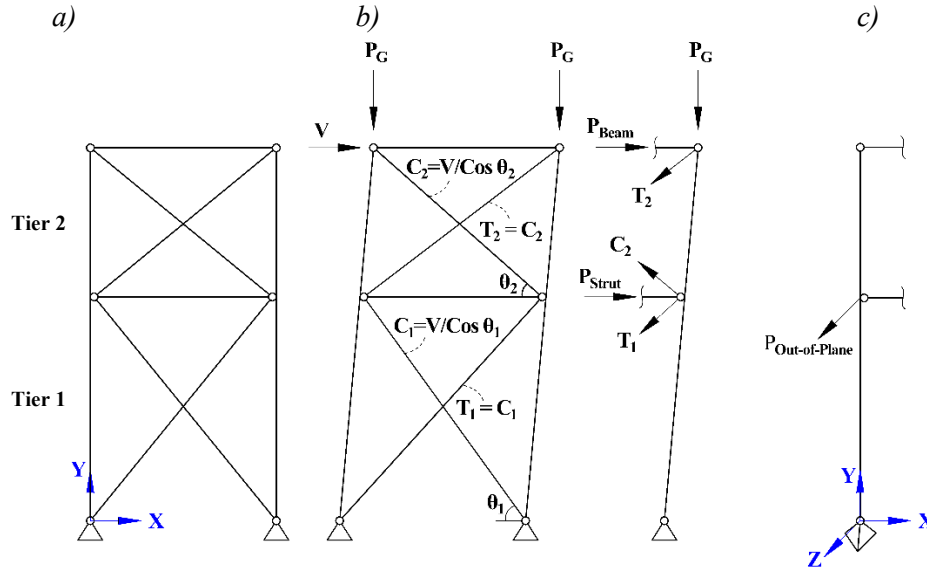
Figure 1.5. Column design forces for a Type CC two-tiered CBF: a) two-tiered CBF; b) column in-plane demands; c) column out-of-plane demands.

1.2   Problem Statement

A large proportion of MT-CBF structures in areas that are not highly seismic are designed to the Limited-Ductility (Type LD) or Conventional Construction (Type CC) seismic provisions to avoid stringent seismic requirements and complex connection detailing. However, CSA S16-14 design requirements for low-ductile MT-CBFs may lead to severe loading conditions for columns and result in larger column sections than if such requirements are not to be considered or are to be relaxed. Furthermore, the application of special seismic design provisions for Type LD MT-CBFs requires a nonlinear static (pushover) analysis (Imanpour and Tremblay 2014) or a series of linear static analyses (Imanpour and Tremblay 2016a), which may become tedious or even complicated, in particular in case of frames with a large number of tiers. Furthermore, CSA S16-14 only permits MT-CBFs with a maximum of three tiers when Moderately Ductile (Type MD) system is selected, and a maximum of five tiers are allowed to be constructed using Type LD CBFs. This can limit the choice of design engineers when selecting the seismic force-resisting system.

7

Extensive numerical simulations and limited experimental testing have been performed on multi-tiered steel concentrically braced frames in the past decade with a focus on high seismic areas. These studies primarily served to better understand the seismic response of such frames. (Imanpour and Tremblay 2016c, 2016b, Imanpour et al. 2016b). The results obtained from such studies were also used to and develop enhanced seismic design provisions in North American steel design standards, AISC Seismic Provisions for Structural Steel Buildings (AISC 2016) in the U.S. and CSA S16 (CSA 2014) in Canada. In Canada, both Type MD and Type LD systems were treated nearly the same in terms of the analysis procedure and design demands. However, Type LD braced frames may experience significantly lower inelastic seismic demands with minimal yielding in seismic fuses, which inspires a simpler analysis method used in design.

Although satisfactory structural behaviour of low-ductile MT-CBFs for typical gravity and wind loading has been well-established, there is little evidence either from existing experimental data or field observation on the response of such frames when subjected to earthquake loading. To date, very limited research has been into the seismic response of Type LD MT-CBFs (Imanpour and Tremblay 2016c, Auger 2017, Agarwal and Fahnestock 2018) and no research, to the author's knowledge, has been conducted to evaluate the seismic performance of Type CC MT-CBFs designed to mimic Canadian design and construction practice, thus the current Canadian steel design standard lack background research to support the seismic design requirements for such low-ductile MT-CBFs. Finally, in moderate and low seismic regions, Type CC MT-CBFs are often not explicitly detailed to achieve a ductile inelastic response, so their governing limit states are mostly unknown (Tremblay et al. 2009, 2010, Gélinas et al. 2012, Decaen 2015).

In view of the extensive use of low-ductile multi-tiered braced frames in regions of low and moderate seismicity, improved and yet simplified seismic design methods are urgently needed that

address the seismic risk outside of high seismic hazard regions for Type LD and Type CC MT-CBFs. Such methods would significantly simplify the seismic design of such buildings and minimize construction costs while maintaining safety. Such improvements can also be used to revisit and update the seismic design provisions of the Canadian steel design standard for Type LD and CC MT-CBFs.

1.3   Research Objectives

The general objective of this M.Sc. research is to investigate the seismic response and design of low-ductile MT-CBFs in Canada.

This thesis has four specific objectives, as follows:

1) To investigate the seismic response of Type LD and Type CC MT-CBFs designed in accordance with CSA S16-14 seismic provisions.

2) To propose a simplified seismic analysis and design procedure for Type LD MT-CBFs in regions of low-to-moderate seismicity.

3) To develop a seismic design method for Type CC MT-CBFs in low-to-moderate seismicity regions.

4) To generate nonlinear response history analyses data for future research studies on steel braced frame structures.

1.4   Research Methodology

Seven steps were followed to achieve the objectives of this research project. These steps include literature review, parametric study matrix development, frame design, numerical model

development, nonlinear response history analysis, seismic response evaluation, and analysis and design method recommendation. The steps are described as follows:

1) Literature Review:

   A literature survey was conducted on the seismic performance of steel concentrically braced frames. The survey mainly focused on multi-tiered brace frames, low-ductile systems, brace nonlinear response, and numerical modelling techniques. Since the present research includes an extensive computer simulation, special attention was paid to numerical simulation techniques and nonlinear analysis procedures.

2) Parametric Study Matrix Development:

   A parametric study matrix was developed to study a wide range of low-ductile steel MT-CBFs. 64 frames were selected by varying the following parameters:

   - Frame ductility level: Type LD ($R_d = 2.0$ & $R_o = 1.3$) and Type CC ($R_d = 1.5$ & $R_o = 1.3$)

   - Number of tiers: two, three, four, and six

   - Frame height: 10 m, 16 m, and 24 m

   - Tier height ratio defined as the height of the first tier to the second tier (h_1 / h_2): 1.0 and 1.75

   - Brace section: Square HSS, single-angle, and built-up double-angle

   - Bracing system: Tension-Compression (T/C) and Tension-Only (T/O)

   - Column section: Square HSS and W-shape

3) Frame Design:

An industrial building was selected in Montreal, Quebec, representing a moderate seismicity region in Canada. Design loads included dead, snow, wind, and seismic, which were calculated in accordance with the 2015 National Building Code of Canada, NBCC (NRC 2015). Member design was then performed using the 2014 edition of the CSA S16 (CSA S16-14). The special seismic design requirements for columns of multi-tiered configurations set by CSA S16-14 for Type LD, as well as the limit on the number of braced tiers, are excluded in design to be able to examine the adequacy and accuracy of current design requirements. For Type CC frames, the amplification factors in frames taller than 15 m in moderate and high seismic regions, as well as the special requirements for columns that are intersected by bracing members at an unbraced location, are excluded in the design to assess the need for such requirements. Note that the 2019 edition of the CSA S16 was published when this document was in preparation. No significant changes that can impact this research study were introduced for the design of Type LD and CC MT-CBFs in this new edition.

4) Numerical Model Development:

The fibre-based nonlinear numerical models of the prototype frames were created using the *OpenSees* software package (McKenna et al. 1997). The frame members expected to experience nonlinear response or instability (i.e. braces and columns) were individually simulated and calibrated against experimental test data.

5) Nonlinear Response History (NLRH) Analysis:

The selected frames in Step 3 were analyzed using the nonlinear response history analysis method under gravity plus horizontal earthquake acceleration.

6) Seismic Response Evaluation:

The seismic response of the frames as obtained from the NLRH analyses were studied to assess various response parameters and to determine the demands on different members with the focus on stability and demands of columns under seismic loading.

7) Analysis and Design Method Recommendation:

The results obtained from the NLRH analyses on the prototype frames were finally used to propose enhanced and simplified analysis and design methods for Type LD and Type CC MT-CBFs.

1.5   Organization of Thesis

This M.Sc. thesis comprises seven chapters. The first chapter introduces the background, problems, objectives, and methodology of the project. In chapter two, a literature review on the cyclic behaviour of steel braces, seismic response of steel CBFs and MT-CBFs, seismic design procedures for steel MT-CBFs, and numerical modelling techniques for steel braced frames are discussed. The third chapter introduces the parametric study matrix and describes the design of prototype frames in this study. Chapter four focuses on the development of the numerical models of the individual braces and columns, as well as the braced frames. Chapter five presents the results of nonlinear response history analyses conducted on the prototype frames. Design recommendations are made for Type LD and Type CC MT-CBFs using the results obtained in Chapter six. The final chapter presents the main findings of the study and recommendations for future research studies.

Chapter 2: Literature Review

2.1   Introduction

This chapter provides a review of past studies concerning seismic response and design of steel Multi-Tiered Concentrically Braced Frames (MT-CBFs). The inelastic hysteretic response of steel braces is first discussed. Then the seismic behaviour of steel Concentrically Braced Frames (CBFs) and MT-CBFs are summarized, followed by a review of the 2014 seismic design guidelines for steel MT-CBFs in Canada. A summary of key research findings on the numerical modelling techniques used in steel braced frame structures is finally presented.

2.2   Cyclic Inelastic Behaviour of Steel Braces

Steel braced frame structures with concentric bracing members are extensively used by designers. The primary reason is that CBFs can efficiently provide a substantial lateral stiffness by forming a vertical truss. The lateral stiffness, in turn, limits the total sway of the structure as well as the inter-storey displacements under earthquake load effects.

Evaluation of the cyclic inelastic response of steel braces has been the focus of numerous research studies over the past 40 years. Extensive experimental and numerical studies have been conducted to improve the understanding of the inelastic behaviour of steel braces under cyclic loading and develop seismic design procedures (Popov et al. 1979, Jain et al. 1980, Astaneh-Asl et al. 1985, Tremblay 2002, 2003, Tremblay et al. 2003, Hsiao et al. 2014).

Seismic design provisions for steel CBFs in modern design standards such as CSA 2014 and AISC 2016, allow yielding and buckling of braces while the other members of the braced frame must

remain elastic under the tensile and compressive capacities of braces. Tension- and compression-acting braces are therefore expected to experience large deformations. Thus, the cyclic inelastic behaviour of such members plays a crucial role in the overall response of the braced frame.

The cyclic behaviour of bracing members is studied by performing quasi-static displacement-controlled testing. In a quasi-static test, a predetermined displacement sequence is applied stepwise to the member in a way that the magnitude of the displacement gradually increases until the specimen fails or is significantly deformed. The hysteretic responses (axial load – axial displacement response) of a Tension-Compression (T/C) Hollow Structural Shape (HSS) brace and a Tension-Only double-angle brace are shown in Figure 2.1. The load-displacement response obtained from the test can provide critical mechanical properties of that specimen, such as tensile yield strength, expected compression capacity, and expected post-buckling capacity. When the specimen is loaded first in compression, it buckles at its compression resistance. After the occurrence of first buckling in compression, due to forming a flexural plastic hinge at the middle of the specimen, the member experiences large in-plane or out-of-plane deformations, and its compression capacity falls drastically during the proceeding cycles. At the tension side, the member might experience a number of cycles of elastic loading and unloading until it reaches its tensile yielding resistance. Then the member elongates in inelastic range while maintaining its tensile yielding capacity. In the subsequent loading cycles, due to residual in-plane or out-of-plane deformations, a larger axial deformation is required to be imposed so that the member can experience tensile yielding again (Tremblay 2001).
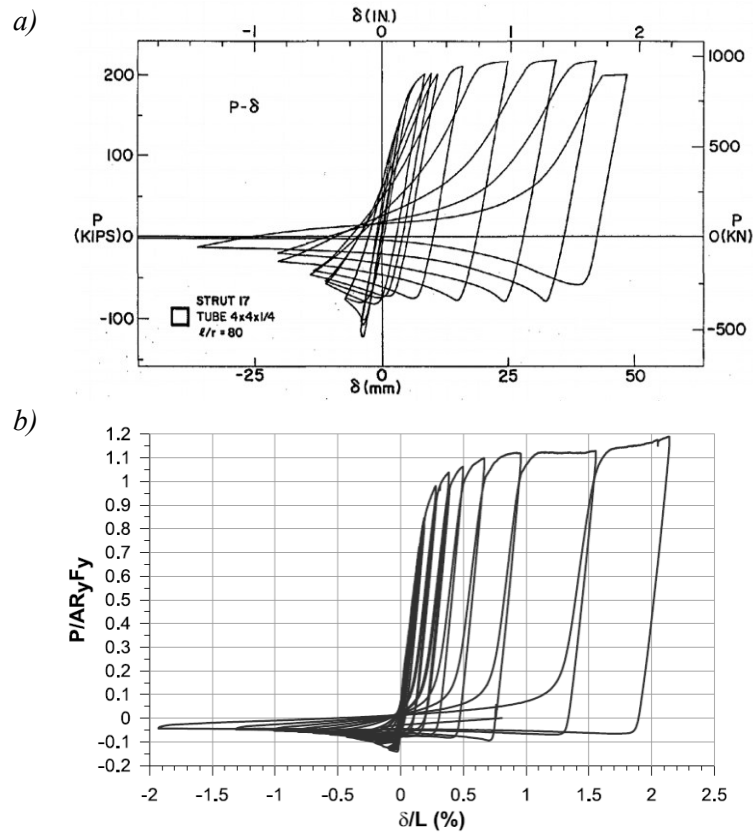
Figure 2.1. Axial force – axial deformation (hysteresis) response of a) a T/C HSS brace (Black et al. 1980), and b) a T/O double-angle brace (Jiang 2013).

2.2.1 Hollow Structural Shape (HSS)

Square and rectangular HSSs are among the most common and efficient structural sections for bracing members. The seismic response of HSS bracing members has thoroughly been examined in the past (Lee and Goel 1987, Tang and Goel 1987, Tremblay and Stiemer 1994, Tremblay 2002, Tremblay et al. 2003, Uriz and Mahin 2004, Fell et al. 2009).

Tremblay (2002) conducted an extensive review of past experimental tests to better understand the inelastic hysteretic response of steel bracing members with various cross-sections, namely Square HSS, Round HSS, pipe, W-shape, and double-angle subjected to various loading protocols. The parameters evaluated in this study were the maximum tensile strength, compression resistance

upon buckling, post-buckling compressive resistance, and the lateral deformation at buckling. Predictive equations were proposed to estimate each of these parameters. It was also found that the lateral deformation at buckling is associated with the buckling mode of the bracing members. (Tremblay 2002) proposed an equation to predict the lateral deformation of the brace at the maximum anticipated compression deformation. A decent correlation was found between the results obtained from this prediction and test data (Figure 2.2).

Upon buckling, a bracing member can be detailed to deform in the plane of the frame (i.e. in-plane buckling mode) or out of the plane frame (i.e. out-of-plane buckling mode). Due to the considerable lateral deformations at the mid-length of the brace at buckling, out-of-plane buckling mode could cause the collapse of partitions attached to the braces (Tremblay et al. 1996). One solution is to provide enough space around the brace so that it can accommodate the out-of-plane lateral deformation corresponding to its out-of-plane buckling mode (Tremblay 2002). Nevertheless, most of the efficient brace-end-connections result in out-of-plane buckling (Astaneh-Asl et al. 1985, Roeder et al. 2011b).
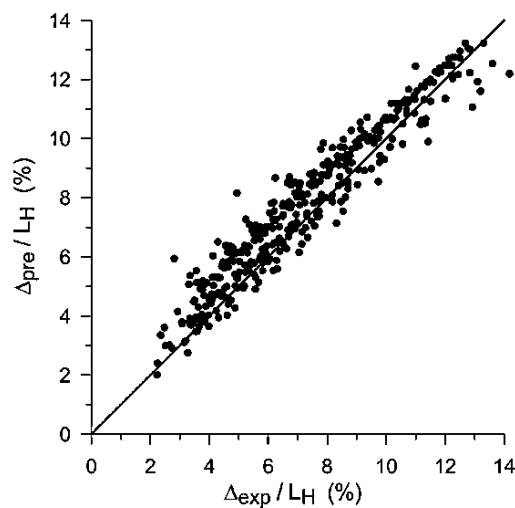
Figure 2.2. Lateral brace deformation (prediction vs. measured) at maximum anticipated compression deformation (Tremblay 2002).

Goggins et al. (2006) also measured the mid-length lateral deformations of steel HSS bracing members by performing a series of quasi-static tests. The comparison between the test results and Tremblay's (Tremblay 2002) equation is shown in Figure 2.3. As shown, the proposed equation well predicts the test measurements when the axial deformation of the brace is not significant. However, for large values of axial displacement, the equation underestimated the test values.
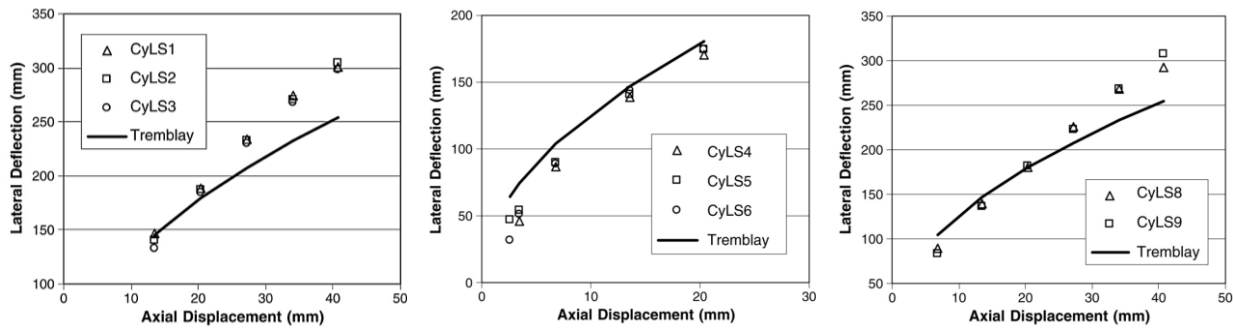
Figure 2.3. Evaluation of Tremblay's (2002) proposed equation using measured data (Goggins et al. 2006).

2.2.2 Built-up Double-Angle Braces

Built-up angle bracing members in CBFs have been commonly used for a long time. One reason being that such braces require connections with relatively simple details, which helps to facilitate the fabrication and erection process (Jiang 2013).

Two key studies on the response of double-angle braces were performed in the 1980s (Astaneh-Asl and Goel 1984, Astaneh-Asl et al. 1985). They investigated the buckling mode of the double-angle braces for in-plane or out-of-plane cases using quasi-static tests.

The key findings for braces with the in-plane buckling (Astaneh-Asl and Goel 1984) are as follows:

- Three plastic hinges formed in the braces: two at the ends of brace close to the gusset plates and one in the middle of the brace. The gusset-plates remained elastic during the tests.

- The deformed shape of nearly all the specimens can be estimated by the buckled shape of a fix-fix axially loaded member (Figure 2.4), which suggests that the effective length factor, *K*, for in-plane buckling of double-angle braces can be taken close to 0.5.

- The forces in the stitches were limited, which implies that the in-plane buckling mode does not involve relative deformations of the individual angles.
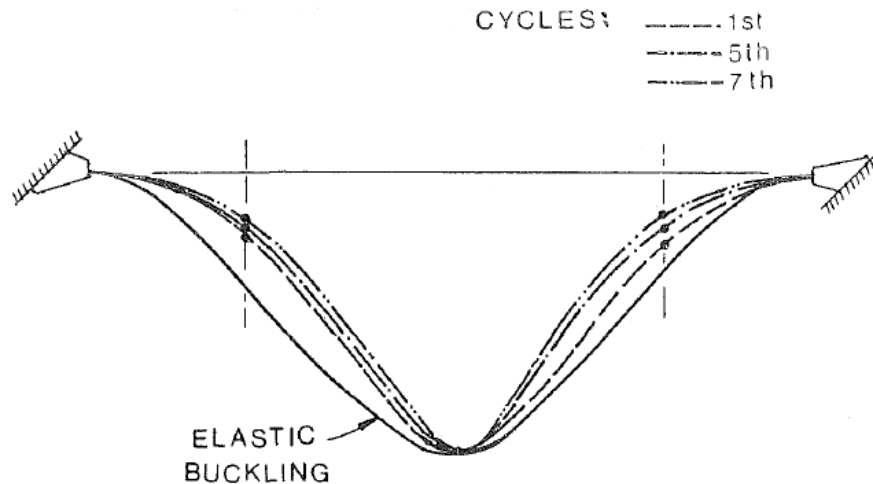
Figure 2.4. In-plane buckling configuration of double-angle braces obtained from specimen AW15 (Astaneh-Asl and Goel 1984).

The results of the tests where out-of-plane buckling of the double-angle braces (Astaneh-Asl et al. 1985) are expected are as follows:

- End gusset plates had a significant impact on the out-of-plane hysteretic response of double-angle braces. The authors proposed connection design recommendations to ensure the connections can undergo large plastic rotations.

- In all of the tests, two plastic hinges formed in end gusset plates and one in the middle of the brace (Figure 2.5).

- The buckled shape of the double-angle braces was approximately a half-sine wave, which is similar to the deformed shape of a simply-supported axially loaded member. Based on this analogy, the study recommended a *K* of approximately 1.0 for out-of-plane buckling.

- The forces in the stitches were considerable. The source of this force is the relative deformations of single-angles. It should be noted that this observation is used in the current research project to calculate the equivalent effective length factor of double-angles, ρ_e.

a)   b)
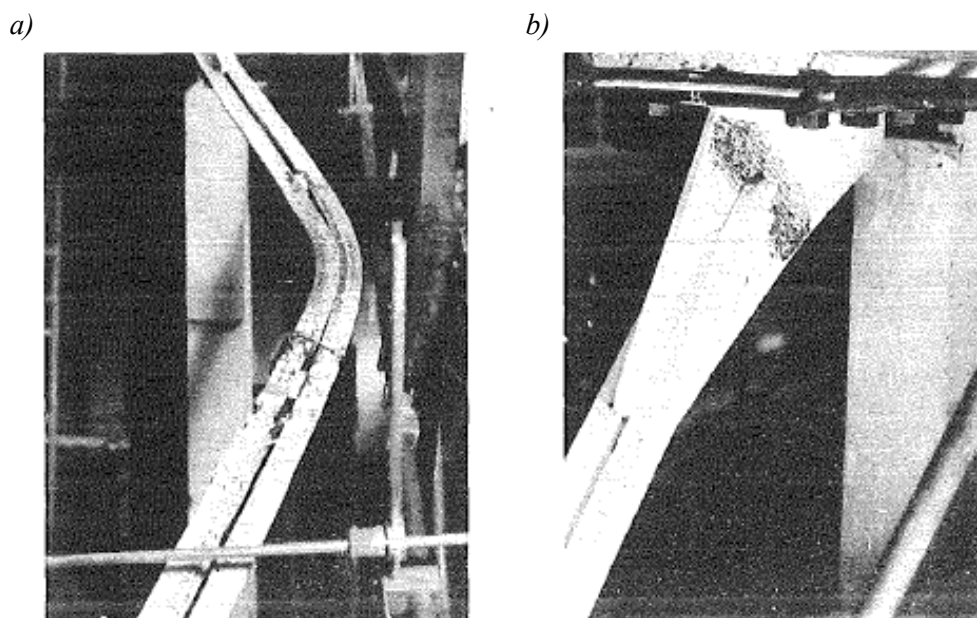
Figure 2.5. Plastic hinge forming in double-angle braces at a) mid-length of the brace, and b) end gusset plates (Astaneh-Asl et al. 1985)

For both buckling modes, a steep degradation was reported in the compressive capacity of the brace upon first buckling. Additionally, as shown in Figure 2.6a, the buckling capacity dropped drastically in the second cycle. In the subsequent cycles, the compression capacity decreased gradually (Figure 2.6b).
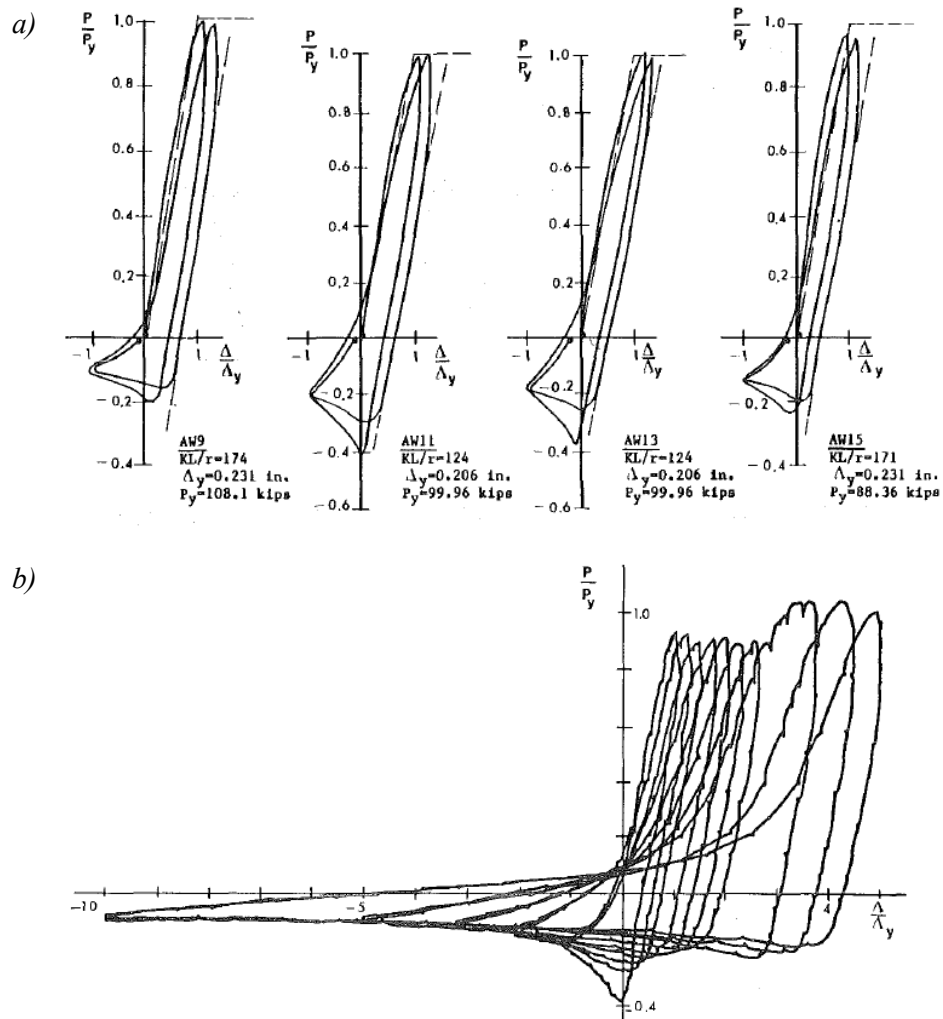
Figure 2.6. a) First two cycles of hysteresis loops of double-angle specimens AW9, AW11, AW13, and AW15; b) Complete hysteresis loop of specimen AW13 (Astaneh-Asl and Goel, 1984)

Jiang (2013) performed a survey on Tension-Only (T/O) CBF buildings constructed in high seismic regions of Canada prior to the introduction of first seismic design provisions in the Canadian steel design standard in 1989. The work focuses on the seismic investigation and retrofit of braced frames with tension-only double-angle braces. Since the bracing connections of such existing buildings had insufficient resistances compared to those required by the recent seismic design requirements (e.g. 2010 edition of CSA S16), retrofit strategies were proposed to avoid non-ductile failure of such connections. To validate the retrofitting methods, experimentally Jiang

(2013) tested full-scale double-angle braces and showed the upgraded connection details outperformed the seismic response. Physical test data was then used to calibrate the numerical models of double-angle braces. Figure 2.7 shows an example of such calibrations. The validated models of double-angles then implemented in the numerical model of a braced frame to investigate the collapse behaviour of original and retrofitted connections of existing braced frames using nonlinear response history analysis.
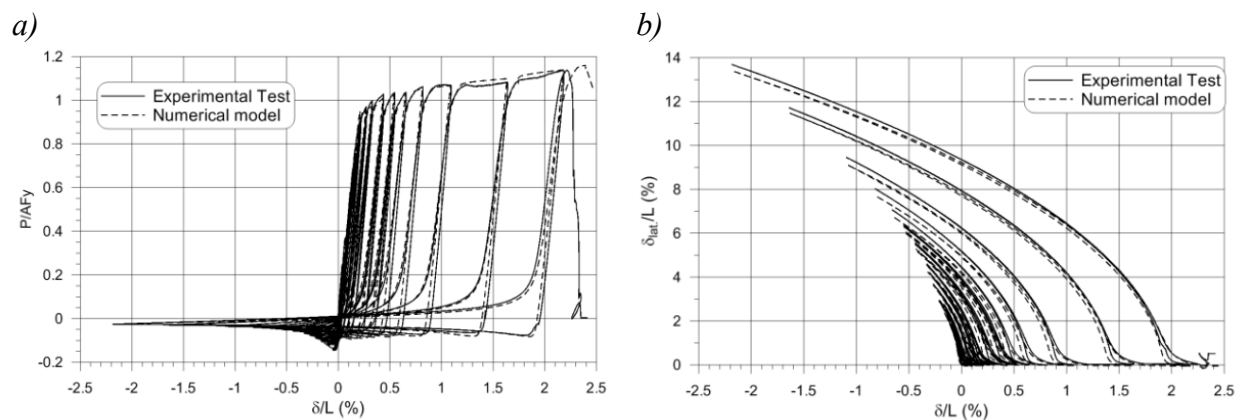
Figure 2.7. Hysteresis response validation of the double-angle brace model against test LF-O-C-1: a) axial force-axial displacement; b) brace axial displacement-lateral deflection (Jiang 2013).

2.3   Seismic Behaviour of Steel CBFs

Steel CBFs are extensively used as the Seismic Force-Resisting System (SFRS) in Canada as they can provide large lateral stiffness and easily satisfy code-specified drift limits while minimizing the weight of the structure. Furthermore, CBF connections are typically designed with simple pin connections, which can significantly reduce the construction cost (Tremblay 2001).

A number of limitations have been reported for CBFs, such as the limited energy dissipation capacity of braces, and the probability of early brace fracture under hysteretic loading. Over the past decades, however, researchers conducted extensive studies to enhance the shortages of CBFs,

which have been implemented in modern steel design standards (Tremblay 2001). North American design standards for steel structures (i.e. CSA S16 and AISC 341) prescribe requirements for CBFs so that they provide a sufficient level of ductility in the event of earthquakes.

In a CBF configuration, the members are connected in a way that seismic-induced forces are transferred to the ground through the axial forces of the members. In conventional CBFs, braces act as the system seismic fuses and are expected to yield in tension and buckle in compression. As required by the capacity design principal, columns, beams, and connections are designed to carry the maximum expected forces arising from inelastic behaviour of braces to ensure they do not experience an inelastic response and maintain the integrity of the system during a severe earthquake. Figure 2.8 shows the desirable behaviour of a multi-storey CBF designed according to the capacity design methodology.
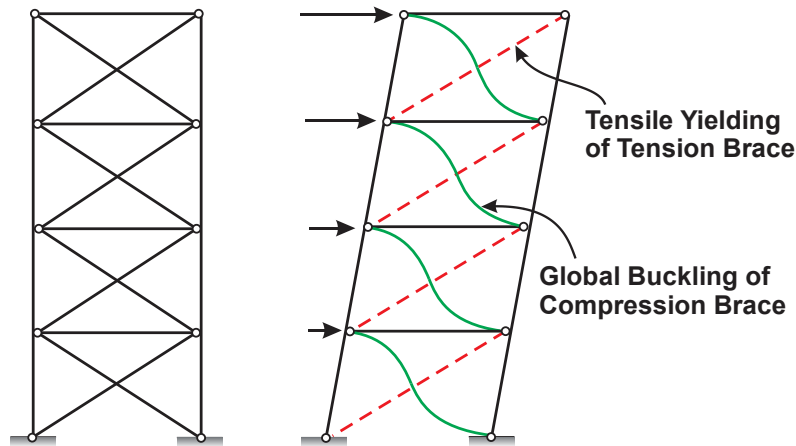
Figure 2.8. Expected seismic performance of steel CBFs.

The braces in CBFs must be designed and detailed to provide a stable inelastic response in tension and compression without brittle fracture in the member or connection or instability of adjacent members, as shown in Figure 2.9.
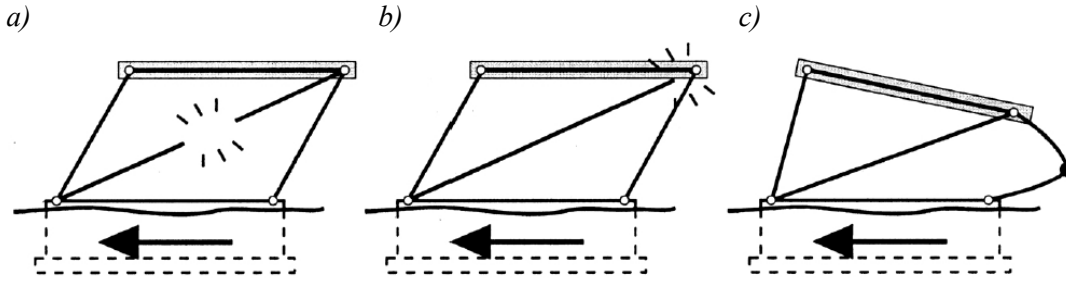
Figure 2.9. Unsatisfactory seismic performance of CBFs: a) brace brittle fracture; b) connection brittle failure; c) column buckling (Tremblay 2001).

2.3.1 Limited Ductility CBFs

Seismic provisions in Canadian steel design standard (CSA S16) and Seismic Provisions for Structural Steel Buildings in the U.S. (AISC 341) classify CBFs based on their ductility level. CSA S16 designates two ductility levels for CBFs, Moderately Ductile (Type MD) with R_dR_o = 3.9 and Limited Ductility (Type LD) with R_dR_o = 2.6. AISC classifies CBFs into two ductility levels, including Special Concentrically Braced Frames (SCBFs) with R = 6 and Ordinary Concentrically Braced Frames (OCBFs) with R = 3.25. R_d is the ductility-related force modification factor, R_o is the over-strength related force modification factor, and R is the response modification factor.

Despite extensive research into the seismic behaviour of low-ductile CBFs (Callister and Pekelnicky 2011, Li and Fahnestock 2013, Bradley et al. 2014, 2017, Fahnestock et al. 2014, Sizemore et al. 2015, 2017) particularly in regions of low-to-moderate seismic hazard, limited research is available on the response of low-ductile MT-CBFs

Most recently, a research project was conducted on low-ductile CBFs at Lehigh University led by the University of Illinois at Urbana-Champaign (Bradley et al. 2014). The performance of CBFs was examined under earthquake load effects in moderate seismic regions with a focus on the

reserve capacity of such frames. In this test program, two full-scale low-ductile braced frames were tested to provide data for the investigation of the failure mechanism of low-ductile CBFs in moderate seismicity regions. One of the prototype frames was a two-storey OCBF of Split-X (Figure 2.10a). As shown in Figure 2.11a, up to a frame drift of 1.5%, the frame experienced a ductile behaviour with several yielding and buckling of braces and drift concentration in both of the storeys. At a drift equal to 1.5%, a sudden fracture in the brace-to-gusset weld in the compression braces was observed. However, the frame showed reserve capacity when the load direction changed, which was originated from re-engagement of the fractured weld when the brace was in tension. Ultimately, the frame experienced a significant reduction in strength because of beam-to-gusset plate weld fracture, which substantially eradicated the load path of the frame.

The second frame was a two-storey chevron CBF with $R = 3$ and not particularly designed and detailed for seismic (Figure 2.10b). Despite the OCBF frame, which showed a limited ductile response, the $R = 3$ frame experienced non-ductile behaviour (Figure 2.11b). The results of this experiment revealed that at a drift of ±0.35%, a substantial capacity loss occurred in both braces of the second storey due to a brace buckling, which is considered as a non-ductile performance compared to the overall response of the system. Subsequently, the frame exhibited significant reserve capacity particularly due to brace connections (Bradley et al. 2017).
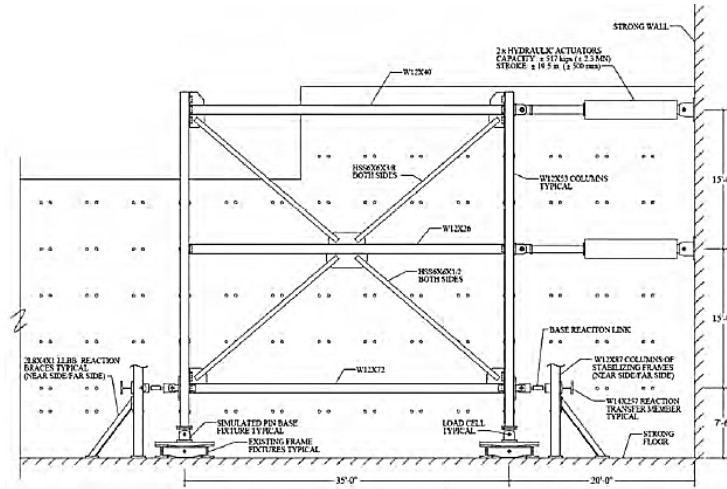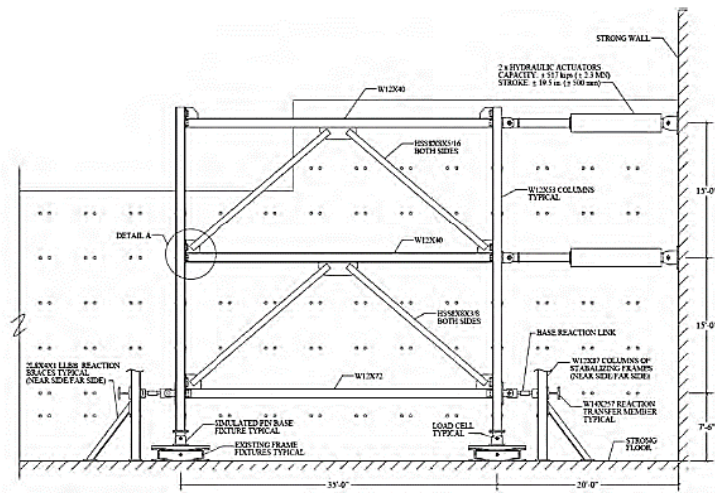
Figure 2.10. Elevation of the two-storey braced frame specimens: a) OCBF Split-X braced frame; b) chevron braced frame (Bradley et al. 2014).
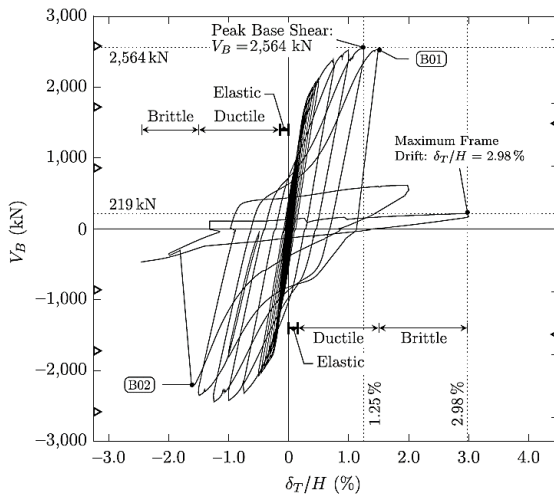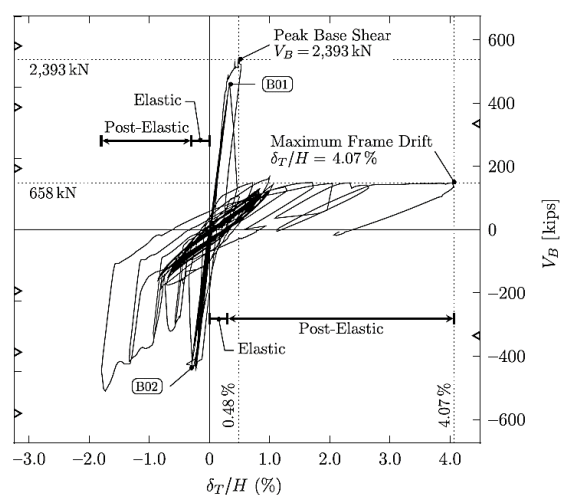
Figure 2.11. Frame base shear vs. frame drift for a) the OCBF and b) the CBF with R = 3.

To extend the test program, Sizemore et al. (2017) performed a parametric numerical study on various combinations of the low-ductile frames that were not tested in the test program. It was reported that system configuration, including Split-X versus chevron, influenced the reserve capacity, which was relatively more for the chevron configuration. Furthermore, the system ductility (OCBF with $R = 3.25$ versus CBF with $R = 3$) affected the response and reserve capacity. However, for the case of the chevron frame, the influence on the reserve capacity was more pronounced (Sizemore et al. 2017).

Choi et al. (2017) recently investigated the effect of the design provisions on the response of steel OCBFs. Nonlinear static and dynamic analyses were performed on multi-storey frames. The results of the analyses indicated that the inter-storey drifts of the frames do not exceed 2%, except for one of the frames.

2.3.2 Conventional Construction CBFs

Conventional Construction (Type CC) is a Seismic Force-Resisting System (SFRS) with the lowest ductility ($R_dR_o=1.5 \times 1.3=1.95$) prescribed by CSA S16-14 for the construction of building structures. An SFRS designed under Type CC category is expected to show modest ductility in the event of an earthquake. Type CC category comprises various SFRSs, including braced frames, moment-resisting frames, and plate shear walls.

Despite all other SFRSs, CSA S16-14 does not prescribe the capacity design procedure for Type CC structures. Due to its relaxed and simple requirements compared to even low-ductile systems such as Type LD CBFs, Type CC system is more favourable in regions of low-to-moderate seismicity.

Limited studies have been dedicated to understanding the behaviour of Type CC CBFs in Canada (Tremblay et al. 2009, 2010, Gélinas et al. 2012, Decaen 2015). Tremblay et al. (2009) investigated the response of Type CC steel CBFs located in a high seismic region, focusing on the behaviour of the connections. The global performance of Type CC steel CBFs under earthquake load effects was evaluated in this study. They carried out nonlinear dynamic analyses on prototype structures by varying various parameters, including total height, the location, and the site class. It was found that the design procedure of the 2006 edition of CSA S16 for Type CC steel CBFs is not applicable for buildings situated in regions of high seismic hazard.

Tremblay et al. (2010) published the results of a parametric study conducted to examine the seismic response of steel CBFs having up to 10 storeys considering two different soil types in high and moderate seismicity regions. The result showed that CSA S16-01 underestimates the connection design force demands for Type CC steel CBFs. Modification factors were proposed to amplify code-specified demands used for the design of the connections in such frames to prevent non-ductile connection failure. These recommendations were later implemented in CSA S16.

Another research study aimed to investigate the behaviour of Type CC steel X-braced frames devoting an exclusive emphasis on the effect of the middle bolted connection detail of the braces on the performance of steel concentrically braced frames with bolted connections (Gélinas et al. 2012). The results confirmed that the detail of the mid-connection influences the buckling response of the discontinuous brace and its effective length in compression. Premature failure was observed in the mid-connections of several frames tested in this study. The study suggested that connection design methods should be revisited to address such failure mode in bolted connections.

Davaran (2019) assessed the elastic and inelastic compressive buckling behaviour of bolted double shear lap connections commonly used in X-bracing CBFs with HSS braces. Due to the lack of a method to determine their compressive strength, these connections are designed for brace tension force. Based on the results of full-scale testing, he reported connection failure as a result of buckling at the connection. A design procedure for bolted double shear lap connections was proposed for which the effective length factor of the connection was obtained using an elastic buckling analysis. He verified the adequacy of the proposed method by non-linear numerical static analyses. It was also reported that the connection compression capacity reduces due to the slip of the connection plates.

2.4   Seismic Behaviour of Steel MT-CBFs

The multi-tiered system is favoured by structural engineers to avoid long braces with large cross-sectional areas in tall storeys of multi-storey buildings or tall single-storey buildings. As opposed to conventional multi-storey CBFs, the columns of MT-CBFs are designed using a shorter unsupported length in the plane of the frame due to the presence of the horizontal struts. Horizontal struts are employed between two adjacent braced panels to prevent the undesired K-type braced frame response, providing a load path when compression braces buckle. Nonetheless, in the out-of-plane direction, the columns are not braced over the full storey height, and therefore, the effective length for out-of-plane buckling of the column is equal to the total height of the frame.

Over the past decade, an extensive study has been carried out on the seismic performance and design of MT-CBFs (Imanpour et al., 2013, 2016b, 2016c, Imanpour and Tremblay 2016b, Imanpour et al. 2016a, Agarwal and Fahnestock 2017, Imanpour and Tremblay 2017, Agarwal and Fahnestock 2018, Cano 2019). The main focus of the majority of these research studies is

moderately-ductile (Type MD) CBFs in Canada and SCBFs in the U.S. A summary of the key findings of those studies is as follows:

- Non-uniform distribution of inelastic deformations over the height of the frame occurs as a result of the yielding of tension-acting braces in one of the braced tiers (Figure 2.12).

- Large bending moments in the plane of the frame are induced in the columns of MT-CBFs due to the drift concentration in one of the tiers.

- The column moment demands, if not considered in the design, may result in plastic hinge forming in the column, which in turn, compromises the stability of the column and, consequently, the integrity of the frame.
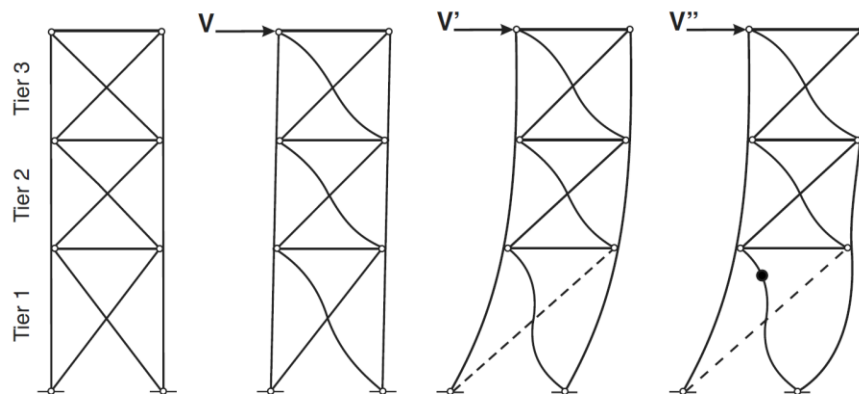
Figure 2.12. Drift concentration in the first tier of a three-tiered CBF (Imanpour et al. 2016b).

Imanpour et al. (2016b) examined the seismic performance of SCBFs designed to the 2010 AISC Seismic Provisions using numerical simulations. This study confirmed that an in-plane flexural bending moment can lead to column instability in the plane of the frame; such instability eventually changes to flexural torsional buckling, resulting in excessive deformations in and out of the plane of the frame.

Imanpour and Tremblay (2016c) studied the performance of moderately ductile (Type MD) CBFs conforming to the 2014 Canadian steel design standard in a high seismic region of Canada. Nither column instability nor frame collapse was reported in this study. An improved design method for tall Type MD MT-CBFs with a large number of tiers exceeding the limitations implicit in CSA S16 was proposed.

The results of past studies led to the development of seismic design provisions for MT-CBFs in Canada and the U.S. (Imanpour and Tremblay 2016b, 2016c, Imanpour et al. 2016b), which have been implemented in North American steel design standards including CSA S16 and AISC Seismic Provisions in the U.S.

A limited number of recent studies investigated low-ductile CBFs (Imanpour and Tremblay 2016c, Imanpour et al. 2016b, Agarwal and Fahnestock 2017, 2018). It was found that bracing members of such low-ductile braced frames may not experience significant inelastic behaviour under seismic load effects. Minimal inelastic demands in such frames result in limited bending moments in their columns. Furthermore, the CSA S16-14 seismic design provisions for the design of Type LD CBFs, which account for brace yielding and buckling, were found to be complex to apply in design. Imanpour and Tremblay (2016b) suggested a series of nonlinear static analyses or multiple linear static analyses on a number of frames generated by removing the yielded bracing members from the original frame to obtain MT-CBF column's seismic demands. An example of such analyses is shown in Figure 2.13 for a three-tiered CBF. A similar analysis method must be used to verify tier drift limits recommended by the 2014 CSA S16.
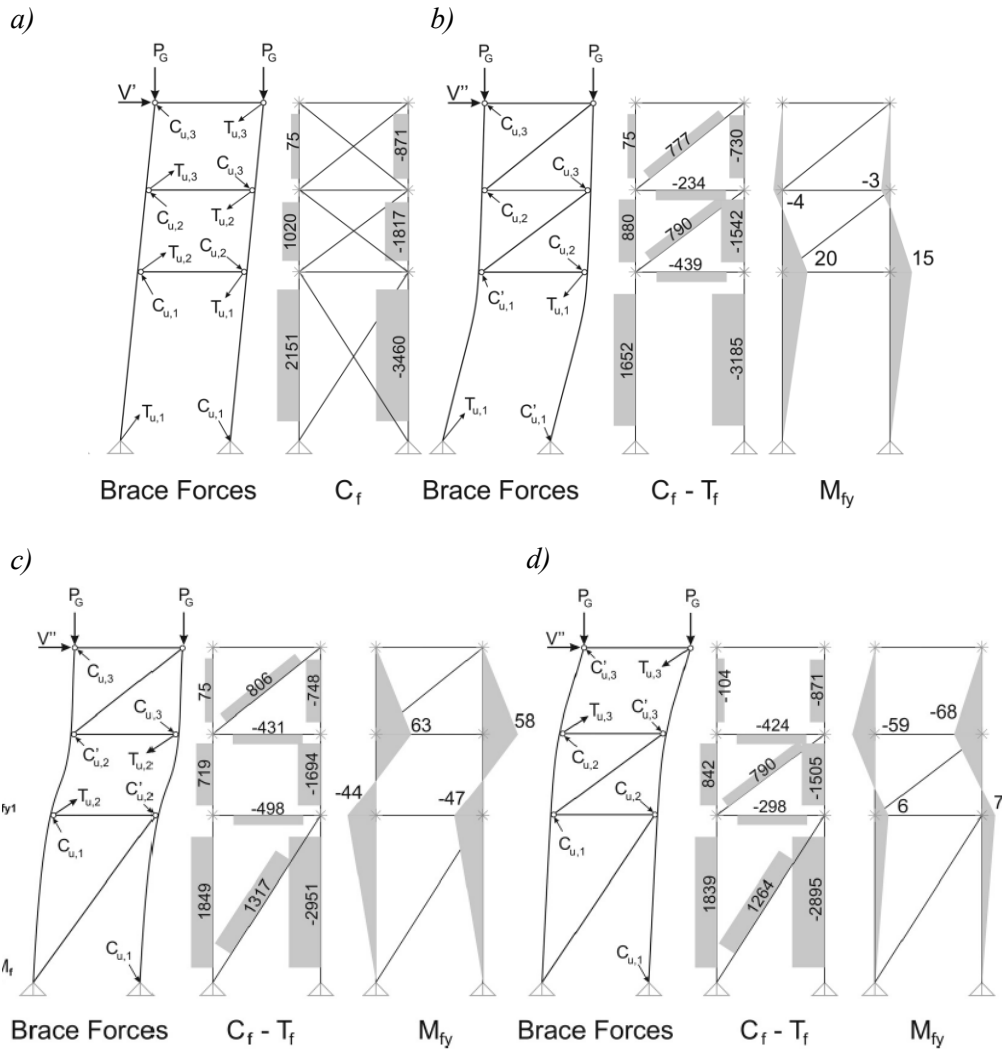
Figure 2.13. Seismic analysis of a non-uniform three-tiered Type MD CBF for axial forces and in-plane bending moments: a) axial column loads under gravity and brace loading condition with all compression braces at buckling; b) axial loads and bending moments in columns from nonlinear static analysis assuming inelastic demand concentrated in Tier 1; c) axial loads and bending moments in columns from nonlinear static analysis assuming inelastic demand concentrated in Tier 2; d) axial loads and bending moments in columns from nonlinear static analysis assuming inelastic demand concentrated in Tier 3.

2.5   Seismic Design of Steel MT-CBFs in Canada

This section presents a review of CSA S16-14 seismic provisions for the design of Type LD and

Type CC CBFs. Note that the 2019 edition of the CSA S16 was published when this document

was in preparation. The key seismic design provisions for these two systems that are used in this research remained unchanged in CSA S16-19.

2.5.1 Design of Type LD Braced Frames

CSA S16-14 requires the capacity design procedure to design all SFRSs with a ductility-related modification factor $R_d > 1.5$, which includes Type LD CBFs. Type CC braced frames need not be designed using this methodology.

The braces in CBFs are designed under design seismic base shear, V, as obtained from the National Building Code of Canada, NBCC (NRC 2015). The design forces in tension, T_i, and in compression, C_i, are shown in Figure 2.14a and Figure 2.14b for two-tiered CBF examples with T/C braces and T/O braces, respectively. For the frame with T/C braces, $C_i = T_i = \frac{V}{2\cos\theta_i}$, where θ_i is shown in Figure 2.14. Similarly, for the T/O braces, the design forces are as $T_i = \frac{V}{\cos\theta_i}$.
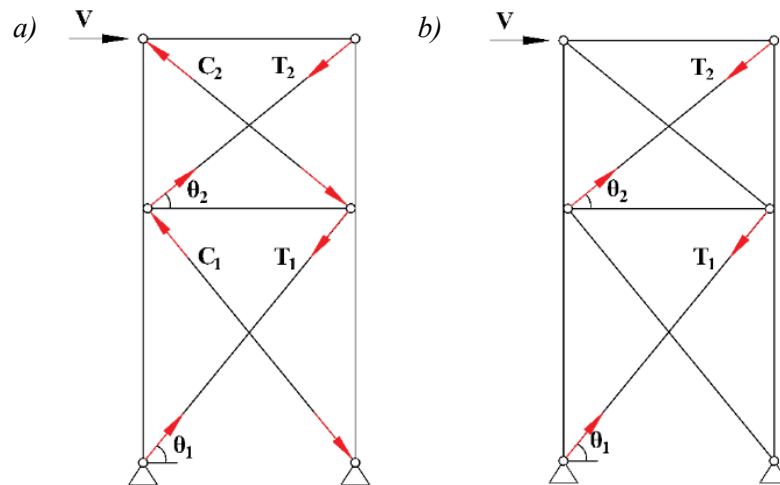
Figure 2.14. CBF brace design forces: a) Tension-Compression braces; b) Tension-Only braces.

The remaining components of the frame are designed under gravity load effects together with loads arising from probable tensile, compressive (at first buckling), and buckled (i.e. compressive

resistance obtained after experiencing several inelastic buckling cycles) resistances of the braces, as shown in Figure 2.15. The probable resistances of braces are defined as follows:

- Probable tensile resistance: $T_u = A_g R_y F_y$, where A_g is the gross cross-sectional area of the brace, F_y is the specified yield stress, and $R_y F_y$ is the probable yield stress of the material.

- Probable compressive resistance: $C_u = \min (A_g R_y F_y, 1.2 C_r /\phi)$, where C_r is the factored compressive resistance of the brace calculated using $R_y F_y$, and $\phi = 0.9$ is the resistance factor.

- Probable buckled resistance: $C'_u = \min (0.2 A_g R_y F_y, C_r /\phi)$.

As shown in Figure 2.15, two brace loading scenarios must be taken into account, and the maximum effects shall be used to design the capacity-protected components:

1) Analysis I: Tension-acting braces yield and reach their T_u in tension while the compression-acting braces reach their C_u.

2) Analysis II: T_u is developed in tensile braces while the compression braces reach their probable buckled resistance (C'_u), representing the force condition of braces after experiencing multiple inelastic cycles in tension and compression.
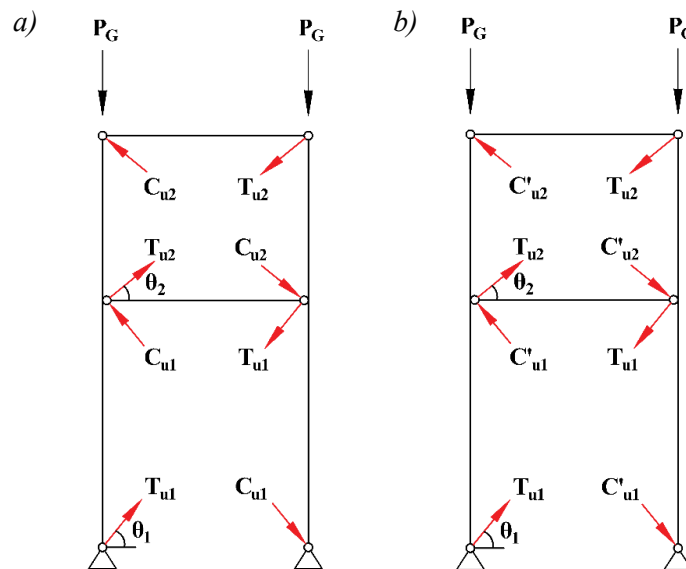
Figure 2.15. Brace loading scenarios for a T/C CBF: a) Analysis I; b) Analysis II.

The storey shear resistance due to any of the two analyses mentioned above shall not exceed the storey shear corresponding to a base shear obtained using $R_oR_d = 1.3$; otherwise, the forces must be redistributed considering C_u in the compression-acting braces, which would result in tension forces in the tensile braces that is less than T_u.

The requirements of CSA S16-14 for the design of Type LD CBFs are as follow:

- Tension-compression braces and tension-only braces are allowed. Other bracing systems are permitted if a stable inelastic response can be confirmed, except for knee bracing and K-bracing, which are not acceptable.

- The slenderness ratio, KL/r, of braces must be limited to 300.

- When $I_EF_aS_a(0.2) > 0.3$, width-to-thickness ratio limit is $330/\sqrt{F_y}$ for HSSs and $145/\sqrt{F_y}$ for legs of angles when $KL/r \leq 100$, and Class 1 requirements for HSS and $170/\sqrt{F_y}$ for legs of angles when $KL/r = 200$. Linear interpolation may be used for $100 < KL/r < 200$.

- In structures with a maximum height of 40 m and $I_EF_aS_a(0.2) < 0.45$, HSS braces need to be at least Class 2, and the width-to-thickness ratio limit is $170/\sqrt{F_y}$ for legs of angles.

- For braces with a slenderness ratio higher than 200, the width-to-thickness ratio limit is waived; otherwise.

- Columns must be continuous, be of a constant cross-section along at least two storeys, and meet Class 1 or 2 limits specified for beam-columns.

- Columns must be designed for interaction of the axial compression and bending moment where the in-plane bending moment is equal to $0.2ZF_y$; Z is the plastic section modulus of the section about the axis of bending.

In addition to the provisions for Type LD CBFs, CSA S16-14 introduces special design requirements for Type LD MT-CBFs. Those requirements are summarized as follows:

1) Braces can meet columns between each pair of adjacent floor levels at up to four points; in other words, up to five tiers are permitted.

2) Columns must be designed for (Figure 2.16):

a) the effects of gravity loads;

b) the induced axial force, shear force, and bending moment demands at the design storey drift conforming the capacity design procedure by performing a set of nonlinear analyses, for each analysis presuming that the braces at only one of the tiers enter the inelastic realm while braces of other tiers respond elastically; and

c) bending moment due to an out-of-plane transverse load equal to 2% of the factored compression load in the column below the strut, applied to the column at every strut level.

3) Horizontal struts must be installed between the columns at each tier level to resist the in-plane unbalanced load due to the unequal forces in tension and compression braces upon buckling of the compression braces.
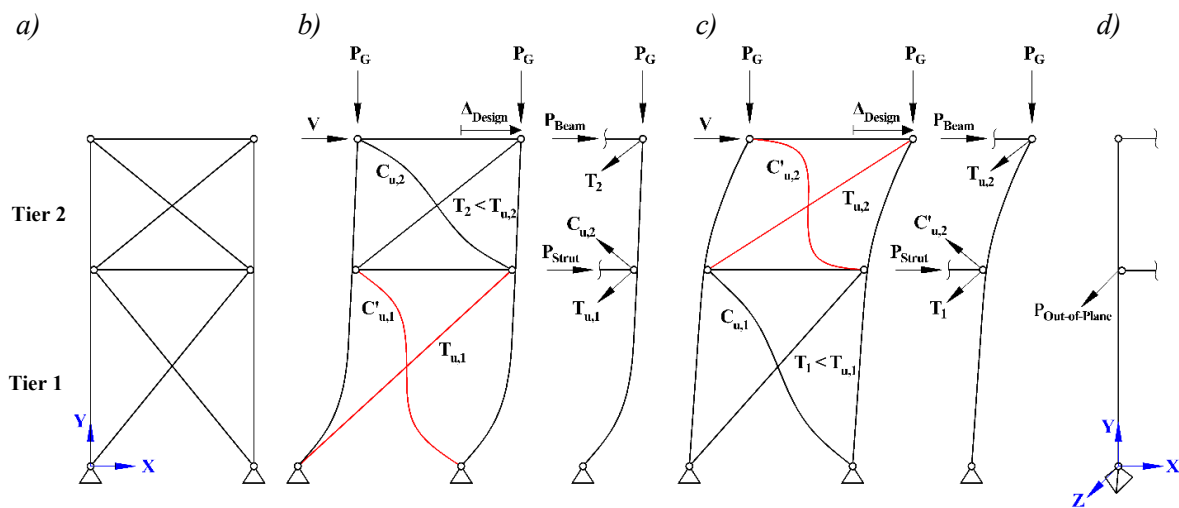
Figure 2.16. Column design forces for a Type LD two-tiered CBF: a) two-tiered CBF; b) in-plane demands for yielding in Tier 1; c) in-plane demands for yielding in Tier 2; d) out-of-plane demands.

2.5.2 Design of Conventional Construction Braced Frames

All members of a Type CC CBF are designed to resist the combined effects of factored gravity load acting together with the factored seismic load. The design forces of braces are similar to Type LD frames (Figure 2.14). Since the capacity design principle is not required for Type CC frames, brace forces are used to determine the design forces of other components of the frame. For structures with the specified short-period spectral acceleration ratio ($I_E F_a S_a(0.2)$) larger than 0.35, frames taller than 15 m must meet the following additional requirements:

- Amplify the factored base shear linearly by 2% per meter of the fraction of the frame height above 15 m when calculating the forces for ultimate limit states. At any event, the amplified effects must be equal or less than the base shear corresponding $R_d R_o = 1.3$.
- Apply another amplification factor equal to 1.3 to the factored seismic forces of the columns.
- Beams, columns, and HSS bracing members are at least Class 2 sections.
- The width-to-thickness ratios of legs of angles of bracing members must be less than $170/\sqrt{F_y}$, if the brace slenderness ratio is equal or less than 200; otherwise, the width-to-thickness ratio limit needs not to be checked.
- In multi-tiered braced frames, out-of-plane transverse loads must be applied to the columns at the intersection of braces and columns. The magnitude of the loads must be equal to 10% of the axial load of the column below the intersection.

2.5.3 Design of Double-Angle Members

The slenderness ratio of built-up double-angles is equal to the maximum of:

a) double-angle slenderness ratio with respect to the X-axis, and

b) an equivalent slenderness ratio, ρ_e, calculated using Equation (2.1 where ρ_{0y} is the slenderness ratio of the double-angle as a whole about Y-axis and ρ_i is the maximum slenderness ratio of individual angles between the stitch-connecters. Figure 2.17 shows the axes of a built-up double-angle section.

$$\rho_e = \sqrt{\rho_{0y}{}^2 + \rho_i{}^2}$$ (2.1)

A minimum number of stitch-connectors must be selected to connect the angles so that the maximum slenderness ratio of the individual angles is equal or less than the maximum slenderness ratio of the double-angle. The maximum slenderness ratio of a single-angle must be calculated based on the distance between the stitches, angle's minimum radius of gyration using an effective length factor $K = 0.65$ (Figure 2.17).
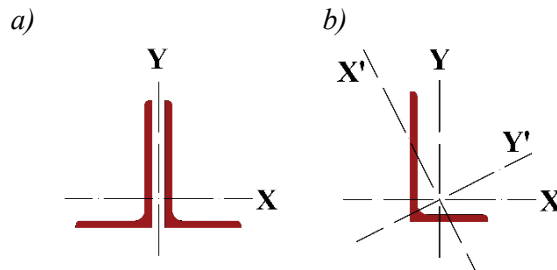
Figure 2.17. a) Principal axes of a built-up double-angle section, and b) principal (X' & Y') and standard (X & Y) axes of a single-angle section.

2.6 Fibre-based numerical simulation of steel braced frames

2.6.1 *OpenSees* Software Framework

Open System for Earthquake Engineering Simulation (*OpenSees*) is a software platform for research and application of simulation for structural and geotechnical systems developed by the Pacific Earthquake Engineering Research Center (PEER) (McKenna et al. 1997). *OpenSees* is capable of creating three-dimensional (3D) models of structures with various geometries, members

and cross-sections. *OpenSees* provides an extensive library of different material models and element types for various structural and geotechnical applications. Numerous analysis algorithms and solution methods have been implemented in *OpenSees,* making this software framework capable of performing nonlinear static and dynamic analyses in structural and earthquake engineering applications.

2.6.2   Fibre-based elements

Although the finite element simulation method is an appropriate tool to investigate the local response of various structures, it becomes computationally expensive when a two- or three-dimensional frame is to be analyzed, particularly when nonlinear response history analysis under a time-varying ground motion history is conducted.

OpenSees offers a nonlinear modelling technique using fibre-based elements with the fibre-discretization of the cross-section. An example of discretization of an HSS cross-section in *OpenSees* is shown in Figure 2.18. Fibre-based elements are capable of integrating the inelastic material response over the cross-section and at respective integration points along each element to calculate the internal forces and deformations of the member. The fibre-based technique is, therefore, an efficient modelling approach while maintaining the necessary accuracy required for the simulation of nonlinear response. Fibre-based elements can also account for residual stresses expected in steel shapes.
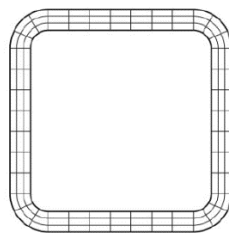
Figure 2.18. Fibre discretization of a steel HSS section.

2.6.3 Simulation of steel cyclic response

OpenSees has been used in the past to simulate the cyclic inelastic response of steel members. Several past studies confirmed this capability of *OpenSees* and validated the simulated response against experimental test data (Uriz and Mahin 2004, Aguero et al. 2006, Lamarche and Tremblay 2011, Hsiao et al. 2013, Jiang 2013, Karamanci and Lignos 2014, Imanpour and Tremblay 2016c, Agarwal and Fahnestock 2018, Balazadeh-Minouei et al. 2018).

The cyclic inelastic response of steel HSS members was validated in past studies (Aguero et al. 2006, Uriz et al. 2008, Lamarche and Tremblay 2011). Two examples of such validation are shown in Figure 2.19.
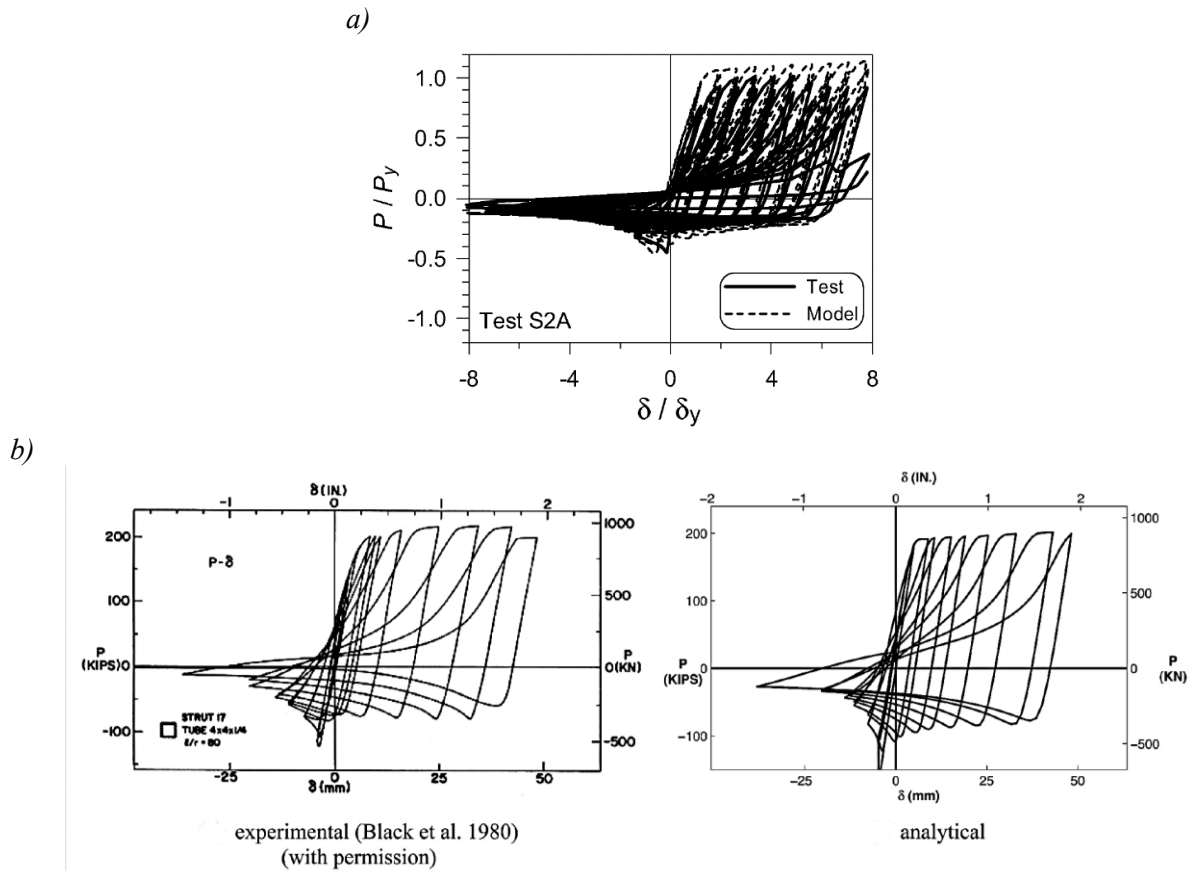
*Figure 2.19. Hysteretic response validation of HSS braces by
a) Aguero et al. (2006), and b) Uriz et al. (2008).*

Uriz and Mahin (2004) developed an analytical method to be used along with the fibre-discretization method implemented in *Opensees* to simulate the low-cycle fatigue fracture along with the inelastic hysteretic response of steel HSS brace. Their simulation was also capable of modelling axial and flexural behaviour and accounting for large deformations.

Aguero et al. (2006) studied the capability of the *OpenSees* software framework in simulating the seismic hysteretic behaviour of steel rectangular and square HSS braces. They conducted sensitivity analyses on various modelling parameters such as the number of fibres, number of integration points, number of elements, and material models. Physical test was used to evaluate the key parameters assumed in numerical simulations. The authors concluded that the quantity of integration points has no substantial influence on brace behaviour. For steel HSS braces, three integration points, eight elements with 16 fibres for the cross-section were suggested in this study.

D'Aniello et al. (2013) conducted sensitivity analyses on braces made of wide-flange sections, square and round HSSs to examine the influence of the number of integration points (IP) on the brace cyclic response. It was recommended using at least four integration points along each element (Figure 2.20).
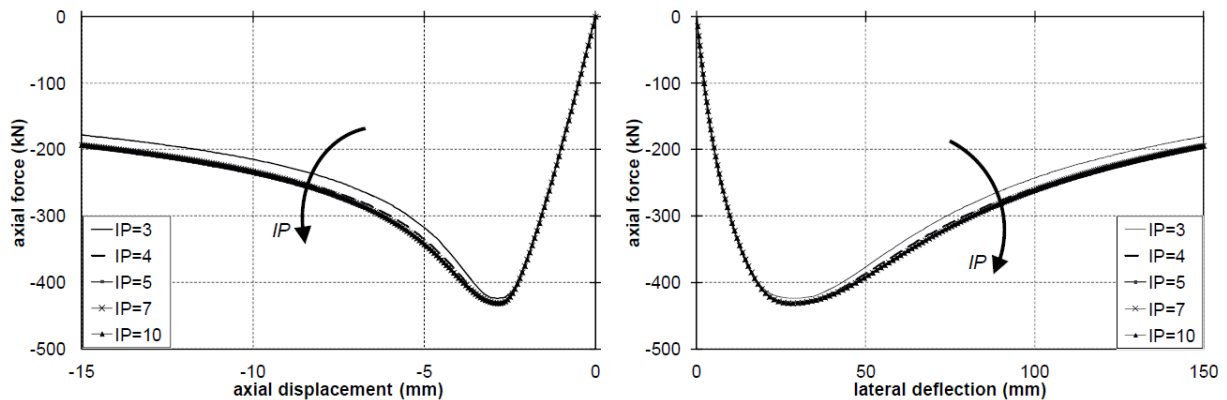
Figure 2.20. Effect of the number of integration points (IP) on the response of steel wide-flange member: a) axial force-axial displacement; b) axial force-lateral deflection.

By performing a sensitivity analysis on a tension-only double-angle brace, Jiang (2013) showed that with two to five integration points, reasonable estimations could be obtained for the buckling load, energy dissipation, and lateral displacements of the bracing member (Figure 2.21). A similar sensitivity analysis was performed on the number of elements of the same double-angle. The result showed that a minimum number of eight elements along the brace length is enough to predict brace buckling. However, employing 16 elements can enhance the prediction of buckling load (Figure 2.22).

a)

b)

c)
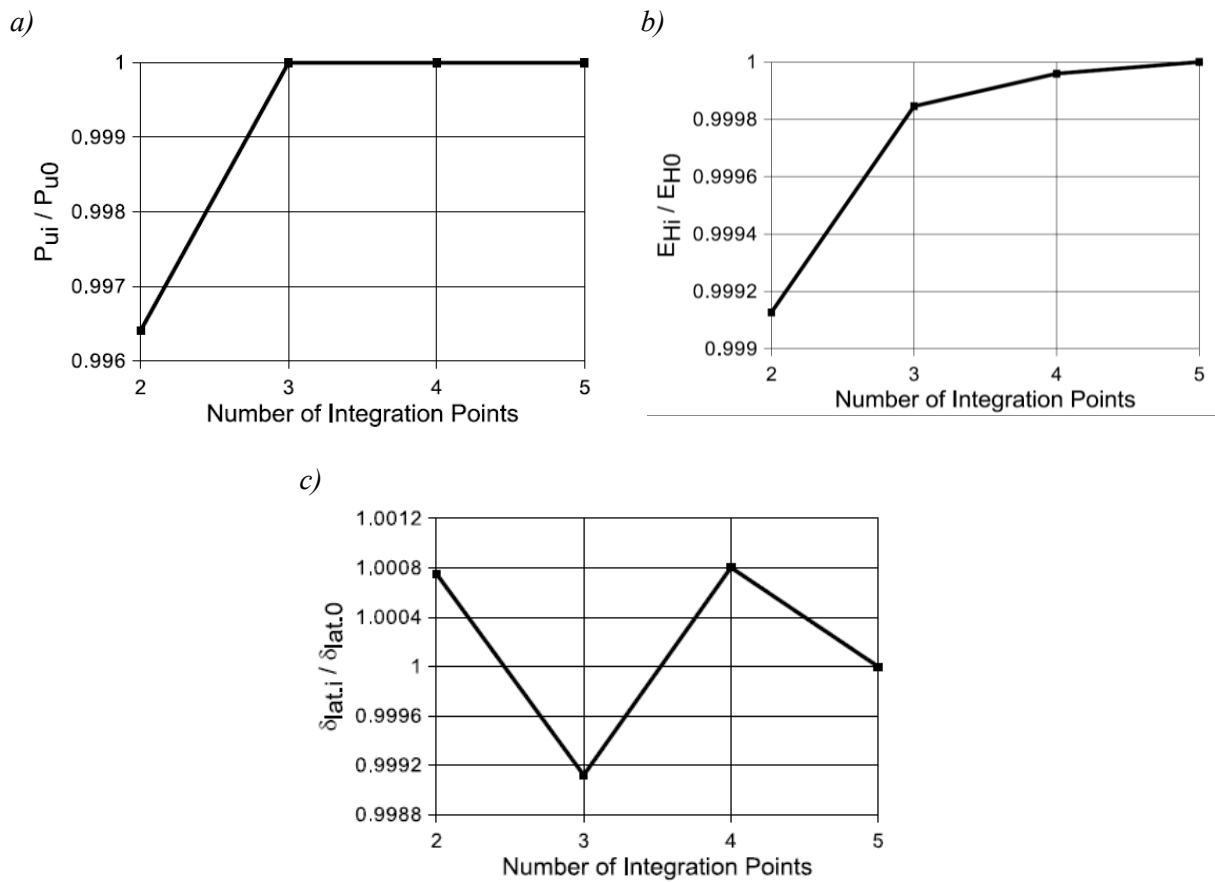
Figure 2.21. Effects of the number of integration points on tension-only double-angle brace a) buckling load, b) energy dissipation capacity, and c) mid-length lateral displacement (Jiang 2013).

a)

b)

c)
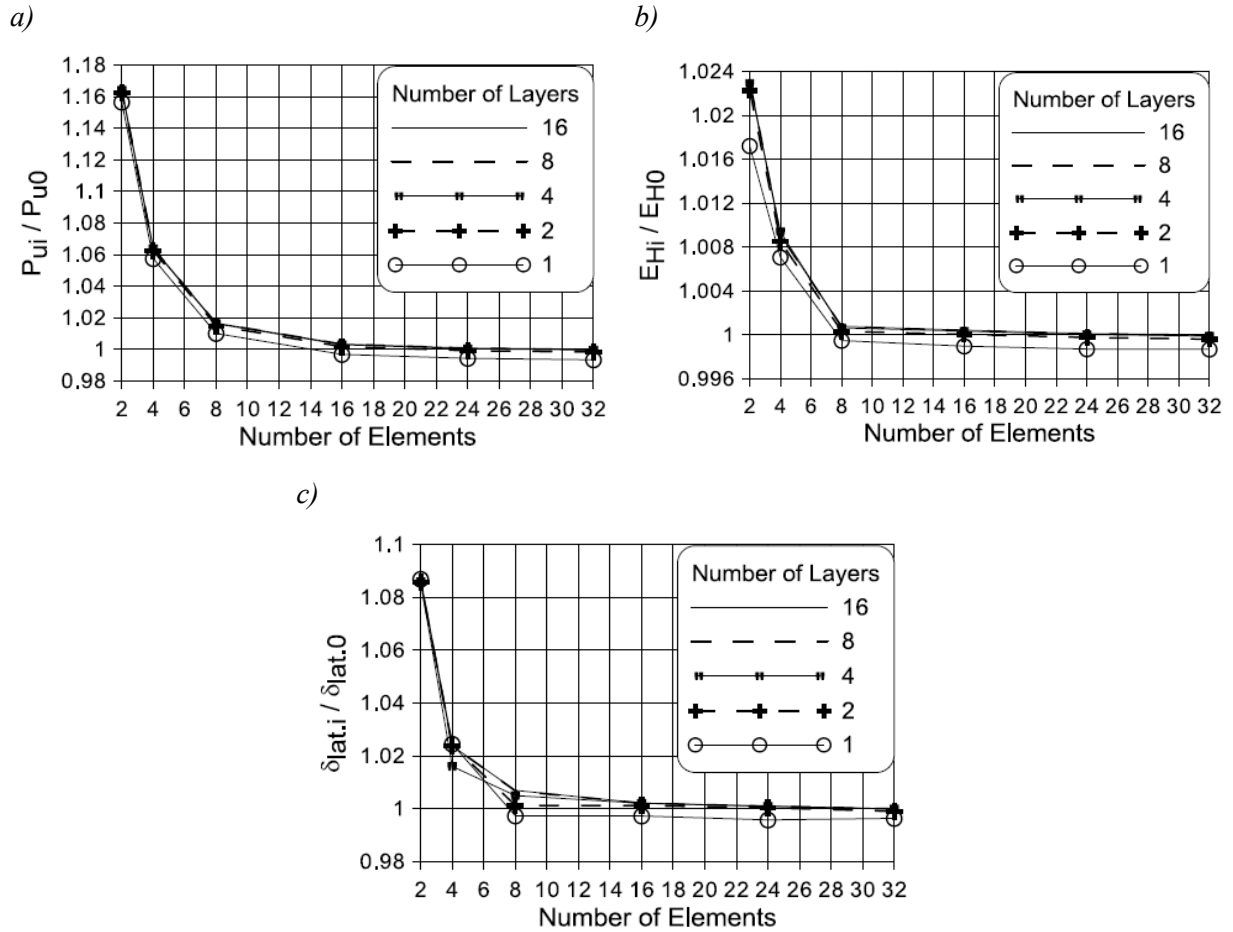
Figure 2.22. Effects of the number of elements on tension-only double-angle brace a) buckling load, b) energy dissipation capacity, and c) mid-length lateral displacement (Jiang 2013).

2.6.4   Material Modelling

Aguero et al. (2006) reported that the uniaxial *Giuffré-Menegotto-Pinto (Steel02)* material model is suitable for modelling the hysteretic behaviour of steel HSS braces. The *Steel02* material model accounts for isotropic and kinematic strain hardening and the Baushinger effects of the steel material. This material model is also capable of the inclusion of residual stresses in the cross-section. An example of fibre discretization of a wide-flange section accounting for residual stresses is shown in Figure 2.23.
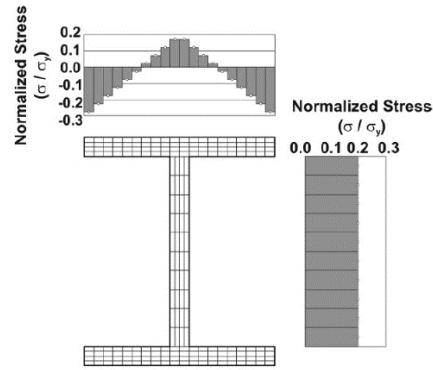
Figure 2.23. Fibre-discretization of a wide-flange section with residual stresses
(Imanpour and Tremblay 2016c).

The parameters required to define *Steel02* in *OpenSees* are:

- Yield stress, F_y

- Young's modulus, E

- Strain-hardening ratio, b, to reproduce kinematic hardening of the steel material

- Parameters to model the transition from elastic to inelastic zones of the steel material stress-strain curve, R_0, cR_1, and cR_2

- Isotropic hardening parameters, a_1, a_2, a_3, and a_4

The fibre-discretization method is not capable of modelling local buckling, which is likely in steel compression members, especially under reversed cyclic loading. Nonetheless, the inclusion of a smooth transition from elastic to inelastic branches (R_0, cR_1, and cR_2), fictitiously alleviates the minor effect of local buckling on the overall cyclic behaviour of steel braces made of compact sections, which is confirmed in past experimental studies (Uriz et al. 2008).

2.6.5   Connection Modelling

A realistic simulation of connections is essential to examine the buckling and post-buckling behaviour of a brace. By employing rotational springs (*Zerolength* elements) at the end of a bracing

member, Aguero et al. (2006) showed a good correlation between the brace hysteresis response obtained from the numerical prediction and that obtained from physical testing. Figure 2.24 shows the proposed model with *Zerolength* elements simulating the end-connections of a brace.
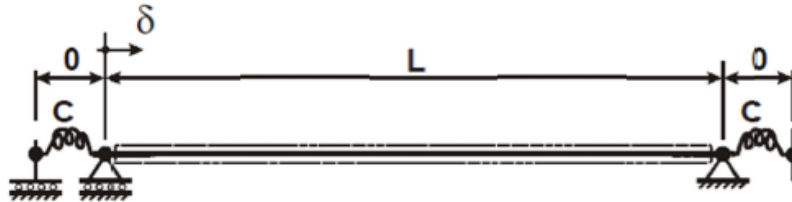
Figure 2.24. Numerical model of an isolated brace with end-connections simulated using rotational springs (Aguero et al. 2006).

Hsiao et al. (2013) proposed a more sophisticated connection modelling technique for the brace-to-beam-to-column connection. In this approach, rotational springs simulated with *Zerolength* elements in *Opensees* are used to reproduce the flexural stiffness and strength of the gusset plate and a set of relatively stiff elastic elements simulated using *ElasticBeamColumn* elements are used to model the connection regions that are expected to remain essentially elastic (Figure 2.25).
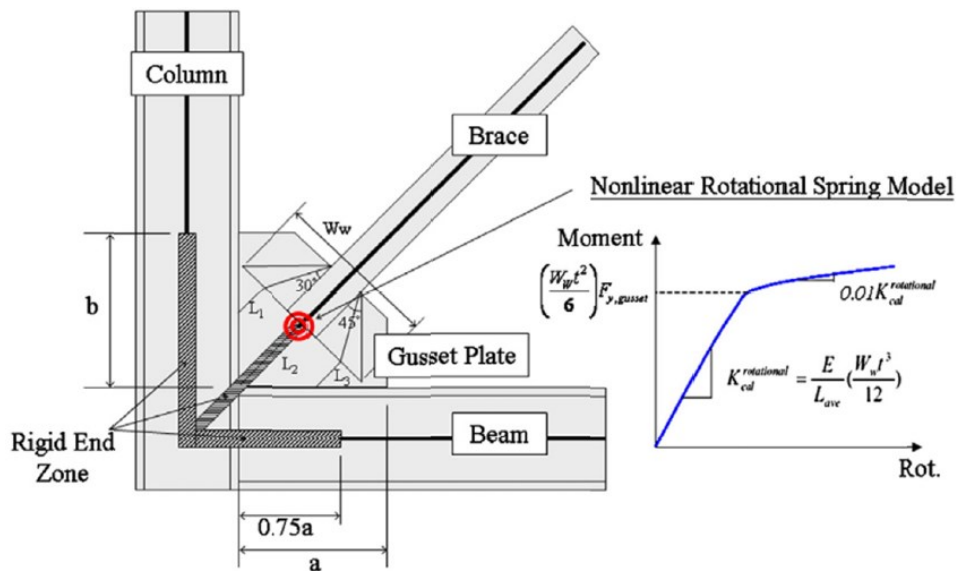
Figure 2.25. Proposed modelling technique for the brace connection using rotational springs and relatively stiff elements (Hsiao et al. 2013).

Chapter 3: Design of Prototype Braced Frames

3.1   Introduction

In this chapter, the geometry and location of the building selected for this study are first introduced, followed by the parametric study matrix, including designated frame configurations. The loading information is then described. Finally, the design assumptions for the selected braced frames with the respective member sizes are given.

3.2   Building Selected

The building selected in this study is a single-storey industrial building with plan dimensions of 42 m × 252 m. The building dimensions were selected to represent an industrial building in the selected location while seismic base shear exceeds the one calcualted under the wind load. Three heights are chosen for the building: 10 m, 16 m, and 24 m (See Section 3.3).

The building is located in Montreal, QC, which is a moderate seismic hazard region in Canada. The building is located on soil class C (very dense soil with shear wave velocity between 360 m/s and 760 m/s). The columns placed in the exterior walls support 42 m long roof trusses that span over the full width of the building. The column spacing is 6 m. Eight steel X-bracing MT-CBFs are placed in the long direction of the building (four braced frames per wall) because of available bays in that direction, whereas, four steel X-bracing MT-CBFs are used in the short direction (two braced frames per wall) to accommodate openings.

3.3 Parametric Study Matrix

One of the MT-CBFs located in the longitudinal direction of the building (**Error! Reference source not found.**) is chosen for the parametric study. To develop a database of the MT-CBF response, a wide-range of braced frames is covered by varying six parameters between the frames as listed below:

- Frame ductility: Limited Ductility (Type LD) and Conventional Construction (Type CC)

- Column section: Wide-flange (W-shape) and Square Hollow Structural Shape (HSS)

- Brace section and bracing system: Square HSS Tension-Compression (T/C), double-angle Tension-Only (T/O), and single-angle T/O

- Frame total height: 10 m, 16 m, and 24 m

- Number of tiers: 2, 3, 4, and 6

- First-tier to second-tier height ratio (h_1 / h_2): 1.0 and 1.75

Figure 3.1 summarizes the parametric study matrix and shows how they are combined to generate various frame configurations that are commonly used in practice (St-Onge 2019). In the figure, W, L, and 2L represent wide-flange, single-angle, and double-angle sections, respectively. The combinations of the parameters shown in Figure 3.1 results in 64 MT-CBFs. The roof beam and struts of all the frames are made of W-shape sections and square HSSs, respectively. The frame span is kept unchanged for the selected frames.
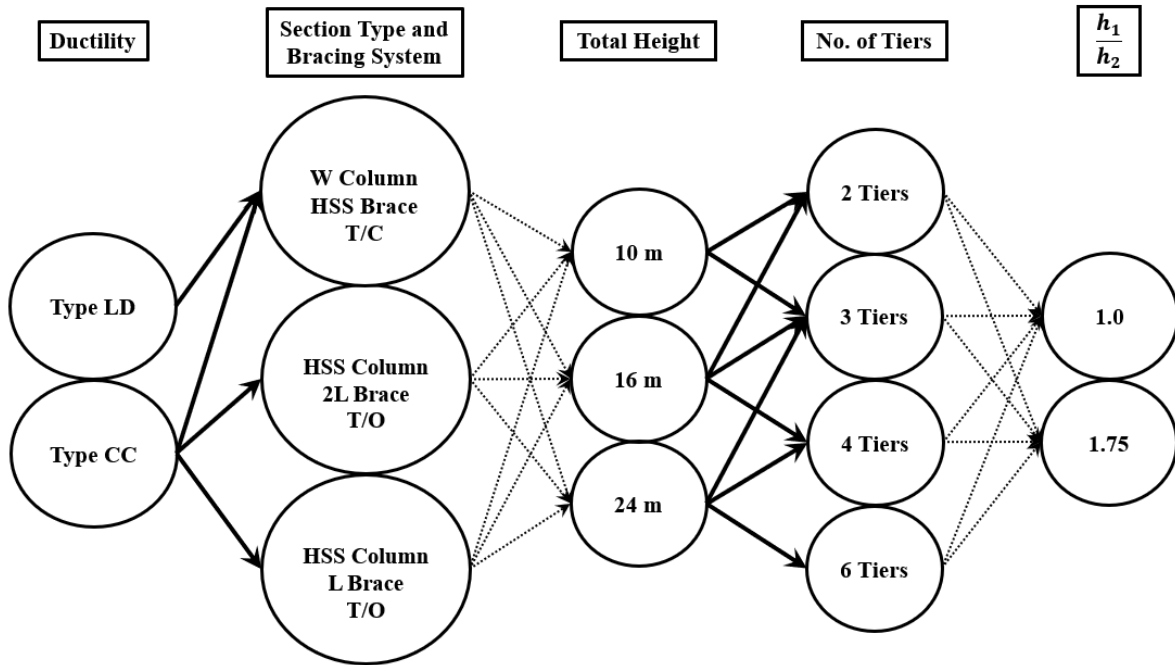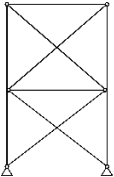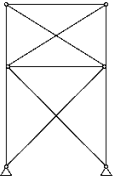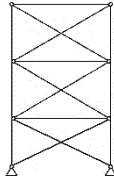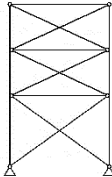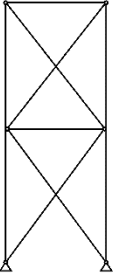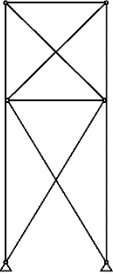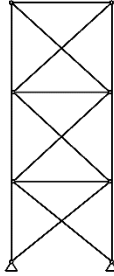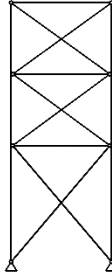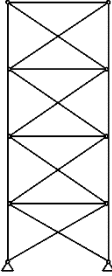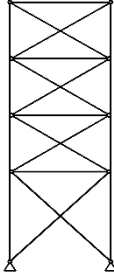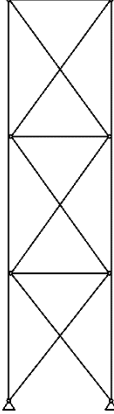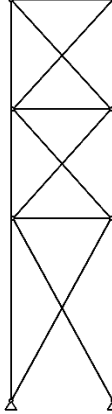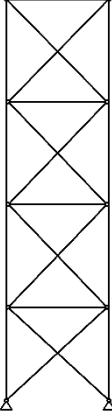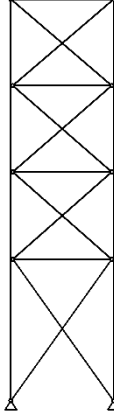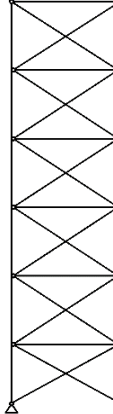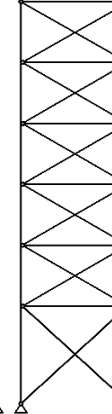
Figure 3.1. Parametric study matrix.

The schematic elevation of the selected frames is given in Table 3.1, where h represents the total height of the structure, h_1 is the first-tier height, and h_2 shows the height of the other tiers, as shown in Figure 3.2.

Table 3.1. Configuration of the selected frames for the parametric study.

	2-Tiered CBF		3-Tiered CBF		4-Tiered CBF		6-Tiered CBF	
$h_1/h_2 =$	1.0	1.75	1.0	1.75	1.0	1.75	1.0	1.75
h = 10 m					-		-	
h = 16 m							-	
h = 24 m	-							

$h_i = h_2$ i = 3 - 6

Figure 3.2. Typical braced frame elevation.

3.4 Gravity and Seismic Loading

The loads are calculated as per the 2015 edition of the National Building Code of Canada, NBCC (NRC 2015). The unfactored gravity loads on the roof are as follows:

- The dead load, D, is equal to 1.0 kPa, including the self-weight of structural components.

- The unit weight of the exterior walls is equal to 0.5 kPa.

- The live load, L, is equal to 1.0 kPa.

- The snow load, S, is 2.48 kPa.

To evalaute the selected frames under seismic and gravity loads, the 2015 NBCC seismic load combination, $1.0D + 1.0E + 0.5L + 0.25S$, is considered. The factored gravity load (i.e. $1.0\ D + 0.5L + 0.25S$) imposed on each column located on the long direction of the building is obtained as $P_G = 208.1$ kN.

As prescribed by 2015 NBCC, the Equivalent Static Force Procedure (ESFP) can be used for this building to calculate the design seismic base shear. The importance factor, I_E, for the selected building is taken as 1.0, as a building in the normal importance category. The higher mode factor, M_v, is equal to 1.0. The ductility-related force modification factor, R_d, and the overstrength-related force modification factor, R_o, for Type LD braced frames are equal to 2.0 and 1.3, respectively. R_d and R_o values are, respectively, equal to 1.5, and 1.3 for Type CC braced frames. As per 2015 NBCC, the fundamental period, T, of the building is taken equal to the minimum of the T obtained from a modal analysis and two times the one calculated using the empirical equation specified in this standard for braced frame structures that is $2 \times 0.025h$, where h is the total height of the building, as shown in Figure 3.2. The design response spectral acceleration, $S(T)$, is obtained using

the NBCC seismic hazard data for 2% probability of exceedance in 50 years on soil class C in Montreal (Figure 3.3).
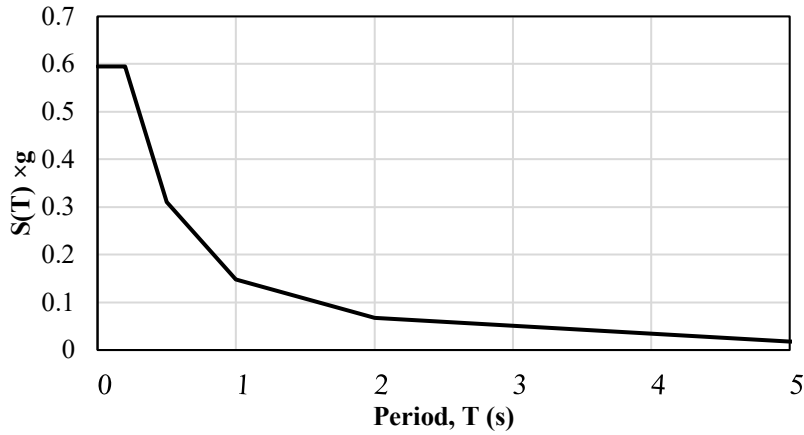
Figure 3.3. Design spectral response acceleration for site class C in Montreal, QC.

The total seismic weight is calculated by adding 25% of the roof snow load to 100% of the roof dead load plus half of the weight of the wall cladding. The total seismic base shear per braced frame, $V_{E/Frame}$, including the effects of accidental torsion, P-Δ, and notional loads, is then calculated. The summary of the seismic load calculation is given in Table 3.2. Note that the loads in the table are provided only for the long direction of the building, since one of the MT-CBFs located in the that direction is selected in this study.

Table 3.2. Summary of the seismic load calculation.

Frame Type	Frame Height	Design Spectral Response Acceleration	Seismic Weight	Factored Seismic Base Shear		Factored Wind Base Shear
	h	S(T)	W	$1.0×V_{E/Frame}$		$1.4×V_{W/Frame}$
	m	×g	kN	kN		kN
Type LD	10	0.31	18498	351	>	38.9
	16	0.21	19830	255	>	67.8
	24	0.13	21006	171	>	114.9
Type CC	10	0.31	18498	464	>	38.9
	16	0.21	19830	336	>	67.8
	24	0.13	21006	224	>	114.9

3.5 Wind Load

The lateral wind load is calculated using Clause 4.1.7.3 of 2015 NBCC (NRC 2015) with the following assumptions:

- Reference velocity pressure, $q = 0.42$ kPa for Montreal City Hall

- Importance factor: $I_w = 1.0$

- Exposure factor, $C_e = 0.7(h/12)^{0.2} \geq 0.7$, where h is the total height of the building

- Topographic factor, $C_t = 1.0$

- Gust effect factor, $C_g = 2.0$

- External pressure coefficient, $C_p = 0.6$ for windward side and, $C_p = -0.3$, for leeward side

The specified wind pressure plus suction, p, on the building, is, therefore, equal to 0.65 kPa.

The governing load combination for the calculation of wind load on the selected building is found to be 1.25D+1.4W+0.5S when considering all of the load combinations in Table 4.1.3.2.-A of 2015 NBCC. Table 3.2 gives the factored base shear per braced frame due to lateral wind, $1.4 \times V_{W/Frame}$. As shown, for all of the selected frame configurations, the seismic base shear, $1.0 \times V_{E/Frame}$, is larger than the wind base shear, and therefore, the seismic load governs the design of the structural members of the selected braced frames.

In addition to the wind base shear computed for the selected braced frames, the calculated wind pressure is used to check each braced frame column individually, as they carry the out-of-plane bending moment due to wind in the presence of the factored gravity load. All the assumptions of the wind load calculation for the columns are the same as those for the building as a whole, except C_p, which is equal to -0.7 for the wind pressure induced in the individual structural components (i.e. columns). The specified wind pressure on the exterior columns is, therefore, equal to 0.51

kPa, which results in a distributed load, q_w, over the column height equal to 3.04 kN/m for the 6 m tributary width of the column.

3.6   Seismic Design of Type LD Braced Frames

This section presents the seismic design of the Type LD braced frames in accordance with CSA S16-14. These braced frames comprise square HSS T/C braces and W-shaped columns. As described in Section 2.5.1, Clause 27.6.6 of CSA S16-14 prescribes special requirements for the seismic design of Type LD MT-CBFs. In this study, the requirements for columns, as well as the limit on the number of tiers, are excluded from the design to examine their effects on the seismic response and design demands of such frames. Note that the additional bending moment demand equal to 20% of the plastic moment of the column section in the direction of the braced bay prescribed by CSA S16 for steel braced frame columns is not required for the columns of MT-CBFs.

HSS bracing members, which are connected using bolted connections to each other and the columns, are made of ASTM A500 Grade C steel (ASTM 2015a) with a yield stress, F_y, of 345 MPa. To design the braces under the axial compression load, the effective length factor, K, is taken as 0.45 to account for the size and fixity of the brace end connections and the mid-support provided by the intersecting tension-acting braces. The selected braces must satisfy the requirements of CSA S16-14 regarding the brace global slenderness ratio, KL/r, limit and width-to-thickness ratio limits, as described in Section 2.5.1. The global slenderness ratio of bracing members must be limited to 200. For HSS braces having a global slenderness ratio smaller than 100, the width-to-thickness ratio limit is $330/\sqrt{F_y}$, while a value of $420/\sqrt{F_y}$ must be used when $KL/r \geq 100$. For the slenderness values between 100 and 200, linear interpolation must be used. The final selected

brace sizes for Type LD prototype frames are shown in Table 3.3. The frame designation format used in this table and the rest of the thesis has been chosen to reflect all the parameters varying between the select frames. For instance, "LD_W_HSS_10_2_1.0" indicates that the frame ductility level is "LD", column section is "W-shaped", braces are "HSS", total frame height is "10" m, the number of tiers is "2", and the height ratio h_1 / h_2 is "1.0". As shown in Figure 3.2, except for the first tier, the geometry of the tiers is always the same for the select frames, and as a result, they are assigned the same brace sizes. Thus, for the frames having unequal tier heights (i.e. $h_1 / h_2 \neq 1.0$), the first row in Table 3.3 provides the summary of design for the first-tier braces and the second row for all other tiers of the frame. For frames with identical tier heights (i.e. $h_1 / h_2 = 1.0$) where the braces of all of the tiers are similar, there is only one row giving the design summary for the braces of all tiers. In the table, L_{Brace} indicates brace lengths, KL/r, is the maximum value of the brace in-plane and out-of-plane slenderness ratios, and b_{el}/t, is the width-to-thickness ratio of the brace section. C_f and C_r are the factored compression demand and the factored compression resistance of the brace, respectively. T_u, C_u, C'_u, are, respectively, the probable tensile, compressive, and buckled resistances of the brace. The probable brace resistance of HSS braces, used to calculate the design forces of the capacity-protected members, namely columns, beams, and struts, are computed using probable yield stress, R_yF_y, equal to 460 MPa. V_u is the storey shear capacity of each tier arising from probable resistances of braces determined as $(T_u + C_u) \cos\theta$, where θ is the angle between the brace and the horizontal plane. As required by the code, V_u at each tier must be limited to the base shear calculated using $R_dR_o = 1.3$ ($V_{1.3}$ in the table); otherwise, the demand of the tension-acting brace must be reduced to mimic the storey shear resistance corresponding to $V_{1.3}$, while keeping C_u in the compression-acting braces. As shown in the table, for all of the selected frames $V_u > V_{1.3}$.

For the columns, wide-flange sections conforming to ASTM A992 (ASTM 2015b) with $F_y = 345$ MPa are chosen to satisfy the strength and stability limit states as given in Clause 13.3 of CSA S16-14. The columns are continuous and are oriented such that the out-of-plane wind load imposes a strong-axis bending moment. To calculate the column resistance in the plane of the frame, the unsupported length is taken equal to the tier height. In contrast, an unsupported length equal to the full height of the frame is used to calculate the out-of-plane buckling resistance. This assumption agrees with the current design practice for MT-CBFs. However, the effective length of columns could have been reduced to account for distributed loading over the column height (Dalal 1969). In this case, an elastic Eigen buckling analysis or available design charts (e.g. Dalal 1969) for stepped columns can be used to achieve a more accurate effective length for the columns. Columns of Type LD braced frames must satisfy Class 1 or 2 beam-columns width-to-thickness ratio limits specified in CSA S16-14.

The column sections are determined under gravity plus seismic loads (i.e. 1.0D + 1.0E + 0.25S); then the capacity of the selected section is verified under gravity plus wind loads (i.e. 1.25D + 1.4W + 0.5S), where gravity loads induce an axial compression force, and the lateral wind load imposes a strong-axis bending moment on the member. Table 3.4 gives the final column sections and a summary of the design calculations. In the table, b_f, t_f, h_w, and t_w, are flange width, flange thickness, web clear depth, and web thickness of the W-shape section, respectively. M_{fx} is the column bending moment demand about its strong axis, and M_{rx} is the respective factored bending moment resistance of the selected section. The indices E and W indicate that the design values are obtained under Earthquake load and Wind load, respectively.

Roof beams are designed using wide-flange sections of ASTM A992, and as beam-column members under an axial compression force due to brace probable resistances and a strong-axis bending

moment as a result of the roof gravity load. Table 3.5 summarizes the selected sections and calculation details for the beams of Type LD braced frames. All of the beams comply with the width-to-thickness ratio limit prescribed for Class 2 section. In the table, the index B stands for Beam. Table 3.5 also gives the member sizes and design calculations for struts, which are shown with index S. The struts made from HSSs conforming to ASTM A500 are designed as a compression member resisting the unbalanced axial force arising from the difference between the brace probable tensile resistance and buckled resistance in adjacent tiers plus a nodal bracing force required to brace the column against in-plane instability because intermediate struts act as lateral braces for the columns in the plane of the frame. The bracing force is calculated using Clause 9.2.6.2 of CSA S16. As compression members, struts must conform to the width-to-thickness ratio limits prescribed for Class 2 as per CSA S16-14.

Once the member sizes are determined, the lateral displacement of each frame, including inelastic effects, $R_d R_o \delta_e / I_E$, is verified against the limit prescribed by 2015 NBCC, 2.5% h, where h is the frame height. δ_e is the elastic roof displacement under the design seismic base shear. The values of design storey drift, defined as the ratio between $R_d R_o \delta_e / I_E$ and the storey height, are given in Table 3.6 for Type LD frames. The tier drift check as recommended by the commentary to CSA S16 (i.e. 2.0% h_i) is not verified for Type LD frames to evaluate the need for such limit. The table also shows the design storey drift under the unfactored wind base shear. This drift is checked against the 2015 NBCC limit for serviceability, 0.2% h, with a wind importance factor $I_w = 0.75$.

The fundamental period used in the design, T_{Design}, must not be taken greater than two times the empirical period calculated using $0.025h$ and the period computed using structural analysis methods, $T_{Analytical}$. As shown in Table 3.6, the product of 2.0 and empirical period is always lower than $T_{Analytical}$. Thus, the period obtained using $2.0 \times 0.025h$ used to design frames remains valid.

Table 3.6 also presents the weakest or critical tier of each frame that possesses the lowest storey shear capacity, V_u, among the tiers. It is expected that brace tensile yielding takes place first in the critical tier (Imanpour and Tremblay 2016c). In the numerical model, slightly lower yield stress equal to $0.9F_y$ is assigned to the braces of the critical tier to account for the various variabilities in design and construction, including variabilities in the material yield stress (Schmidt and Bartlett 2002), cross-sectional area, member length, connection effects, initial geometric imperfections (ASTM 2015c). For the frames with identical tier geometry, the $0.9F_y$ is assigned to the first tier; thus, the first tier is designated as the critical tier in the table for those frames.

Table 3.3. Summary of design for braces of Type LD frames.

Frame Designation	Tier	L_{Brace} m	Section (HSS)	$\frac{KL}{r}$	b_{el}/t Design	b_{el}/t Limit	C_f kN	C_r kN	$\frac{C_f}{C_r}$	T_u kN	C_u kN	C'_u kN	V_u kN		$V_{1.3}$ kN
LD_W_HSS_10_2_1.0	All Tiers	7.8	88.9×88.9×6.4	105	12.0	18.0	228	234	1.0	865	336	169	922	>	691
LD_W_HSS_10_2_1.75	First Tier	8.7	101.6×101.6×6.4	102	14.2	17.9	256	281	0.9	998	405	195	963	>	691
	Other Tiers	7.0	88.9×88.9×4.8	92	17.1	17.8	205	215	1.0	667	315	131	840	>	691
LD_W_HSS_10_3_1.0	All Tiers	6.9	88.9×88.9×4.8	90	17.1	17.8	201	221	0.9	667	325	131	867	>	691
LD_W_HSS_10_3_1.75	First Tier	7.6	88.9×88.9×6.4	102	12.0	17.9	222	243	0.9	865	350	169	959	>	691
	Other Tiers	6.6	88.9×88.9×4.8	86	17.1	17.8	192	233	0.8	667	345	131	925	>	691
LD_W_HSS_16_2_1.0	All Tiers	10.0	101.6×101.6×6.4	117	14.2	18.6	212	231	0.9	998	327	195	795	>	499
LD_W_HSS_16_2_1.75	First Tier	11.8	114.3×114.3×6.4	121	16.3	18.8	251	249	1.0	1141	351	223	757	>	499
	Other Tiers	8.4	88.9×88.9×6.4	112	12.0	18.4	177	212	0.8	865	302	169	837	>	499
LD_W_HSS_16_3_1.0	All Tiers	8.0	88.9×88.9×4.8	105	17.1	18.0	171	180	1.0	667	258	131	691	>	499
LD_W_HSS_16_3_1.75	First Tier	9.6	101.6×101.6×6.4	112	14.2	18.3	203	247	0.8	998	351	195	845	>	499
	Other Tiers	7.4	88.9×88.9×4.8	97	17.1	17.8	156	202	0.8	667	294	131	783	>	499
LD_W_HSS_16_4_1.0	All Tiers	7.2	88.9×88.9×4.8	95	17.1	17.8	153	208	0.7	667	303	131	807	>	499
LD_W_HSS_16_4_1.75	First Tier	8.4	88.9×88.9×6.4	113	12.0	18.4	179	210	0.9	865	299	169	830	>	499
	Other Tiers	6.9	76.2×76.2×4.8	107	14.2	18.1	146	148	1.0	561	212	110	674	>	499
LD_W_HSS_24_3_1.0	All Tiers	10.0	88.9×88.9×6.4	134	12.0	19.4	142	160	0.9	865	223	169	653	>	331
LD_W_HSS_24_3_1.75	First Tier	12.7	114.3×114.3×6.4	130	16.3	19.2	181	222	0.8	1141	310	223	685	>	331
	Other Tiers	8.8	88.9×88.9×4.8	115	17.1	18.5	125	158	0.8	667	223	131	609	>	331
LD_W_HSS_24_4_1.0	All Tiers	8.5	88.9×88.9×4.8	111	17.1	18.3	121	166	0.7	667	236	131	638	>	331
LD_W_HSS_24_4_1.75	First Tier	10.7	101.6×101.6×6.4	125	14.2	19.0	152	209	0.7	998	293	195	725	>	331
	Other Tiers	7.8	76.2×76.2×4.8	122	14.2	18.8	112	122	0.9	561	171	110	560	>	331
LD_W_HSS_24_6_1.0	All Tiers	7.2	76.2×76.2×4.8	112	14.2	18.3	103	138	0.7	561	197	110	631	>	331
LD_W_HSS_24_6_1.75	First Tier	8.6	88.9×88.9×4.8	113	17.1	18.4	123	161	0.8	667	229	131	622	>	331
	Other Tiers	7.0	76.2×76.2×4.8	108	14.2	18.2	99	145	0.7	561	208	110	661	>	331

Table 3.4. Summary of design for columns of Type LD frames.

Frame Designation	Section (W)	$\dfrac{KL}{r}$	$\dfrac{b_f}{2t_f}$	$\dfrac{h_w}{t_w}$	$C_{f,E}$ kN	$C_{r,E}$ kN	$\dfrac{C_{f,E}}{C_{r,E}}$	$C_{f,w}$ kN	$C_{r,w}$ kN	$M_{fx,w}$ kN.m	$M_{rx,w}$ kN.m	$\dfrac{C_{f,W}}{C_{r,W}}+\dfrac{0.85U_{1x}M_{f,Wx}}{M_{rx,W}}$
LD_W_HSS_10_2_1.0	250×67	98	6.5	22.5	1144	1175	1.0	322	1175	43	254	0.5
LD_W_HSS_10_2_1.75	250×73	99	8.9	23.1	1168	1259	0.9	322	1259	43	274	0.4
LD_W_HSS_10_3_1.0	410×60	77	6.9	46.5	1202	1267	1.0	322	1267	43	339	0.4
LD_W_HSS_10_3_1.75	250×67	94	6.5	22.5	1241	1285	1.0	322	1285	43	260	0.4
LD_W_HSS_16_2_1.0	310×107	119	9.0	22.6	1276	1414	0.9	322	1723	121	478	0.5
LD_W_HSS_16_2_1.75	310×129	131	7.5	18.9	1436	1473	1.0	322	1473	121	548	0.4
LD_W_HSS_16_3_1.0	360×91	105	7.8	30.4	1367	1425	1.0	322	1858	121	477	0.5
LD_W_HSS_16_3_1.75	360×110	119	6.4	25.4	1478	1466	1.0	322	1466	121	523	0.4
LD_W_HSS_16_4_1.0	460×82	95	6.0	41.1	1372	1509	0.9	322	1509	121	494	0.5
LD_W_HSS_16_4_1.75	360×101	105	7.0	27.5	1516	1613	0.9	322	1854	121	523	0.4
LD_W_HSS_24_3_1.0	460×113	122	8.1	37.8	1353	1423	1.0	322	1456	306	601	0.7
LD_W_HSS_24_3_1.75	610×174	150	7.5	39.2	1574	1571	1.0	322	1571	306	904	0.5
LD_W_HSS_24_4_1.0	460×113	122	8.1	37.8	1366	1423	1.0	322	2181	306	730	0.6
LD_W_HSS_24_4_1.75	460×144	131	6.4	30	1592	1625	1.0	322	1625	306	782	0.6
LD_W_HSS_24_6_1.0	530×101	110	6.0	43.6	1422	1498	1.0	322	2034	306	533	0.7
LD_W_HSS_24_6_1.75	690×125	118	7.8	52.7	1601	1658	1.0	322	1658	306	877	0.5

Table 3.5. Summary of design for beams and struts of Type LD frames.

Frame Designation	Beam Section (W)	$C_{f,B}$ kN	$C_{r,B}$ kN	$M_{fx,B}$ kN.m	$M_{rx,B}$ kN.m	$\dfrac{C_{f,B}}{C_{r,B}}+\dfrac{0.85U_{1x}M_{fx,B}}{M_{rx,B}}$	Strut Section (HSS)	$C_{f,S}$ kN	$C_{r,S}$ kN	$\dfrac{C_{f,S}}{C_{r,S}}$
LD_W_HSS_10_2_1.0	250×32.7	87	220	22	56	0.8	127×127×6.4	178	213	0.8
LD_W_HSS_10_2_1.75	310×38.7	228	325	22	87	0.9	127×127×4.8	146	167	0.9
LD_W_HSS_10_3_1.0	360×32.9	61	139	22	43	0.9	127×127×4.8	126	167	0.8
LD_W_HSS_10_3_1.75	250×32.7	84	220	22	56	0.7	114.3×114.3×4.8	102	123	0.8
LD_W_HSS_16_2_1.0	360×32.9	53	139	22	43	0.8	114.3×114.3×4.8	109	123	0.9
LD_W_HSS_16_2_1.75	250×32.7	136	220	22	56	1.0	114.3×114.3×4.8	107	123	0.9
LD_W_HSS_16_3_1.0	360×32.9	57	139	22	43	0.9	114.3×114.3×4.8	117	123	1.0
LD_W_HSS_16_3_1.75	250×32.7	85	220	22	56	0.7	101.6×101.6×4.8	42	87	0.5
LD_W_HSS_16_4_1.0	250×25.3	0	72	22	23	0.8	101.6×101.6×4.8	3	87	0.0
LD_W_HSS_16_4_1.75	250×32.7	120	220	22	56	0.9	114.3×114.3×4.8	104	123	0.8
LD_W_HSS_24_3_1.0	310×32.7	32	93	22	36	0.9	101.6×101.6×4.8	66	87	0.8
LD_W_HSS_24_3_1.75	250×32.7	87	220	22	56	0.7	101.6×101.6×4.8	34	87	0.4
LD_W_HSS_24_4_1.0	250×25.3	0	72	22	23	0.8	101.6×101.6×4.8	3	87	0.0
LD_W_HSS_24_4_1.75	250×32.7	94	220	22	56	0.8	101.6×101.6×4.8	38	87	0.4
LD_W_HSS_24_6_1.0	250×25.3	2	72	22	23	0.9	101.6×101.6×4.8	6	87	0.1
LD_W_HSS_24_6_1.75	250×28.4	26	86	22	30	0.9	101.6×101.6×4.8	3	87	0.0

Table 3.6. Summary of drift and period calculations for Type LD frames.

Frame Designation	$\dfrac{R_d R_o \delta_e}{\% \, h}$	$\dfrac{\delta_{e,W}}{\% \, h}$	$T_{Analytical}$	T_{Design}	Critical Tier
LD_W_HSS_10_2_1.0	0.41	0.01	0.66	0.5	Tier 1
LD_W_HSS_10_2_1.75	0.44	0.01	0.68	0.5	Tier 2
LD_W_HSS_10_3_1.0	0.51	0.01	0.73	0.5	Tier 1
LD_W_HSS_10_3_1.75	0.48	0.01	0.71	0.5	Tier 2
LD_W_HSS_16_2_1.0	0.37	0.02	0.95	0.8	Tier 1
LD_W_HSS_16_2_1.75	0.38	0.02	0.95	0.8	Tier 1
LD_W_HSS_16_3_1.0	0.41	0.02	1.00	0.8	Tier 1
LD_W_HSS_16_3_1.75	0.37	0.02	0.94	0.8	Tier 2
LD_W_HSS_16_4_1.0	0.40	0.02	0.99	0.8	Tier 1
LD_W_HSS_16_4_1.75	0.41	0.02	1.00	0.8	Tier 2
LD_W_HSS_24_3_1.0	0.33	0.05	1.38	1.2	Tier 1
LD_W_HSS_24_3_1.75	0.32	0.04	1.34	1.2	Tier 2
LD_W_HSS_24_4_1.0	0.33	0.05	1.38	1.2	Tier 1
LD_W_HSS_24_4_1.75	0.32	0.05	1.35	1.2	Tier 2
LD_W_HSS_24_6_1.0	0.35	0.05	1.42	1.2	Tier 1
LD_W_HSS_24_6_1.75	0.33	0.05	1.38	1.2	Tier 1

3.7 Seismic Design of Type CC Braced Frames

Type CC braced frames include three sets: 1) frames with T/C square HSS braces and wide-flange columns; 2) frames with T/O single-angle braces and HSS columns; 3) frames with T/O double-angle braces and HSS braces. T/C braces must resist seismic effects in tension and compression, whereas T/O braces are sized assuming that only the tension-acting brace carries 100% of the lateral seismic forces. In all Type CC frames, wide-flange beams and HSS struts are used.

3.7.1 Frames with T/C HSS Braces and wide-flange Columns

Type CC HSS braces are made from ASTM A500 Grade C steel with F_y = 345 MPa. Their design forces are obtained using the same method used for HSS braces of Type LD frames, and the braces are deisgned assuming in-plane and out-of-plane effective length factors, K_x and K_y, equal to 0.45. As opposed to Type LD, no upper or lower limit is specified by CSA S16-14 for the global slenderness ratio, KL/r, of braces in Type CC frames. The width-to-thickness ratio limit for braces in frames taller than 15 m in moderate and high seismic regions must be taken $525/\sqrt{F_y}$ = 28.3 (Class 2). This limit is applied to all Type CC frames in this study for consistency. The selected sections and the summary of the design are shown in Table 3.7. Bolted connections are used for the middle and end of the braces.

As opposed to Type LD frames, no capacity design is required for the design of other structural members in Type CC frames, including columns, beams, and struts. Those members are sized to resist gravity effects plus the seismic design base shear, as shown in Table 3.2. The requirements specified in CSA S16-14 for Type CC frames taller than 15 m in moderate and high seismic regions to increase the induced seismic forces linearly by 2% per meter of height above 15 m are excluded

in the seismic load calculation to examine the need for such requirements when multi-tiered configurations are employed. The standard also requires the seismic-induced forces of the columns of Type CC frames taller than 15 m in moderate and high seismic regions to be amplified by a factor of 1.3 to protect the columns from potential yielding or instability when the braces experience inelastic behaviour. This factor is also excluded in design as this study aims to investigate the necessity for such amplification factors for multi-tiered CBFs. Furthermore, for columns in Type CC multi-tiered configurations taller than 15 m in moderate and high seismic regions, CSA S16-14 specifies an out-of-plane transverse force equal to 10% of the axial load carried by the columns at the brace-to-column intersection point; however, this additional demand is excluded in the design to evaluate the need for such requirements in Type CC MT-CBFs. Columns of Type CC frames taller than 15 m in moderate and high seismic regions must satisfy Class 2 width-to-thickness ratios. This limit is applied to all Type CC frames in this study for consistency.

The design requirements for beams and struts of Type CC frames with T/C HSS braces are similar to Type LD frames. The section slenderness ratios specified for the frames taller than 15 m in moderate and high seismic regions are assumed for all Type CC frames in this study for consistency. Table 3.8 and Table 3.9 summarizes the final sections and design details, respectively, for columns, and beams and struts.

The storey drift limit for Type CC frames is identical to that of Type LD frames. For Type CC frames with T/C HSS braces, the storey drifts under seismic and wind loads, the fundamental period used in the design, and the critical tier are given in Table 3.10. As shown, two times the empirical period given by 2015 NBCC is always smaller than the analytical value; thus, the latter is used in the

design. Similar to Type LD frsmes, the tier drift is not verified for Type CC frames with T/C HSS braces.

Table 3.7. Summary of design for braces of Type CC frames with T/C braces.

Frame Designation	Tier	L_{Brace} m	Section (HSS)	$\dfrac{KL}{r}$	Design b_{el}/t	C_f kN	C_r kN	$\dfrac{C_f}{C_r}$
CC_W_HSS_10_2_1.0	All Tiers	7.8	114.3×114.3×4.8	79	22.9	302	335	0.9
CC_W_HSS_10_2_1.75	First Tier	8.7	127×127×4.8	79	25.7	338	375	0.9
	Other Tiers	7.0	101.6×101.6×4.8	80	20.0	271	289	0.9
CC_W_HSS_10_3_1.0	All Tiers	6.9	101.6×101.6×4.8	78	20.0	266	296	0.9
CC_W_HSS_10_3_1.75	First Tier	7.6	114.3×114.3×4.8	77	22.9	294	344	0.9
	Other Tiers	6.6	101.6×101.6×4.8	75	20.0	254	310	0.8
CC_W_HSS_16_2_1.0	All Tiers	10.0	127×127×4.8	90	25.7	280	322	0.9
CC_W_HSS_16_2_1.75	First Tier	11.8	127×127×6.4	109	18.5	331	329	1.0
	Other Tiers	8.4	101.6×101.6×4.8	95	20.0	234	235	1.0
CC_W_HSS_16_3_1.0	All Tiers	8.0	101.6×101.6×4.8	92	20.0	225	247	0.9
CC_W_HSS_16_3_1.75	First Tier	9.6	114.3×114.3×4.8	97	22.9	268	262	1.0
	Other Tiers	7.4	88.9×88.9×4.8	97	17.1	206	202	1.0
CC_W_HSS_16_4_1.0	All Tiers	7.2	88.9×88.9×4.8	95	17.1	202	208	1.0
CC_W_HSS_16_4_1.75	First Tier	8.4	101.6×101.6×4.8	96	20.0	236	233	1.0
	Other Tiers	6.9	88.9×88.9×4.8	90	17.1	193	220	0.9
CC_W_HSS_24_3_1.0	All Tiers	10.0	101.6×101.6×4.8	114	20.0	187	183	1.0
CC_W_HSS_24_3_1.75	First Tier	12.7	127×127×4.8	115	25.7	237	231	1.0
	Other Tiers	8.8	101.6×101.6×4.8	100	20.0	164	220	0.7
CC_W_HSS_24_4_1.0	All Tiers	8.5	88.9×88.9×4.8	111	17.1	159	166	1.0
CC_W_HSS_24_4_1.75	First Tier	10.7	114.3×114.3×4.8	108	22.9	200	226	0.9
	Other Tiers	7.8	88.9×88.9×4.8	103	17.1	147	185	0.8
CC_W_HSS_24_6_1.0	All Tiers	7.2	88.9×88.9×3.2	93	27.2	135	145	0.9
CC_W_HSS_24_6_1.75	First Tier	8.6	88.9×88.9×4.8	113	17.1	162	161	1.0
	Other Tiers	7.0	88.9×88.9×3.2	90	27.2	130	151	0.9

Table 3.8. Summary of design for columns of Type CC frames with T/C braces.

Frame Designation	Section (W)	$\dfrac{KL}{r}$	$\dfrac{b_f}{2t_f}$	$\dfrac{h_w}{t_w}$	$C_{f,E}$ kN	$C_{r,E}$ kN	$\dfrac{C_{f,E}}{C_{r,E}}$	$C_{f,W}$ kN	$C_{r,W}$ kN	$M_{fx,W}$ kN.m	$M_{rx,W}$ kN.m	$\dfrac{C_{f,W}}{C_{r,W}}+\dfrac{0.85U_{1x}M_{f,Wx}}{M_{rx,W}}$
CC_W_HSS_10_2_1.0	250×58	99	7.5	25.0	788	995	0.8	322	995	43	211	0.5
CC_W_HSS_10_2_1.75	310×67	129	7.0	29.6	736	773	1.0	322	773	43	243	0.6
CC_W_HSS_10_3_1.0	360×57.8	85	6.6	39.6	853	1187	0.7	322	1187	43	286	0.4
CC_W_HSS_10_3_1.75	250×58	93	7.5	25.0	801	1089	0.7	322	1089	43	216	0.5
CC_W_HSS_16_2_1.0	310×79	127	8.7	28.1	880	942	0.9	322	942	121	298	0.8
CC_W_HSS_16_2_1.75	250×101	155	6.6	16.7	819	857	1.0	322	857	121	342	0.8
CC_W_HSS_16_3_1.0	360×64	111	7.5	37.4	955	932	1.0	322	932	121	279	0.8
CC_W_HSS_16_3_1.75	310×79	120	8.7	28.1	895	1026	0.9	322	1050	121	312	0.7
CC_W_HSS_16_4_1.0	360×64	108	7.5	37.4	992	970	1.0	322	1357	121	326	0.7
CC_W_HSS_16_4_1.75	310×74	121	6.3	26.8	939	946	1.0	322	981	121	296	0.8
CC_W_HSS_24_3_1.0	360×122	156	5.9	22.4	955	1025	0.9	322	1446	306	573	0.8
CC_W_HSS_24_3_1.75	310×129	175	7.5	18.9	896	886	1.0	322	1257	306	521	1.0
CC_W_HSS_24_4_1.0	410×100	136	7.7	35.9	993	1057	0.9	322	1770	306	569	0.8
CC_W_HSS_24_4_1.75	360×122	156	5.9	22.4	940	1025	0.9	322	1227	306	541	0.9
CC_W_HSS_24_6_1.0	410×100	136	7.7	35.9	1030	1057	1.0	322	2706	306	569	0.8
CC_W_HSS_24_6_1.75	410×100	136	7.7	35.9	989	1057	0.9	322	1687	306	557	0.8

Table 3.9. Summary of design for beams and struts of Type CC frames with T/C braces.

Frame Designation	Beam Section (W)	$C_{f,B}$ kN	$C_{r,B}$ kN	$M_{f\times,B}$ kN.m	$M_{r\times,B}$ kN.m	$\frac{C_{f,B}}{C_{r,B}}+\frac{0.85U_{1\times}M_{f\times,B}}{M_{r\times,B}}$	Strut Section (HSS)	$C_{f,S}$ kN	$C_{r,S}$ kN	$\frac{C_{f,S}}{C_{r,S}}$
CC_W_HSS_10_2_1.0	310×38.7	232	325	22	87	0.94	88.9×88.9×3.2	3	55	0.05
CC_W_HSS_10_2_1.75	310×38.7	232	325	22	87	0.94	88.9×88.9×3.2	3	55	0.05
CC_W_HSS_10_3_1.0	310×38.7	232	325	22	87	0.94	88.9×88.9×3.2	4	55	0.07
CC_W_HSS_10_3_1.75	310×38.7	232	325	22	87	0.94	88.9×88.9×3.2	4	55	0.07
CC_W_HSS_16_2_1.0	250×38.5	168	267	22	77	0.89	88.9×88.9×3.2	3	55	0.06
CC_W_HSS_16_2_1.75	250×38.5	168	267	22	77	0.89	88.9×88.9×3.2	3	55	0.06
CC_W_HSS_16_3_1.0	250×38.5	168	267	22	77	0.89	88.9×88.9×3.2	5	55	0.08
CC_W_HSS_16_3_1.75	250×38.5	168	267	22	77	0.89	88.9×88.9×3.2	6	55	0.10
CC_W_HSS_16_4_1.0	250×38.5	168	267	22	77	0.89	88.9×88.9×3.2	6	55	0.10
CC_W_HSS_16_4_1.75	250×38.5	168	267	22	77	0.89	88.9×88.9×3.2	7	55	0.13
CC_W_HSS_24_3_1.0	250×32.7	112	220	22	56	0.86	88.9×88.9×3.2	6	55	0.10
CC_W_HSS_24_3_1.75	250×32.7	112	220	22	56	0.86	88.9×88.9×3.2	8	55	0.14
CC_W_HSS_24_4_1.0	250×32.7	112	220	22	56	0.86	88.9×88.9×3.2	7	55	0.13
CC_W_HSS_24_4_1.75	250×32.7	112	220	22	56	0.86	88.9×88.9×3.2	9	55	0.16
CC_W_HSS_24_6_1.0	250×32.7	112	220	22	56	0.86	88.9×88.9×3.2	8	55	0.14
CC_W_HSS_24_6_1.75	250×32.7	112	220	22	56	0.86	88.9×88.9×3.2	11	55	0.19

Table 3.10. Summary of drift and period calculations for Type CC frames with T/C braces.

Frame Designation	$\dfrac{R_d R_o \delta_e}{\% \text{ h}}$	$\dfrac{\delta_{e,W}}{\% \text{ h}}$	$T_{Analytical}$	T_{Design}	Critical Tier
CC_W_HSS_10_2_1.0	0.39	0.01	0.64	0.5	Tier 1
CC_W_HSS_10_2_1.75	0.40	0.01	0.65	0.5	Tier 2
CC_W_HSS_10_3_1.0	0.44	0.01	0.68	0.5	Tier 1
CC_W_HSS_10_3_1.75	0.43	0.01	0.67	0.5	Tier 1
CC_W_HSS_16_2_1.0	0.37	0.02	0.95	0.8	Tier 1
CC_W_HSS_16_2_1.75	0.35	0.02	0.93	0.8	Tier 2
CC_W_HSS_16_3_1.0	0.38	0.02	0.97	0.8	Tier 1
CC_W_HSS_16_3_1.75	0.39	0.02	0.97	0.8	Tier 2
CC_W_HSS_16_4_1.0	0.41	0.02	0.99	0.8	Tier 1
CC_W_HSS_16_4_1.75	0.39	0.02	0.98	0.8	Tier 1
CC_W_HSS_24_3_1.0	0.32	0.05	1.36	1.2	Tier 1
CC_W_HSS_24_3_1.75	0.32	0.04	1.35	1.2	Tier 1
CC_W_HSS_24_4_1.0	0.33	0.05	1.38	1.2	Tier 1
CC_W_HSS_24_4_1.75	0.30	0.04	1.32	1.2	Tier 1
CC_W_HSS_24_6_1.0	0.39	0.05	1.50	1.2	Tier 1
CC_W_HSS_24_6_1.75	0.38	0.05	1.48	1.2	Tier 2

3.7.2   Frames with T/O single-angle or double-angle braces and HSS columns

The braces are selected from angle sections made of A36 steel with F_y = 248 MPa as one of the steel grades commonly used in the construction of steel structures in North America. The single-angle bracing members are selected from equal-leg angles (Figure 2.17), while the built-up double-angles are made using unequal-leg angles to achieve a more economical cross-section where the radius of gyration about both principal axes (Figure 2.17) of the section are close. Double-angles are connected Long-Leg Back-to-Back (LLBB) using one stitch per each brace half and oriented such that the out-of-plane buckling occurs about their *Y*-axis of Figure 2.17.

CSA S16-14 requires no limit for the global slenderness ratio, KL/r, of the braces in Type CC frames. Width-to-thickness ratio of the legs of angles in frames taller than 15 m in moderate and high seismic regions must be verified using $170/\sqrt{F_y}$ when $KL/r \leq 200$, however, no limit is imposed on the width-to-thickness ratio when the global slenderness ratio of single-angle or double-angle braces exceed 200. This limit is applied to Type CC frames in this study for consistency.

When calculating the slenderness ratios of both single-angle and double-angle braces, the effective length factors about their X- and Y-axes, K_x and K_y, are taken equal to 1.0 with 0.45 times the full length of the brace as the unsupported length about both axes, L_x and L_y. For double-angles, an equivalent slenderness ratio, ρ_e, is required in the design, as described in Section 2.5.3. For single-angle braces, the global slenderness ratio about the section minor axis, $(KL/r)_{x'}$, is calculated using $K_{x'} = 0.85$, as recommended by Goel and El-Tayem (1986). The unsupported length of the single-angle brace about X′-axis, $L_{x'}$, is also taken as 0.45 times the total length of the brace, considering the beneficial effect of the tensile brace and gusset plates. Table 3.11 and Table 3.12 give the selected member sizes for double-angle and single-angle braces, respectively. T_f and T_r in these tables are the design tension load induced in the brace and the factored tensile resistance, respectively.

The remaining structural elements of Type CC frames with T/O braces, including columns, beams, and struts are designed to resist the forces induced by gravity loads plus seismic loads assuming that only the tension-acting braces deliver axial forces to their adjacent members. Columns, beams, and struts in frames taller than 15 m in moderate and high seismic regions must meet the width-to-thickness ratio prescribed for Class 1 or 2 sections. This limit is applied to all Type CC frames in

this study for consistency. The selected sections and the summary of design calculations for the columns and beams are given in Table 3.13 and Table 3.14, respectively.

For Type CC with T/O double angle-braces and single-angle braces T/O braces, the design storey drift, fundamental period used in design, and critical tier are presented in Table 3.15 and Table 3.16, respectively. It is worth noting that as opposed to frames with T/C braces, the drift and period of frames with T/O braces are calculated by neglecting the effect of compression braces. Similar to the other frame categories, the tier drift is not verified for this frames category.

Table 3.11. Summary of design for braces of Type CC frames with T/O double-angles braces.

Frame Designation	Tier	L_{Brace} m	Section (2L)	ρ_e	b_{el}/t Design	b_{el}/t Limit	T_f kN	T_r kN	$\dfrac{T_f}{T_r}$
CC_HSS_2L_10_2_1.0	All Tiers	7.8	89×64×9.5-12 LLBB	147	9.3	10.8	604	608	1.0
CC_HSS_2L_10_2_1.75	First Tier	8.7	89×76×9.5-12 LLBB	142	9.3	10.8	677	662	1.0
	Other Tiers	7.0	76×64×9.5-12 LLBB	134	8.0	10.80	543	554	1.0
CC_HSS_2L_10_3_1.0	All Tiers	6.9	76×64×9.5-12 LLBB	131	8.0	10.8	531	554	1.0
CC_HSS_2L_10_3_1.75	First Tier	7.6	76×51×11.1-12 LLBB	172	6.9	10.8	588	574	1.0
	Other Tiers	6.6	76×51×9.5-12 LLBB	150	8.0	10.8	508	500	1.0
CC_HSS_2L_16_2_1.0	All Tiers	10.0	76×64×9.5-12 LLBB	191	8.0	10.8	560	554	1.0
CC_HSS_2L_16_2_1.75	First Tier	11.8	76×51×12.7-12 LLBB	265	6.0	No Need	662	648	1.0
	Other Tiers	8.4	76×64×7.9-12 LLBB	158	9.6	10.8	468	467	1.0
CC_HSS_2L_16_3_1.0	All Tiers	8.0	76×64×7.9-12 LLBB	152	9.6	10.8	450	467	1.0
CC_HSS_2L_16_3_1.75	First Tier	9.6	76×64×9.5-12 LLBB	183	8.0	10.8	537	554	1.0
	Other Tiers	7.4	76×51×7.9-12 LLBB	170	9.6	10.8	412	422	1.0
CC_HSS_2L_16_4_1.0	All Tiers	7.2	76×51×7.9-12 LLBB	166	9.6	10.8	404	422	1.0
CC_HSS_2L_16_4_1.75	First Tier	8.4	76×64×7.9-12 LLBB	159	9.6	10.8	471	467	1.0
	Other Tiers	6.9	76×51×7.9-12 LLBB	159	9.6	10.8	385	422	0.9
CC_HSS_2L_24_3_1.0	All Tiers	10.0	76×51×7.9-12 LLBB	231	9.6	No Need	374	422	0.9
CC_HSS_2L_24_3_1.75	First Tier	12.7	76×64×7.9-12 LLBB	240	9.6	No Need	475	467	1.0
	Other Tiers	8.8	76×51×6.4-12 LLBB	204	12.0	No Need	328	342	1.0
CC_HSS_2L_24_4_1.0	All Tiers	8.5	76×51×7.9-12 LLBB	196	9.6	10.8	317	422	1.0
CC_HSS_2L_24_4_1.75	First Tier	10.7	89×64×6.4-12 LLBB	203	14.0	No Need	399	414	1.0
	Other Tiers	7.8	76×51×7.9-12 LLBB	181	9.6	10.8	293	422	1.0
CC_HSS_2L_24_6_1.0	All Tiers	7.2	76×51×7.9-12 LLBB	166	9.6	10.8	269	422	1.0
CC_HSS_2L_24_6_1.75	First Tier	8.6	76×51×6.4-12 LLBB	201	12.0	No Need	323	342	1.0
	Other Tiers	7.0	76×51×7.9-12 LLBB	161	9.6	10.8	261	422	1.0

Table 3.12. Summary of design for braces of Type CC frames with T/O single-angles braces.

Frame Designation	Tier	L_{Brace} m	Section (L)	$\frac{KL}{r}$	b_{el}/t Design	b_{el}/t Limit	T_f kN	T_r kN	$\frac{T_f}{T_r}$
CC_HSS_L_10_2_1.0	All Tiers	7.8	102×102×15.9	150	6.4	10.8	604	668	0.9
CC_HSS_L_10_2_1.75	First Tier	8.7	102×102×15.9	168	6.4	10.8	677	668	1.0
	Other Tiers	7.0	102×102×12.7	135	8.0	10.8	543	542	1.0
CC_HSS_L_10_3_1.0	All Tiers	6.9	102×102×12.7	132	8.0	10.8	531	542	1.0
CC_HSS_L_10_3_1.75	First Tier	7.6	102×102×15.9	146	6.4	10.8	588	668	0.9
	Other Tiers	6.6	102×102×12.7	126	8.0	10.8	508	542	0.9
CC_HSS_L_16_2_1.0	All Tiers	10.0	102×102×15.9	192	6.4	10.8	560	668	0.8
CC_HSS_L_16_2_1.75	First Tier	11.8	102×102×15.9	227	6.4	No Need	662	668	1.0
	Other Tiers	8.4	89×89×12.7	184	7.0	10.8	468	468	1.0
CC_HSS_L_16_3_1.0	All Tiers	8.0	89×89×12.7	177	7.0	10.8	450	468	1.0
CC_HSS_L_16_3_1.75	First Tier	9.6	102×102×12.7	184	8.0	10.8	537	542	1.0
	Other Tiers	7.4	102×102×9.5	140	10.7	10.8	412	414	1.0
CC_HSS_L_16_4_1.0	All Tiers	7.2	76×76×12.7	186	6.0	10.8	404	396	1.0
CC_HSS_L_16_4_1.75	First Tier	8.4	89×89×12.7	186	7.0	10.8	471	468	1.0
	Other Tiers	6.9	76×76×12.7	177	6.0	10.8	385	396	1.0
CC_HSS_L_24_3_1.0	All Tiers	10.0	76×76×12.7	258	6.0	No Need	374	396	0.9
CC_HSS_L_24_3_1.75	First Tier	12.7	89×89×12.7	280	7.0	No Need	475	468	0.9
	Other Tiers	8.8	64×64×12.7	271	5.0	No Need	328	324	1.0
CC_HSS_L_24_4_1.0	All Tiers	8.5	64×64×12.7	263	5.0	No Need	317	324	1.0
CC_HSS_L_24_4_1.75	First Tier	10.7	76×76×12.7	276	6.0	No Need	399	396	1.0
	Other Tiers	7.8	76×76×9.5	201	8.0	No Need	293	304	0.9
CC_HSS_L_24_6_1.0	All Tiers	7.2	76×76×9.5	185	8.0	10.8	269	304	0.9
CC_HSS_L_24_6_1.75	First Tier	8.6	64×64×12.7	267	5.0	No Need	323	324	0.8
	Other Tiers	7.0	76×76×7.9	178	9.6	10.8	261	256	1.0

Table 3.13. Summary of design for columns of Type CC frames with T/O single- or double-angle braces.

Frame Designation	Section	$\dfrac{KL}{r}$	$\dfrac{b_{el}}{t}$	$C_{f,E}$ kN	$C_{r,E}$ kN	$\dfrac{C_{f,E}}{C_{r,E}}$	$C_{f,W}$ kN	$C_{r,W}$ kN	$M_{fx,W}$ kN.m	$M_{rx,W}$ kN.m	$\dfrac{C_{f,W}}{C_{r,W}}+\dfrac{U_{1x}M_{f,Wx}}{M_{rx,W}}$
CC_HSS_2L/L_10_2_1.0											
CC_HSS_2L/L_10_2_1.75											
CC_HSS_2L/L_10_3_1.0	228.6×228.6×12.7	114	16.4	982	1086	0.9	322	1086	322	246	0.5
CC_HSS_2L/L_10_3_1.75											
CC_HSS_2L/L_16_2_1.0											
CC_HSS_2L/L_16_2_1.75											
CC_HSS_2L/L_16_3_1.0											
CC_HSS_2L/L_16_3_1.75	304.8×304.8×12.7	134	22.8	1104	1148	1.0	322	1148	322	456	0.6
CC_HSS_2L/L_16_4_1.0											
CC_HSS_2L/L_16_4_1.75											
CC_HSS_2L/L_24_3_1.0											
CC_HSS_2L/L_24_3_1.75											
CC_HSS_2L/L_24_4_1.0											
CC_HSS_2L/L_24_4_1.75	355.6×355.6×19	175	17.0	1105	1246	0.9	322	1246	322	900	0.7
CC_HSS_2L/L_24_6_1.0											
CC_HSS_2L/L_24_6_1.75											

Table 3.14. Summary of design for beams and struts of Type CC frames T/O single- or double-angle braces.

Frame Designation	Beam Section (W)	$C_{f,B}$ kN	$C_{r,B}$ kN	$M_{fx,B}$ kN.m	$M_{rx,B}$ kN.m	$\dfrac{C_{f,B}}{C_{r,B}}+\dfrac{0.85U_{1x}M_{fx,B}}{M_{rx,B}}$	Strut Section (HSS)	$C_{f,S}$ kN	$C_{r,S}$ kN	$\dfrac{C_{f,S}}{C_{r,S}}$
CC_HSS_2L/L_10_2_1.0	310×38.7	232	325	22	87	0.9	177.8×177.8×6.4	472	642	0.7
CC_HSS_2L/L_10_2_1.75	310×38.7	232	325	22	87	0.9	177.8×177.8×6.4	472	642	0.7
CC_HSS_2L/L_10_3_1.0	310×38.7	232	325	22	87	0.9	177.8×177.8×6.4	475	642	0.7
CC_HSS_2L/L_10_3_1.75	310×38.7	232	325	22	87	0.9	177.8×177.8×6.4	476	642	0.7
CC_HSS_2L/L_16_2_1.0	250×38.5	168	267	22	77	0.9	139.7×139.7×6.4	345	354	1.0
CC_HSS_2L/L_16_2_1.75	250×38.5	168	267	22	77	0.9	139.7×139.7×6.4	345	354	1.0
CC_HSS_2L/L_16_3_1.0	250×38.5	168	267	22	77	0.9	139.7×139.7×6.4	349	354	1.0
CC_HSS_2L/L_16_3_1.75	250×38.5	168	267	22	77	0.9	139.7×139.7×6.4	349	354	1.0
CC_HSS_2L/L_16_4_1.0	250×38.5	168	267	22	77	0.9	139.7×139.7×6.4	351	354	1.0
CC_HSS_2L/L_16_4_1.75	250×38.5	168	267	22	77	0.9	139.7×139.7×6.4	351	354	1.0
CC_HSS_2L/L_24_3_1.0	250×32.7	112	220	22	56	0.9	127×127×6.4	237	274	0.9
CC_HSS_2L/L_24_3_1.75	250×32.7	112	220	22	56	0.9	127×127×6.4	237	274	0.9
CC_HSS_2L/L_24_4_1.0	250×32.7	112	220	22	56	0.9	127×127×6.4	239	274	0.9
CC_HSS_2L/L_24_4_1.75	250×32.7	112	220	22	56	0.9	127×127×6.4	239	274	0.9
CC_HSS_2L/L_24_6_1.0	250×32.7	112	220	22	56	0.9	127×127×6.4	240	274	0.9
CC_HSS_2L/L_24_6_1.75	250×32.7	112	220	22	56	0.9	127×127×6.4	242	274	0.9

Table 3.15. Summary of drift and period of Type CC frames with T/O double-angle braces.

Frame Designation	$\dfrac{R_dR_o\delta_e}{\% \text{ h}}$	$\dfrac{\delta_{e,W}}{\% \text{ h}}$	$T_{\text{Analytical}}$	T_{Design}	Critical Tier
CC_HSS_2L_10_2_1.0	0.63	0.01	0.82	0.5	Tier1
CC_HSS_2L_10_2_1.75	0.66	0.02	0.83	0.5	Tier1
CC_HSS_2L_10_3_1.0	0.75	0.02	0.89	0.5	Tier1
CC_HSS_2L_10_3_1.75	0.79	0.02	0.91	0.5	Tier1
CC_HSS_2L_16_2_1.0	0.66	0.04	1.26	0.8	Tier1
CC_HSS_2L_16_2_1.75	0.69	0.04	1.29	0.8	Tier1
CC_HSS_2L_16_3_1.0	0.65	0.04	1.26	0.8	Tier1
CC_HSS_2L_16_3_1.75	0.67	0.04	1.28	0.8	Tier1
CC_HSS_2L_16_4_1.0	0.71	0.04	1.32	0.8	Tier1
CC_HSS_2L_16_4_1.75	0.72	0.04	1.33	0.8	Tier1
CC_HSS_2L_24_3_1.0	0.57	0.08	1.81	1.2	Tier1
CC_HSS_2L_24_3_1.75	0.64	0.09	1.93	1.2	Tier1
CC_HSS_2L_24_4_1.0	0.51	0.07	1.72	1.2	Tier1
CC_HSS_2L_24_4_1.75	0.54	0.08	1.78	1.2	Tier1
CC_HSS_2L_24_6_1.0	0.51	0.07	1.72	1.2	Tier1
CC_HSS_2L_24_6_1.75	0.54	0.08	1.78	1.2	Tier1

Table 3.16. Summary of drift and period of Type CC frames with T/O single-angle braces.

Frame Designation	$\dfrac{R_dR_o\delta_e}{\% \text{ h}}$	$\dfrac{\delta_{e,W}}{\% \text{ h}}$	$T_{\text{Analytical}}$	T_{Design}	Critical Tier
CC_HSS_L_10_2_1.0	0.59	0.01	0.79	0.5	Tier1
CC_HSS_L_10_2_1.75	0.66	0.02	0.83	0.5	Tier1
CC_HSS_L_10_3_1.0	0.76	0.02	0.89	0.5	Tier1
CC_HSS_L_10_3_1.75	0.74	0.02	0.88	0.5	Tier2
CC_HSS_L_16_2_1.0	0.58	0.03	1.19	0.8	Tier1
CC_HSS_L_16_2_1.75	0.68	0.04	1.28	0.8	Tier1
CC_HSS_L_16_3_1.0	0.65	0.04	1.26	0.8	Tier1
CC_HSS_L_16_3_1.75	0.68	0.04	1.29	0.8	Tier1
CC_HSS_L_16_4_1.0	0.74	0.04	1.34	0.8	Tier1
CC_HSS_L_16_4_1.75	0.74	0.04	1.34	0.8	Tier1
CC_HSS_L_24_3_1.0	0.59	0.08	1.86	1.2	Tier1
CC_HSS_L_24_3_1.75	0.65	0.09	1.95	1.2	Tier1
CC_HSS_L_24_4_1.0	0.61	0.09	1.88	1.2	Tier1
CC_HSS_L_24_4_1.75	0.63	0.09	1.91	1.2	Tier1
CC_HSS_L_24_6_1.0	0.63	0.09	1.91	1.2	Tier1
CC_HSS_L_24_6_1.75	0.70	0.10	2.01	1.2	Tier1

Chapter 4: Numerical Simulation

4.1 Introduction

This chapter describes the development of a three-dimensional fibre-based numerical model capable of simulating the seismic response of multi-tiered steel concentrically braced frames of Figure 3.1. The model is created in the environment of the Open System for Earthquake Engineering Simulation (*OpenSees*) (McKenna et al. 1997).

4.2 Material Model

The steel material model used in this research is *Giuffre-Menegotto-Pinto* (*Steel02*), which has been implemented in the *OpenSees* library of material. The *Steel02* material accounts for isotropic and kinematic strain hardening and the Baushinger effects of steel material. The parameters required to define this material in *OpenSees*, which has been introduced in Section 2.6.4, is obtained from Ashrafi and Imanpour (2019). The authors optimized the input parameters for the *Steel02* material using the hysteretic test results of an experimental study (Dehghani et al. 2017) on CSA G40.21-350WT steel coupons (Figure 4.1). The parameters reported include $b = 0.0067$, $R_0 = 23.43$, $CR_1 = 0.89$, $CR_2 = 0.07$, $a_1 = 0.35$, $a_2 = 12.12$, $a_3 = 0.33$, and $a_4 = 12.09$. Young's modulus $E = 200$ GPa is assigned to the steel material. The yield strength $F_y = 345$ MPa is used for columns, beams, struts, while probable yield strength, $R_yF_y = 460$ MPa for HSSs and 385 MPa for angles is considered for the bracing members as these members are expected to yield under seismic loads.
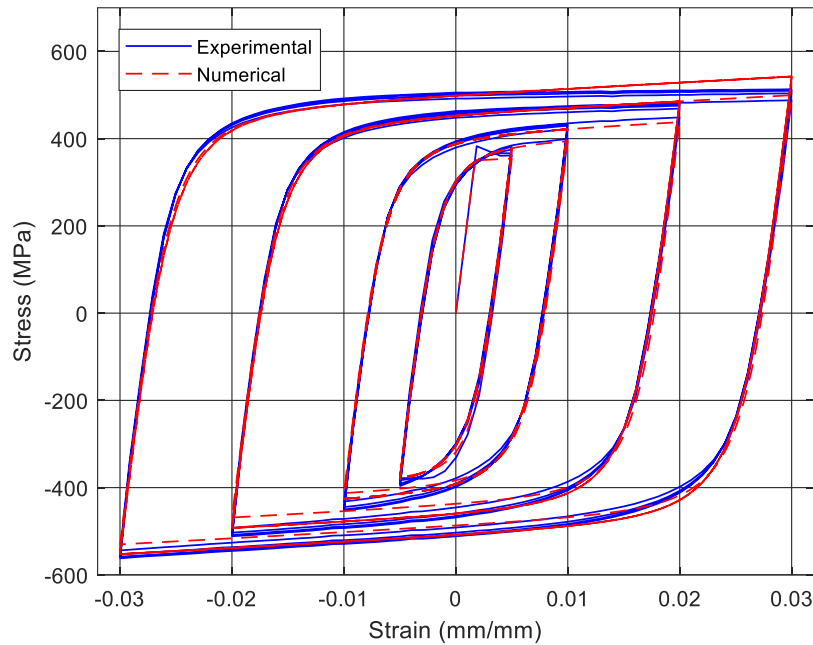
Figure 4.1. Calibration of Steel02 material model under cyclic loading (Ashrafi and Imanpour 2019).

4.3 Braced Frame Model

Prior to creating the model of the frame in *OpenSees*, braces and columns are individually simulated and calibrated against the available test data. The modelling techniques and assumptions used in such individual models are then employed in the frame model.

4.3.1 Isolated HSS and Single-angle Brace Models

A simply-supported member is modelled in *OpenSees* using forced-based nonlinear elements (*nonlinearBeamColumn*). The modelling technique used for this purpose has been verified in the past for HSS bracing members (Aguero et al. 2006, Uriz et al. 2008) and angle bracing members (Jiang 2013).

4.3.1.1 Single-angle Model

To adequately reproduce the buckling response, the member is divided into elements, and the implemented corotational geometric coordinate transformation in *OpenSees*, accounting for P-Delta and large deformations, is assigned to the elements.

Figure 4.2 shows the fibre discretization of the cross-section for the angle brace. Considering the cross-section as two rectangular segments (along the legs and excluding the overlapping area), each segment is modelled using *quadrilateral* fibres. Four layers of fibres are employed across the thickness of the legs (Jiang 2013) and 14 layers along the width of each rectangular segment. In tototal, 16 elements are used for the member as recommended by Jiang (2013). Additionally, they suggested assigning two to five integration points to each element; therefore, five integration points are employed per element for the single-angle model of this study.
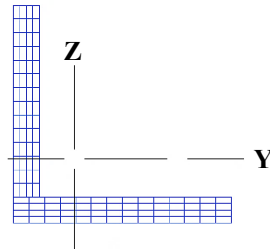
Figure 4.2. Discretization of the cross-section for the single-angle.

Steel02 material is assigned to the fibres with the parameters, as described in Section 4.2. Residual stresses are assigned to the cross-section based on the test data measured by Adluri and Madugula (1996). The distribution of the residual stresses is linear along the legs of the angles, as illustrated in Figure 4.3.
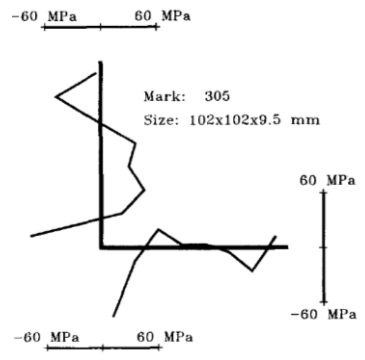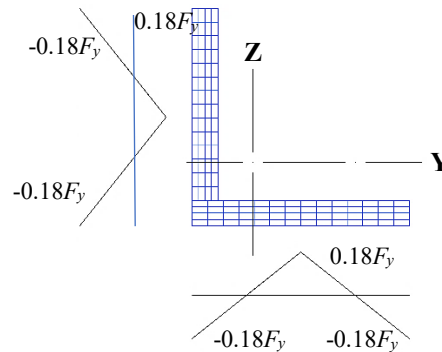
Figure 4.3. Residual stress distribution in angles: a) Measured data (Adluri and Madugula 1996); b) Numerical simulation.

Elastic torsional stiffness is assigned to the fibres corresponding to the *GJ* values of the sections, where *G* is the shear modulus of elasticity of steel, and *J* is the torsional constant of the section.

The numerical model of the individual single-angle is verified by comparing the buckling capacity of the member obtained from the model with that calculated using the equation specified in CSA S16-14 for the compression capacity of single-angle members.

L76×76×11.1 is selected and assigned to a two-span continuous beam-column, as shown in Figure 4.4. The brace section is kept unchanged, while various lengths are selected covering a wide-range of slenderness ratios. The length is varied from 800 mm to 10000 mm with intervals of 400 mm to produce 26 slenderness ratios ranging from 23 to 286. The compression capacity corresponding to each slenderness ratio is calculated based on CSA S16-14 equation for single-angle members in compression, considering effective length factors equal to the design assumptions in Section 3.7.2, described for the braced frame (i.e. $K_X = K_Y = 1.0$ and $K_{X'} = 0.85$), while the unbraced length is taken equal to 0.5 times the brace length excluding the connection areas (*L* in Figure 4.4).
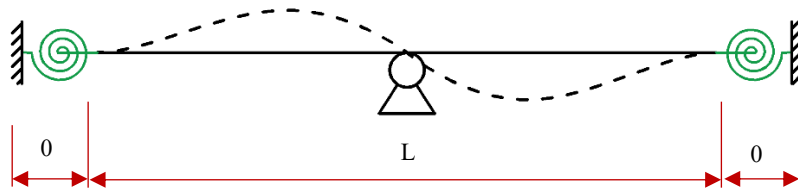
Figure 4.4. Single-angle OpenSees model (the expected buckled shape shown with dashed line).

Very similar boundary conditions to the braced frame model are considered for the single-angle brace model; fixed supports with rotational springs are assigned to the ends and a roller to the mid-length of the member. The end rotational springs represent the brace-to-column gusset plate connection with the out-of-plane rotational stiffness properties of the respective gusset plate. The roller at the mid-length represents the middle connection in an X-bracing configuration with single-angle bracing members in which braces are often connected using a single bolt (Figure 4.5).
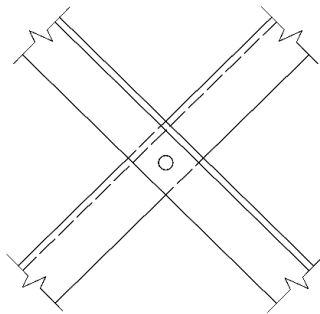
Figure 4.5. Typical middle connection of an X-bracing braced frame with single-angle braces.

To trigger the global buckling of the member, an Initial Out-of-Straightness (IOS) is introduced in the model. The IOS is estimated with a sinusoidal shape corresponding to the first global buckling mode-shape of the member. The maximum amplitude of the sine-wave is assigned to the middle of each half of the brace as a fraction of the brace length, L. Two IOS amplitudes are employed in the model: $0.001L$ and $0.002L$. Although the single-angles are expected to buckle about their minor axis (X′-axis in Figure 2.17), the IOS is applied only about the X-axis of the member. The reason

is to reproduce the misalignment of the member in the braced frame when buckling takes place in the out-of-plane direction of the frame, as driven by the detail of the brace end-connections. Each brace is then subjected to a gradually increasingly negative displacement of 100 mm to determine the brace buckling load.

Figure 4.6 shows the compression capacity of the single-angle brace calculated as per CSA S16-14 along with the buckling load obtained from the *OpenSees* models. As shown, the model underpredicted the code-specified compression capacity of the brace, despite neglecting the torsional buckling mode in the fibre-based model developed in *OpenSees*. However, further effort to achieve a better calibration was not taken, because the single-angle braces of the selected frames in this study act as tension-only and such slender braces are not expected to considerably affect the frame seismic response. The average value of the design slenderness ratios, *KL/r*, of single-angle braces used in this study is 195 (see Table 3.12). Additionally, as demonstrated in Figure 4.6, for IOS equal to 0.001*L*, a relatively better prediction was achieved. Although the IOS magnitude has minimal impact on the compression capacity of the braces used in this study (for *KL/r* values of around 200), the initial out-of-straightness of 0.001*L* is chosen for the single-angle braces in the frame.
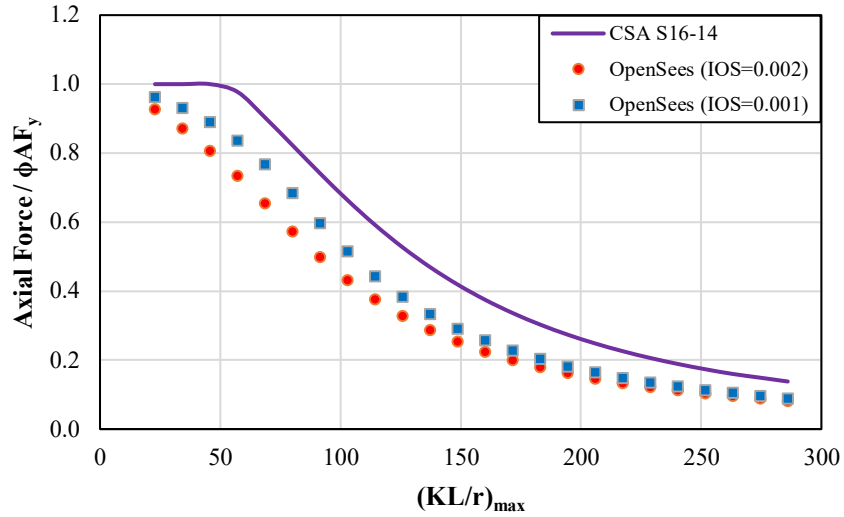
Figure 4.6. Single-angle brace buckling load: CSA S16 vs. the numerical model.

4.3.1.2 HSS Brace Model

The fibres discretization of the HSS braces is shown in Figure 4.7. The straight edges of the cross-sections are modelled using *quadrilateral* fibres, and *circular* fibres are used to create the curved corners. 16 elements are used for the HSS model, which is identical to the number of elements used in the angle model. As recommended by Karamanci and Lignos (2013), ten layers along the width of each side of the cross-section are utilized; six for the straight parts and four in the circumferential direction of the corners. Five layers of fibres are used through the thickness of the segments.
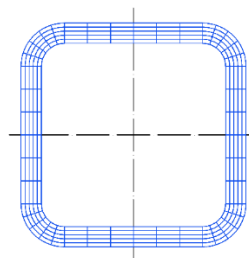
Figure 4.7. Discretization of the cross-section for HSS

No residual stresses were assigned to the HSS section to avoid numerical convergence issues. This assumption is not expected to significantly influence the yielding and buckling response of HSS braces as reported by Uriz et al. (2008).

The HSS brace model is validated using available experimental data from a cyclic quasi-static test program (Jiang 2019) conducted on HSS braces. The modelling assumptions are kept close to the test condition. Similar to the test, a 4500 mm-long brace with an HSS127×127×7.9 section is modelled and analyzed using the cyclic pushover analysis method under the cyclic displacement history imposed in the experiment (Figure 4.8). Pin supports are assigned to both ends of the member. The measured yield stress, $F_y = 410$ MPa, reported in the test program is used.

Similar to the angle model, a sinusoidal IOS is assigned to the brace to avoid bifurcation and initiate global buckling. The maximum amplitude of the sine-wave at the middle of the brace is 0.002 times the brace length.
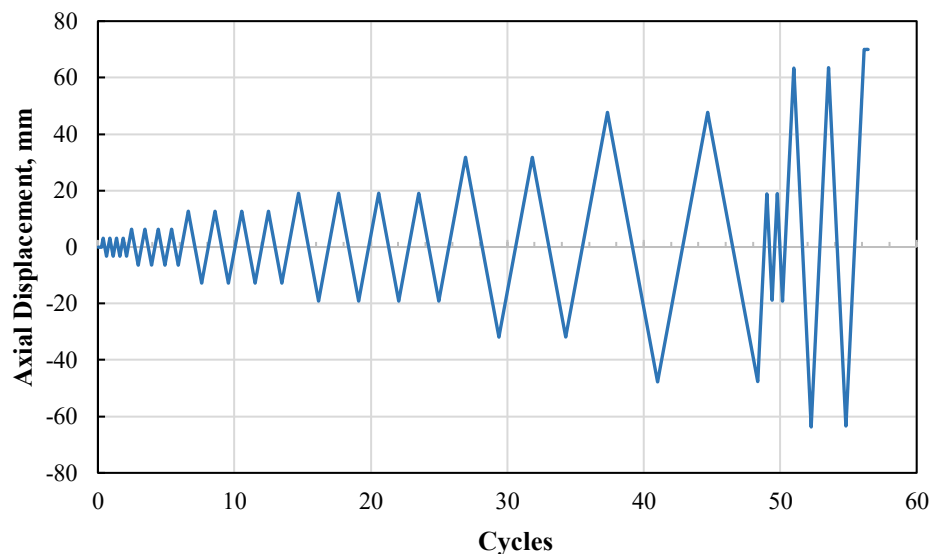
Figure 4.8. Displacement sequence applied to HSS brace specimen (Jiang 2019).

Figure 4.9 shows the hysteretic response of the HSS brace obtained from the numerical model and experimental test, in which the normalized axial force of the brace, C_f, with respect to the yielding capacity of the brace cross-section, AF_y, is plotted versus the applied axial displacement. A very good match is observed between the results of the HSS brace simulation and the experimental data, which confirmed that the *OpenSees* model is able to appropriately simulate the cyclic inelastic response of the HSS brace and predict the buckling, post-buckling, and tensile yielding capacities of the member.
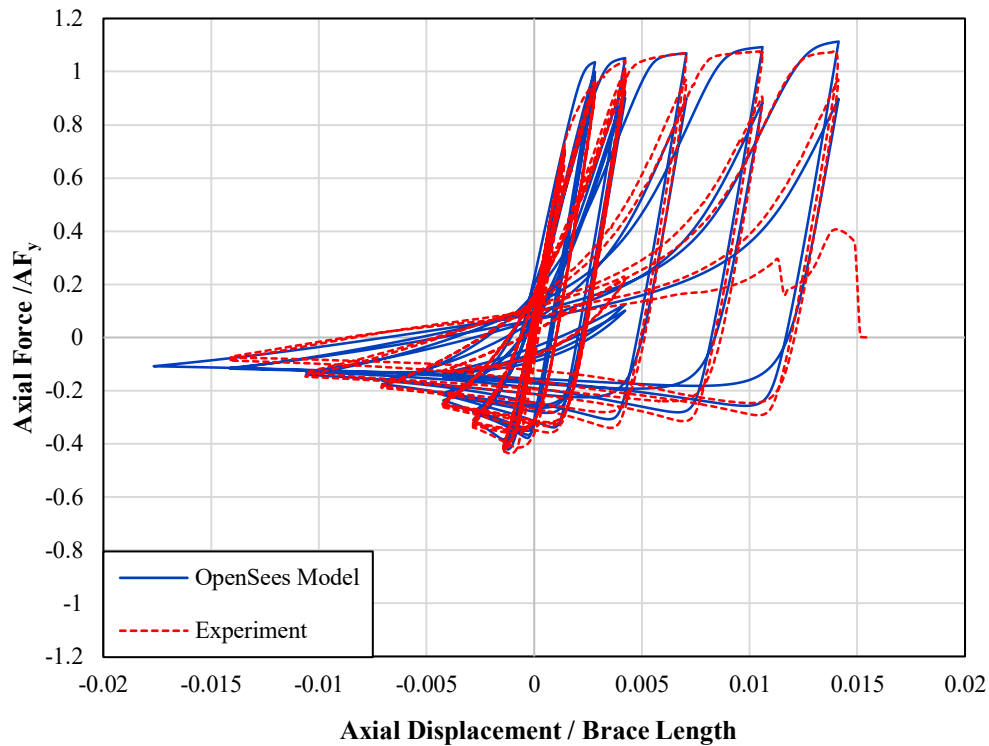
Figure 4.9. Hysteretic response of HSS brace.

4.3.2 Isolated Built-up Double-angle Model

Special attention is paid to reproduce the nonlinear cyclic response of double-angle braces, including yielding, buckling, and post-buckling responses, as well as the interaction between individual angles. A double-angle member model is created by expanding the single-angle model

described in Section 4.3.1. The modelling technique and most of the modelling assumptions used for the double-angle brace model are identical to those of the single-angle brace model, including the material model, residual stress amplitude and pattern, number of layers used in fibre discretization of the cross-section (Figure 4.10), type and number of elements, geometric coordinate transformation system, and number of integration points.
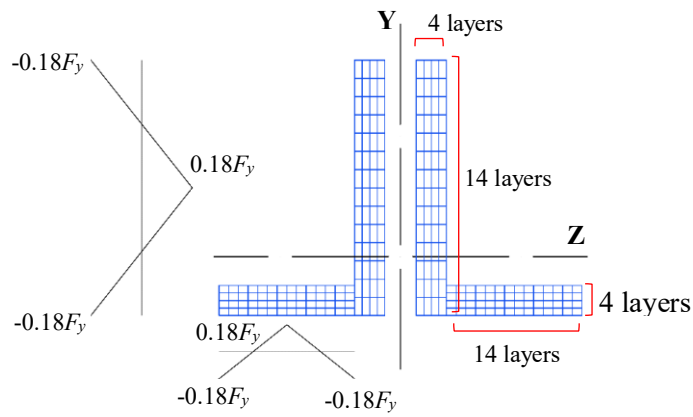
Figure 4.10. Fibre discretization of the double-angle brace with residual stresses

The double-angle model is calibrated against the physical test conducted on double-angle braces by (Jiang 2013). The assumptions of the numerical model are set such that the numerical results can adequately reproduce the results of the experimental test. A 2L127×76×9.5 connected Long-Leg Back-to-Back (LLBB) is selected with a back-to-back clear gap of 12.7 mm, as shown in Figure 4.11a. The clear length of the brace (brace length excluding the end gusset plates) is 6095 mm. The built-up member consists of one stitch in the middle of its length, connecting the long legs of the two angles. Figure 4.11b schematically shows the *OpenSees* model of the double-angle brace. To model the components of the brace, various element types from the *OpenSees* element library are used:

- *nonlinearBeamColumn* element to simulate the individual angles and relatively Stiff *elasticBeamColumn* element to model stitch-fastener

- Relatively Stiff *elasticBeamColumn* element along with *zeroLength* element (rotational spring) to simulate the end-connection

- Relatively Stiff *elasticBeamColumn* element together with *zeroLength* element (axial spring) to reproduce the physical contact between the angles
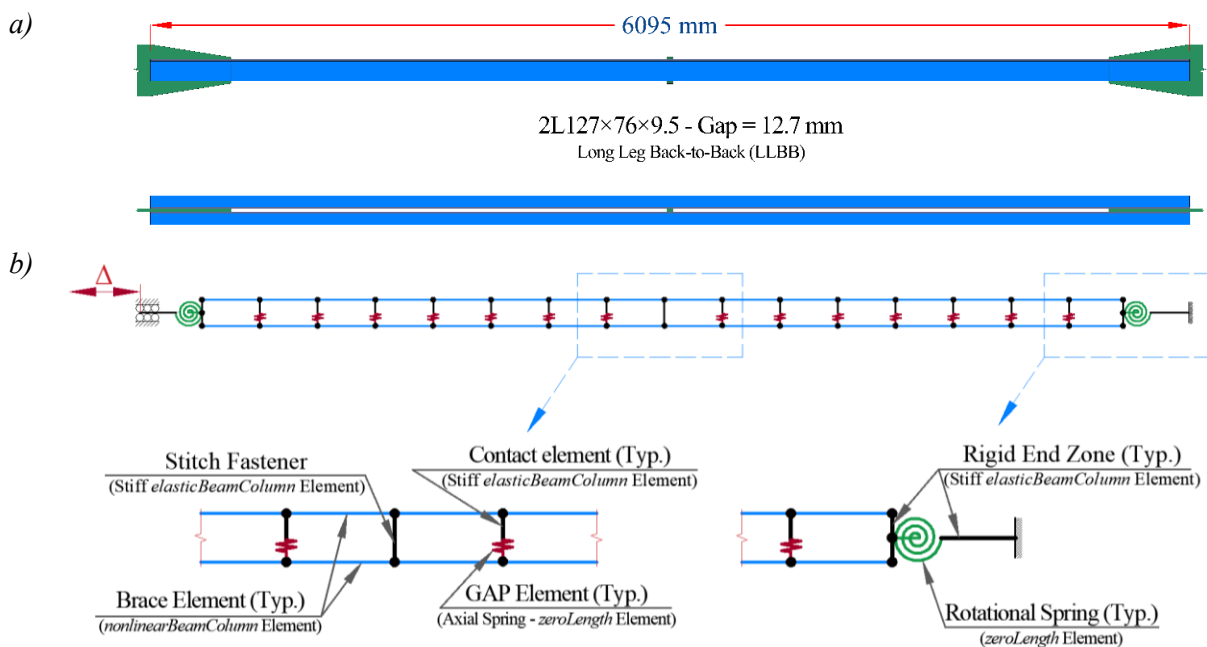
Figure 4.11. Model of the built-up double-angle: a) Brace configuration used in physical test and brace model elevation; b) Contact, Gap, and stitch-connector elements.

4.3.2.1 Individual Angles

As shown in Figure 4.11b, the individual angles are modelled using *nonLinearBeamColumn* elements and are assigned the corotational geometric coordinate transformation comprising P-Delta and large deformations. The centres of gravity of the two angles are connected using relatively stiff elastic elements (*elasticBeamColumn*) in the middle of the brace representing the only stitch connector used in the experiment and at the ends simulating the influence of the end-

connections. Large cross-sectional area and moments of inertia as compared to the brace are assigned to these elements to provide relatively large axial and flexural stiffness.

For the double-angle brace, two sources of instability are expected under a compression load: buckling of the built-up section as a whole, and buckling of individual single-angles between the stitch fastener and the end-connection. To initiate the global buckling modes, an IOS corresponding to a half-sine wave is assigned to the individual angles in the direction parallel to the short legs of the angles (Z-axis in Figure 4.10). The maximum amplitude of the sine-wave is equal to 12 mm that is 0.002 times the brace unbraced length, which agrees with the average value of misalignments measured in the experimental program reported by Jiang (2013).

The uniaxial *Steel02* material model with the parameters similar to those described in Section 4.2 is employed with a yield stress F_y = 336 MPa and Young's modulus, E, equals to 200 GPa, which are identical to the values measured in the experimental program (Jiang 2013).

4.3.2.2   End-Connections

As shown in Figure 4.11b, the end-connections of the double-angle are simulated using the modelling technique described in Section 2.6.5. The ends of the built-up section are fixed in flexure about both principal axes of the section. A translational fixity in the longitudinal direction, together with a torsional restraint, are assigned to one end of the brace. A rotational spring is implemented at each end of the brace using the *zeroLength* element to reproduce the nonlinear response of the end gusset plate connections, including their stiffness and strength when the brace buckles in the Z-axis (Figure 4.10) direction. The *Steel02* material is used for this purpose with the stiffness properties of the gusset plate. Elastic torsional stiffness of the gusset plate is assigned to the rotational spring to reproduce the torsional behaviour.

A finite element model of the end-connection is then created in SAP2000 (CSI 2009) using Shell elements to determine the elastic properties of the gusset plate connection. As shown in Figure 4.12, the connection is analyzed under a bending moment, M, applied about the Y-axis of the section (Figure 4.10) at the free end of the brace (Point A in Figure 4.12a). The flexural stiffness of the gusset plate is equal to $K_\theta = M / \theta$, where θ is the amount of rotation in the gusset-plate under the applied moment, measured at the end of the brace (Point B in Figure 4.12a).
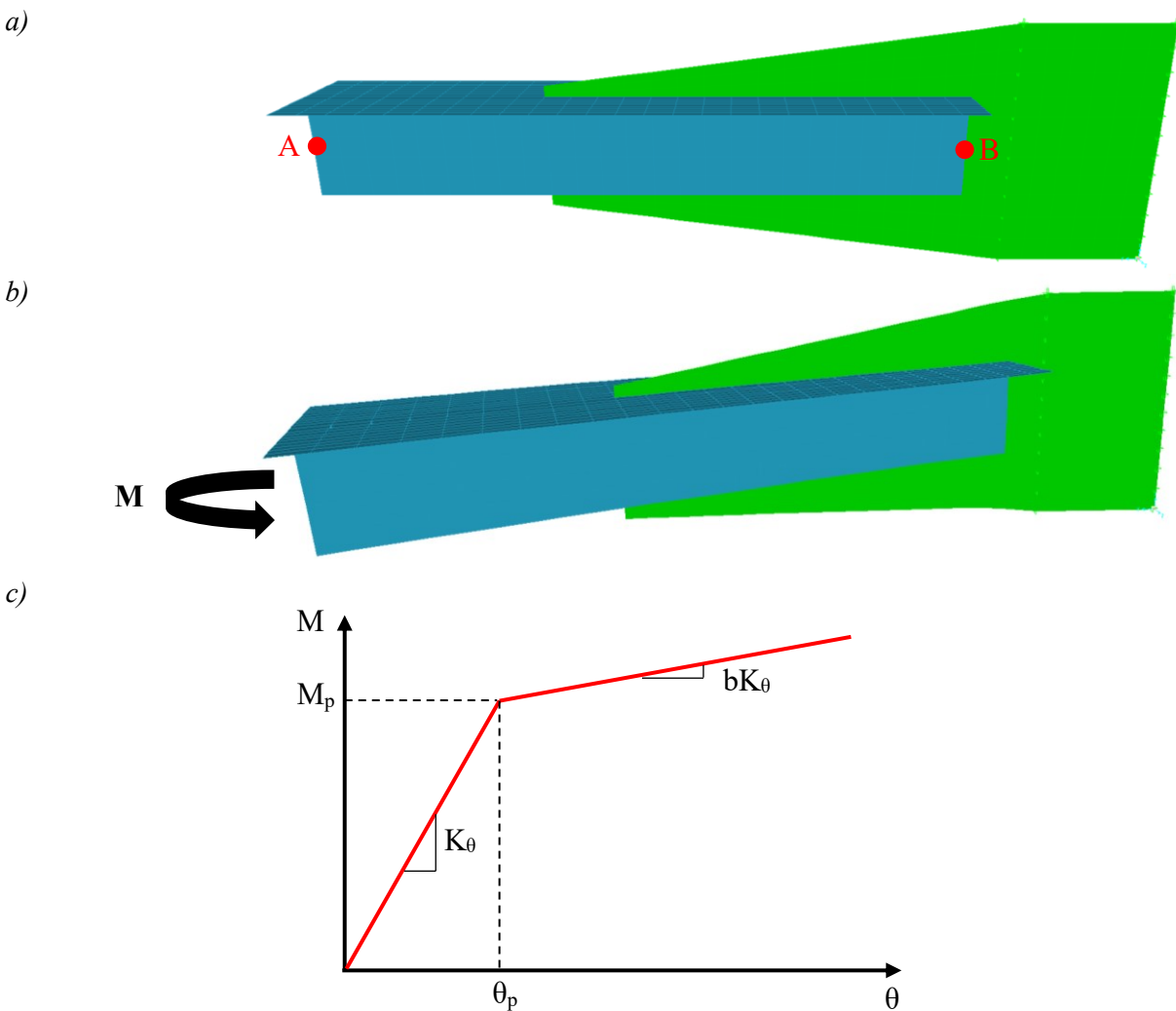
Figure 4.12. Finite element model of the double-angle brace end-connection: a) Undeformed shape; b) deformed shape under bending moment M. c) Moment-rotation response of the gusset plate connection assigned to OpsenSees model

Once K_θ is calculated using the finite element model, a spring represented by moment-rotation response shown in Figure 4.12c is assigned to the brace connections in the frame model in *OpenSees*. In the figure, M_p is the plastic moment of the gusset plate at point B, θ_p is the rotation corresponding to M_p, and b is the strain-hardening ratio parameter of the *Steel02* material model which is equal to 0.0067 for the material used in this study (see Section 4.2).

4.3.2.3 Physical Contact Between the Angles

A critical feature associated with modelling built-up members is to simulate the physical contact between two individual components. In order to simulate this phenomenon, two criteria should be considered:

1) The individual angles are fixed to one another at the locations of end-connections and stitch fasteners to ensure that the angles are not entirely separated during the loading.

2)   The remaining parts of the angles stay free to touch one another or separate from each other under applied loads.

As shown in Figure 4.11b, the first constraint is carried out in the model by tieing the nodes of two single-angles using Stiff *elasticBeamColumn* elements. For the brace nodes outside the stitch fasteners and end-connections, Contact elements (Stiff *elasticBeamColumn* elements) are used together with Gap elements, as shown in Figure 4.11b.

The Gap element is simulated using a translational spring (*zeroLength* element) with an Elastic-Perfectly Plastic Gap (*ElasticPPGap*) material or merely "Gap material", as shown in Figure 4.13. Relatively high yield stress is assigned to the Gap material with Young's modulus of 200 GPa so that it remains elastic during the cyclic loading.
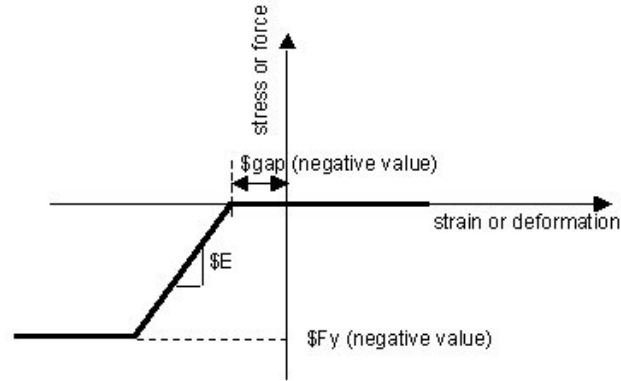
Figure 4.13. Elastic-Perfectly Plastic Gap (ElasticPPGap) material (Mazzoni et al. 2006)

As shown in Figure 4.13, the Gap elements implemented in the model deform only under the axial compression load. This feature allows the nodes at both ends of a Gap element to move inwards when single-angles buckle individually, which causes contraction in the Gap element. However, no load is induced in the Gap element, while the brace nodes are getting closer to each other until the contraction amplitude exceeds a predefined value corresponding to the back-to-back clear distance between the angles. Beyond this point, the Gap element develops axial forces and negligible elastic contraction, which prevents further significant inward movement of its end nodes.

Since the *zeroLength* elements used to model the Gap can only connect two nodes with the same coordinates (i.e. the element length is zero), Contact elements, which are Stiff *elasticBeamColumn* elements, are required to attach the centre of gravity of an angle to one end of the Gap element (see Figure 4.11b). Once any of the Gap elements under the compression load reaches a displacement equal to its predefined value, the Contact element connected to that Gap element is engaged. This resembles the case where two angles physically touch each other upon buckling of each component individually.

The model of the double-angle was verified to ensure that the combination of the Contact and Gap elements can appropriately simulate the physical contact between the individual angles. To do so, the double-angle was subjected to gradually increasing longitudinal displacement of 150 mm to create a compression load in the member. Figure 4.14a shows the deformed shape of the double-angle model at the end of the analysis. As expected, the angles remained untouched at the location of the end-connections and the stitch-fastener, and were free to touch one another everywhere else. The displacements of the sperate angles in the Z-axis (Figure 4.10) direction were recorded at each node along the member. The relative deformation of each angle was then achieved by subtracting the displacement of each node on one of the angles from that of the adjacent node on the other angle (Figure 4.14b). As shown, the quantities vary from zero to -12.7 mm on the negative side, and +30 mm on the positive side. Zero represents no relative displacement between the two angles as expected in the stitch fastener and end-connections. A negative value means the angles moved towards one another, and 12.7 corresponds to the clear distance between the angles; hence, a value of -12.7 in the figure shows that the angles came into a complete contact. The positive number, however, means the angles were separated from each other. The results of the analysis confirmed that the model is able to adequately simulate the physical contact between the angles upon buckling.
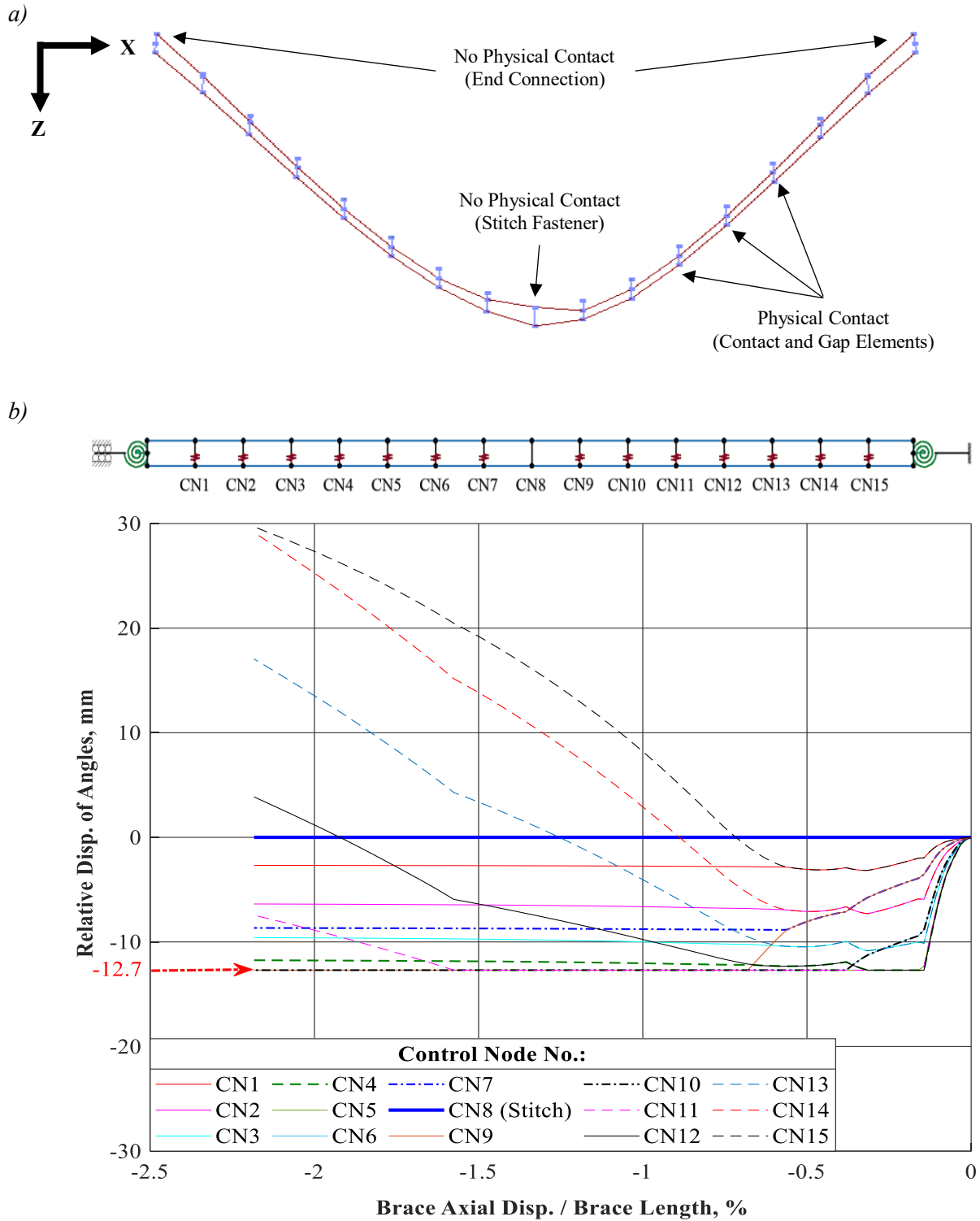
Figure 4.14. Simulation of the physical contact between the components of the built-up double-angle: a) deformed-shape of the double-angle under at buckling; b) relative displacement of the individual angles in Z-axis direction.

Also shown in Figure 4.15a and Figure 4.15b, the deformed-shape obtained from two undesirable alternatives of the double-angle model without the consideration of the modelling techniques described here. In the first case (Figure 4.15a), Contact and Gap elements were both excluded from the model to demonstrate their effectiveness, which caused the individual angles to pass over each other. The second case (Figure 4.15b) shows the deformed-shape of a double-angle with only Contact elements in which both angles worked entirely as a unit, similar to the case of having stitch connectors over the full length of the brace. These alternative models were built to reaffirm the modelling techniques used in this study to reproduce the cyclic inelastic response of double-angle braces. As a result, it was confirmed that when the Contact and Gap elements are properly simulated, as shown in Figure 4.11, the components of the built-up member are expected to touch each other upon buckling where there is no stitch fastener. Similar to single-angle brace model, the effect of torsional buckling, which affects the stability response of double-angle braces, is ignored when using the fibre-based elements in *OpenSees*.
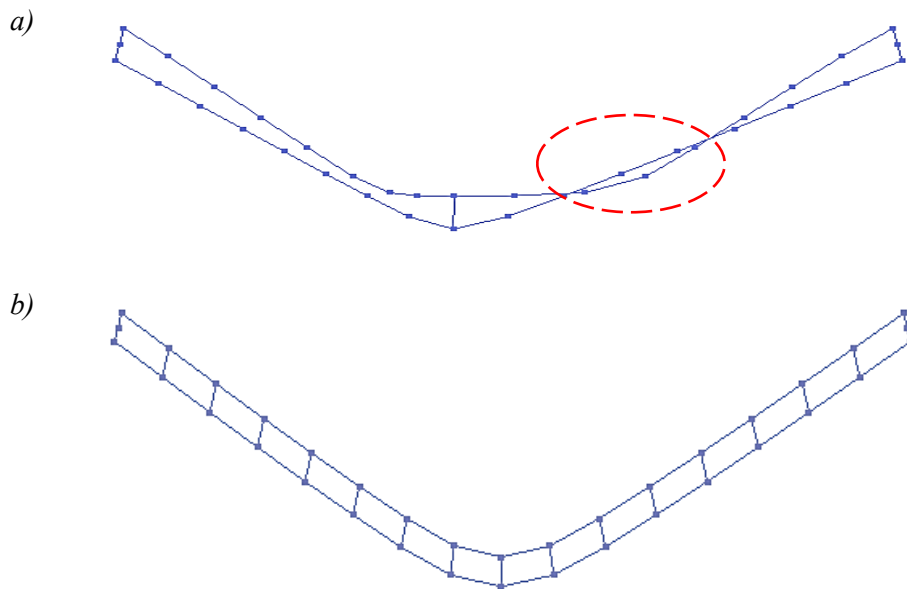
Figure 4.15. Undesirable deformed-shape of a double-angle brace at buckling: a) in the absence of Contact and Gap elements; b) when only Contact elements present.

4.3.2.4 Double-angle Model Calibration Against Hysteretic Test Data

To calibrate the cyclic inelastic behaviour of the isolated double-angle model, the results of the experimental test program performed by Jiang (2013) was used. The loading protocol used in this study is shown in Figure 4.16.
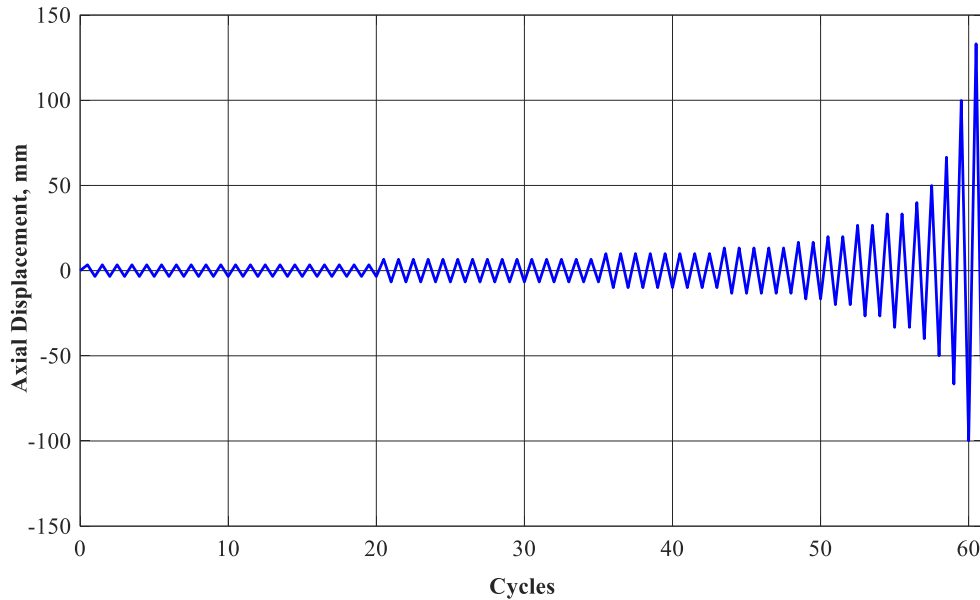
Figure 4.16. Double-angle brace displacement sequence adopted from (Jiang 2013).

Comparison between the brace hysteretic response obtained from the experimental test and that from the static analysis under incrementally increasing cyclic displacement is shown in Figure 4.17 with tension force shown positive. In the figure, the brace was normalized by the yielding capacity of the brace, AF_y, where A is the cross-sectional area of the brace and F_y is the steel material yield strength measures in the test.
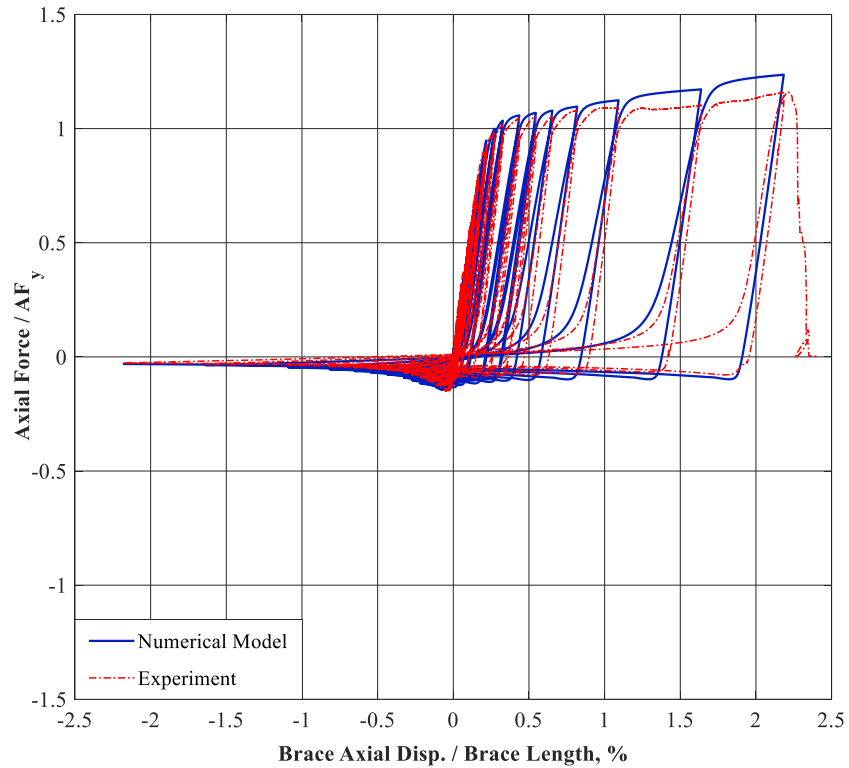
Figure 4.17. Hysteretic response of the double-angle brace made of 2L127×76×9.5 (LLBB).

As shown, an excellent agreement is observed between the results of the experimental test and the numerical model, which suggests that the fibre-based numerical model of the double-angle brace can appropriately predict the nonlinear cyclic response of the brace including tensile yielding, hardening, strength and stiffness degradations due to global buckling. Additionally, the brace compression capacity was calculated according to CSA S16-14 using the equivalent slenderness ratio, as described in Section 2.5.3. The compression capacity normalized by AF_y is equal to 0.14, which is in a good agreement with the normalized brace buckling load obtained from the experimental test and the numerical model (i.e. 0.15 and 0.15) reassuring the prediction obtained from the numerical model.

4.3.3 HSS column

HSS column is selected for Type CC frames with T/O braces, as shown in Figure 3.1. To validate the modelling of HSS columns, the fibre-based model of an isolated pinned-ended column is first created, and a nonlinear static (pushover) analysis is conducted by subjecting the column to an incrementally increasing axial dispalcement to reproduce its buckling response in the presence of a bending moment. For this purpose, an HSS228.6×228.6×9.5 made of ASTM A500 Gr. C steel with F_y = 345 MPa and a length of 10 m is selected. Similar to the HSS brace model, residual stresses are not assigned to the HSS column model, as it is believed to have minimal effect on the buckling behaviour of HSS members. The column is divided into ten elements to reproduce global buckling, as suggested by Aguero et al. (2006). Additionally, a half-sine-shaped IOS is applied to the column to initiate the buckling with two maximum amplitudes at the middle of the member equal to 0.001L and 0.002L, where L is the total length of the member.

The bending moment is first applied, to one end of the column, followed by an incrementally increasing axial displacement until column instability occurs. The analysis is repeated seven times with various moment amplitudes. The buckling load of the column, C_f, is then obtained from the model. The axial compression force – bending moment (P-M) interaction curve of the member is then plotted using the results obtained from the numerical model and compared with the one specified by CSA S16-14 (Figure 4.18). In this plot, M_p is the plastic moment of the section and C_r is the compression capacity of the member calculated using CSA S16-14 equation for members in compression. C_r is computed using an effective length factor K = 1.0 and the resistance factor ϕ of unity. To account for the P-δ effects in the member, the U_1 factor is calculated according to CSA S16-14.

As shown in the figure, overall, the *OpenSees* model overestimated the P-M capacity of the HSS column, which could be attributed to:

- definition of material strain hardening in the model,

- neglecting residual stresses,

- neglecting the higher material yield stress in the corners of the HSS,

- ignoring local buckling in the fibre-based elements used for the simulation,

- the fact that the code interaction equation has been developed based on the best fit to the experimental data.

The prediction by the model with IOS = 0.002L was found to be closer to the CSA S16-14 prediction. Hence, IOS=0.002L is used in the braced frame model for the HSS columns.
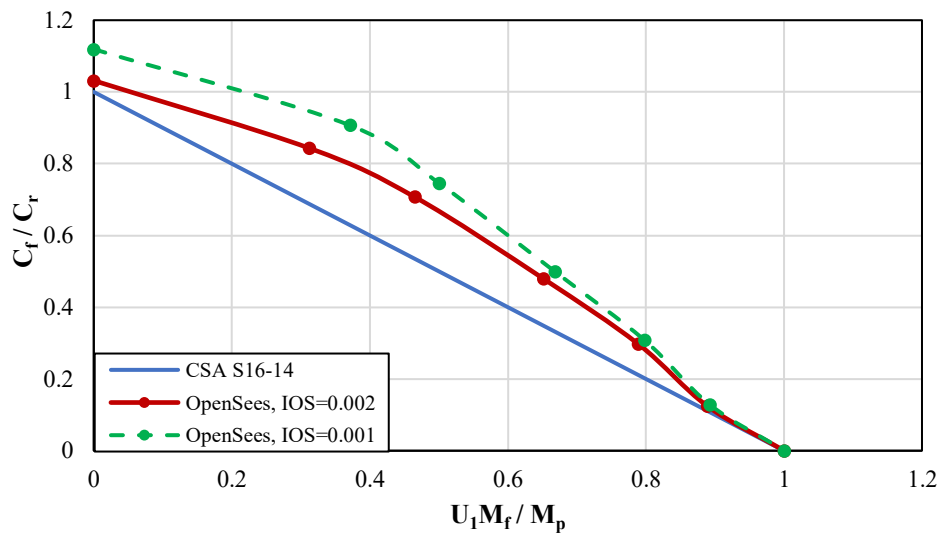
Figure 4.18. HSS column P-M interaction.

4.3.4 Braced Frame Numerical Model

A three-dimensional (3D) fibre-based numerical model capable of simulating the seismic response of low-ductile multi-tiered concentrically braced frames shown in Figure 4.19 is developed in the

OpenSees software framework. Figure 4.19a shows the 3D view of the model of a two-tiered braced frame with double-angle braces; the elevation of the frame is shown in Figure 4.19b. The numerical models of the prototype frames with single-angle and HSS braces are identical to this model, except for the braces as they do not consist of Contact and Gap elements. The techniques and assumptions used in modelling the braced frame mimic those used for individual members.

a)
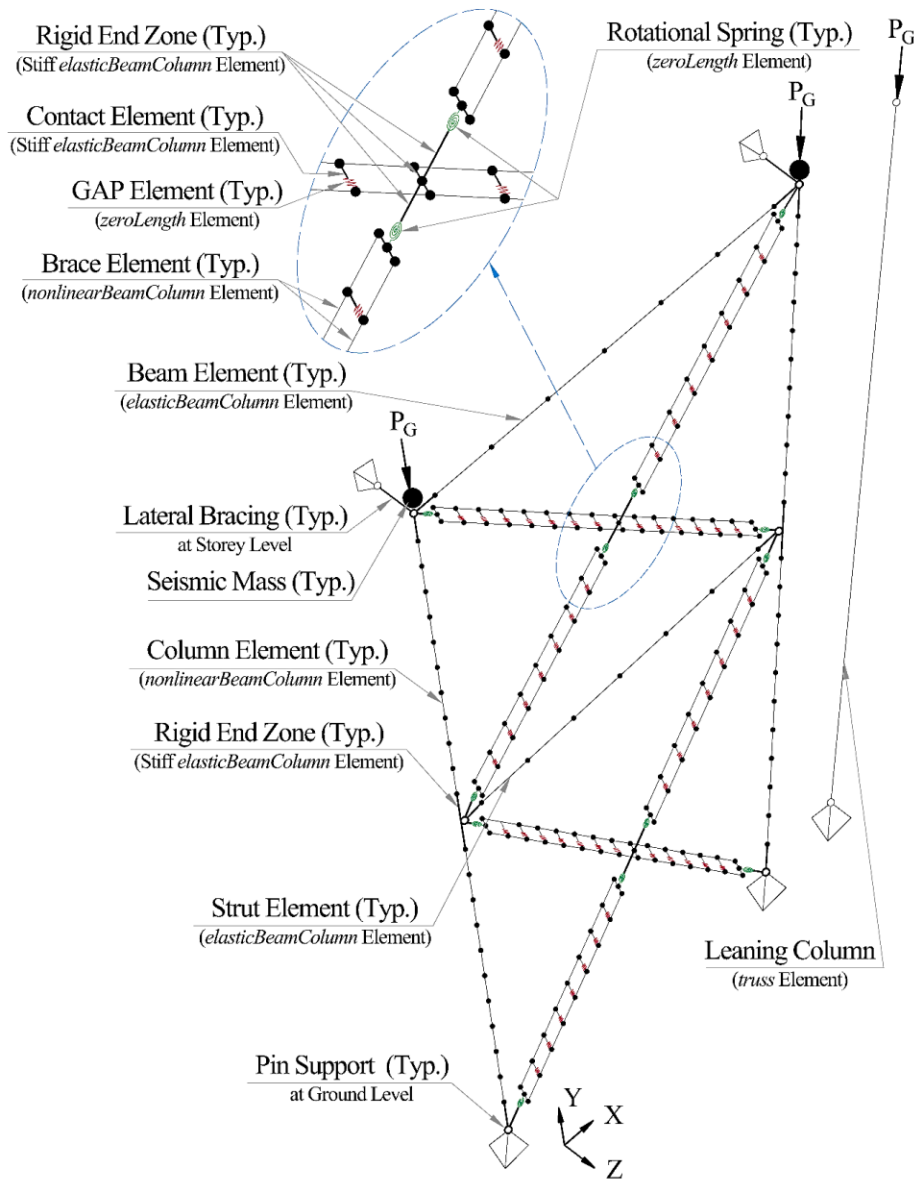
Figure 4.19. Fibre-based numerical model of a two-tiered CBF with double-angle braces: a) 3D model; b) X-Y elevation.
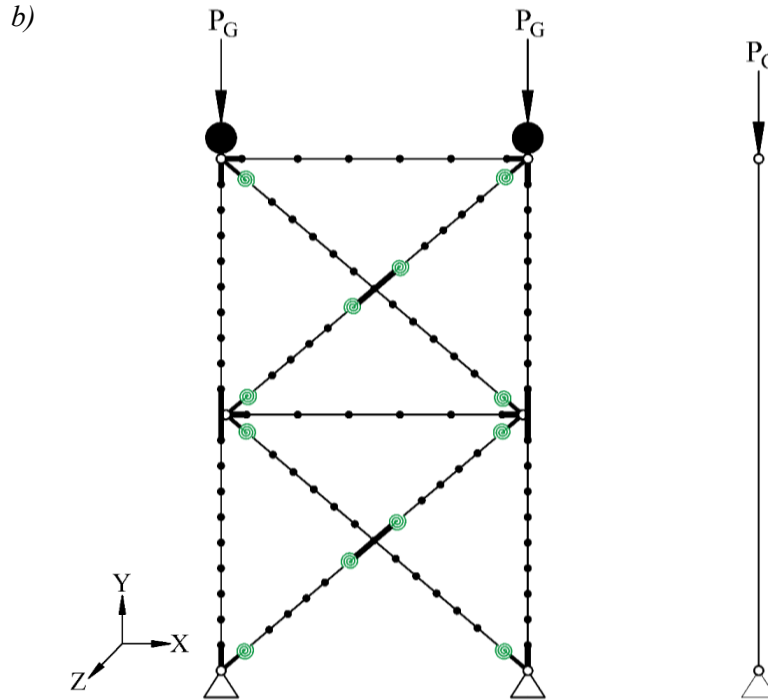
Figure 4.19. Schematic of the fibre-based numerical model of a two-tiered CBF with double-angle braces: a) 3D model; b) X-Y elevation. (Continued)

4.3.4.1 Boundary Conditions and Connections

As shown in Figure 4.19, the braced frame columns are pined at their base and laterally braced in the out-of-plane direction at their top ends, simulating the lateral restraint provided by the roof truss in the perpendicular direction. The beam and struts are pin-connected to the columns.

Brace-to-column and brace-to-brace connections are modelled using the technique described in Section 2.6.5. The out-of-plane flexural stiffness and strength of the gusset plate is assigned to the rotational springs (*zeroLength* elements). The thick lines in Figure 4.19 represent *elasticBeamColumn* elements with a stiffness corresponding to the properties of the beam or brace connection used to reproduce connection sizes. The lengths of the rigid links are set to match the connection geometries obtained from the connection design.

The gravity load tributary of the braced frame columns, P_G, (see Section 3.4) is applied at the top end of the columns, as shown in Figure 4.19. Additionally, as shown, the building seismic weight (see Section 3.4) tributary of the braced frame is assigned as lumped masses to the top of the columns.

4.3.4.2 Elements

The braces and HSS columns are modelled using *nonlinearBeamColumn* elements with fibre-discretization of the cross-sections, as described in Sections 4.3.1 to 4.3.3. The wide-flange columns are simulated using the method described in Imanpour et al. (2016a). The inelastic buckling response of wide-flange steel columns, simulated using *nonlinearBeamColumn* elements in *OpenSees*, was validated in the past (Lamarche and Tremblay 2011, Imanpour 2015). 16 elements are used along the length of the braces and 10 elements for the columns over the height of each Tier. The beam and struts are simulated using six *elasticBeamColumn* elements to improve the computational efficiency of the model since they are not expected to experience nonlinear behaviour.

For double-angle braces, Contact and Gap elements are used to reproduce the physical contact between the components of the built-up member following the technique and assumptions described in Section 4.3.2.

4.3.4.3 Material

The material model assigned to the braces and columns of the braced frame is as described in Sections 4.3.1 to 4.3.3. The beam and strut modelled using elastic elements are assigned an elastic material with Young's modulus equal to 200 GPa.

The probable yield strength (R_yF_y) of the braces of the critical tiers, as determined in Table 3.6, Table 3.10, and Table 3.15, along the height of the frame is reduced by 10% to trigger yielding first in that panel, while accounting for plausible variabilities in the material, geometry, and end-conditions expected in actual frames. Examples of such variabilities in braces are the material yield stress (Schmidt and Bartlett 2002), the initial out-of-straightness, the cross-sectional area, member length, and end or middle connections. It is worth mentioning that although the discrepancy of the measured yield stress for HSS braces is higher than angles, for consistency between the braced frames studied here, a 10% reduction in R_yF_y value is used for all brace sections. Although a reduction in R_yF_y of the braces slightly reduces brace forces induced in columns, beams, and struts, it is deemed unrealistic to increase R_yF_y in the critical tier as the test data (Schmidt and Bartlett 2002) showed that the measured yield strength of HSSs on average is expected to be lower than the upper bound value of R_yF_y given in CSA S16.

4.3.4.4   Initial Out-of-Straightness

To trigger the global buckling of braces and columns, sinusoidal IOS is assigned to the members in the model. As shown in Figure 4.20a and Figure 4.20b for a three-tiered braced frame example, sinusoidal IOS corresponding to the first in-plane and out-of-plane buckling modes of the columns are considered (both frame-columns are assigned same IOS). For braces, however, a full sin-wave IOS is applied only in the out-of-plane direction (Figure 4.20c), because the brace-to-column connections are designed to trigger buckling out-of-plane.

For the braces, the maximum amplitude of the sinusoidal shape has been adjusted (as described in Sections 4.3.1 and 4.3.2) such that an accurate estimation of the brace buckling load is obtained when compared to the available experimental test data or code-specified buckling force. Thus, the

single-angle braces are assigned a maximum IOS of 0.001 times the member length, whereas 0.002 times the member length is assigned to the double-angle and HSS braces.

A similar approach is taken for HSS and wide-flange columns, for which the maximum IOS amplitude assigned in the middle of their unbraces length, are respectively 0.002 and 0.001 times the unbraced length. The unbraced length of the column is defined as its total length for out-of-plane buckling and the tier heights for in-plane buckling.

a)   b)   c)

Tier 3

Tier 2

Tier 1
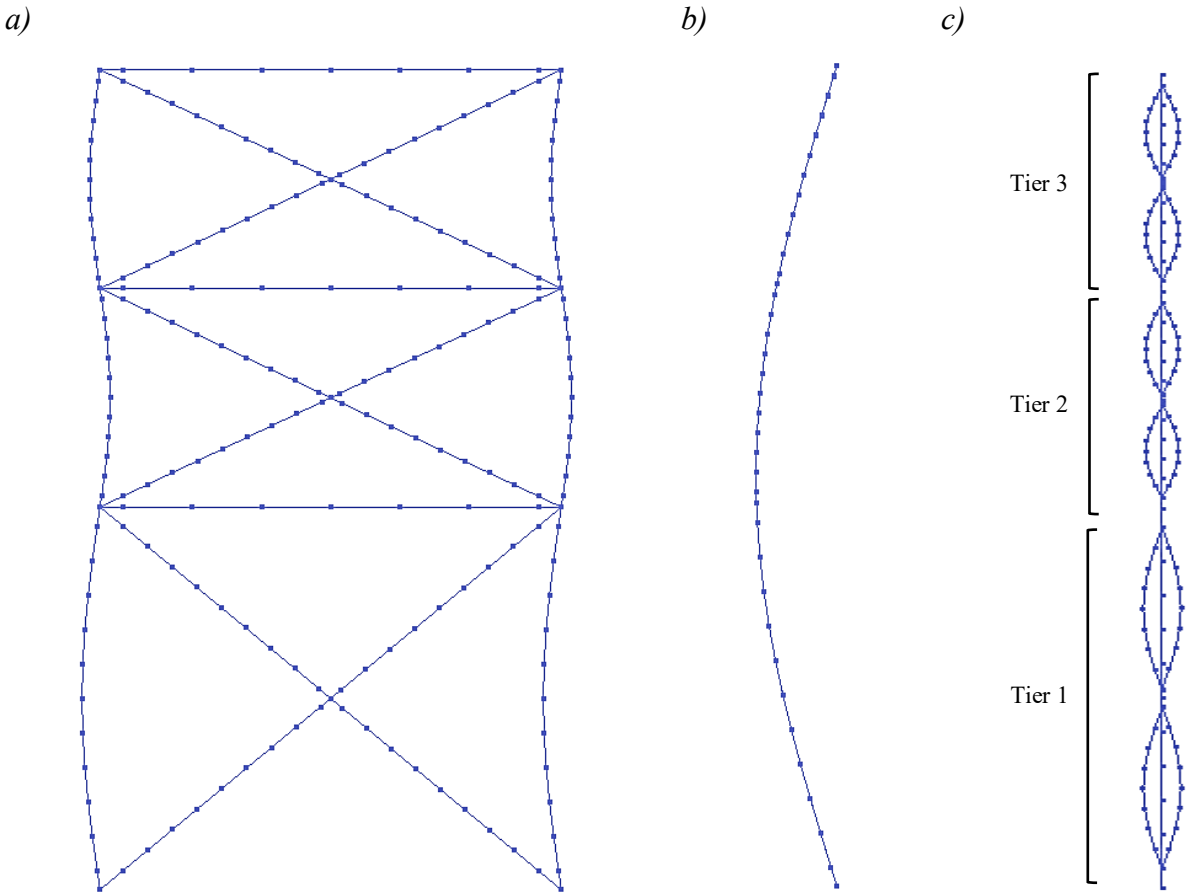
Figure 4.20. Initial out-of-straightness pattern: a) column in-plane; b) column out-of-plane (one of the columns shown); c) brace out-of-plane (amplitudes magnified for the illustration purpose).

4.4 Geometric nonlinearity and P-Delta effects

A corotational formulation that accounts for P-Δ effects and large deformations is employed in the model. As shown in Figure 4.19, a leaning column is included in the model to account for large P-Δ effects developed by the portion of the gravity loads of the adjacent gravity-load resisting system tributary to the braced frame. The leaning column is simulated by an elastic *truss* element with relatively large axial and flexural stiffness. Pinned base condition is considered for the leaning column to ensure that it does not contribute to the lateral stiffness of the system. The horizontal translations (X and Z) of the top end of the leaning column are constrained to the braced frame roof, while the vertical translation (Y) and all three rotational degrees of freedom remain free.

4.5 Nonlinear incremental static (pushover) analysis

Nonlinear static (pushover) analyses are first performed on two of the selected frames, LD_W_HSS_16_2_1.0 and CC_HSS_L_24_4_1.75, by incrementally increasing the lateral displacement at the roof level. The maximum lateral displacement applied to the roof is 3% times the height of the frame, $0.03h$. The purpose of these analyses is to assess the overall seismic behaviour of the selected frames and examine the capability of the model to simulate the key response parameters under seismic loading. The case studies are selected so that they cover the majority of the parameters introduced in the parametric study. Pushover analysis can provide a good understanding of the lateral response of such single-storey multi-tiered braced frames. Because, when subjected to dynamic loading, a single-storey MT-CBF acts as a single-degree-of-freedom system with masses lumped at the roof level. A pushover analysis can also provide insight into the capability of the numerical model in predicting the overall frame response and inelastic response of the frame components.

4.6 Nonlinear response history analysis

A set of Nonlinear Response History (NLRH) analyses is conducted on the selected braced frames of the parametric study matrix (see Figure 3.1). The dynamic analysis is performed under 30 ground motion records imposed on the frame in the horizontal direction.

4.6.1 Earthquake ground motion

Ground motion time histories are selected and scaled in accordance with the 2015 NBCC (NRC 2015) using the procedure described by Tremblay et al. (2015) to match the design response spectra of the selected site (Montreal Soil Type C). A database of 180 ground motion accelerations consisting of historical (Ancheta et al. 2014) and simulated (Engineering Seismology Toolbox, www.seismotoolbox.ca) ground motions are first selected using NBCC seismic hazard deaggregation (Halchuk and Adams 2004). Two magnitude-distance (M-R) scenarios identified by Atkinson (2009) for the selected site of the building are considered: 1) M6 events having a fault distance ranging between 10 and 30 km, and 2) M7 events occurring at greater distances between 20 and 70 km. For each ground motion record, two ratios are then calculated:

- the ratio between $S_T(T)$ that is the target response spectrum as specified in NBCC; and

- $S_g(T)$ that is the 5% damped pseudo-acceleration spectrum of the individual ground motion component.

The mean and standard deviation of the computed ratios, $S_T(T)/S_g(T)$, over the period range corresponding to the fundamental period of the selected frames are used to select the final suite of ground motions, meaning that 30 records having the lowest standard deviation and mean of $S_T(T)/S_g(T)$ are chosen. The mean value of $S_T(T)/S_g(T)$ for each ground motion record is finally utilized as the first scaling factor. A second scaling factor is calculated so that the mean response

spectrum of each scenario suite of time histories does not fall more than 10% below $S_T(T)$ over the corresponding period range. The response spectra of the individual scaled ground motions are plotted in Figure 4.21.
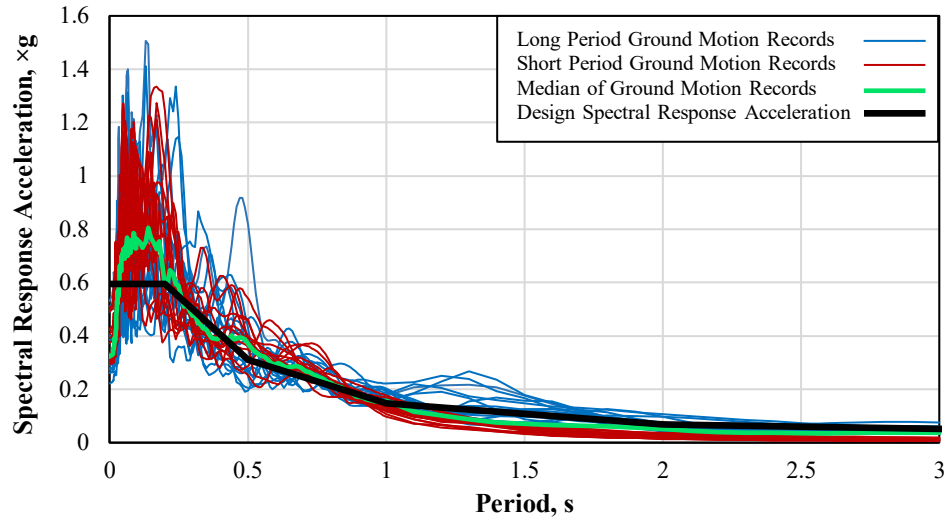
Figure 4.21. Scaled response spectra of the selected ground motion records.

4.6.2 Inertia and damping definitions

As shown in Figure 4.19, lumped masses representing the inertia forces tributary of the braced frame are assigned to the top end of the columns. Rayleigh damping method is employed to construct the classical damping matrix. In Rayleigh damping, a linear combination of mass and stiffness matrices are used to define damping with mass-proportional and stiffness-proportional coefficients. As given in Equation (4.1, the damping matrix, *C*, is composed of two terms: mass-proportional damping, αM, and stiffness-proportional damping, βK (Chopra 2005). For a single-degree-of-freedom system, $\alpha = 2\xi\omega$ and $\beta = 2\xi / \omega$, where ξ is the critical damping ratio, and ω is the natural frequency of the structure. The critical damping ratio for standard steel structures, ξ, is recommended to be taken 0.02 (Naeim 1989).

$$C = \alpha M + \beta K \qquad\qquad\qquad\qquad\qquad\qquad (4.1)$$

Figure 4.22 shows how super-positioning of the mass proportional damping and stiffness proportional damping results in Rayleigh damping for various angular frequencies.
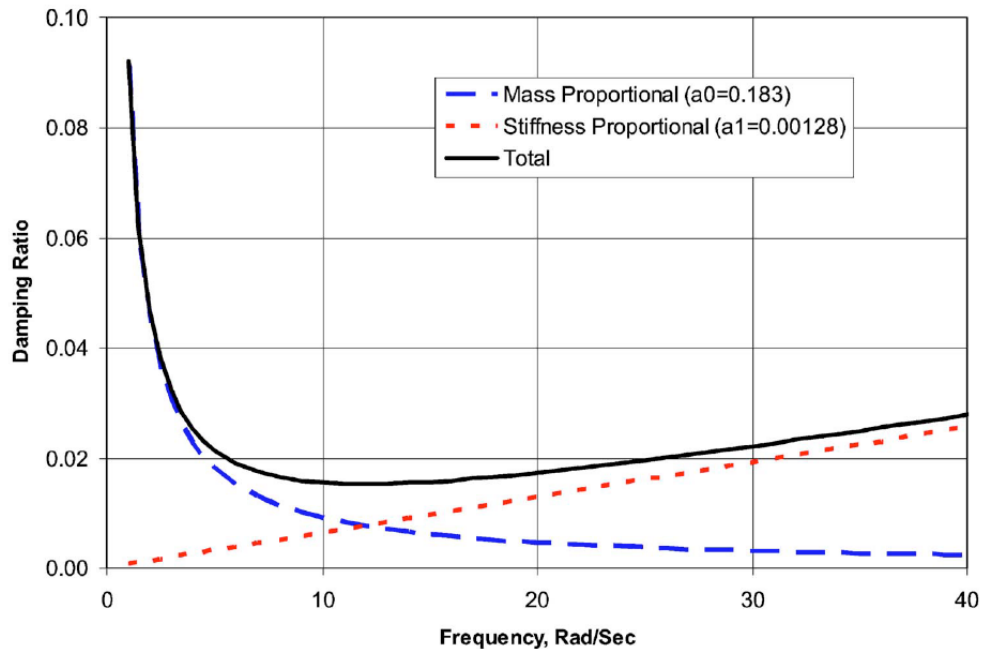
Figure 4.22. Rayleigh damping (Charney 2008).

Past studies (Bernal 1994, Medina and Krawinkler 2004, Hall 2006, Zareian and Medina 2010) showed that calculating Rayleigh damping using the initial stiffness matrix, causes unrealistic damping forces in the structural elements that experience sudden stiffness changes such as braces in the current study. The reason is that as soon as the stiffness of the elements varies throughout the inelastic response, the degrees-of-freedom with small inertias tend to experience rapid variations in velocity (Bernal 1994). Consequently, undesirable damping forces are generated at those degrees-of-freedom, which in turn result in an underestimation of the displacement demands in the structure (Medina and Krawinkler 2004). Instead, it is recommended that the tangent (i.e. modified to account for material and geometric nonlinearity) stiffness matrix of the structure be

employed. Nonetheless, updating the stiffness matrix at each step of the analysis to obtain the tangent stiffness matrix is computationally expensive, and often leads to convergence issues (Zareian and Medina 2010).

Advanced structural analysis programs are capable of creating the damping matrix based on the approaches described here. *OpenSees* is one of the programs capable of creating damping using all three methods (Charney 2008).

A comparative study is performed to evaluate the influence of various damping parameters when using Rayleigh damping definition. To examine the response of the structure, the roof displacement of a two-tiered CBF (Frame LD_W_HSS_10_2_1.0) is compared when implementing Mass Proportional Damping (MPD) plus Initial Stiffness Proportional Damping (ISPD) and Tangent Stiffness Proportional Damping (TSPD) versus the case where only the mass proportional damping is considered (Figure 4.23).

As shown in Figure 4.23, when Rayleigh damping includes TSPD, a numerical convergence issue halted the NLRH analysis under both of the ground motions (the red curves Figure 4.23). The other two approaches to apply damping were successful. The damping matrix created by the inclusion of the MPD+ISPD coefficients resulted in an underestimation in the roof displacement of both frames, which agrees with the results reported by Medina and Krawinkler (2004). Hence, the damping definition using only MPD is found to be an acceptable option in this study to avoid underestimation of the demands on the frame while ensuring smooth convergence in NLRH analyses.
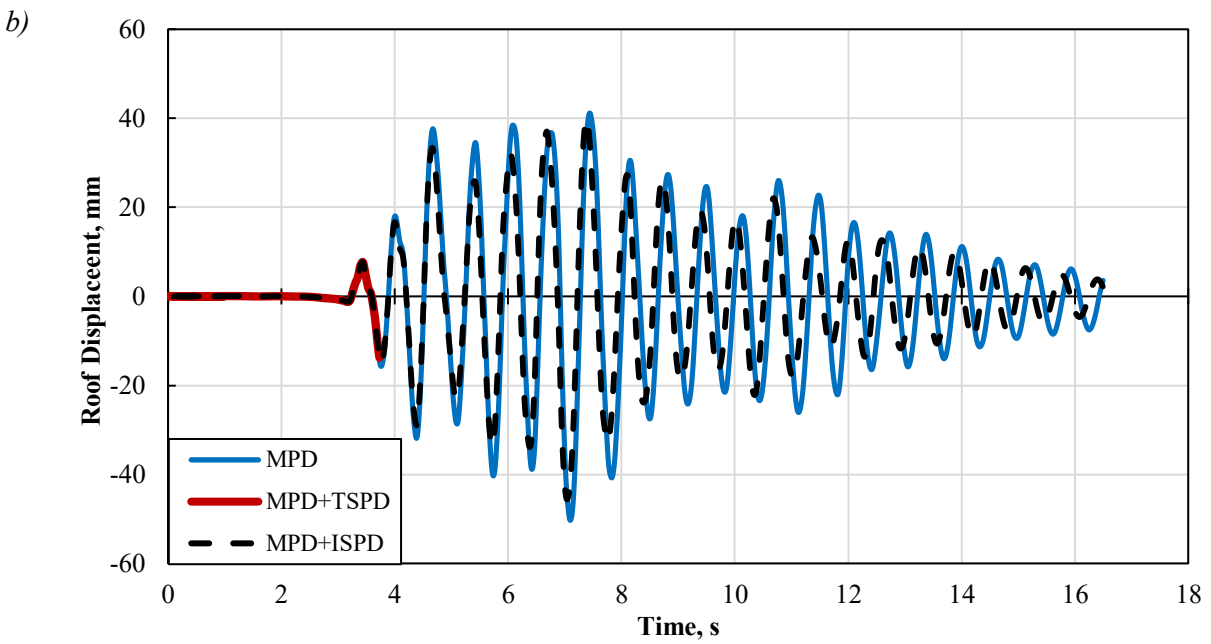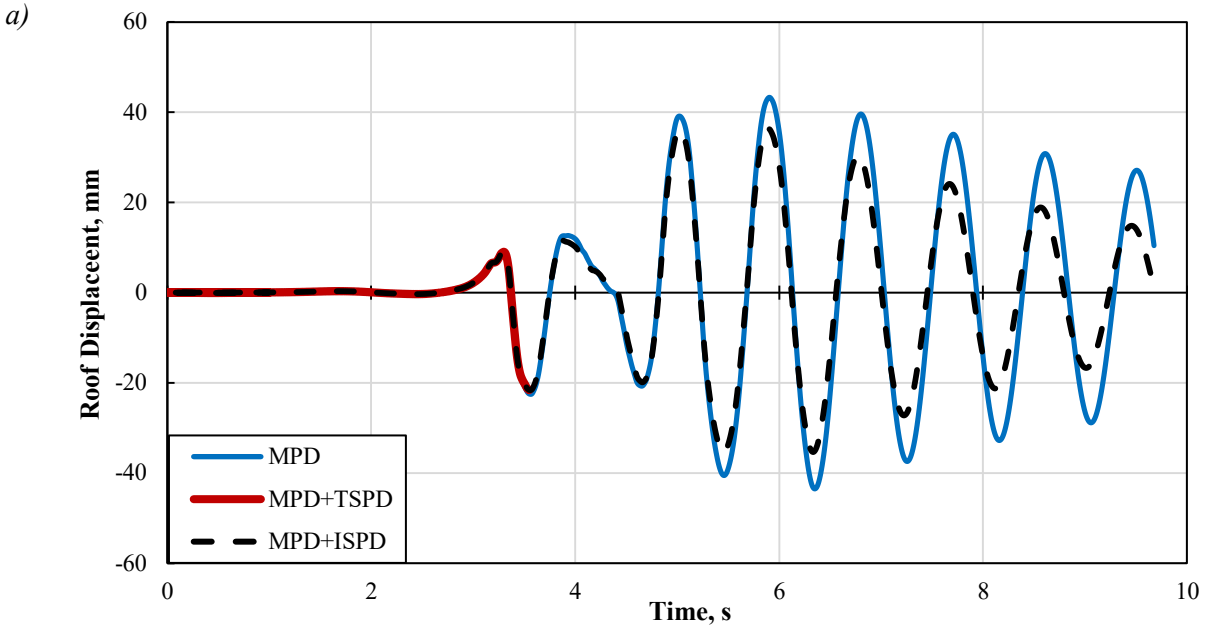
Figure 4.23. Roof displacement of frame LD_W_HSS_10_2_1.0 using three damping definitions under a) a short-period ground motion record, and b) a long-period ground motion record.

Chapter 5: Seismic Response of Steel MT-CBFs

5.1   Introduction

This chapter first presents the results of nonlinear static (pushover) analyses conducted on two braced frames, including a Type LD two-tiered braced frame with W-shape columns and T/C HSS braces and a Type CC four-tiered braced frame with HSS columns and T/O single-angle braces (see Section 3.3). The results obtained from the Nonlinear Response History (NLRH) analysis performed on frames of Figure 3.1 are then presented.

5.2   Nonlinear Static (Pushover) Analysis Results

The pushover analysis was performed on two selected braced frames: LD_W_HSS_16_2_1.0 and CC_W_HSS_L_24_4_1.75. This analysis was used to examine the lateral performance of the frames and access the buckling response of braces and columns. The key response parameters of the selected frames obtained from pushover analyses are presented here, including base shear, tier drifts, brace axial forces, and column demands. A gradually increasing lateral displacement with a maximum of $0.03h$, where h is the total frame height, was applied at the roof level of the selected frames. It should be noted that the applied lateral displacement is higher than the anticipated storey drift of the frames; however, the goal of the analysis was to examine the frame overall lateral performance while verifying the model capability in predicting the buckling response of braces and columns.

5.2.1 Lateral Response of Frame LD_W_HSS_16_2_1.0

Figure 5.1a to Figure 5.1g show the results obtained from the pushover analysis for LD_W_HSS_16_2_1.0. The frame base shear versus the storey drift (pushover curve) is shown in Figure 5.1a. Three key points can be characterized: buckling of compression-acting braces, yielding in the tension-acting brace of the critical tier, and buckling of the compression column. As explained in Section 4.3.4.3, to trigger brace tensile yielding in one of the tiers (i.e. critical tier) of frames with identical tier heights, including LD_W_HSS_16_2_1.0, the first tier was intentionally weakened by reducing the probable yield stress of the braces in that tier by 10%. Up to a drift of approximately 0.35%, the frame responded in the elastic range. At that point, the compression-acting brace of both tiers buckled. The tension-acting brace in the first tier then yielded at a drift of 0.65%, and despite a slight increase due to the strain-hardening effect, it maintained its tensile capacity. The storey shear resistance of the frame reduced beyond this point because of large strength degradation in the compression brace of the first tier as the tension brace elongates (Figure 5.1c). Tension brace yielding in Tier 1 capped the shear resistance of the frame (Figure 5.1a) and prevented tensile yielding of the tension brace and strength degradation of the compression brace in Tier 2 (Figure 5.1c). The normalized axial demands of braces in both tiers are given in Figure 5.1c. This response led to a large inelastic drift concentration in Tier 1 (Figure 5.1b), which in turn resulted in flexing the column in a single-curvature in the plane of the frame. The column in-plane curvature kept increasing as the lateral displacement increases. This large in-plane bending moment (Figure 5.1e) combined with large axial compression force due to gravity and brace axial forces finally led to column flexural buckling in the plane of the frame, as shown in Figure 5.1f at a drift of 2.56%. As depicted in Figure 5.1g, the column buckling mode was then changed to out-of-plane due to the lack of out-of-plane bracing in the strut level and the presence

of initial geometric imperfections in the out-of-plane direction. The drift response shown in Figure 5.1b confirms that large inelastic deformations concentrated in Tier 1; however, drift in the second tier remained nearly the same as the roof displacement increases.

The results obtained from the pushover analysis agree with similar results reported in the past studies on high-ductile MT-CBFs (Imanpour et al. 2016b, Cano 2019). In particular, out-of-plane buckling of braces is well reproduced, and the biaxial buckling response of wide-flange columns under the axial compression force and biaxial bending moments is appropriately predicted.
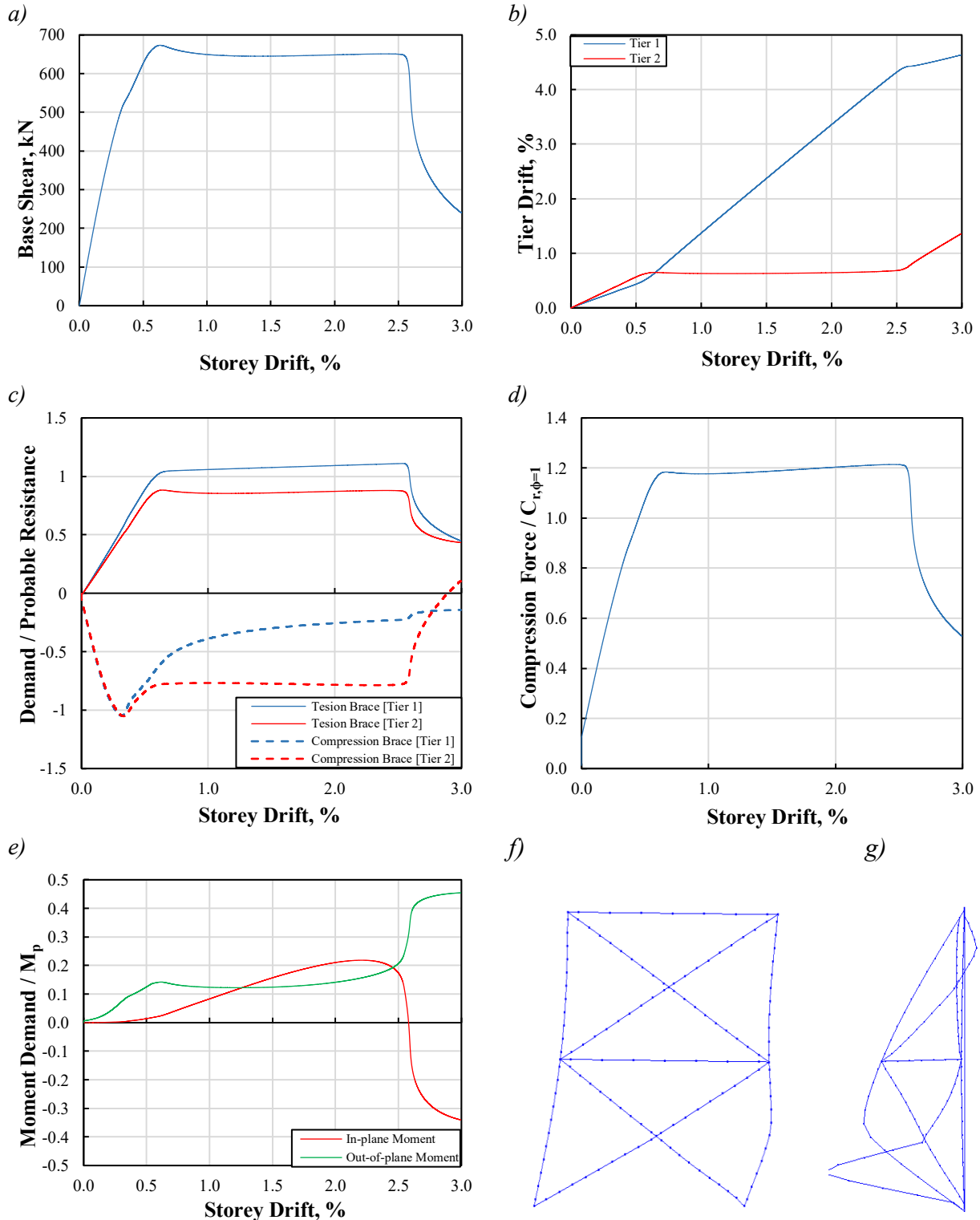
Figure 5.1. Pushover analysis of frame LD_W_HSS_16_2_1.0: a) base shear; b) tier drifts; c) brace tension and compression demands normalized to the probable resistances; d) column axial force demand normalized to the design force; e) column moments normalized to its plastic moment; f) in-plane deformed shape at 3% storey drift; g) out-of-plane deformed shape at 3% storey drift.

5.2.2 Lateral Response of Frame CC_W_HSS_L_24_4_1.75

Results obtained from the pushover analysis of frame CC_HSS_L_24_4_1.0 are shown in Figure 5.2a to Figure 5.2g. The frame roof displacement was gradually increased to 3.0%*h*. No column buckling was observed in this frame. As opposed to the 2-tiered braced fame of Section 5.2.1, frame lateral deformations were distributed between four tiers. Compared to the two-tiered CBF, braces in all tiers of the four-tiered CBF buckled nearly simultaneously at a much lower storey drift of 0.1% (Figure 5.2c). The reason being that the braces were designed as tension-only members and thus had a relatively low axial compression capacity. By further increasing the lateral displacement of the frame, tensile yielding took place in the first tier at approximately 0.5% of storey drift (Figure 5.2c), which led to an increase in the drift amplitude in Tier 1 (Figure 5.2b). Beyond this point, the capacity of the compression brace in the first tier degraded significantly, which reduced the storey shear resistance of the frame, as shown in Figure 5.2a. As the lateral roof displacement increased, brace yielding and strength degradation in the compression brace propagated to other tiers from bottom to top. As tensile yielding was initiated in any tier, the drift in that tier increased significantly (Figure 5.2b)

Figure 5.2c shows the tension and compression forces of braces. As shown, tension brace in the critical (first) tier yielded first, followed by braces of other tiers. It was also found that the compression capacity of braces slightly exceeded their probable compressive resistances. This could be attributed to the fact that a single-angle brace tends to buckle about its minor axis (X' in Figure 2.17b); however, the end connection detail forces the brace to buckle about its X-axis, which results in an increase in the brace buckling resistance.

Figure 5.2d shows the normalized axial force, and Figure 5.2e shows the normalized in-plane and out-of-plane moments of the right-hand-side compression column of the frame. As shown, the compression demand of the column was approximately 30% higher than the design force with $\phi =$ 1.0, which can be attributed to the increase in brace force demands as compared to the design demands and confirms the need for the overstrength factor of 1.3 prescribed by CSA S16-14 (Section 0), which was neglected in the design of the selected frames. As shown in Figure 5.2e, limited in-plane and out-of-plane moments arising from the multi-tiered response, as described in Section 2.4, were observed in the column, although such moments were not considered in design. Despite higher demands than those assumed in the design, the column stability was not compromised in the analysis. This additional capacity can be the result of a lower effective length factor ($K < 1.0$) than that assumed in the design (Toutant 2016) (Section 3.6), resistance factor smaller than one, and reserved capacity of the column when the bending moment is induced in axially loaded column (Newell and Uang 2008, Balazadeh Minouei 2017).

Frame final deformed-shapes are shown in Figure 5.2e and Figure 5.2f. As shown, yielding and buckling of the single-angle brace were appropriately predicted using the numerical model developed in this study.
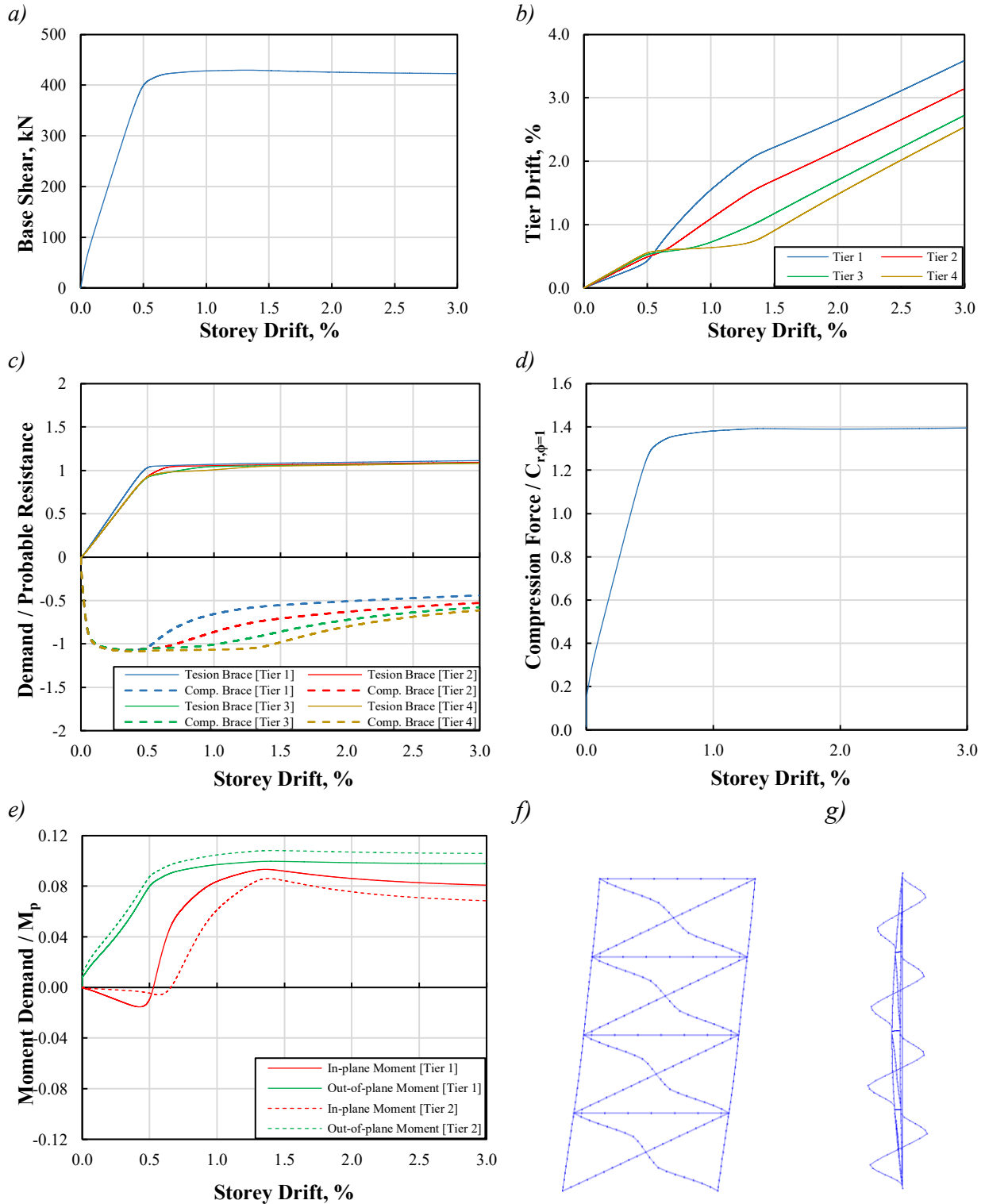
Figure 5.2. Pushover analysis of frame CC_HSS_L_24_4_1.0: a) base shear; b) tier drifts; c) brace tension and compression demands normalized to the probable resistances; d) column axial force demand normalized to the design force; e) column moments normalized to its plastic moment; f) in-plane deformed shape at 3% storey drift; g) out-of-plane deformed shape at 3% storey drift.

113

5.3 Nonlinear Response History Analyses Results

The key assumptions and details of the NLRH analyses were described in Section 4.6. The results of the NLRH analyses are given here for each of the braced frame categories separately: Type LD frames, Type CC frames with T/C HSS braces (CC-W-HSS frames), Type CC frames with T/O double-angle braces (CC-HSS-2L frames), and Type CC T/O frames with single-angle braces (CC-HSS-L frames).

5.3.1 Statistical Analysis

The statistics of key seismic response parameters are reported for each frame in accordance with the recommendation specified in the Commentary J of the 2015 NBCC (NRC_Commentaries 2015). According to this recommendation, when using at least two sets of ground motion records, given that all sets include at least 11 records, a structural response parameter, such as force or displacement, can be obtained following three steps:

1) take the peak response parameter obtained under each individual ground motion record,

2) for each earthquake ensemble, calculate the average of the peak parameters computed in Step 1, and

3) report the maximum of the mean values of all earthquake ensembles as the peak response parameter.

As described in Section 4.6.1, two suites of ground motion records are used in this study, each included more than 11 records, which permits the use of the NBCC recommendation for the purpose of determining the design demands. The final NLRH analysis results reported here are referred to as "statistics of response parameter". As recommended in the Commentary, the results of ground motion records are removed where the frame experienced instability (e.g. column

buckling in this study). Then, the design seismic demands are calculated based on the results obtained from the remaining ground motion records.

5.3.2 Column Instability Criteria

Given the likelihood of column instability under gravity plus seismic loads in the frames studied here and the large number of NLRH analyses performed, determining whether a column has buckled or not is not possible by investigation of every single analysis. Therefore, column buckling cases are determined using an automated method by developing an algorithm to check the column axial force and axial deformation amplitudes while the frame deforms laterally. In the algorithm, the axial compression force of the column is tracked while comparing the axial deformation of the member at every two consecutive time steps of the analysis. If the column is shortened while the axial compression force reduces, the column is deemed to buckle.

Examining several analyses showed that as a result of the numerical algorithm used in the dynamic analysis, there are cases where the column axial force drops slightly in one single time step, but the column returns to a stable condition for the rest of the analysis. Although the column does not buckle in this case, it is considered as buckled when using the automated method. Hence, a second criterion is defined to filter those cases out by measuring the in-plane and out-of-plane lateral deformations of the columns that were reported as buckled using the first criterion. Based on the second criterion, if the lateral deformation of the column exceeds three times the maximum Initial Out-of-Straightness (IOS) amplitude assigned to the column (see Section 4.3.4), the column is reported as buckled. This lateral deformation threshold is deemed large enough in this study to exceed the elastic deformation of the column under applied loads.

To illustrate the criteria set to identify column buckling, Figure 5.3a shows the first criterion for frame CC_W_HSS_16_2_1.0. As marked on the figure, at an axial shortening of approximately 10 mm in the first inelastic cycle, the compression capacity of the column started to degrade while its axial shortening kept increasing. Column shortening reached nearly 14 mm with an axial force reduction of almost 10% before the column was unloaded as a result of reversing lateral displacement sign. A similar and more pronounced response was observed in the subsequent loading cycles when the column underwent significant axial shortening while loosing its axial compression capacity. Figure 5.3b shows the second criterion set to check column buckling where the out-of-plane lateral deformation of the column drastically exceeded three times the maximum IOS amplitude (indicated by a green dashed line on the figure) reached approximately 270 mm (>> IOS = 48 mm) at t = 11s. Therefore, this column was considered that has buckled.
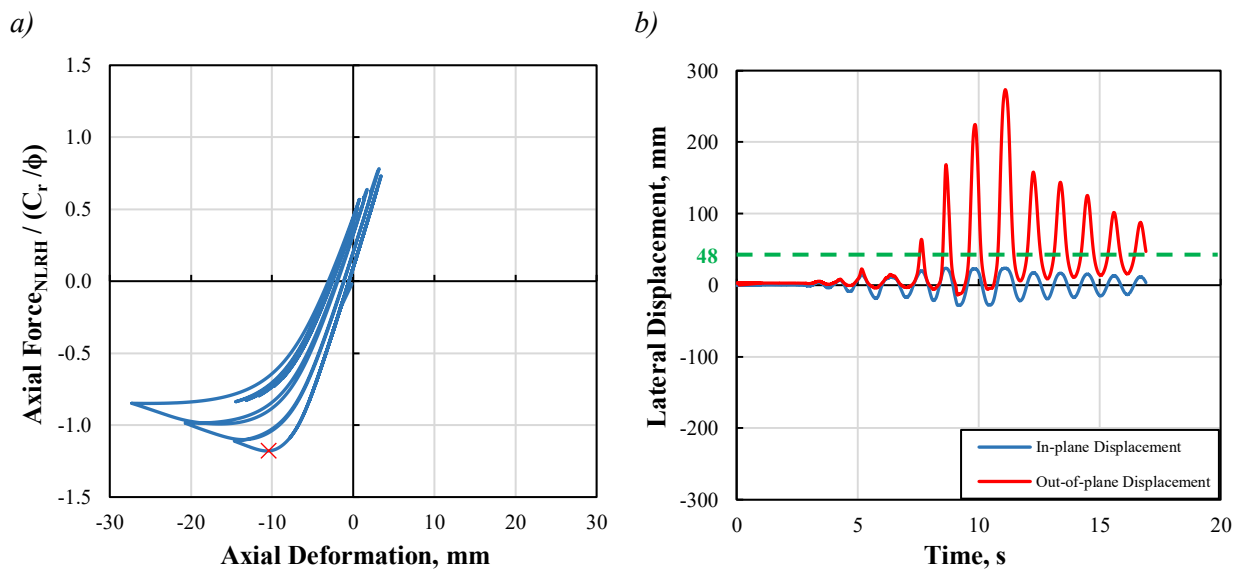
Figure 5.3. Column buckling identification shown for frame CC_W_HSS_16_2_1.0: a) axial force vs. axial deformation; b) lateral deformation history.

5.3.3 Type LD Frames

5.3.3.1 Frame Global Response

All of the 480 NLRH analyses performed on Type LD frames were completed successfully. Table 5.1 shows the statistics of the key displacement response parameters (i.e. the maximum of means over each earthquake ensemble of the peak response parameter) for Type LD frames under the selected ground motion records plus the number of analyses where the column buckling was observed. Except for frame LD_W_HSS_24_3_1.0, which experienced column buckling under two ground motion records, neither column buckling nor frame instability was observed for Type LD frames. The buckling of the columns was determined using the criteria described in Section 5.3.2.

In the table, δ_{St}/h represents the statistics of maximum storey drifts, where δ_{St} is the maximum total lateral deflection of the storey measured at the roof level, and h is the total story height. $R_d R_o \delta_e/h$ is the anticipated (design) storey drift, including the inelastic effects, where δ_e is the lateral deflection of the frame obtained from a linear elastic analysis under the design seismic base shear. δ_i/h_i characterizes the maximum drift in Tier i, in which h_i is the height of Tier i, and δ_i is calculated by subtracting the lateral displacement measured at the bottom of the tier from the lateral displacement at the top of the tier.

Drift Concentration Factor, DCF, is a parameter to investigate the distribution of lateral displacements over the frame height. DCF is computed by dividing the maximum tier drift in the tier that experienced the largest drift by the maximum storey drift, both obtained from the NLRH analyses at an identical time step where both parameters reached their respective maximum values.

A DCF value higher than one indicates a non-uniform distribution of the lateral displacement, which is expected to produce in-plane moment demands in the columns.

Critical tier, where the majority of the frame lateral deformations take place, is identified by comparing the tier drifts under each ground motion and reported in Table 5.1. For each frame, the number of cases where a tier was identified as the critical tier is given in the brackets. For instance, for frame LD_W_HSS_16_3_1.0, Critical Tier row reads 2[1] 3[29], which means that the second tier was identified as the critical tier under one of the records, and 29 records led to a critical Tier 3. In the same table, the expected critical tier of the frame, as defined in Section 4.3.4, is also given. In low-ductile frames studied here, it was found that the critical tier is not necessarily the same tier where brace tensile yielding is expected to initiate first due to reduced storey shear resistance (expected critical tier as defined in Section 3.6). The reason being the frame lateral deformations are often small in such frames and nearly uniformly distributed between tiers. Very limited inelasticity developing due to inelastic buckling of braces, combined with limited bending of the column, leads to a slightly higher tier drift in one of the tiers, which is identified as the critical tier. This response was observed in the majority of the frames analyzed here, which explains why the observed critical tier is not the expected critical tier in the majority of the frames. Due to no or limited inelastic deformations in the braced tiers, the location of the critical tier also varies between tiers, as shown in Table 5.1. A similar response was observed in the pushover analysis (Figure 5.1b), where the tier drift was slightly higher than the one in the critical tier before tensile yielding took place in the critical tier. This can be attributed to the insignificant difference between the lateral stiffness of each braced tier in the elastic range.

As shown in Table 5.1, the maximum storey drifts, ranging from 0.33 to 0.47 between frames (higher in short frames and lower in tall ones), were found to be significantly lower than the 2015

NBCC limit (i.e. 2.5%), which also confirms the limited inelastic deformation expected in Type

LD frames and the observed response in braces as it is discussed in Section 5.3.3.2.

Table 5.1. Statistics of peak drift demands for Type LD frames.

Parameter	LD_W_HSS_10_2_1.0	LD_W_HSS_10_2_1.75	LD_W_HSS_10_3_1.0	LD_W_HSS_10_3_1.75	LD_W_HSS_16_2_1.0	LD_W_HSS_16_2_1.75	LD_W_HSS_16_3_1.0	LD_W_HSS_16_3_1.75	LD_W_HSS_16_4_1.0	LD_W_HSS_16_4_1.75	LD_W_HSS_24_3_1.0	LD_W_HSS_24_3_1.75	LD_W_HSS_24_4_1.0	LD_W_HSS_24_4_1.75	LD_W_HSS_24_6_1.0	LD_W_HSS_24_6_1.75
Instability	—	—	—	—	—	—	—	—	—	—	2	—	—	—	—	—
δ_{St}/h (%)	0.40	0.40	0.47	0.45	0.35	0.34	0.36	0.35	0.37	0.36	0.34	0.33	0.36	0.34	0.37	0.36
$\dfrac{\delta_{St}/h}{R_d R_o \delta_e}$	0.97	0.92	0.92	0.94	0.94	0.91	0.87	0.94	0.91	0.88	1.01	1.04	1.07	1.06	1.05	1.06
δ_1/h_1 (%)	0.38	0.33	0.43	0.34	0.32	0.36	0.31	0.30	0.30	0.25	0.26	0.30	0.26	0.24	0.25	0.27
δ_2/h_2 (%)	0.43	0.57	0.50	0.60	0.38	0.32	0.38	0.40	0.36	0.43	0.35	0.37	0.35	0.39	0.32	0.34
δ_3/h_3 (%)			0.49	0.51			0.40	0.39	0.40	0.44	0.39	0.36	0.40	0.41	0.37	0.37
δ_4/h_4 (%)									0.41	0.43			0.42	0.40	0.41	0.39
δ_5/h_5 (%)															0.43	0.41
δ_6/h_6 (%)															0.44	0.41
DCF	1.07	1.40	1.07	1.33	1.11	1.05	1.13	1.18	1.16	1.23	1.20	1.13	1.21	1.22	1.22	1.21
Critical Tier	2[30]	2[30]	2[25] 3[5]	2[28] 3[2]	2[30]	1[30]	2[1] 3[29]	2[12] 3[18]	3[5] 4[25]	2[2] 3[11] 4[17]	3[28]	2[6] 3[24]	4[30]	2[3] 3[4] 4[23]	5[4] 6[26]	5[8] 6[22]
Expected Critical Tier	1	2	1	2	1	1	1	2	1	2	1	2	1	2	1	1

120

Figure 5.4 shows the statistics of the peak storey drift, δ_{St}/h, normalized to the design storey drift, $R_dR_o\delta_e/h$. As shown, this ratio is close to 1.0 between frames, which confirms that 2015 NBCC well predicts the design storey drift. In 10 m- and 16 m-tall frames, the observed storey drifts are slightly (3% - 13%) smaller than the respective design values. However, the results of the NLRH analyses are 1% to 7% larger than the code values for the 24 m-tall frames. Additionally, the variations of the drift statistics for the frames with the same height and a different number of tiers or different tier height ratios are insignificant, which suggests that the number of tiers or tier height ratios do not significantly affect the drift prediction.
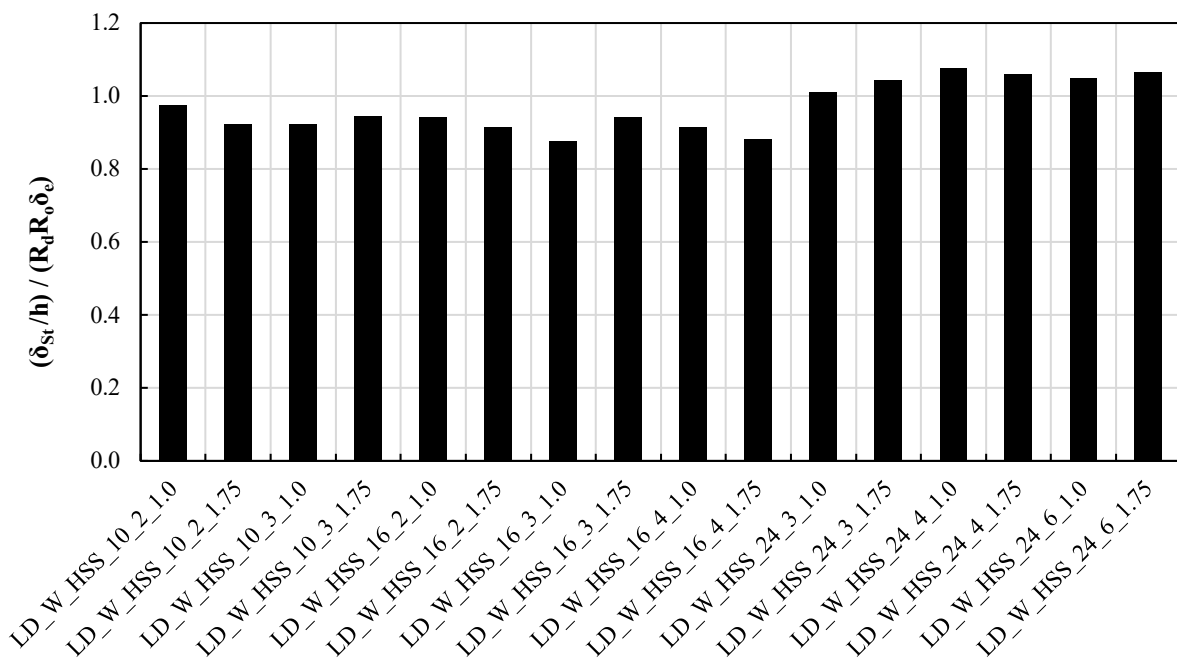
Figure 5.4. Statistics of normalized peak storey drift demands for Type LD frames.

Figure 5.5 shows the statistics of the DCF for Type LD frames. A limited drift concentration was observed in tall frames; however, 10 m-tall frames with non-uniform tier heights experienced slightly higher DCFs. This can, in part, be attributed to the fact that the total frame drift is distributed between more tiers in tall frames, as braces buckle in nearly all tiers, which reduces the

possibility of drift concentration in tiers of such frames. Additionally, in 10 m-tall frames with non-uniform tier heights, brace compressive buckling may not take place simultaneously in all tiers, which can contribute to more non-uniformity of inelastic lateral deformations. This aspect should be further investigated in future studies.
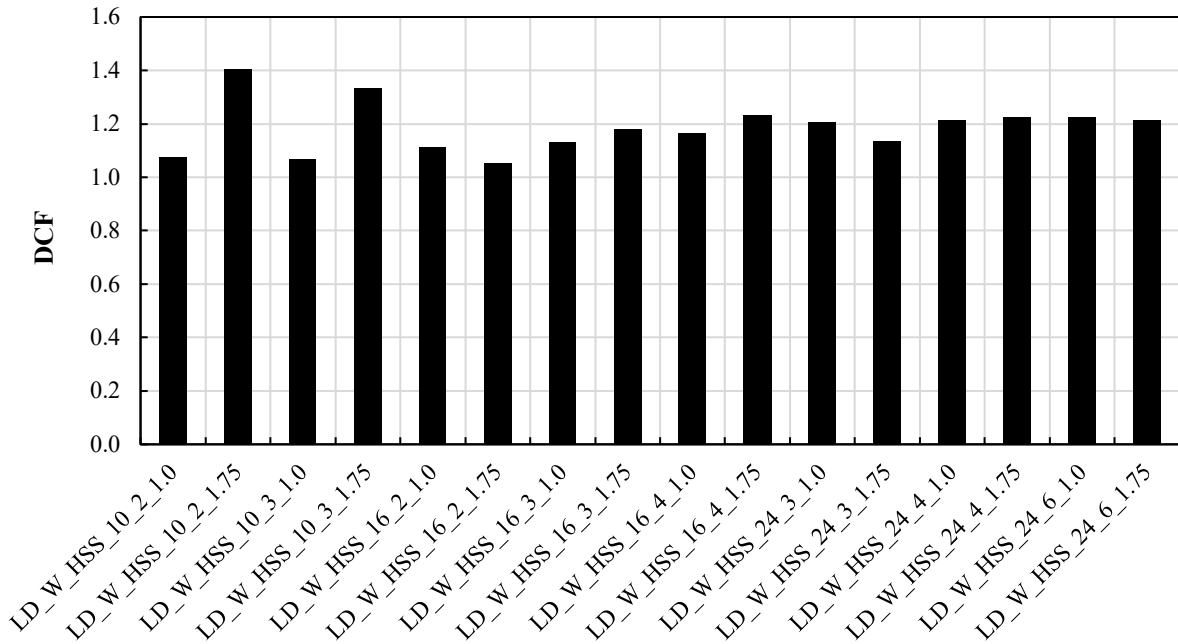
Figure 5.5. Statistics of peak Drift Concentration Factors (DCFs) for Type LD frames.

Figure 5.6 shows the profile of tier drift demands over the height of the frame. As shown, relatively low tier drifts, ranging from 0.25 to 0.60, were observed in Type LD frames, which confirms the potential for limited yielding and post-buckling degradation in braces of such frames as expected in design. The results of past experimental studies confirmed that the fracture life of HSS braces is a function of the material yield stress, section slenderness ratio, and global slenderness ratio, which for braces commonly used in building construction varies between 2.0% and 2.5% inter-storey drift or tier drift in the case of the multi-tiered configuration. Although the numerical model did not take into account the influence of brace fracture, the limited tier drifts in the frames studied indicates that HSS braces in Type LD braced frames are not prone to fracture.
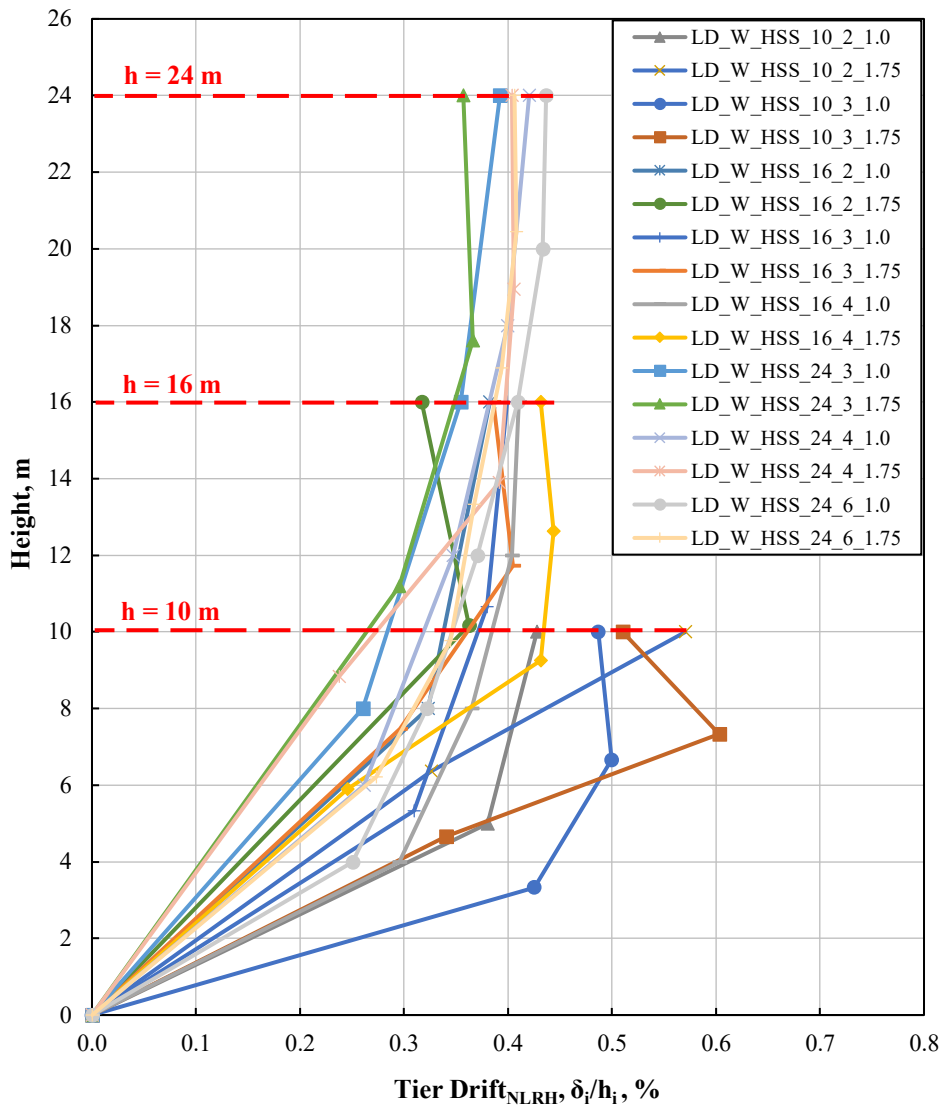
Figure 5.6. Profile of peak tier drifts for Type LD frames.

5.3.3.2 Brace Behavior

Table 5.2 gives the statistics of the peak tension, $T_{b\text{-}NLRH}$, and compression, $C_{b\text{-}NLRH}$, forces (i.e. the maximum of means over each earthquake ensemble of the peak response parameter) induced in the braces of Type LD frames. These demands are normalized to their corresponding tension and compression probable resistances, T_u and C_u, respectively, as defined in Table 3.3. These statistics are plotted visually in Figure 5.7a and Figure 5.7b for tension and compression brace forces,

respectively. As shown, on average, brace tensile yielding did not occur in the frames studied here. The results of tension brace forces follow the pattern observed for the DCF (Figure 5.5) as the tier drift demand is affected by the elongation and shortening of the braces, which themselves affect brace forces. The results obtained from the compression braces show that, on average, the compression brace forces in the majority of braced tiers are close to their respective probable compressive resistances, which indicates that the majority of braces buckled in compression. However, the compression braces did not reach their respective post-buckling resistances because the tension braces remained elastic, which prevented further strength degradation in the companion compression braces. As shown, in a few cases, the compression brace force obtained from the NLRH analysis exceeds the respective probable compressive resistance, which can be attributed to numerical simulation overestimation (Section 0), underestimation by the code compressive resistance equation, or the effects of dynamic loading on the brace buckling response (Kazemzadeh Azad et al. 2018). The compression force in the majority of the braces of 24 m-tall frames, however, are lower than the corresponding probable compressive resistances. This behaviour, combined with the results of the brace tension force in 24 m-tall frames, indicates that those frames remained substantially elastic under the selected ground motion records.

Table 5.2. Statistics of normalized peak tension and compression force demands of braces for Type LD frames.

Parameter	Frame															
	LD_W_HSS_10_2_1.0	LD_W_HSS_10_2_1.75	LD_W_HSS_10_3_1.0	LD_W_HSS_10_3_1.75	LD_W_HSS_16_2_1.0	LD_W_HSS_16_2_1.75	LD_W_HSS_16_3_1.0	LD_W_HSS_16_3_1.75	LD_W_HSS_16_4_1.0	LD_W_HSS_16_4_1.75	LD_W_HSS_24_3_1.0	LD_W_HSS_24_3_1.75	LD_W_HSS_24_4_1.0	LD_W_HSS_24_4_1.75	LD_W_HSS_24_6_1.0	LD_W_HSS_24_6_1.75
$(T_{b\text{-}NLRH}/T_u)_1$	0.79	0.60	0.81	0.62	0.62	0.67	0.65	0.52	0.58	0.44	0.47	0.45	0.53	0.38	0.49	0.57
$(T_{b\text{-}NLRH}/T_u)_2$	0.68	0.89	0.71	0.79	0.54	0.46	0.57	0.65	0.52	0.66	0.42	0.57	0.47	0.61	0.45	0.44
$(T_{b\text{-}NLRH}/T_u)_3$			0.68	0.63			0.57	0.54	0.52	0.59	0.42	0.49	0.47	0.54	0.45	0.44
$(T_{b\text{-}NLRH}/T_u)_4$									0.50	0.57			0.47	0.52	0.45	0.44
$(T_{b\text{-}NLRH}/T_u)_5$															0.45	0.44
$(T_{b\text{-}NLRH}/T_u)_6$															0.44	0.43
$(C_{b\text{-}NLRH}/C_u)_1$	1.03	1.02	1.00	1.02	1.02	1.01	1.00	1.00	0.94	0.98	0.99	0.95	0.93	0.93	0.96	0.93
$(C_{b\text{-}NLRH}/C_u)_2$	1.04	1.07	0.98	0.99	1.02	1.06	0.97	0.99	0.91	1.05	0.97	1.01	0.90	1.06	0.91	0.91
$(C_{b\text{-}NLRH}/C_u)_3$			1.02	1.08			1.00	1.06	0.91	1.08	0.98	1.05	0.90	1.06	0.91	0.90
$(C_{b\text{-}NLRH}/C_u)_4$									0.93	1.13			0.92	1.12	0.91	0.90
$(C_{b\text{-}NLRH}/C_u)_5$															0.91	0.90
$(C_{b\text{-}NLRH}/C_u)_6$															0.95	0.93

a)
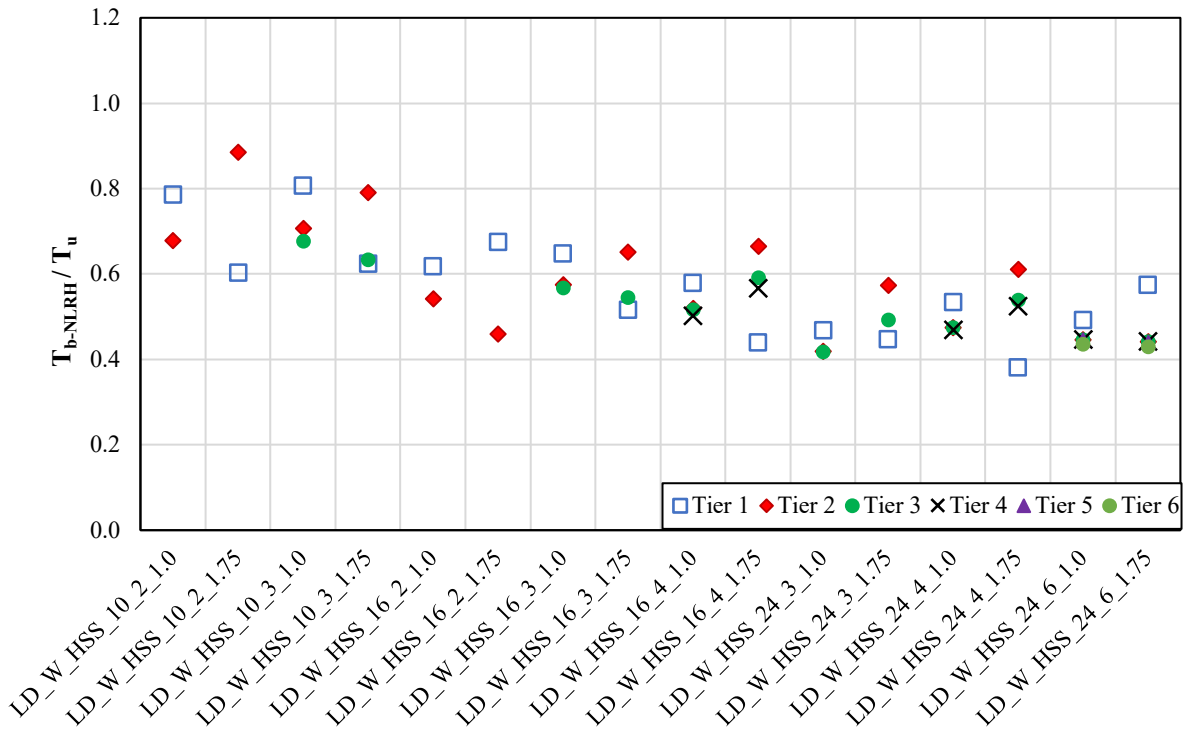
b)
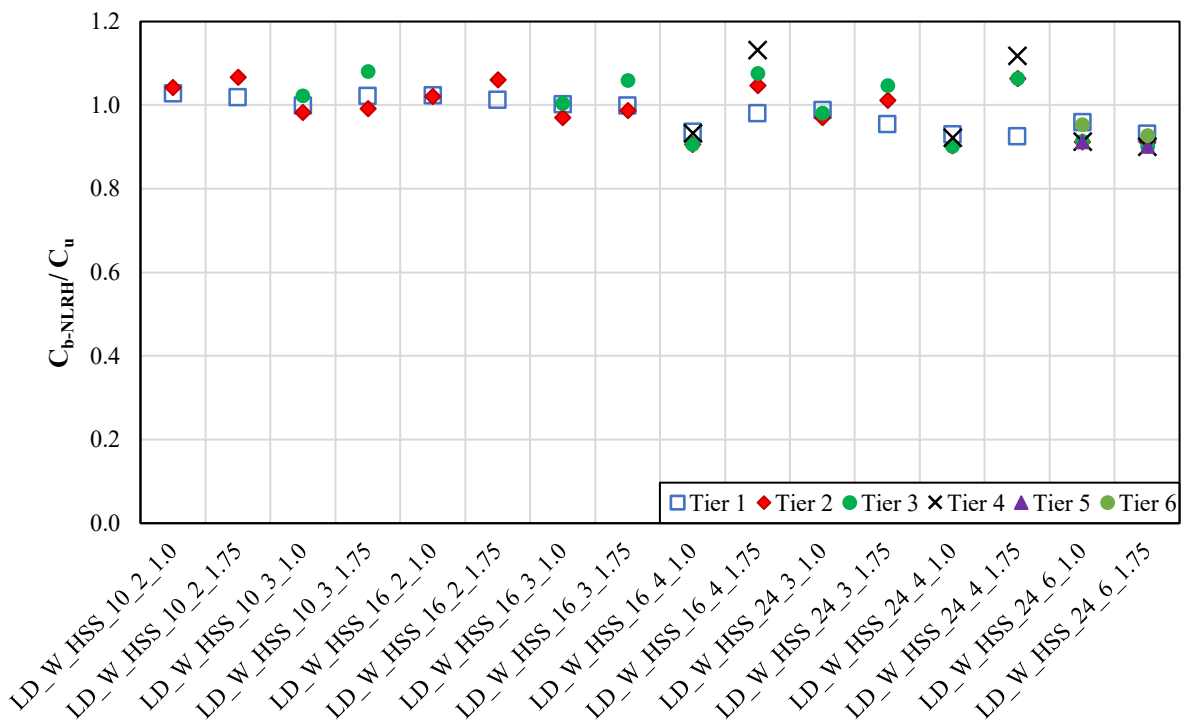
Figure 5.7. Statistics of normalized peak brace axial force demands for Type LD frames: a) tension brace; b) compression brace.

5.3.3.3 Column Behaviour

Table 5.3 presents the statistics of the peak axial force, in-plane and out-of-plane moments (i.e. the maximum of means over each earthquake ensemble of the peak response parameter) induced in the columns of Type LD frames. These demands are normalized to their respective axial compression resistances (i.e. the least resistance obtained from flexural and flexural-torsional buckling modes) and the in-plane and out-of-plane plastic moments, respectively. For each ground motion, the reported values are the maximum of the demands induced in the Left-Hand-Side (LHS) and the Right-Hand-Side (RHS) columns. In the table, $C_{c\text{-}NLRH}$ is the column axial compression demand obtained from the NLRH analysis recorded in the first tier level (the largest column axial force), and $C_{r,\phi=1}$ is the column compressive resistance calculated in accordance with Clause 13.3 of CSA S16-14 under axial compression force with a resistance factor of $\phi = 1.0$. $(M_{cy\text{-}NLRH}/M_{py})_i$ and $(M_{cx\text{-}NLRH}/M_{px})_i$ are the maximum column in-plane and out-of-plane moments, respectively, at the Tier i level, normalized to the corresponding plastic moments.

Figure 5.8 shows the statistics of $C_{c\text{-}NLRH}/C_{r,\phi=1}$ for the columns of Type LD frames. As shown, the normalized compression forces in the columns vary between 71% and 97%. Since the columns of Type LD frames were designed to carry probable brace resistances, lower axial force ratios observed in the columns could be the consequence of brace tension demands being smaller than the respective probable tensile resistance, as discussed in Section 5.3.3.2.

Parameter	Frame															
	LD_W_HSS_10_2_1.0	LD_W_HSS_10_2_1.75	LD_W_HSS_10_3_1.0	LD_W_HSS_10_3_1.75	LD_W_HSS_16_2_1.0	LD_W_HSS_16_2_1.75	LD_W_HSS_16_3_1.0	LD_W_HSS_16_3_1.75	LD_W_HSS_16_4_1.0	LD_W_HSS_16_4_1.75	LD_W_HSS_24_3_1.0	LD_W_HSS_24_3_1.75	LD_W_HSS_24_4_1.0	LD_W_HSS_24_4_1.75	LD_W_HSS_24_6_1.0	LD_W_HSS_24_6_1.75
$C_{c\text{-NLRH}}/C_{r,\phi=1}$	0.90	0.76	0.83	0.80	0.85	0.79	0.82	0.84	0.85	0.71	0.78	0.84	0.97	0.80	0.92	0.84
$(M_{cy\text{-NLRH}}/M_{py})_1$	0.02	0.05	0.02	0.06	0.02	0.03	0.01	0.04	0.02	0.04	0.02	0.04	0.01	0.04	0.01	0.04
$(M_{cy\text{-NLRH}}/M_{py})_2$			0.03	0.06			0.01	0.02	0.02	0.01	0.02	0.01	0.01	0.01	0.01	0.01
$(M_{cy\text{-NLRH}}/M_{py})_3$									0.01	0.01			0.01	0.01	0.01	0.01
$(M_{cy\text{-NLRH}}/M_{py})_4$															0.01	0.00
$(M_{cy\text{-NLRH}}/M_{py})_5$															0.01	0.01
$(M_{cx\text{-NLRH}}/M_{px})_1$	0.06	0.04	0.03	0.07	0.08	0.03	0.05	0.05	0.03	0.04	0.06	0.02	0.06	0.04	0.03	0.02
$(M_{cx\text{-NLRH}}/M_{px})_2$			0.02	0.04			0.04	0.03	0.04	0.04	0.05	0.01	0.07	0.03	0.05	0.02
$(M_{cx\text{-NLRH}}/M_{px})_3$									0.03	0.02			0.04	0.02	0.05	0.02
$(M_{cx\text{-NLRH}}/M_{px})_4$															0.04	0.02
$(M_{cx\text{-NLRH}}/M_{px})_5$															0.02	0.01
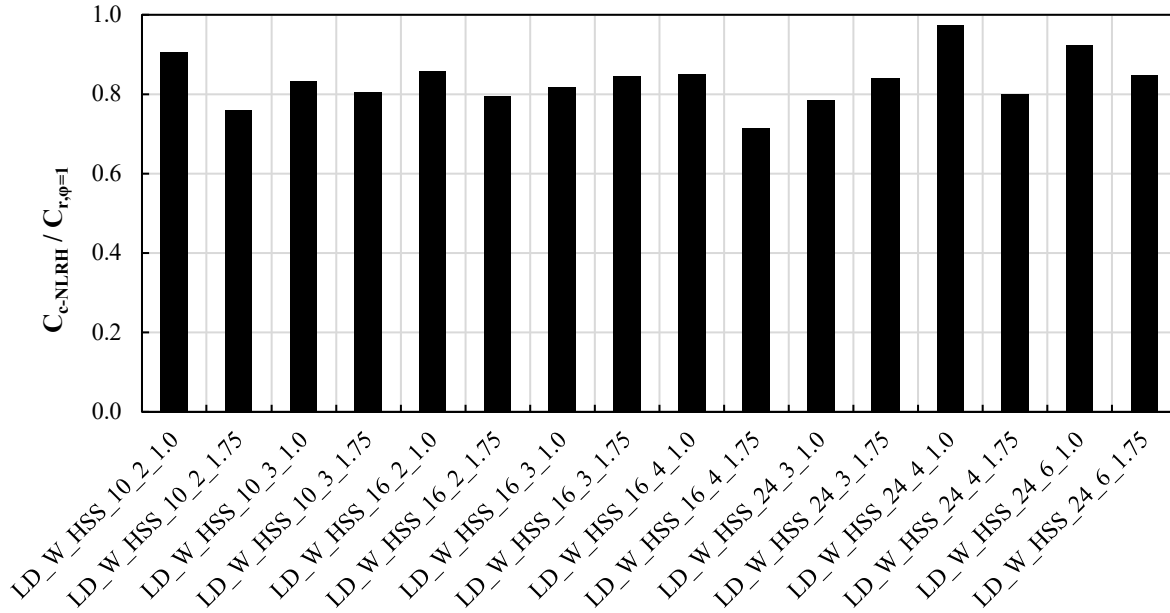
Figure 5.8. Statistics of normalized peak column axial compression forces for Type LD frames.

Figure 5.9a and Figure 5.9b show the peak in-plane and out-of-plane moment demands in columns at every tier level normalized to the respective plastic moments. As shown in Figure 5.9a, the in-plane moment results ranging between $0.01M_{py}$ and $0.06M_{py}$ indicate that minimal in-plane moment demands are induced in the columns. Except for frame LD_W_HSS_10_3_1.0, the peak column in-plane moment in the first tier is always higher than the other tiers. Additionally, larger in-plane moments were developed in the first tier of the frames with $h_1/h_2 = 1.75$ than their counterparts having tiers with identical heights; the difference is more pronounced for 10 m-tall frames.

Column peak out-of-plane moments (Figure 5.9b) range from $0.02M_{px}$ to $0.08M_{px}$ with higher moments typically observed in the first-tier column segments. The key sources of column out-of-plane moments in MT-CBFs are the brace out-of-plane displacement upon brace buckling out-of-plane for braces intersecting with the compression column and the P-Delta effects due to initial geometric imperfections (Cano 2019).

a)
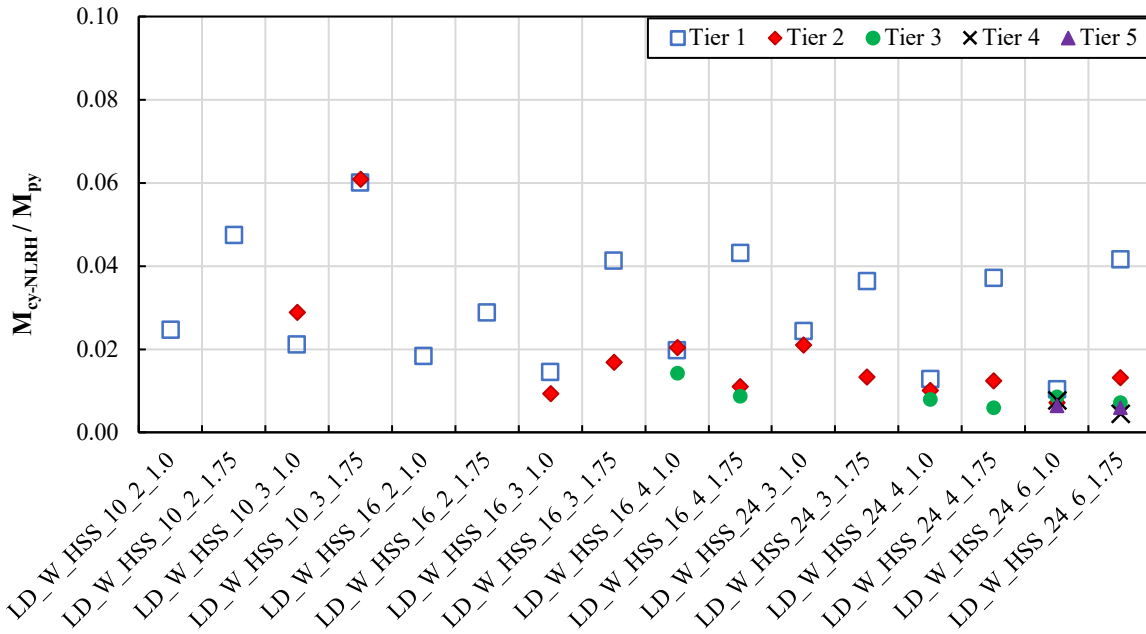
b)
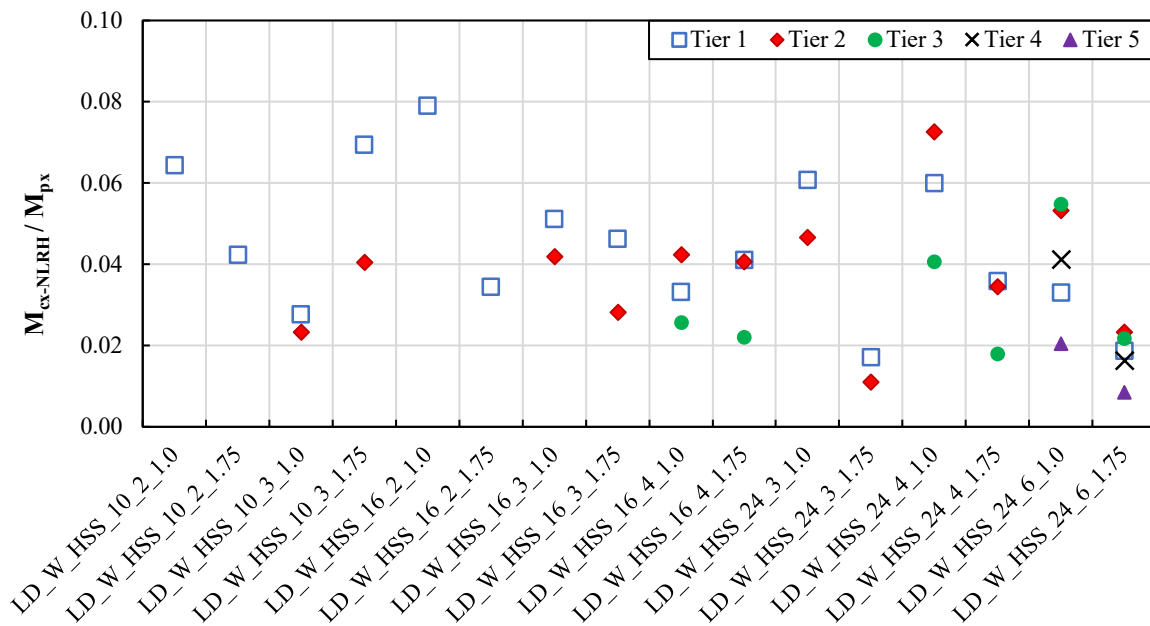
Figure 5.9. Statistics of normalized peak column moment demands for Type LD frames: a) in-plane moment; b) out-of-plane moment.

5.3.4   Type CC Frames with T/C Braces

5.3.4.1   Frame Global Response

All 480 NLRH analyses of Type CC braced frames with T/C HSS braces (CC-W-HSS) were completed successfully. Table 5.4 provides the statistics of key displacement response parameters. The number of instability cases observed for these frames and the critical tier location are included in the table, as well. All of the variables used in the table were introduced in Section 5.3.3.1. Column instability was observed in the majority of 16 m- and 24 m-tall frames. The instability consisted of in-plane, out-of-plane or the combination of both modes (see Section 5.2). No column instability was detected in 10 m-tall frames. The method described in Section 5.3.2 was employed to determine columns buckling cases.

As shown in Table 5.4, the location of the critical tier over the height of the frame does not agree with the predictions provided in Table 3.7 (expected critical tier), which is because of the similar response observed in and described for LD-W-HSS frames.

As shown in Table 5.4, relatively lower (0.29% – 0.44%) storey drift demands were observed in the CC-W-HSS frames compared to those reported for LD-W-HSS frames. This was expected because of a lower ductility capacity of such Type CC frames. Furthermore, the 2015 NBCC storey drift limit of 2.5% was well met in CC-W-HSS frames studied. Additionally, for a given frame height, the variation of storey drift demands is limited regardless of the number of tiers.

Storey drift demands of CC-W-HSS frames are compared to the respective design storey drift and reported in Table 5.4 and Figure 5.10. As shown, the results for 10 m- and 24 m-tall frames correlate well with the design storey drift. A lower storey drift demand-to-design ratio was

achieved for the majority of the 16 m-tall frames. The reason being the analysis results of these frames only include the cases where columns did not buckle (Table 5.4). For instance, frame CC_W_HSS_16_3_1.0, which has the lowest drift demand in Figure 5.10, experienced column instability under 10 ground motion records.

Figure 5.11 shows the DCF for CC-W-HSS frames. All of the frames experienced drift concentration. For the taller 16 m and 24 m frames, DCF range between 1.16 to 1.25; however, more discrepancy was observed in the DCF of 10 m-tall frames; frames with uniform tier heights experienced lower DCF while a DCF as high as 1.33 occurred in frames with non-uniform tier heights. This response agrees with the results obtained for LD-W-HSS frames.

Figure 5.12 shows the distribution of tier drifts over the height of the frames. As shown in the figure, the maximum of tier drifts observed in CC-W-HSS frames is 0.59%, which is significantly lower than the tier drift corresponding to HSS braces fracture life due to low-cycle fatigue (2.0% to 2.5% as explained in Section 5.3.3.1 for Type LD frames). Although the brace fracture was not explicitly simulated in the numerical model of the frame, the limited tier drifts in the frames studied indicates that HSS braces in Type CC MT-CBFs are not prone to fracture, which suggests that a tier drift check may not be required for Type CC MT-CBFs.

Table 5.4. Statistics of peak drift demands for CC-W-HSS frames.

Parameter	CC_W_HSS_10_2_1.0	CC_W_HSS_10_2_1.75	CC_W_HSS_10_3_1.0	CC_W_HSS_10_3_1.75	CC_W_HSS_16_2_1.0	CC_W_HSS_16_2_1.75	CC_W_HSS_16_3_1.0	CC_W_HSS_16_3_1.75	CC_W_HSS_16_4_1.0	CC_W_HSS_16_4_1.75	CC_W_HSS_24_3_1.0	CC_W_HSS_24_3_1.75	CC_W_HSS_24_4_1.0	CC_W_HSS_24_4_1.75	CC_W_HSS_24_6_1.0	CC_W_HSS_24_6_1.75
Instability	—	—	—	—	7	2	10	1	3	6	5	3	5	4	—	—
(δ_{St}/h) (%)	0.39	0.39	0.44	0.44	0.32	0.35	0.25	0.36	0.32	0.31	0.30	0.32	0.30	0.29	0.38	0.38
$\dfrac{(\delta_{St}/h)}{R_d R_o \delta_e}$	1.00	0.98	1.01	1.02	0.86	0.99	0.66	0.93	0.79	0.79	0.93	1.03	0.95	0.98	0.97	1.00
(δ_1/h_1) (%)	0.37	0.35	0.39	0.35	0.27	0.32	0.19	0.31	0.25	0.25	0.23	0.28	0.22	0.24	0.28	0.25
(δ_2/h_2) (%)	0.43	0.50	0.51	0.59	0.37	0.40	0.27	0.42	0.31	0.32	0.31	0.34	0.29	0.29	0.32	0.38
(δ_3/h_3) (%)			0.44	0.49			0.30	0.41	0.37	0.35	0.36	0.39	0.35	0.34	0.37	0.40
(δ_4/h_4) (%)									0.38	0.37			0.38	0.36	0.42	0.43
(δ_5/h_5) (%)															0.45	0.46
(δ_6/h_6) (%)															0.46	0.47
DCF	1.10	1.28	1.15	1.33	1.16	1.14	1.20	1.18	1.20	1.21	1.21	1.19	1.23	1.22	1.21	1.25
Critical Tier	1[7] 2[23]	2[30]	2[18] 3[12]	2[19] 3[11]	2[23]	2[28]	3[20]	2[7] 3[22]	4[27]	4[24]	3[25]	3[27]	4[25]	4[26]	5[1] 6[29]	6[30]
Expected Critical Tier	1	2	1	1	1	2	1	2	1	1	1	1	1	1	1	2
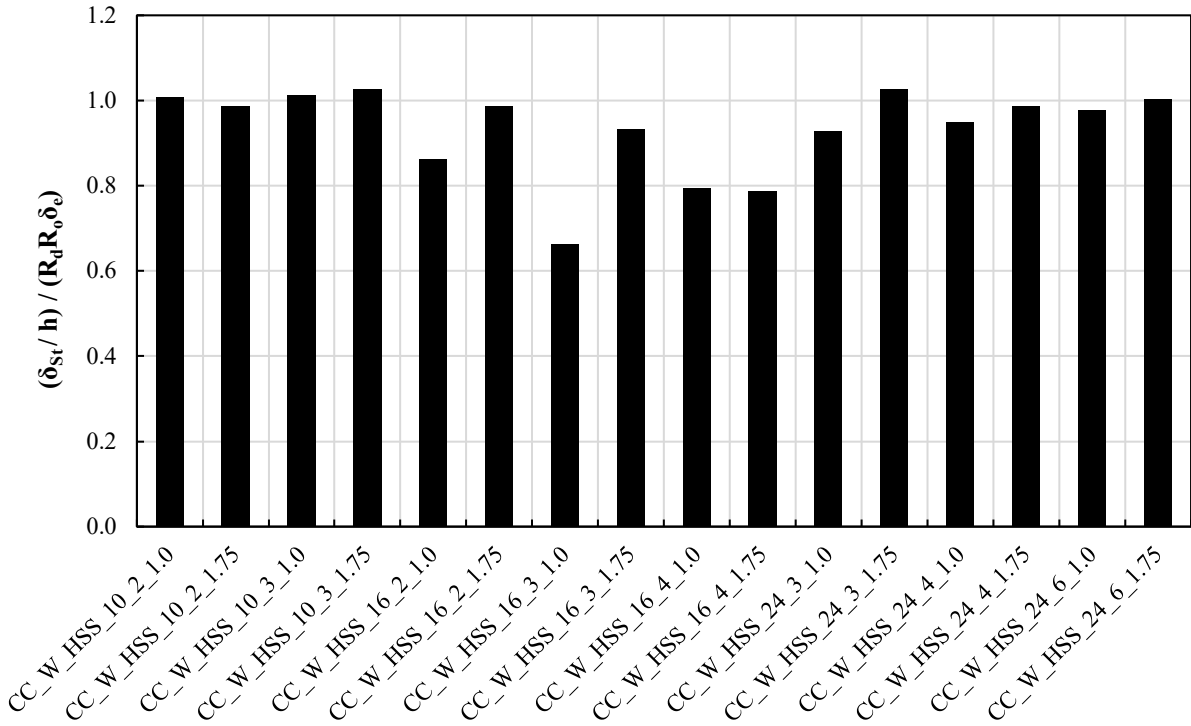
Figure 5.10 Statistics of normalized peak storey drift demands for CC-W-HSS frames.
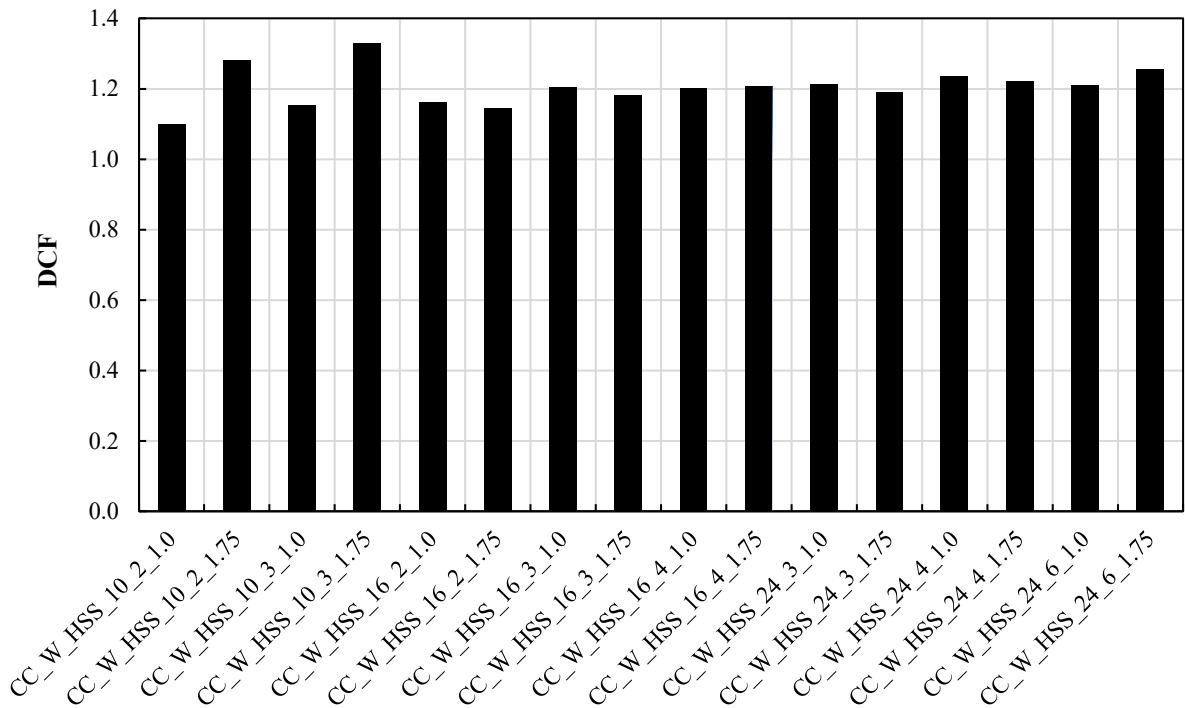
Figure 5.11. Statistics of peak Drift Concentration Factors (DCFs) for CC-W-HSS frames.

134
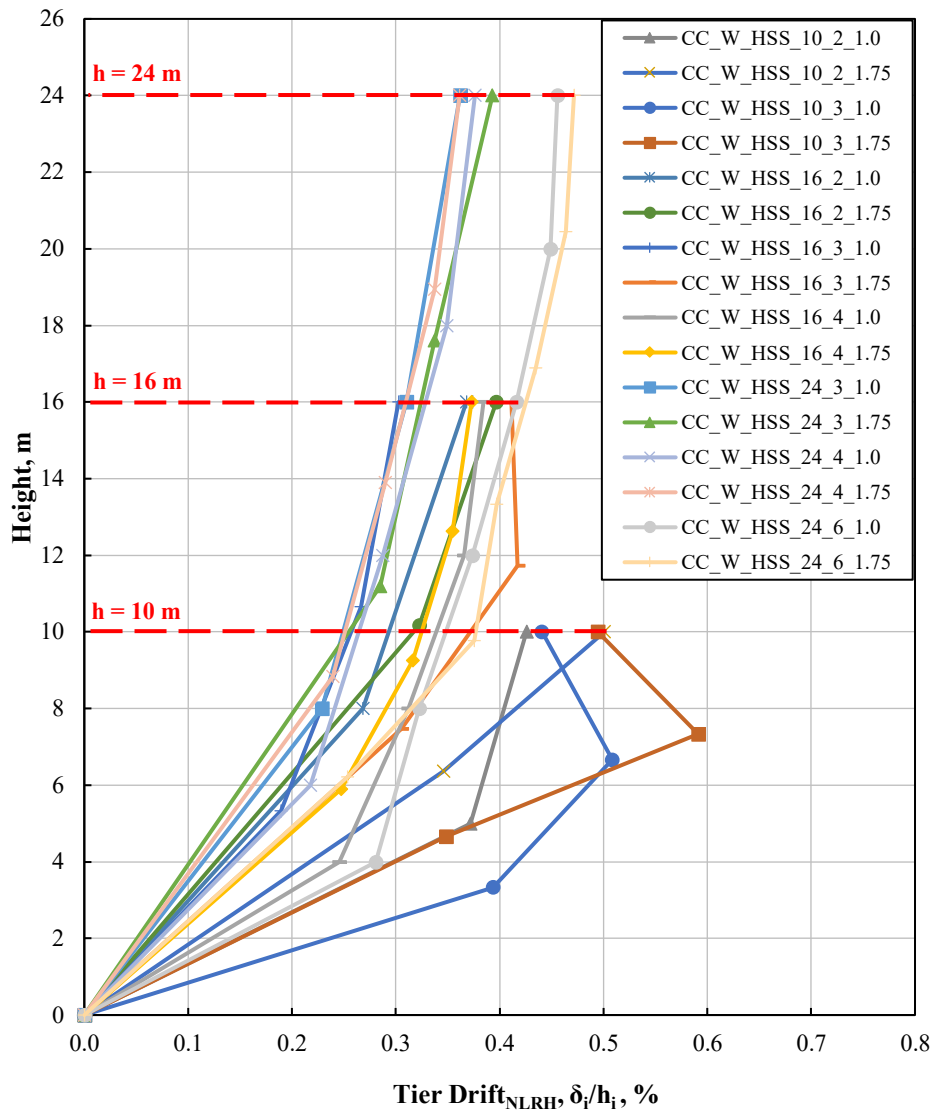
Figure 5.12. Statistics of peak tier drifts over the frame height for CC-W-HSS frames.

5.3.4.2   Brace Behavior

The statistics of the peak brace tension demand, $T_{b\text{-}NLRH}$, at each tier level obtained from the NLRH analyses normalized to the respective probable resistance, T_u, and their design forces, T_f, are presented in Table 5.5. Similarly, the statistics of the peak brace compression demand, $C_{b\text{-}NLRH}$, normalized to the respective probable resistance, C_u, and the design force, C_f, are given in Table

5.6 as well as Figure 5.13 and Figure 5.14. It should be noted that in the seismic design of Type CC frames, brace probable resistances need not be resisted by other members. As shown in Figure 5.13a, tension demands in all tiers are considerably lesser than their respective T_u, which suggests that no tension yielding has occurred in the braces of the selected CC-W-HSS frames. Figure 5.13b shows that the induced tension forces in braces are higher than the design forces; the peak ratios range from 1.09 to 1.95. The relatively low values for 16 m-tall frames, particularly CC_W_HSS_16_3_1.0, is mainly because of excluding the results of the cases where column buckling took place.

Brace compression demands normalized to the probable resistance and design force are shown in Figure 5.14a and Figure 5.14b, respectively. As shown, the peak brace forces, when normalized to the respective probable resistances range from 0.69 to 0.96, and when normalized to the design forces, range from 1.12 to 1.71. On average, both tension and compression braces of CC-W-HSS frames carried higher forces when subjected to ground acceleration. Additionally, the results obtained for compression braces show that brace buckling was less likely in the majority of 16 m- and 24 m- tall frames as shown in Figure 5.14b, which is on the one hand against the brace nonlinear mechanism in such Tension-Compression bracing systems, and on the other hand, confirms a limited nonlinear response expected in Type CC frames. For 10 m-tall frames, comparing the tension and compression brace forces (Figure 5.13b and Figure 5.14b) indicates that on average, brace buckling took place in most of the braced tiers, although the load is slightly overestimated by CSA S16-14 equation in some cases resulting in $C_{b\text{-}NLRH} / C_u < 1.0$ (Figure 5.14a). The limited nonlinear response in the MT-CBF cases studied here also contributes to the reduction of in-plane and out-of-plane bending moments induced in the column.

Since the columns of CC-W-HSS frames are designed for forces arising from tension- and compression-acting braces, relatively higher brace forces observed in NLRH analyses of such frames, suggests the need to amplify the column design forces for Type CC MT-CBFs with T/C braces. This is discussed in detail in Section 6.2.

Table 5.5. Statistics of normalized peak tension demands of braces for CC-W-HSS frames.

Parameter	Frame															
	CC_W_HSS_10_2_1.0	CC_W_HSS_10_2_1.75	CC_W_HSS_10_3_1.0	CC_W_HSS_10_3_1.75	CC_W_HSS_16_2_1.0	CC_W_HSS_16_2_1.75	CC_W_HSS_16_3_1.0	CC_W_HSS_16_3_1.75	CC_W_HSS_16_4_1.0	CC_W_HSS_16_4_1.75	CC_W_HSS_24_3_1.0	CC_W_HSS_24_3_1.75	CC_W_HSS_24_4_1.0	CC_W_HSS_24_4_1.75	CC_W_HSS_24_6_1.0	CC_W_HSS_24_6_1.75
$(T_{b\text{-NLRH}}/T_u)_1$	0.74	0.61	0.73	0.63	0.48	0.46	0.36	0.50	0.46	0.43	0.42	0.40	0.41	0.38	0.55	0.44
$(T_{b\text{-NLRH}}/T_u)_2$	0.61	0.76	0.63	0.72	0.42	0.59	0.33	0.57	0.41	0.42	0.37	0.39	0.37	0.40	0.49	0.54
$(T_{b\text{-NLRH}}/T_u)_3$			0.59	0.57			0.32	0.49	0.40	0.38	0.37	0.32	0.36	0.35	0.48	0.47
$(T_{b\text{-NLRH}}/T_u)_4$									0.40	0.39			0.36	0.34	0.48	0.47
$(T_{b\text{-NLRH}}/T_u)_5$															0.49	0.47
$(T_{b\text{-NLRH}}/T_u)_6$															0.49	0.47
$(T_{b\text{-NLRH}}/T_f)_1$	1.91	1.77	1.89	1.85	1.49	1.79	1.09	1.63	1.35	1.39	1.55	1.64	1.55	1.64	1.68	1.81
$(T_{b\text{-NLRH}}/T_f)_2$	1.76	1.91	1.82	1.95	1.46	1.72	1.11	1.65	1.34	1.32	1.53	1.65	1.54	1.62	1.65	1.70
$(T_{b\text{-NLRH}}/T_f)_3$			1.69	1.71			1.09	1.57	1.33	1.33	1.53	1.50	1.54	1.59	1.64	1.66
$(T_{b\text{-NLRH}}/T_f)_4$									1.33	1.33			1.53	1.56	1.64	1.66
$(T_{b\text{-NLRH}}/T_f)_5$															1.65	1.67
$(T_{b\text{-NLRH}}/T_f)_6$															1.65	1.66

Table 5.6. Statistics of normalized peak compression demands of braces for CC-W-HSS frames.

Parameter	Frame															
	CC_W_HSS_10_2_1.0	CC_W_HSS_10_2_1.75	CC_W_HSS_10_3_1.0	CC_W_HSS_10_3_1.75	CC_W_HSS_16_2_1.0	CC_W_HSS_16_2_1.75	CC_W_HSS_16_3_1.0	CC_W_HSS_16_3_1.75	CC_W_HSS_16_4_1.0	CC_W_HSS_16_4_1.75	CC_W_HSS_24_3_1.0	CC_W_HSS_24_3_1.75	CC_W_HSS_24_4_1.0	CC_W_HSS_24_4_1.75	CC_W_HSS_24_6_1.0	CC_W_HSS_24_6_1.75
$(C_{b\text{-NLRH}}/C_u)_1$	0.92	0.93	0.95	0.91	0.85	0.95	0.72	0.90	0.83	0.82	0.84	0.78	0.86	0.77	0.91	0.93
$(C_{b\text{-NLRH}}/C_u)_2$	0.94	0.98	0.93	0.92	0.83	0.99	0.68	0.95	0.82	0.77	0.87	0.62	0.85	0.73	0.85	0.86
$(C_{b\text{-NLRH}}/C_u)_3$			0.94	0.96			0.69	0.96	0.82	0.76	0.83	0.62	0.84	0.73	0.87	0.86
$(C_{b\text{-NLRH}}/C_u)_4$									0.81	0.76			0.85	0.75	0.87	0.86
$(C_{b\text{-NLRH}}/C_u)_5$															0.85	0.85
$(C_{b\text{-NLRH}}/C_u)_6$															0.89	0.89
$(C_{b\text{-NLRH}}/C_f)_1$	1.47	1.56	1.53	1.62	1.39	1.35	1.12	1.28	1.21	1.18	1.14	1.08	1.25	1.24	1.39	1.31
$(C_{b\text{-NLRH}}/C_f)_2$	1.57	1.51	1.57	1.63	1.40	1.40	1.10	1.32	1.23	1.26	1.21	1.17	1.26	1.30	1.34	1.42
$(C_{b\text{-NLRH}}/C_f)_3$			1.59	1.71			1.12	1.33	1.22	1.24	1.16	1.18	1.26	1.29	1.37	1.43
$(C_{b\text{-NLRH}}/C_f)_4$									1.22	1.23			1.26	1.34	1.37	1.42
$(C_{b\text{-NLRH}}/C_f)_5$															1.34	1.41
$(C_{b\text{-NLRH}}/C_f)_6$															1.40	1.47

Figure 5.13. Statistics of peak tension demands of braces for CC-W-HSS frames normalized to their a) probable tensile resistances, and b) design forces.

a)
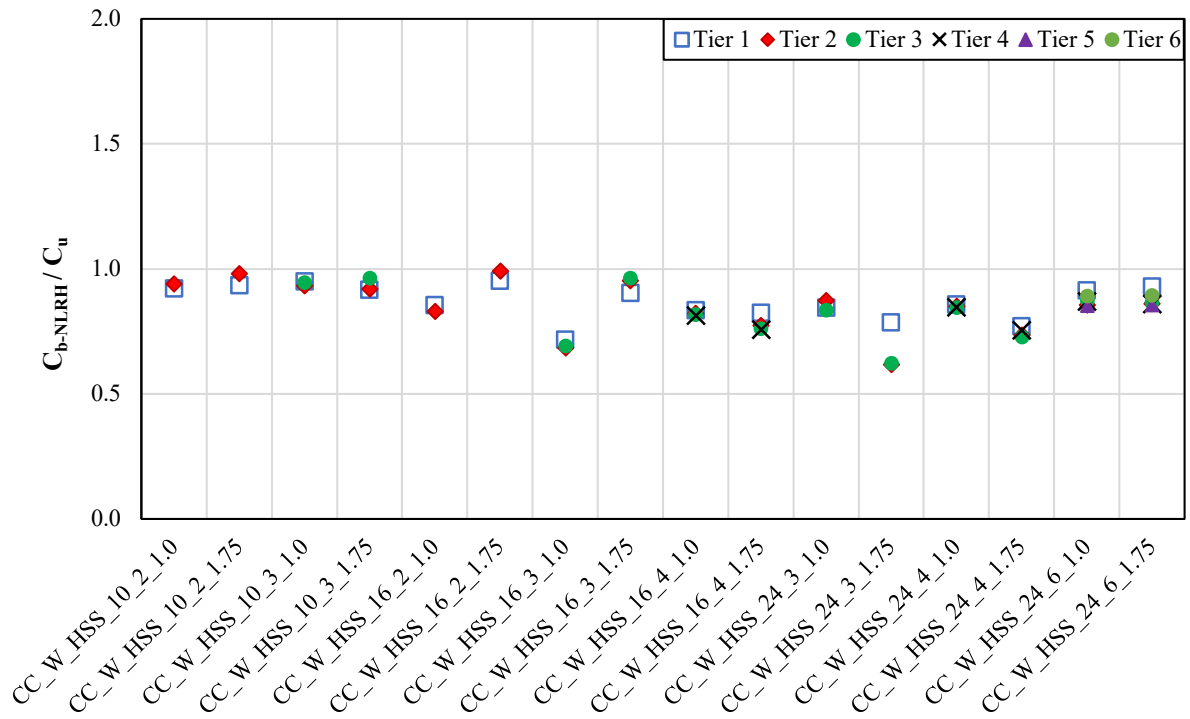
b)
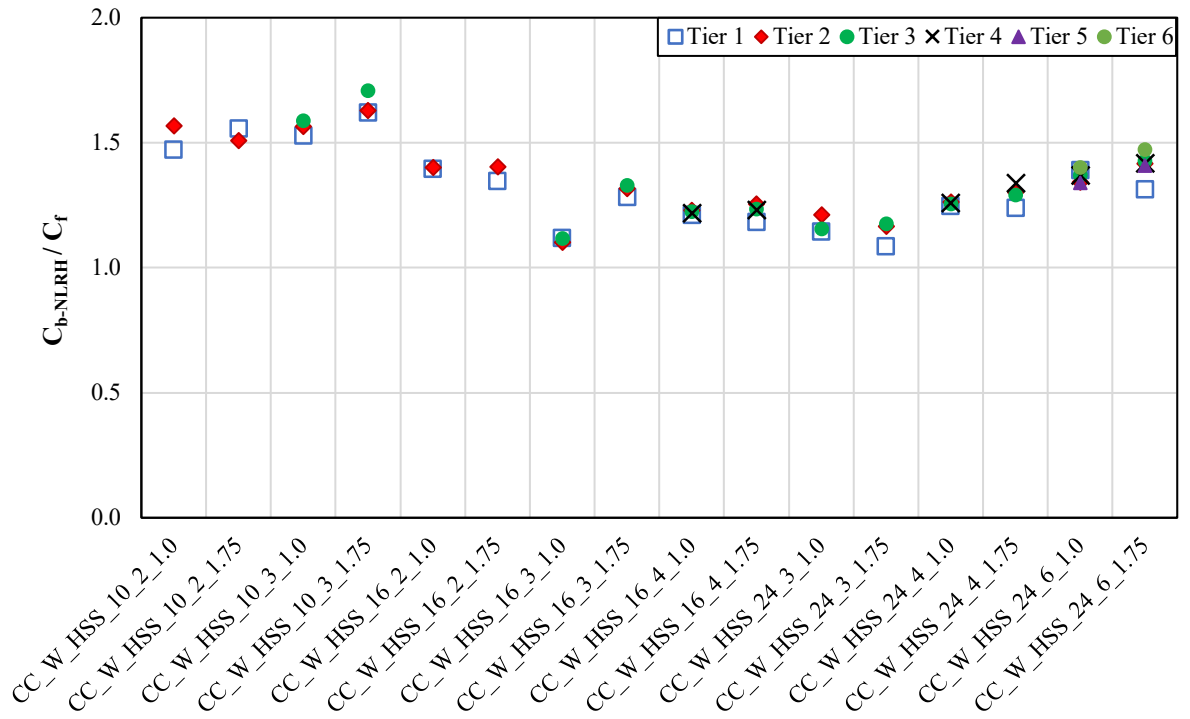
Figure 5.14. Statistics of peak compression demands of braces for CC-W-HSS frames normalized to their a) probable compressive resistances, and b) design forces.

5.3.4.3 Column Behaviour

Table 5.7 gives the statistics of peak column demands for CC-W-HSS frames, including the axial force, in-plane and out-of-plane moments. The demands are normalized to their respective capacities that are the least design axial compression resistance with $\phi = 1.0$, in-plane and out-plane plastic moments, respectively. All of the parameters used in Table 5.7 were introduced in Section 5.3.3.3. The axial forces were recorded in Tier 1, where the largest axial force is expected to occur, and moments were recorded at every strut-to-column connection-level. Similar to Type LD frames, the demands reported are the maximum of LHS and RHS columns. The statistics provided in the table are shown in Figure 5.15, Figure 5.16a, and Figure 5.16b, respectively, for the axial force, in-plane and out-of-plane moments.

As shown in Figure 5.15, axial forces induced in columns of the selected frames range from 0.97 to 1.28 times their design capacities (with $\phi = 1.0$). The discrepancy in the ratios can be explained by the overstrength due to sizing of columns, resistance factor less than one assumed in design, higher brace forces (see Figure 5.13b and Figure 5.14b) than design values. The latter is the most important reason contributing significantly to increase the column axial force demands. The higher column compression forces along with having several cases of column instability indicate that the amplification factors recommended in CSA S16-14 for Type CC frames, namely the amplification of the design seismic forces and column design demands (= 1.3) for frames taller than 15 m, need to be considered for MT-CBFs of Type CC category with T/C braces. However, such amplification factors may be required for Type CC T/C MT-CBFs regardless of the frame height. Such additional design requirements are presented in Section 6.2.3.

Table 5.7. Statistics of normalized peak column demands for CC-W-HSS frames.

Parameter	Frame															
	CC_W_HSS_10_2_1.0	CC_W_HSS_10_2_1.75	CC_W_HSS_10_3_1.0	CC_W_HSS_10_3_1.75	CC_W_HSS_16_2_1.0	CC_W_HSS_16_2_1.75	CC_W_HSS_16_3_1.0	CC_W_HSS_16_3_1.75	CC_W_HSS_16_4_1.0	CC_W_HSS_16_4_1.75	CC_W_HSS_24_3_1.0	CC_W_HSS_24_3_1.75	CC_W_HSS_24_4_1.0	CC_W_HSS_24_4_1.75	CC_W_HSS_24_6_1.0	CC_W_HSS_24_6_1.75
$C_{c\text{-NLRH}}/C_{r,\varphi=1}$	1.08	1.28	0.97	1.02	1.12	1.27	0.99	1.08	1.12	1.11	1.08	1.20	1.11	1.13	1.24	1.23
$(M_{cy\text{-NLRH}}/M_{py})_1$	0.04	0.07	0.03	0.06	0.06	0.08	0.03	0.07	0.02	0.06	0.02	0.05	0.01	0.05	0.01	0.04
$(M_{cy\text{-NLRH}}/M_{py})_2$			0.04	0.06			0.03	0.02	0.02	0.03	0.02	0.02	0.01	0.02	0.01	0.01
$(M_{cy\text{-NLRH}}/M_{py})_3$									0.02	0.01			0.01	0.01	0.01	0.01
$(M_{cy\text{-NLRH}}/M_{py})_4$															0.01	0.01
$(M_{cy\text{-NLRH}}/M_{py})_5$															0.00	0.00
$(M_{cx\text{-NLRH}}/M_{px})_1$	0.13	0.04	0.05	0.14	0.22	0.20	0.09	0.20	0.13	0.18	0.17	0.28	0.12	0.19	0.09	0.14
$(M_{cx\text{-NLRH}}/M_{px})_2$			0.04	0.08			0.07	0.11	0.16	0.16	0.12	0.15	0.14	0.16	0.14	0.17
$(M_{cx\text{-NLRH}}/M_{px})_3$									0.09	0.08			0.08	0.08	0.14	0.15
$(M_{cx\text{-NLRH}}/M_{px})_4$															0.10	0.10
$(M_{cx\text{-NLRH}}/M_{px})_5$															0.05	0.05
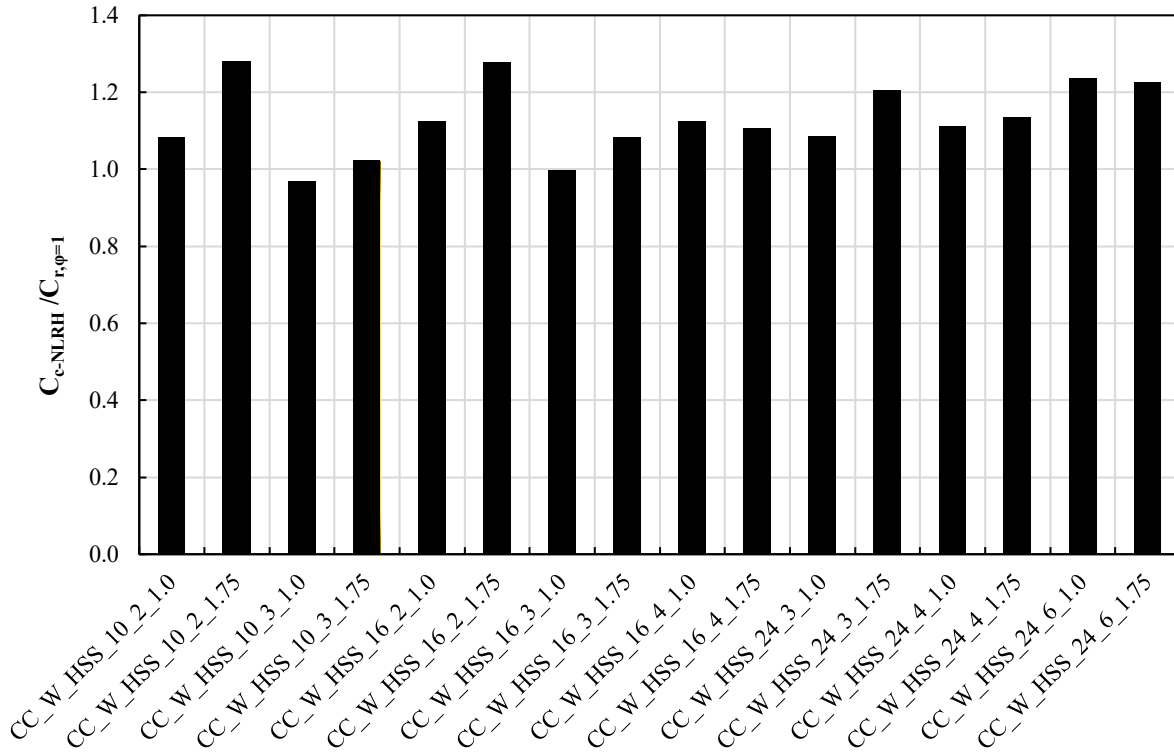
Figure 5.15. Statistics of normalized peak column axial compression forces for CC-W-HSS frames.

As shown in Figure 5.16a, peak in-plane moments induced in the columns of CC-W-HSS frames were found to vary from nearly zero to $0.08M_{py}$ with higher moments observed in the first- or second-tier column segments. Additionally, the moments in the frames with non-uniform tiers were found to be higher than those induced in frames with uniform tiers.

The statistics of normalized peak out-of-plane moment demands induced in the columns of CC-W-HSS frames are shown in Figure 5.16b. The out-of-plane moments vary between $0.04M_{px}$ and $0.28M_{px,}$ with a maximum value observed in the first or second tier segment of the column. The out-of-plane moment was developed in the columns, mainly due to the P-Delta effects under large axial forces and initial geometric imperfections. This moment is expected to be higher in the frames where the location of the maximum axial force and the maximum out-of-plane imperfection is the same (i.e. tall two-tiered CBFs) as shown in Figure 5.16b.

a)
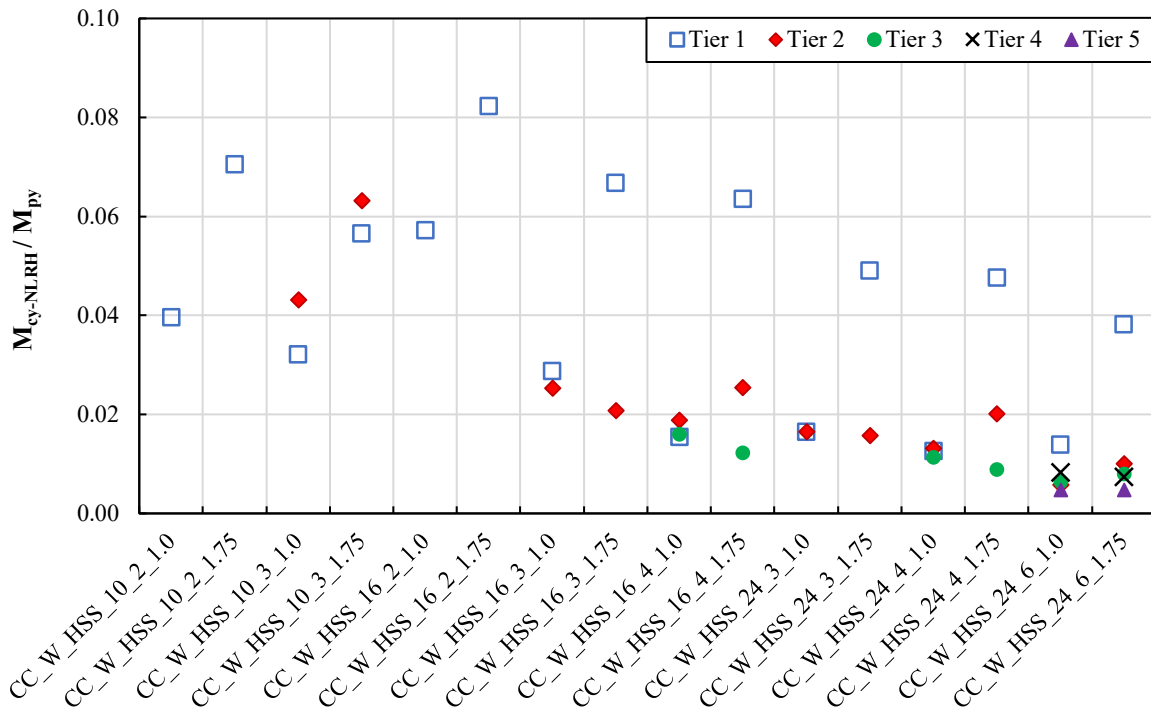
b)
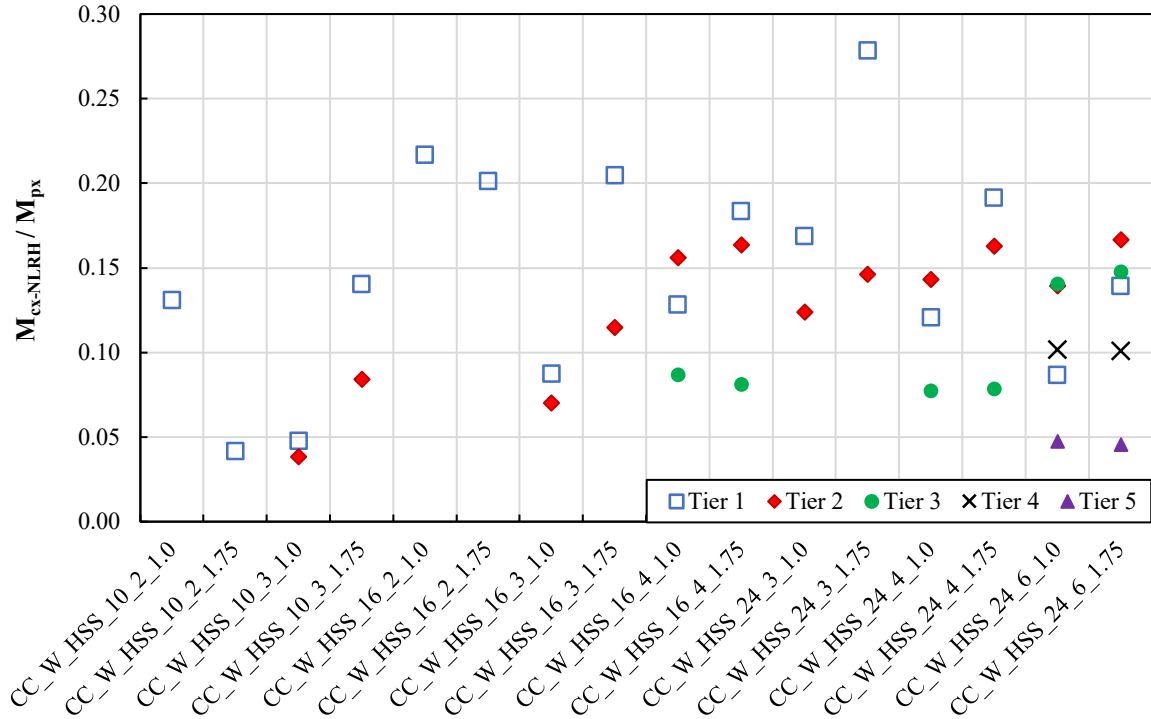
Figure 5.16. Statistics of normalized peak column moment demands for CC-W-HSS frames: a) in-plane moment; b) out-of-plane moment.

5.3.5   Type CC Frames with T/O Braces

5.3.5.1   Frame Global Response

The 960 NLRH analyses of CC-HSS-2L and CC-HSS-L frames were completed without frame collapse or column instability. The statistics of peak lateral displacements, including total storey drifts and tier drifts, are presented in Table 5.8 and Table 5.9, respectively, for CC-HSS-2L frames and CC-HSS-L frames. The tables also include the number of buckling cases observed for these frames and the critical tier location. All of the parameters in the tables were defined earlier in Section 5.3.3.1.

The location of the critical tier is not necessarily the same as the expected critical tier, which can be as a result of the limited inelastic deformations in these frames, as described earlier for LD-W-HSS and CC-W-HSS frames.

Total storey drifts vary between 0.30% and 0.42% for CC-HSS-2L frames (Table 5.8) and between 0.34% and 0.37% for CC-HSS-L frames (Table 5.9). The peak storey drifts for all frames are always smaller than the code-specified drift limit (i.e. 2.5%).

Figure 5.17a and Figure 5.17b show the statistics of peak storey drifts normalized to the respective design storey drifts. As shown, the ratios range from 0.47 to 0.65 for CC-HSS-2L frames and 0.57 to 0.62 for CC-HSS-L. On average, the drift demand for all the frames was found to be approximately half of the design storey drift. As described in Section 3.7.2, the design storey drift for these tension-only braced frames was calculated by neglecting the presence of compression-acting braces because the contribution of such slender braces to the frame lateral stiffness in the inelastic range of the response is negligible, once they buckle in compression. However, the results

obtained from NLRH analyses showed that CC-HSS-2L and CC-HSS-L frames remained nearly elastic with no or a minimal number of braces experiencing post-buckling resistance, which led to a higher lateral stiffness (almost two times the one computed in design) and in turn reduced the frame lateral deflection. Comparing the results of peak storey drifts for CC-HSS-2L and CC-HSS-L frames (Figure 5.17a versus Figure 5.17b) shows more discrepancy in frames with double-angle braces with higher values observed in taller frames.

The results of DCF for CC-HSS-2L and CC-HSS-L frames are shown in Figure 5.18a and Figure 5.18b, respectively. Nonuniformity of drift was found to be very limited (DCF range from 1.04 to 1.21) mainly because of limited inelastic response developed in the frames as the elastic deformations are nearly uniformly distributed between tiers (see Figure 5.2b).

The consistency in the drift values in CC-HSS-L frames can also be seen in Figure 5.19b, which shows a nearly uniform distribution of tier drifts over the frame height. The tier drifts range from 0.29% to 0.42% for frames with single-angle braces, whereas for frames having double-angle braces, the variation is more scattered (0.24% - 0.50%).

Table 5.8. Statistics of peak drift demands for CC-HSS-2L frames.

Parameter	CC_HSS_2L_10_2_1.0	CC_HSS_2L_10_2_1.75	CC_HSS_2L_10_3_1.0	CC_HSS_2L_10_3_1.75	CC_HSS_2L_16_2_1.0	CC_HSS_2L_16_2_1.75	CC_HSS_2L_16_3_1.0	CC_HSS_2L_16_3_1.75	CC_HSS_2L_16_4_1.0	CC_HSS_2L_16_4_1.75	CC_HSS_2L_24_3_1.0	CC_HSS_2L_24_3_1.75	CC_HSS_2L_24_4_1.0	CC_HSS_2L_24_4_1.75	CC_HSS_2L_24_6_1.0	CC_HSS_2L_24_6_1.75
Instability	—	—	—	—	—	—	—	—	—	—	—	—	—	—	—	—
δ_{St}/h (%)	0.35	0.34	0.35	0.42	0.36	0.38	0.33	0.35	0.35	0.35	0.36	0.37	0.33	0.33	0.30	0.31
$\dfrac{\delta_{St}/h}{R_d R_o \delta_e}$	0.55	0.52	0.47	0.53	0.54	0.55	0.51	0.52	0.49	0.49	0.63	0.57	0.65	0.61	0.59	0.58
δ_1/h_1 (%)	0.32	0.32	0.32	0.34	0.33	0.39	0.30	0.31	0.31	0.29	0.31	0.37	0.27	0.38	0.24	0.38
δ_2/h_2 (%)	0.38	0.40	0.38	0.50	0.39	0.37	0.35	0.40	0.36	0.39	0.37	0.37	0.32	0.30	0.27	0.28
δ_3/h_3 (%)			0.38	0.49			0.36	0.40	0.38	0.40	0.40	0.37	0.36	0.31	0.30	0.28
δ_4/h_4 (%)									0.38	0.40			0.37	0.32	0.33	0.30
δ_5/h_5 (%)															0.34	0.31
δ_6/h_6 (%)															0.34	0.31
DCF	1.11	1.17	1.10	1.21	1.11	1.08	1.13	1.16	1.12	1.17	1.12	1.04	1.16	1.12	1.19	1.17
Critical Tier	1[3] 2[27]	2[30]	2[9] 3[21]	2[27] 3[3]	2[30]	1[28] 2[2]	2[3] 3[27]	2[11] 3[19]	3[9] 4[21]	3[14] 4[16]	3[30]	1[22] 3[8]	3[2] 4[28]	1[29] 4[1]	5[5] 6[25]	1[16] 6[14]
Expected Critical Tier	1	1	1	1	1	1	1	1	1	1	1	1	1	1	1	1

148

Table 5.9. Statistics of peak drift demands for CC-HSS-L frames.

Parameter	Frame															
	CC_HSS_L_10_2_1.0	CC_HSS_L_10_2_1.75	CC_HSS_L_10_3_1.0	CC_HSS_L_10_3_1.75	CC_HSS_L_16_2_1.0	CC_HSS_L_16_2_1.75	CC_HSS_L_16_3_1.0	CC_HSS_L_16_3_1.75	CC_HSS_L_16_4_1.0	CC_HSS_L_16_4_1.75	CC_HSS_L_24_3_1.0	CC_HSS_L_24_3_1.75	CC_HSS_L_24_4_1.0	CC_HSS_L_24_4_1.75	CC_HSS_L_24_6_1.0	CC_HSS_L_24_6_1.75
Instability	—	—	—	—	—	—	—	—	—	—	—	—	—	—	—	—
δ_{St}/h (%)	0.34	0.36	0.36	0.35	0.35	0.37	0.36	0.35	0.37	0.37	0.36	0.37	0.36	0.35	0.35	0.35
$\dfrac{\delta_{St}/h}{R_d R_o \delta_e}$	0.57	0.61	0.60	0.60	0.58	0.62	0.60	0.59	0.62	0.62	0.61	0.62	0.61	0.60	0.59	0.59
δ_1/h_1 (%)	0.31	0.34	0.32	0.29	0.32	0.36	0.32	0.33	0.32	0.31	0.32	0.36	0.31	0.34	0.29	0.30
δ_2/h_2 (%)	0.38	0.42	0.37	0.42	0.39	0.38	0.38	0.38	0.37	0.40	0.37	0.38	0.36	0.36	0.32	0.35
δ_3/h_3 (%)			0.39	0.41			0.40	0.38	0.40	0.42	0.40	0.38	0.39	0.37	0.35	0.36
δ_4/h_4 (%)									0.41	0.42			0.40	0.37	0.37	0.38
δ_5/h_5 (%)															0.39	0.39
δ_6/h_6 (%)															0.39	0.39
DCF	1.12	1.15	1.10	1.20	1.12	1.06	1.12	1.08	1.13	1.17	1.12	1.05	1.12	1.06	1.15	1.12
Critical Tier	2[30]	1[1] 2[29]	2[6] 3[24]	2[24] 3[6]	2[30]	1[13] 2[17]	2[1] 3[29]	2[5] 3[25]	3[6] 4[24]	3[11] 4[19]	3[30]	1[4] 2[4] 3[22]	3[6] 4[24]	1[8] 3[3] 4[19]	5[5] 6[25]	5[4] 6[26]
Expected Critical Tier	1	1	1	2	1	1	1	1	1	1	1	1	1	1	1	1

a)
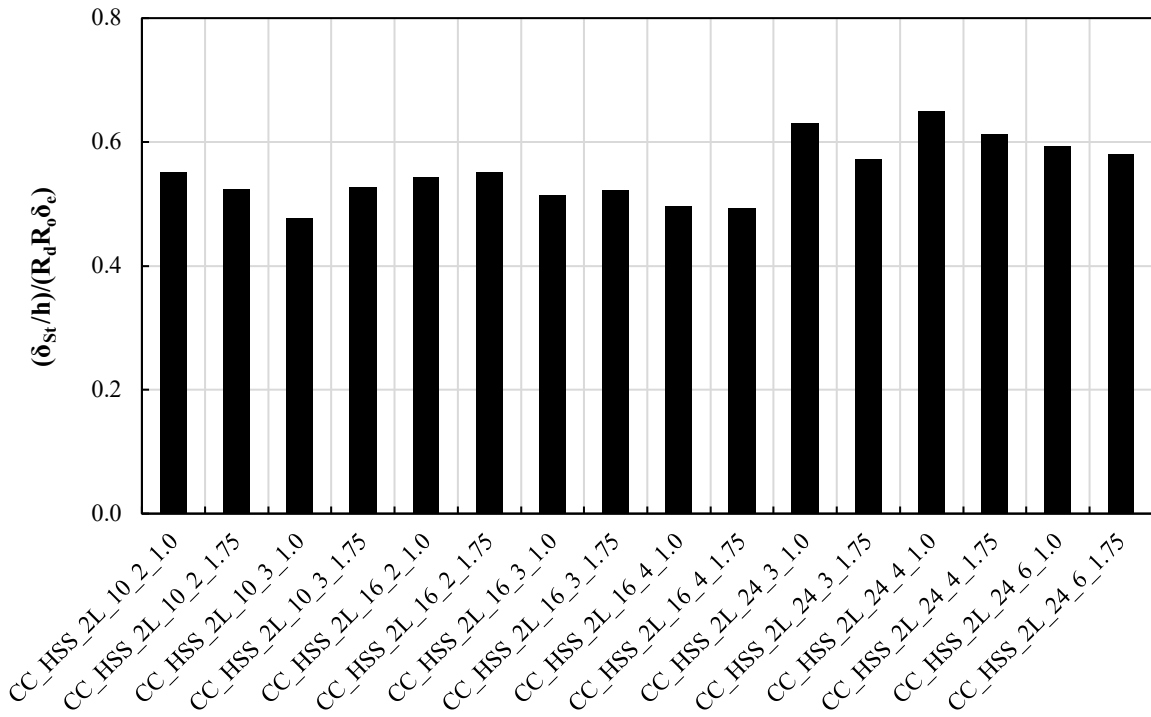
b)
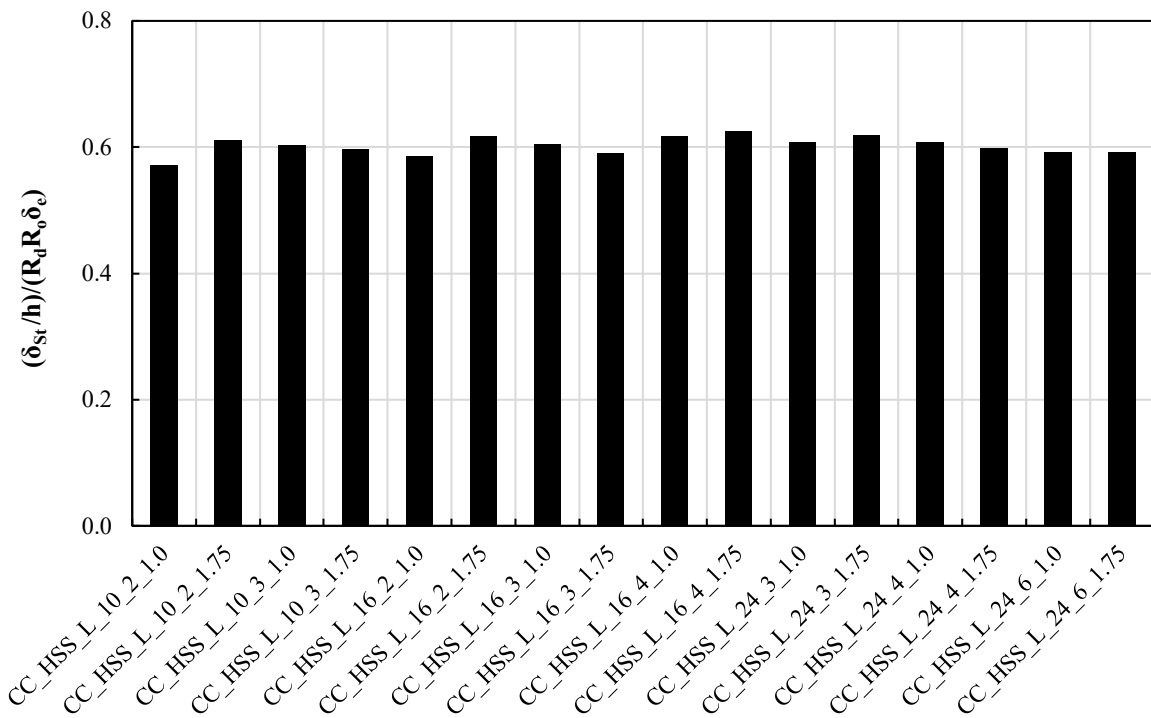
Figure 5.17. Statistics of normalized peak storey drifts for a) CC-HSS-2L frames, and b) CC-HSS-L frames.

a)
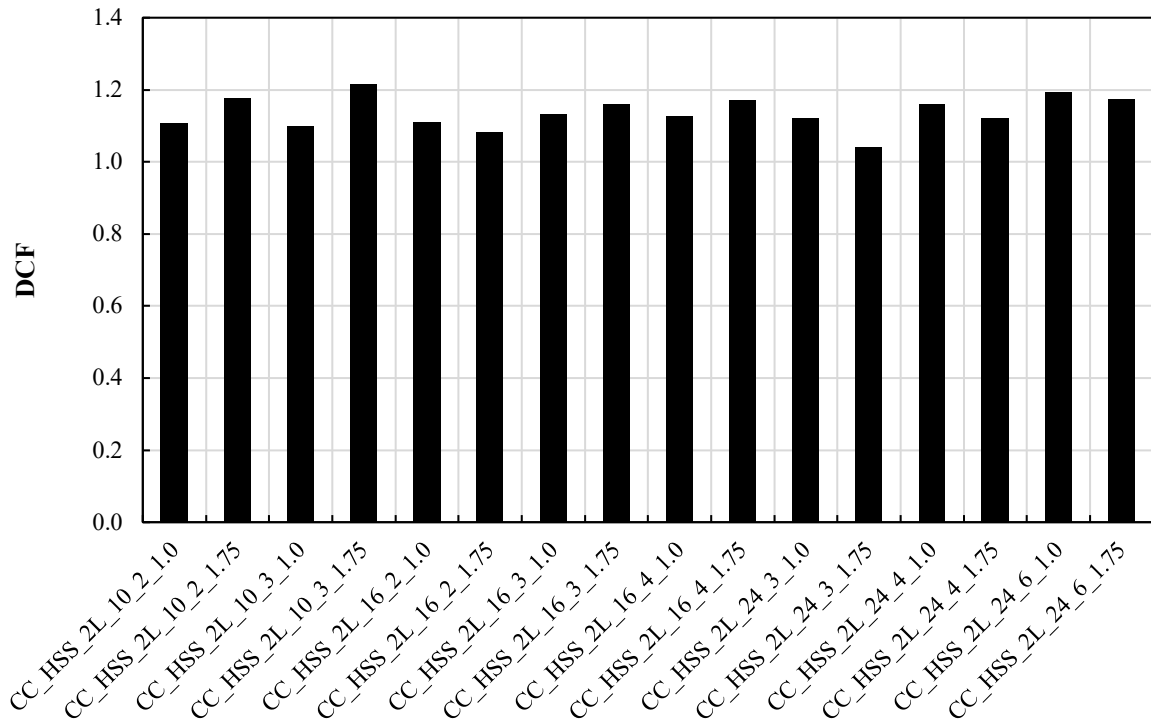
b)
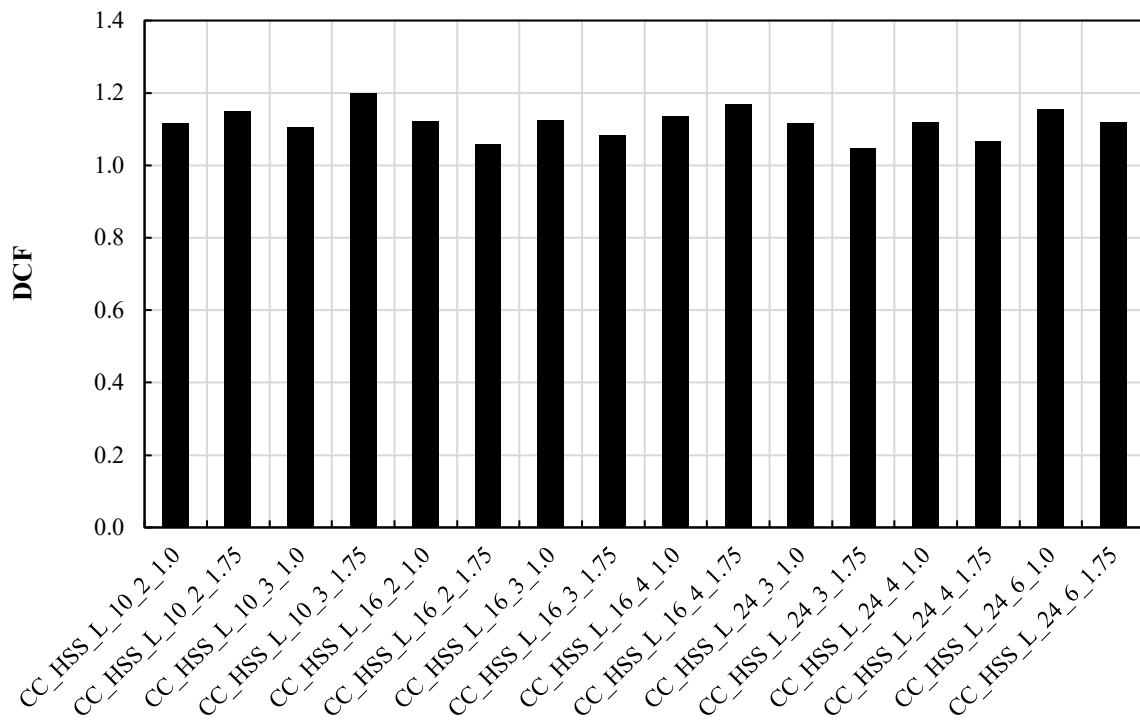
Figure 5.18. Statistics of peak Drift Concentration Factors (DCFs) for a) CC-HSS-2L frames, and b) CC-HSS-L frames.

Figure 5.19. Statistics of peak tier drifts for a) CC-HSS-2L frames, and b) CC-HSS-L frames.

152
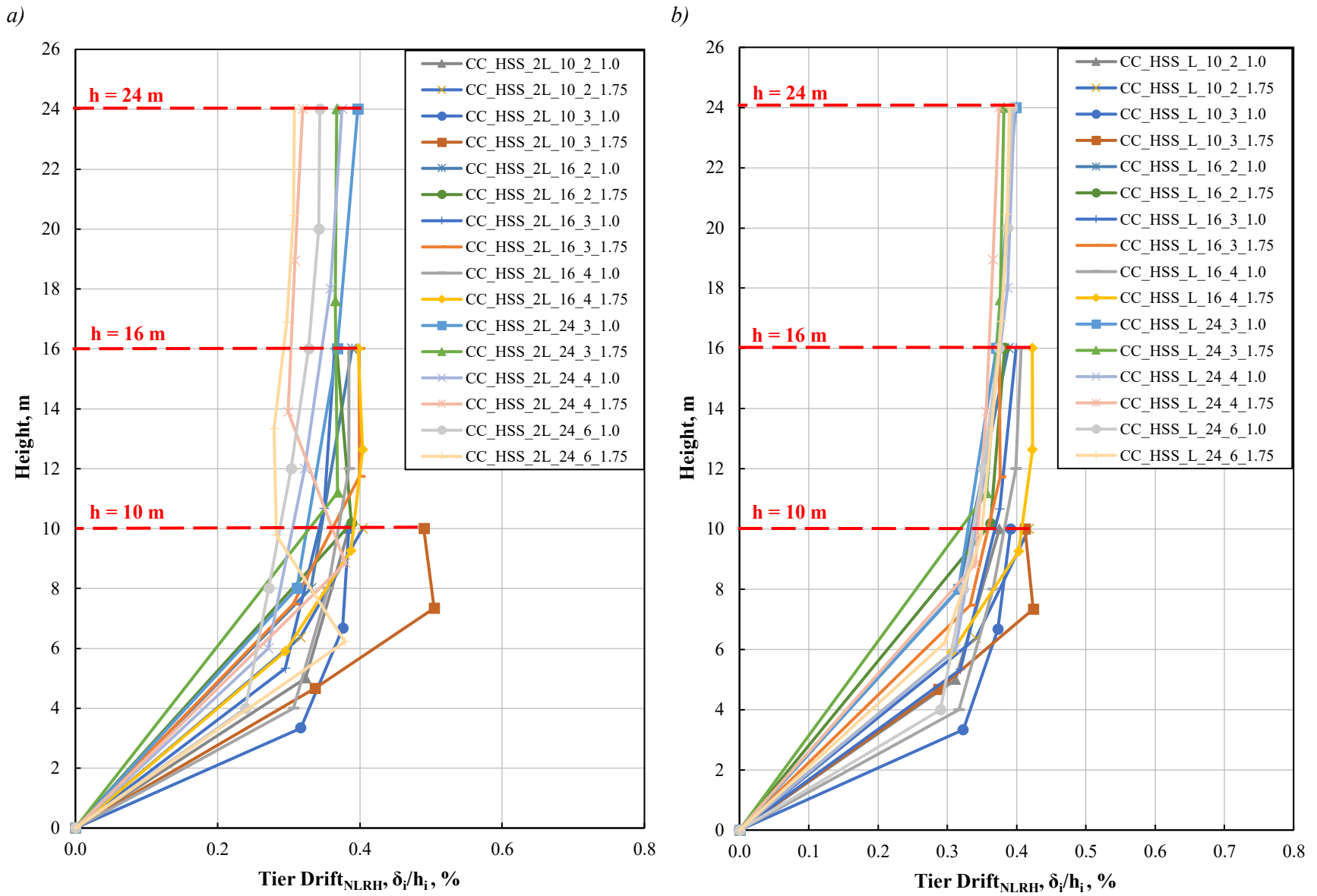
5.3.5.2 Brace Behavior

Table 5.10 and Table 5.11, respectively, provide the statistics of normalized peak tension and compression forces for the braces of CC-HSS-2L frames. In the tables, the forces are normalized to the respective probable resistances and design forces. It is worth noting that both tension and compression demands are normalized to the design tension forces, T_f, because the braces were designed as T/O. Thus, there was no design compression force considered in design (see Section 3.7.2). The statistics mentioned above for CC-HSS-2L were also presented in Figure 5.20 and Figure 5.21, respectively, for brace tension and compression forces. Similar results are provided in Table 5.12 and Table 5.13 for CC-HSS-L frames as well as in Figure 5.22 and Figure 5.23 for tension and compression forces of CC-HSS-L braces, respectively.

As shown in Figure 5.20a, the tension brace forces in double-angle braces are considerably lesser than their probable tensile resistances, which means none of the braces have yielded in tension. Figure 5.20b shows that tension double-angle brace in the majority of tiers experienced higher forces than their design forces with a maximum of 28%.

As depicted in Figure 5.20b and Figure 5.21b, the compression forces induced in the double-angle braces are drastically smaller than the tension forces. This indicates that all of the double-angle braces have buckled in compression; otherwise, the induced tension and compression forces would have been close to one another if they both would have responded in the elastic region. Additionally, the out-of-plane displacement of the braces recorded at the mid-length of the brace half reaffirms that the braces have buckled. However, as Figure 5.21a shows, the maximum compression forces for some of the braces at buckling, were smaller than their respective probable compressive resistances calculated using CSA S16-14. The discrepancy in the prediction of the

153

double-angle brace compression capacity, in part, pertains to the capability of the numerical model used in this study.

An example of the calculation of the probable compressive resistance of braces located in the first tier of frame CC_HSS_2L_10_2_1.0 according to Clause 13.3.2 of CSA S16-14 and using the equivalent slenderness ratio described in Section 2.5.3 are provided here:

2L89×64×9.5 LLBB; Gap = 12 mm; Brace total length: L_{br} = 7810 mm; R_yF_y = 347 MPa

Single-angle (SA):

$r_{min,SA}$ = 13.65 mm; $K_{x',SA}$ = 0.65; L_{SA} = 0.9×7810 / 4 = 1757 mm (unbraced length of SA)

$\rho_i = \dfrac{K_{x',SA}L_{SA}}{r_{min,SA}}$ = 0.65 × 1757 / 13.65 = 83.68 (slenderness ratio of SA about minor axis)

Double-angle (DA):

A = 2723 mm^2; $r_{x,DA}$ = 27.98 mm, $r_{y,DA}$ = 29.18 mm; J = 85800 mm^4; C_w = 3.84E+07 mm^6

x_0 = 0; y_0 = 24.44 mm → $\bar{r}_0$ = 47.2 mm and Ω = 0.732

$K_{x,DA} = K_{y,DA} = K_{z,DA}$ = 1.0; L_{DA} = 0.9 × 7810 / 2 = 3515 mm (unbraced length of DA)

$\rho_{0x} = \dfrac{K_{x,DA}L_{DA}}{r_{x,DA}}$ = 1.0 × 3515 / 27.98 = 125.61 (slenderness ratio of DA about its X-axis)

$\rho_{0y} = \dfrac{K_{y,DA}L_{DA}}{r_{y,DA}}$ = 1.0 × 3515 / 29.18 = 120.46 (slenderness ratio of DA about its Y-axis)

$\rho_e = \sqrt{\rho_{0y}{}^2 + \rho_i{}^2}$ = 146.7 (equivalent slenderness ratio of DA)

$F_{ex} = \dfrac{\pi^2 E}{\rho_{0x}{}^2}$ = 125 MPa; $F_{ey} = \dfrac{\pi^2 E}{\rho_e{}^2}$ = 92 MPa; $F_{ez} = \left(\dfrac{\pi^2 E C_w}{(K_{z,DA}L_{DA})^2} + GJ \right)\dfrac{1}{A\bar{r}_0{}^2}$ = 1087 MPa

$F_{eyz} = \dfrac{F_{ey}+F_{ez}}{2\Omega}\left[1 - \sqrt{1 - \dfrac{4F_{ey}F_{ez}\Omega}{(F_{ey}+F_{ez})^2}}\right]$ = 93 MPa; $\lambda_{max} = \sqrt{\dfrac{R_yF_y}{\min\ (F_{ex},F_{eyz})}}$ = 1.94

$C_{r,min} = \dfrac{\phi A R_y F_y}{(1+\lambda_{max}{}^{2n})^{1/n}}$ = 202 kN → C_u = min (1.2$C_{r,min}$ / ϕ, AR_yF_y) = 270 kN

Table 5.10. Statistics of normalized peak tension forces of braces for CC-HSS-2L frames.

Parameter	CC_HSS_2L_10_2_1.0	CC_HSS_2L_10_2_1.75	CC_HSS_2L_10_3_1.0	CC_HSS_2L_10_3_1.75	CC_HSS_2L_16_2_1.0	CC_HSS_2L_16_2_1.75	CC_HSS_2L_16_3_1.0	CC_HSS_2L_16_3_1.75	CC_HSS_2L_16_4_1.0	CC_HSS_2L_16_4_1.75	CC_HSS_2L_24_3_1.0	CC_HSS_2L_24_3_1.75	CC_HSS_2L_24_4_1.0	CC_HSS_2L_24_4_1.75	CC_HSS_2L_24_6_1.0	CC_HSS_2L_24_6_1.75
$(T_{b\text{-NLRH}}/T_u)_1$	0.73	0.65	0.65	0.69	0.70	0.68	0.67	0.60	0.65	0.61	0.72	0.69	0.63	0.78	0.51	0.79
$(T_{b\text{-NLRH}}/T_u)_2$	0.64	0.67	0.57	0.71	0.62	0.61	0.59	0.67	0.57	0.61	0.64	0.71	0.56	0.47	0.44	0.41
$(T_{b\text{-NLRH}}/T_u)_3$			0.56	0.64			0.58	0.61	0.57	0.55	0.64	0.63	0.56	0.44	0.45	0.37
$(T_{b\text{-NLRH}}/T_u)_4$									0.57	0.54			0.56	0.44	0.44	0.37
$(T_{b\text{-NLRH}}/T_u)_5$															0.44	0.37
$(T_{b\text{-NLRH}}/T_u)_6$															0.44	0.37
$(T_{b\text{-NLRH}}/T_f)_1$	1.14	1.09	1.05	1.16	1.08	1.15	1.07	1.07	1.05	1.04	1.27	1.18	1.31	1.25	1.23	1.30
$(T_{b\text{-NLRH}}/T_f)_2$	1.11	1.06	1.03	1.09	1.06	0.94	1.05	1.07	1.03	1.03	1.25	1.14	1.29	1.16	1.18	1.14
$(T_{b\text{-NLRH}}/T_f)_3$			1.01	1.08			1.05	1.07	1.03	1.03	1.25	1.13	1.29	1.10	1.21	1.04
$(T_{b\text{-NLRH}}/T_f)_4$									1.02	1.02			1.29	1.10	1.20	1.04
$(T_{b\text{-NLRH}}/T_f)_5$															1.19	1.02
$(T_{b\text{-NLRH}}/T_f)_6$															1.19	1.03

Table 5.11. Statistics of normalized peak compression forces of braces for CC-HSS-2L frames.

Parameter	CC_HSS_2L_10_2_1.0	CC_HSS_2L_10_2_1.75	CC_HSS_2L_10_3_1.0	CC_HSS_2L_10_3_1.75	CC_HSS_2L_16_2_1.0	CC_HSS_2L_16_2_1.75	CC_HSS_2L_16_3_1.0	CC_HSS_2L_16_3_1.75	CC_HSS_2L_16_4_1.0	CC_HSS_2L_16_4_1.75	CC_HSS_2L_24_3_1.0	CC_HSS_2L_24_3_1.75	CC_HSS_2L_24_4_1.0	CC_HSS_2L_24_4_1.75	CC_HSS_2L_24_6_1.0	CC_HSS_2L_24_6_1.75
$(C_{b\text{-NLRH}}/C_u)_1$	0.91	1.01	0.97	0.90	1.01	0.86	0.97	1.02	0.90	0.99	0.90	0.98	0.90	0.96	0.87	0.95
$(C_{b\text{-NLRH}}/C_u)_2$	0.93	0.99	1.00	0.90	1.02	0.99	1.00	0.92	0.92	0.91	0.90	0.93	0.91	0.90	0.89	0.87
$(C_{b\text{-NLRH}}/C_u)_3$			0.99	0.93			0.99	0.94	0.92	0.93	0.89	0.94	0.91	0.89	0.89	0.86
$(C_{b\text{-NLRH}}/C_u)_4$									0.92	0.93			0.90	0.88	0.89	0.85
$(C_{b\text{-NLRH}}/C_u)_5$															0.88	0.85
$(C_{b\text{-NLRH}}/C_u)_6$															0.87	0.84
$(C_{b\text{-NLRH}}/T_f)_1$	0.40	0.47	0.54	0.29	0.27	0.12	0.42	0.31	0.33	0.38	0.20	0.17	0.31	0.24	0.48	0.25
$(C_{b\text{-NLRH}}/T_f)_2$	0.42	0.52	0.56	0.38	0.28	0.38	0.44	0.32	0.34	0.38	0.20	0.24	0.32	0.40	0.49	0.53
$(C_{b\text{-NLRH}}/T_f)_3$			0.56	0.39			0.43	0.33	0.34	0.39	0.20	0.24	0.32	0.39	0.50	0.52
$(C_{b\text{-NLRH}}/T_f)_4$									0.34	0.39			0.32	0.39	0.50	0.52
$(C_{b\text{-NLRH}}/T_f)_5$															0.49	0.52
$(C_{b\text{-NLRH}}/T_f)_6$															0.49	0.52

156

Table 5.12. Statistics of normalized peak tension demands of braces for CC-HSS-L frames.

Parameter	CC_HSS_L_10_2_1.0	CC_HSS_L_10_2_1.75	CC_HSS_L_10_3_1.0	CC_HSS_L_10_3_1.75	CC_HSS_L_16_2_1.0	CC_HSS_L_16_2_1.75	CC_HSS_L_16_3_1.0	CC_HSS_L_16_3_1.75	CC_HSS_L_16_4_1.0	CC_HSS_L_16_4_1.75	CC_HSS_L_24_3_1.0	CC_HSS_L_24_3_1.75	CC_HSS_L_24_4_1.0	CC_HSS_L_24_4_1.75	CC_HSS_L_24_6_1.0	CC_HSS_L_24_6_1.75
$(T_{b\text{-}NLRH}/T_u)_1$	0.68	0.70	0.65	0.57	0.65	0.64	0.70	0.66	0.68	0.63	0.75	0.68	0.77	0.72	0.66	0.68
$(T_{b\text{-}NLRH}/T_u)_2$	0.61	0.68	0.58	0.62	0.58	0.66	0.62	0.64	0.60	0.64	0.66	0.74	0.68	0.69	0.58	0.64
$(T_{b\text{-}NLRH}/T_u)_3$			0.58	0.55			0.63	0.56	0.60	0.58	0.67	0.67	0.68	0.61	0.59	0.59
$(T_{b\text{-}NLRH}/T_u)_4$									0.60	0.58			0.68	0.61	0.58	0.59
$(T_{b\text{-}NLRH}/T_u)_5$															0.58	0.58
$(T_{b\text{-}NLRH}/T_u)_6$															0.59	0.59
$(T_{b\text{-}NLRH}/T_f)_1$	1.17	1.20	1.04	1.12	1.19	1.11	1.14	1.16	1.04	1.08	1.23	1.15	1.22	1.23	1.16	1.18
$(T_{b\text{-}NLRH}/T_f)_2$	1.16	1.06	1.02	1.02	1.18	1.02	1.12	0.99	1.02	1.03	1.21	1.13	1.20	1.11	1.12	0.98
$(T_{b\text{-}NLRH}/T_f)_3$			1.02	1.01			1.12	0.97	1.02	1.03	1.22	1.13	1.20	1.09	1.14	1.01
$(T_{b\text{-}NLRH}/T_f)_4$									1.02	1.03			1.21	1.10	1.14	1.00
$(T_{b\text{-}NLRH}/T_f)_5$															1.12	0.99
$(T_{b\text{-}NLRH}/T_f)_6$															1.14	1.00

Table 5.13. Statistics of normalized peak compression demands of braces for CC-HSS-L frames.

Parameter	Frame															
	CC_HSS_L_10_2_1.0	CC_HSS_L_10_2_1.75	CC_HSS_L_10_3_1.0	CC_HSS_L_10_3_1.75	CC_HSS_L_16_2_1.0	CC_HSS_L_16_2_1.75	CC_HSS_L_16_3_1.0	CC_HSS_L_16_3_1.75	CC_HSS_L_16_4_1.0	CC_HSS_L_16_4_1.75	CC_HSS_L_24_3_1.0	CC_HSS_L_24_3_1.75	CC_HSS_L_24_4_1.0	CC_HSS_L_24_4_1.75	CC_HSS_L_24_6_1.0	CC_HSS_L_24_6_1.75
$(C_{b\text{-}NLRH}/C_u)_1$	0.70	0.67	0.73	0.69	0.67	0.65	0.68	0.66	0.68	0.67	0.67	0.65	0.69	0.67	0.67	0.68
$(C_{b\text{-}NLRH}/C_u)_2$	0.68	0.73	0.72	0.75	0.66	0.68	0.67	0.75	0.68	0.69	0.67	0.70	0.69	0.68	0.67	0.69
$(C_{b\text{-}NLRH}/C_u)_3$			0.72	0.76			0.67	0.75	0.68	0.70	0.66	0.69	0.69	0.68	0.67	0.70
$(C_{b\text{-}NLRH}/C_u)_4$									0.68	0.70			0.68	0.67	0.67	0.70
$(C_{b\text{-}NLRH}/C_u)_5$															0.67	0.69
$(C_{b\text{-}NLRH}/C_u)_6$															0.66	0.69
$(C_{b\text{-}NLRH}/T_f)_1$	0.50	0.36	0.58	0.54	0.34	0.22	0.35	0.32	0.31	0.31	0.18	0.14	0.17	0.15	0.35	0.16
$(C_{b\text{-}NLRH}/T_f)_2$	0.50	0.55	0.58	0.65	0.34	0.32	0.36	0.52	0.31	0.35	0.18	0.16	0.17	0.29	0.35	0.33
$(C_{b\text{-}NLRH}/T_f)_3$			0.58	0.67			0.35	0.52	0.31	0.36	0.18	0.16	0.17	0.28	0.36	0.34
$(C_{b\text{-}NLRH}/T_f)_4$									0.31	0.35			0.17	0.28	0.35	0.34
$(C_{b\text{-}NLRH}/T_f)_5$															0.35	0.34
$(C_{b\text{-}NLRH}/T_f)_6$															0.35	0.33

a)
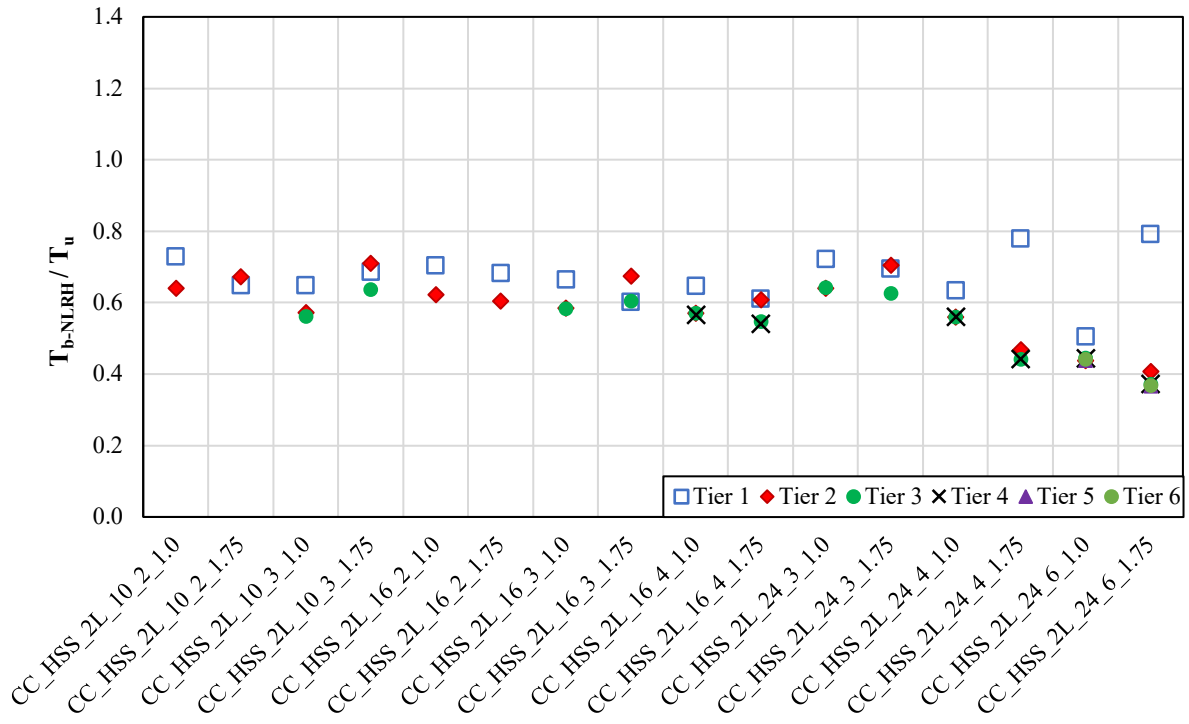
b)
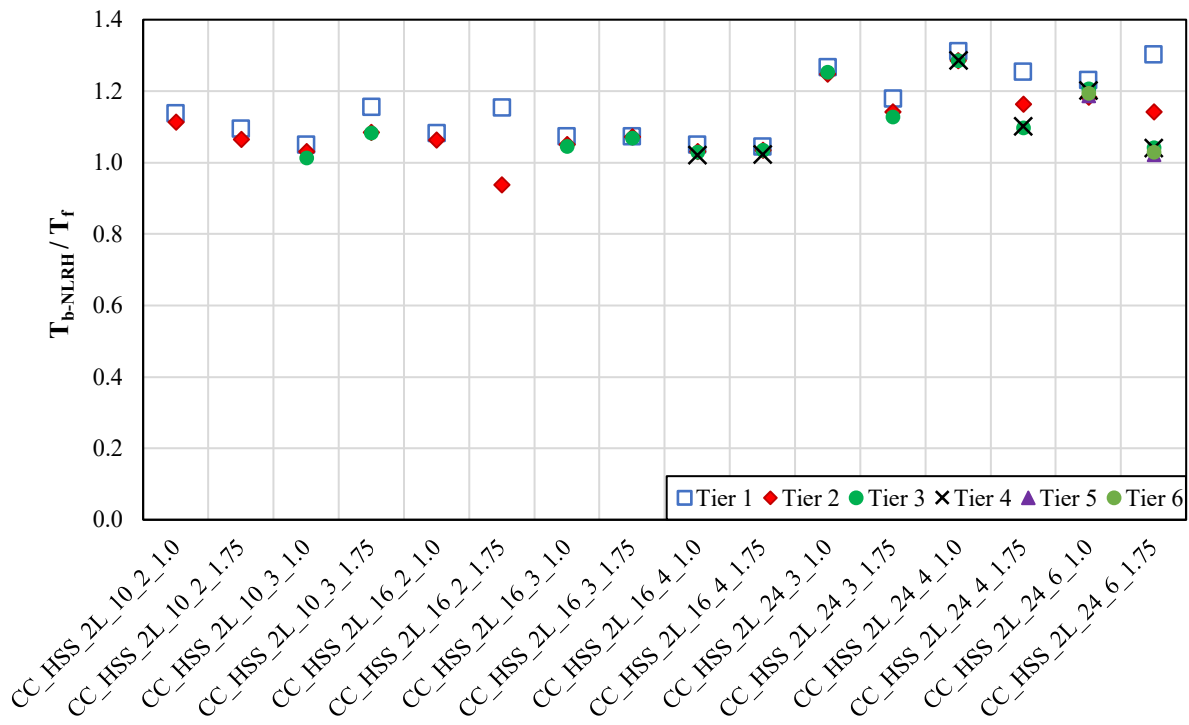
Figure 5.20. Statistics of peak tension brace forces for CC-HSS-2L frames normalized to their a) probable tensile resistances, and b) design forces.

a)
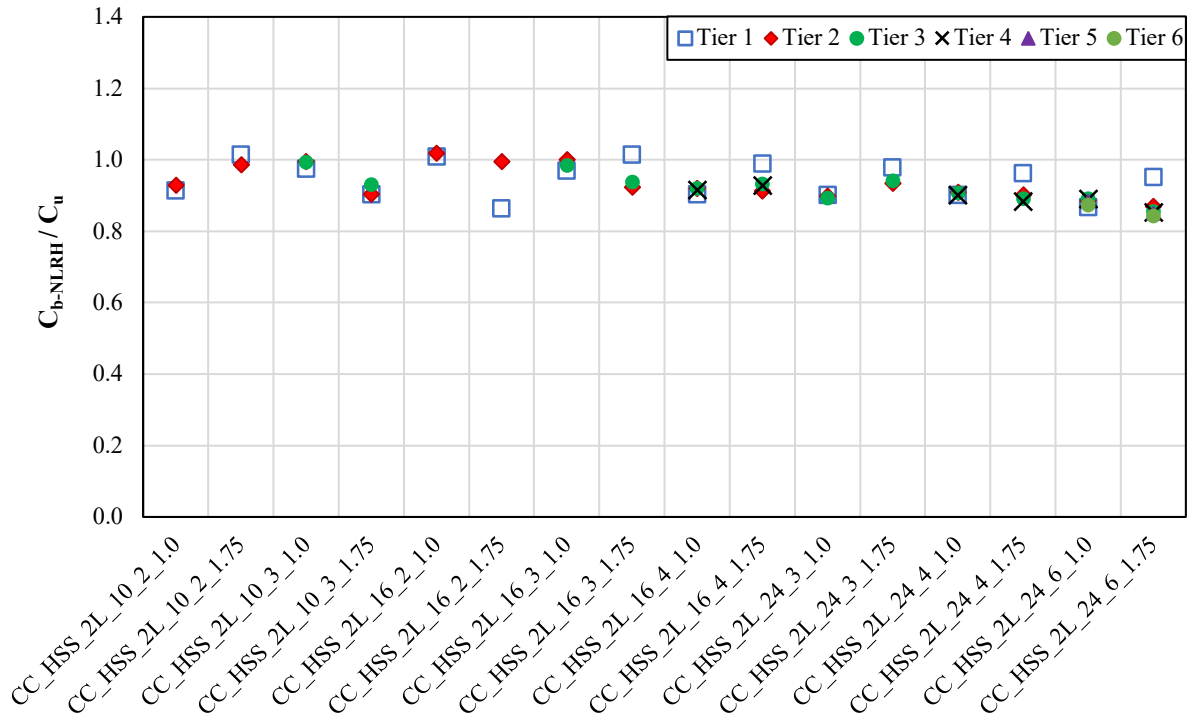
b)
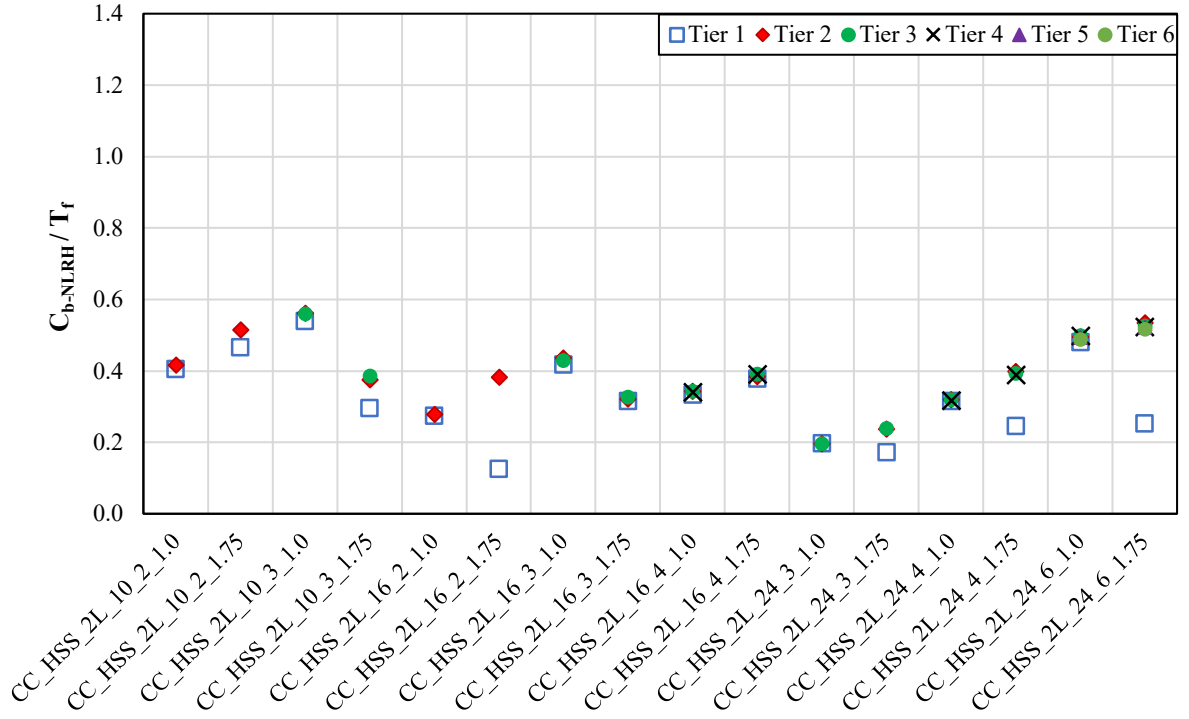
Figure 5.21. Statistics of peak compression brace forces for CC-HSS-2L frames normalized to their a) probable compressive resistances, and b) design forces.

The results of tension brace forces shown in Figure 5.22 for CC-HSS-L confirm that no yielding occurred in the single-angle braces, and the brace forces are appreciably lesser than their respective tensile capacities. However, as shown in Figure 5.22b for single-angle braces, larger tensile forces compared to their design forces were observed in a large number of CC-HSS-L frames.

Similar to double-angles, as shown in Figure 5.22b and Figure 5.23b, significantly larger tension forces induced in the single-angle braces compared to the compression forces indicates that all of the single-angle braces have buckled. In addition, noticeably large out-of-plane displacement of the braces measured at the mid-length of the brace half confirms that the braces have buckled. However, as shown in Figure 5.23a, the maximum compression demands in single-angle braces of CC-HSS-L frames were found to be smaller than the respective probable compressive resistances, as expected from the calibration of the single-angle brace (see Section 4.3.1.1). This underestimation could be attributed to the capability of the numerical model used in this study. It should be noted that in such tension-only braced frames, the influence of the compression brace force on the frame seismic response is expected to be insignificant because of lower forces in the slender compression-acting braces.

A sample calculation of the probable compressive resistance of single-angle braces are presented here for braces located in tier 1 of frame CC_HSS_L_10_2_1.0 in accordance with Clause 13.3.2 of CSA S16-14:

L102×102×15.9; Brace total length: L_{br} = 7810 mm; $R_y F_y$ = 347 MPa

A = 2991 mm^2; $r_x = r_y$ = 30.66 mm; $r_{x'}$ = 19.87 mm; J = 252034 mm^4; C_w = 1.83E+08 mm^6

$x_0 = y_0$ = 23.34 mm → $\bar{r_0}$ = 54.49 mm

$K_x = K_y$ = 1.0; $K_{x'}$ = 0.85; $L_x = L_y = L_{x'}$ = 0.9×7810 / 2 = 3515 mm (unbraced length of brace)

$$\frac{K_x L_x}{r_x} = \frac{K_y L_y}{r_y} = 1.0 \times 3515 / 30.66 = 115 \text{ (slenderness ratio about X- or Y-axis)}$$

$$\frac{K_{x'} L_{x'}}{r_{x'}} = 0.85 \times 3515 / 19.87 = 150 \text{ (slenderness ratio about minor axis)}$$

$$F_{ex} = F_{ey} = \frac{\pi^2 E}{\rho_{0x}^2} = 150 \text{ MPa}; \; F_{ez} = \left(\frac{\pi^2 E C_w}{(K_{x'} L_{x'})^2} + GJ\right) \frac{1}{A \bar{r}_0^2} = 2201 \text{ MPa}$$

$$(F_e - F_{ex})(F_e - F_{ey})(F_e - F_{ez}) - F_e^2 (F_e - F_{ey})\left(\frac{x_0}{\bar{r}_0}\right)^2 - F_e^2 (F_e - F_{ex})\left(\frac{y_0}{\bar{r}_0}\right)^2 = 0 \rightarrow F_e = 146 \text{ MPa}$$

$$\lambda_{\max} = \sqrt{\frac{R_y F_y}{F_e}} = 1.54$$

$$C_{r,\min} = \frac{\phi A R_y F_y}{(1 + \lambda_{\max}^{2n})^{1/n}} = 321 \text{ kN} \rightarrow C_u = \min\left(1.2 C_{r,\min}/\phi, \; A R_y F_y\right) = 428 \text{ kN}$$

a)
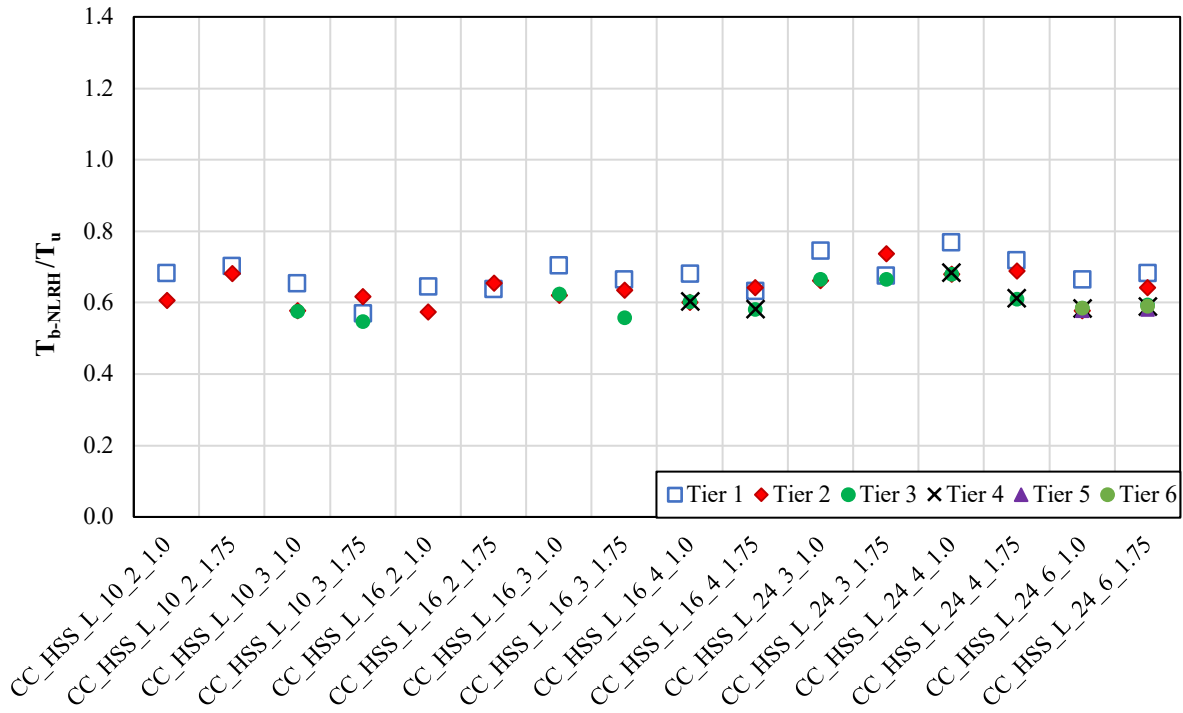
b)
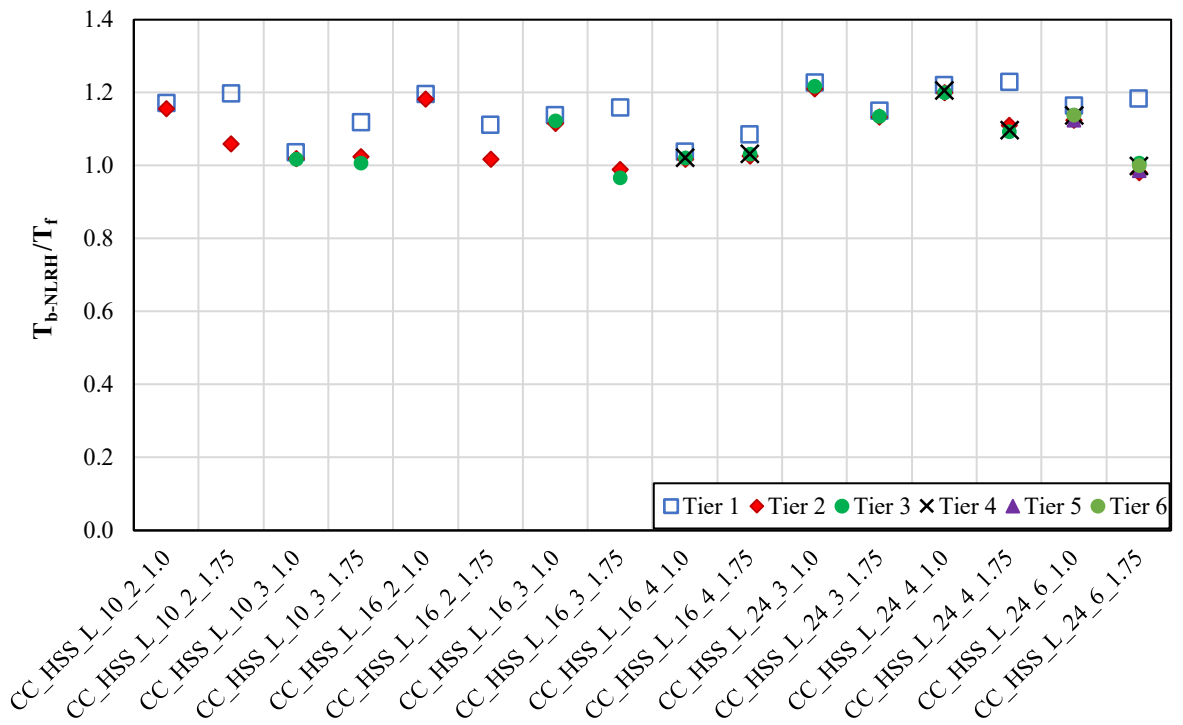
Figure 5.22. Statistics of peak tension demands of braces for CC-HSS-L frames normalized to their a) probable tensile resistances, and b) design forces.

163

a)
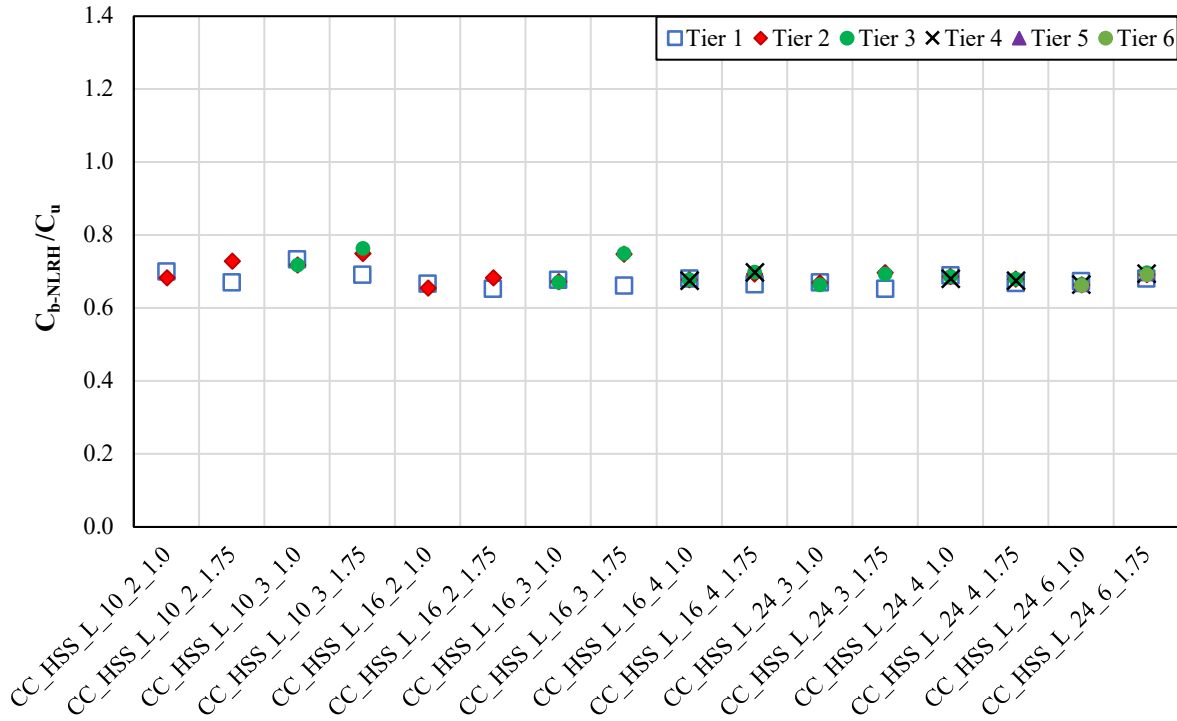
b)
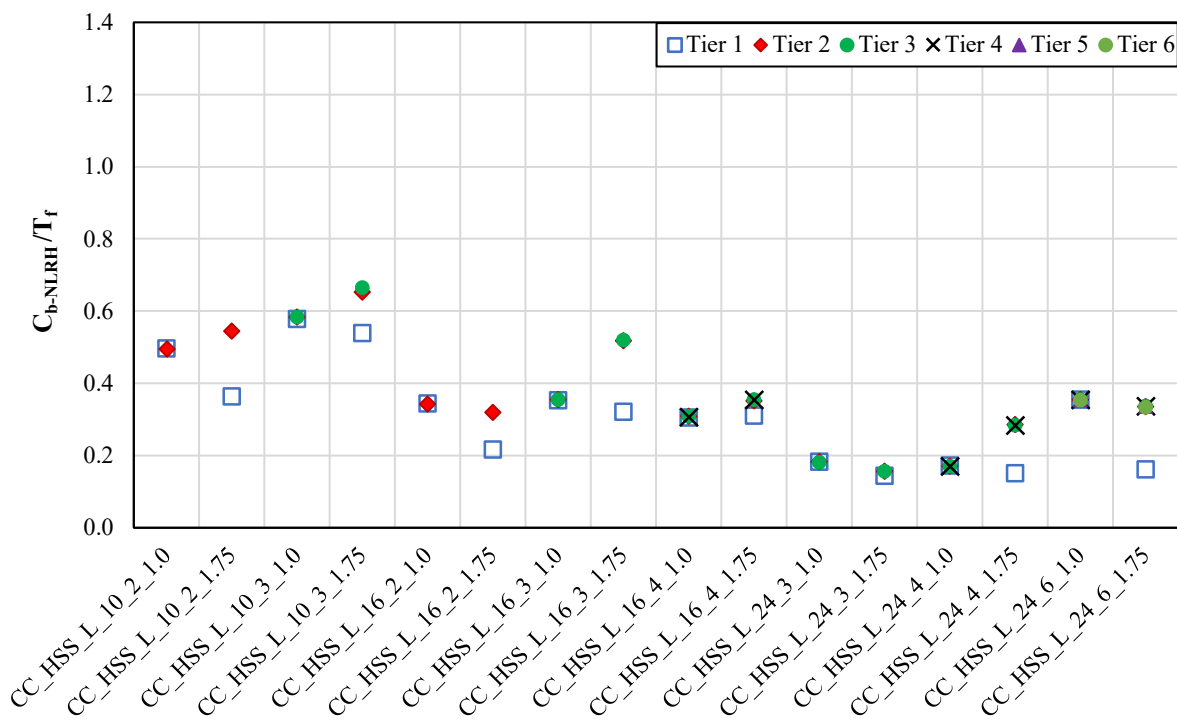
Figure 5.23. Statistics of peak compression demands of braces for CC-HSS-L frames normalized to their a) probable tensile resistances, and b) design forces.

5.3.5.3 Column Behaviour

The statistics of peak column demands, including the axial force, in-plane moment, and out-of-plane moment for CC-HSS-2L and CC-HSS-L frames, are given in Table 5.14 and Table 5.15, respectively. The tables provide column axial forces normalized to the respective minimum design compression capacities at the first-tier segment with a resistance factor $\phi = 1.0$, and the ratios of in-plane and out-of-plane moments to the respective plastic moments at strut-to-column connection levels. Similar to LD-W-HSS and CC-W-HSS frames, the reported quantities are the maximum of LHS and RHS columns. The columns of these frames are square HSS for which the plastic moments about both principal axes (X and Y) are the same and shown using M_p in the tables. All other symbols were introduced in Section 5.3.3.3. Figure 5.24 and Figure 5.25 show the quantities of the column demands in a plot format.

As shown in Figure 5.24, peak normalized column axial force ratios range from 0.96 to 1.16 for CC-HSS-2L frames, and from 0.94 to 1.12 for CC-HSS-L frames. The higher compression forces are caused mainly because of higher tension brace forces (Figure 5.20 to Figure 5.23) than design values and the fact that the compression braces induce additional forces in the column not considered in the design. This response indicates that the requirements of CSA S16-14 for Type CC frames taller than 15 m in moderate and high seismic regions to increase the design base shear (by 2% per meter of height above 15 m) and amplify the columns force (by an amplification factor of 1.3), are deemed necessary in design of Type CC MT-CBFs with T/O braces to protect the columns with an exception that the latter, should be considered for Type CC T/O MT-CBFs of any height. This improved design recommendation is described in Section 6.2.3.

As shown in Table 3.13, the design forces of columns in Type CC frames with T/O braces are affected only by the height and the span of the frame; in other words, the number of tiers or the tier heights does not affect the column design force. Although, as shown in Figure 5.24, the actual axial forces induced in the columns of the frames with the same frame height but different tier configurations were not the same. The first reason being that in the design of T/O frames, the presence of compression braces is neglected; however, they contribute to the frame lateral response under NLRH analyses, and although small, they induce compression forces to the columns. The second reason is that the columns of Type CC frames are designed for forces corresponding to seismic base shear, meaning that the magnitudes of forces transferred from braces to the columns are independent of the inclination of braces; however, induced brace forces can vary between frames and under various ground motion records.

Table 5.14. Statistics of normalized peak column demands for CC-HSS-2L frames.

Parameter	CC_HSS_2L_10_2_1.0	CC_HSS_2L_10_2_1.75	CC_HSS_2L_10_3_1.0	CC_HSS_2L_10_3_1.75	CC_HSS_2L_16_2_1.0	CC_HSS_2L_16_2_1.75	CC_HSS_2L_16_3_1.0	CC_HSS_2L_16_3_1.75	CC_HSS_2L_16_4_1.0	CC_HSS_2L_16_4_1.75	CC_HSS_2L_24_3_1.0	CC_HSS_2L_24_3_1.75	CC_HSS_2L_24_4_1.0	CC_HSS_2L_24_4_1.75	CC_HSS_2L_24_6_1.0	CC_HSS_2L_24_6_1.75
$C_{c\text{-NLRH}}/C_{r,\phi=1}$	1.00	0.96	1.04	0.98	1.00	1.00	1.07	1.01	1.04	1.03	1.03	0.96	1.12	1.05	1.16	1.11
$(M_{cy\text{-NLRH}}/M_p)_1$	0.02	0.04	0.02	0.06	0.02	0.03	0.02	0.04	0.03	0.04	0.01	0.01	0.02	0.02	0.02	0.04
$(M_{cy\text{-NLRH}}/M_p)_2$			0.01	0.04			0.01	0.01	0.01	0.01	0.00	0.01	0.01	0.01	0.01	0.01
$(M_{cy\text{-NLRH}}/M_p)_3$									0.01	0.02			0.01	0.01	0.01	0.01
$(M_{cy\text{-NLRH}}/M_p)_4$															0.01	0.00
$(M_{cy\text{-NLRH}}/M_p)_5$															0.01	0.01
$(M_{cx\text{-NLRH}}/M_p)_1$	0.17	0.12	0.15	0.12	0.14	0.10	0.13	0.11	0.09	0.11	0.09	0.08	0.08	0.09	0.06	0.07
$(M_{cx\text{-NLRH}}/M_p)_2$			0.11	0.07			0.10	0.07	0.10	0.10	0.06	0.04	0.09	0.07	0.08	0.08
$(M_{cx\text{-NLRH}}/M_p)_3$									0.06	0.05			0.05	0.04	0.08	0.07
$(M_{cx\text{-NLRH}}/M_p)_4$															0.06	0.05
$(M_{cx\text{-NLRH}}/M_p)_5$															0.03	0.03

Table 5.15. Statistics of normalized peak column demands for CC-HSS-L frames.

Parameter	CC_HSS_L_10_2_1.0	CC_HSS_L_10_2_1.75	CC_HSS_L_10_3_1.0	CC_HSS_L_10_3_1.75	CC_HSS_L_16_2_1.0	CC_HSS_L_16_2_1.75	CC_HSS_L_16_3_1.0	CC_HSS_L_16_3_1.75	CC_HSS_L_16_4_1.0	CC_HSS_L_16_4_1.75	CC_HSS_L_24_3_1.0	CC_HSS_L_24_3_1.75	CC_HSS_L_24_4_1.0	CC_HSS_L_24_4_1.75	CC_HSS_L_24_6_1.0	CC_HSS_L_24_6_1.75
$C_{c\text{-NLRH}}/C_{r,\phi=1}$	1.07	1.02	1.06	1.06	1.12	1.00	1.11	1.09	1.04	1.05	1.02	0.94	1.01	1.00	1.07	0.98
$(M_{cy\text{-NLRH}}/M_p)_1$	0.02	0.04	0.01	0.04	0.01	0.03	0.01	0.02	0.02	0.04	0.01	0.01	0.01	0.01	0.02	0.02
$(M_{cy\text{-NLRH}}/M_p)_2$			0.03	0.04			0.01	0.02	0.01	0.01	0.00	0.01	0.01	0.01	0.01	0.00
$(M_{cy\text{-NLRH}}/M_p)_3$									0.01	0.02			0.01	0.01	0.00	0.00
$(M_{cy\text{-NLRH}}/M_p)_4$															0.00	0.00
$(M_{cy\text{-NLRH}}/M_p)_5$															0.01	0.01
$(M_{cx\text{-NLRH}}/M_p)_1$	0.20	0.13	0.16	0.16	0.17	0.10	0.13	0.13	0.08	0.10	0.08	0.07	0.06	0.07	0.05	0.05
$(M_{cx\text{-NLRH}}/M_p)_2$			0.11	0.09			0.09	0.08	0.10	0.09	0.06	0.04	0.06	0.06	0.07	0.06
$(M_{cx\text{-NLRH}}/M_p)_3$									0.06	0.05			0.04	0.03	0.07	0.06
$(M_{cx\text{-NLRH}}/M_p)_4$															0.05	0.04
$(M_{cx\text{-NLRH}}/M_p)_5$															0.03	0.02

a)
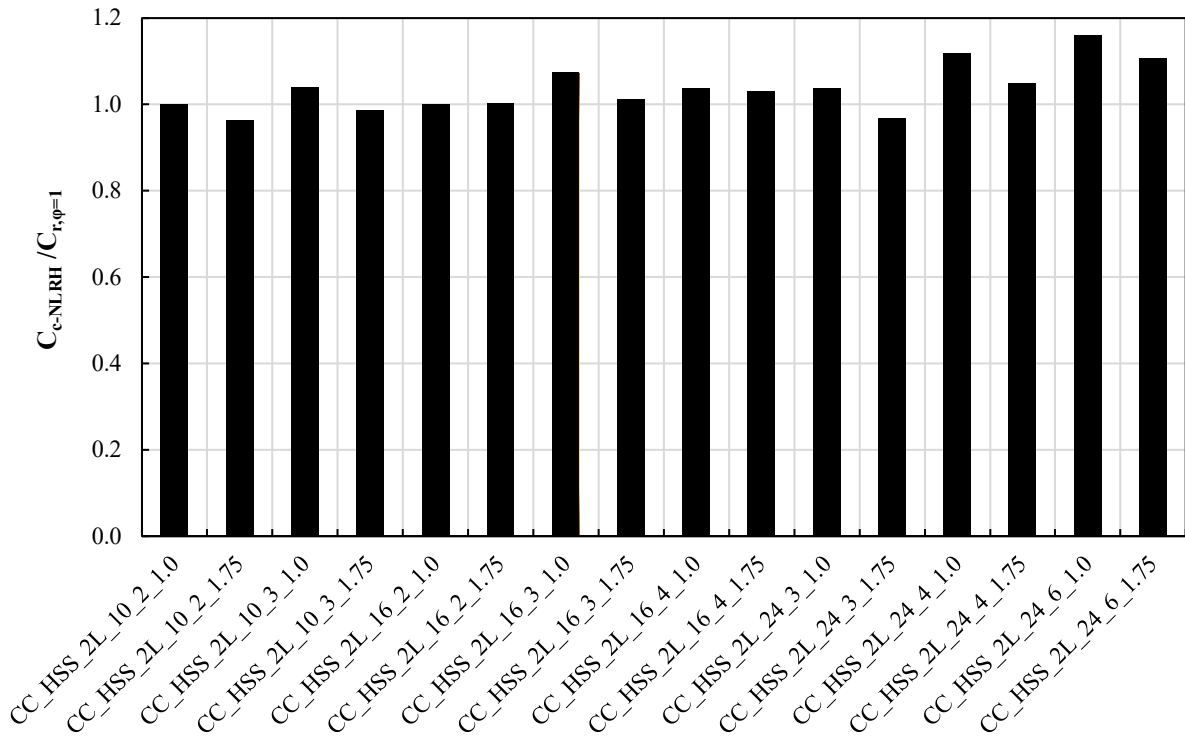
b)
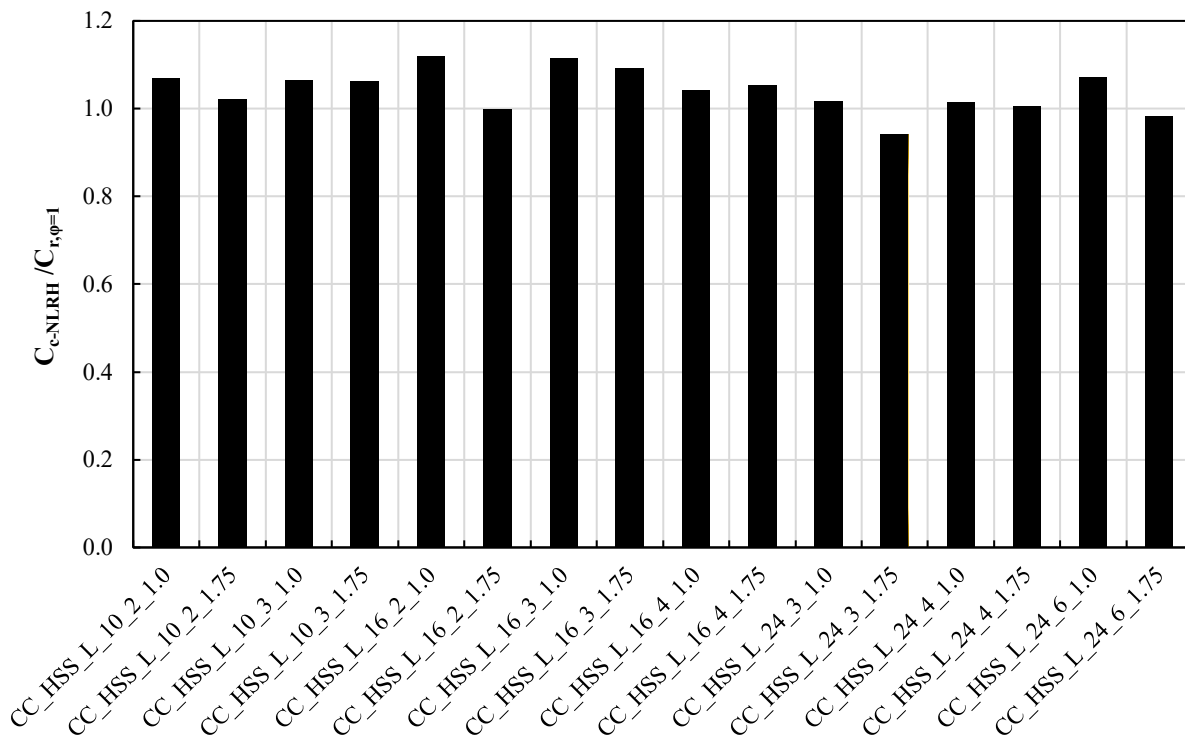
Figure 5.24. Statistics of normalized peak column axial compression forces for a) CC-HSS-2L frames, and b) CC-HSS-L frames.

169

Figure 5.25a and Figure 5.25b show the normalized peak in-plane moment demands of the columns of CC-HSS-2L and CC-HSS-L frames, respectively. As shown, the in-plane moments are significantly lesser than the respective section plastic moments. The maximum normalized in-plane moments are 0.06 and 0.04 for CC-HSS-2L and CC-HSS-L frames, respectively, with peak moments that occur in either the first tier or the second one. In both sets of frames, brace cross-section choice did not significantly affect the moments induced in the columns. It was also found that frames having taller first tier experienced higher in-plane moments than the same frames with identical tier heights. This trend is more pronounced in the case of shorter frames.

The statistics of normalized peak columns out-of-plane moments for CC-HSS-2L and CC-HSS-L frames are shown in Figure 5.26a and Figure 5.26b, respectively. The maximum out-of-plane moment demands observed in CC-HSS-2L and CC-HSS-L frames are $0.17M_p$ and $0.2M_p$, respectively. The maximum out-of-plane moment always occurs in Tier 1 or Tier 2, as column segments of these tiers have the first and second highest axial compression forces, which results in larger moments due to P-Delta effects. Furthermore, as shown in Figure 5.26a and Figure 5.26b, the peak column out-of-plane moments reduce as the number of tiers increases because the location of the maximum induced axial compression force (e.g. Tier 1 column segment) is not the same as the location of the maximum initial geometric imperfection (i.e. column mid-height).
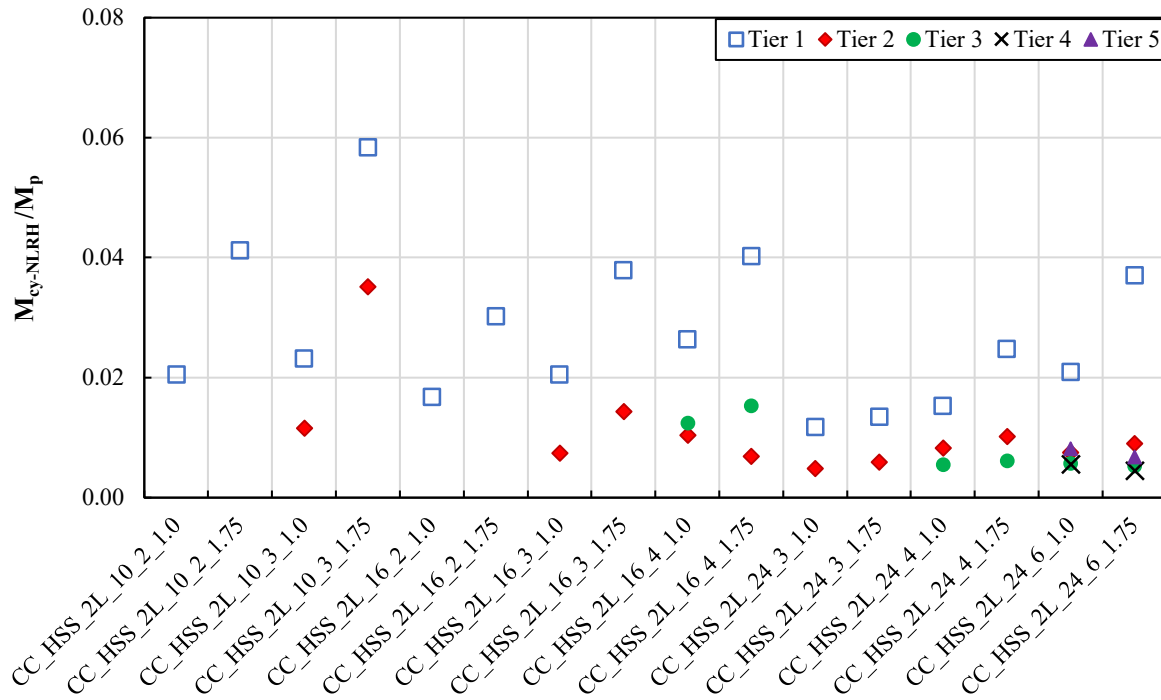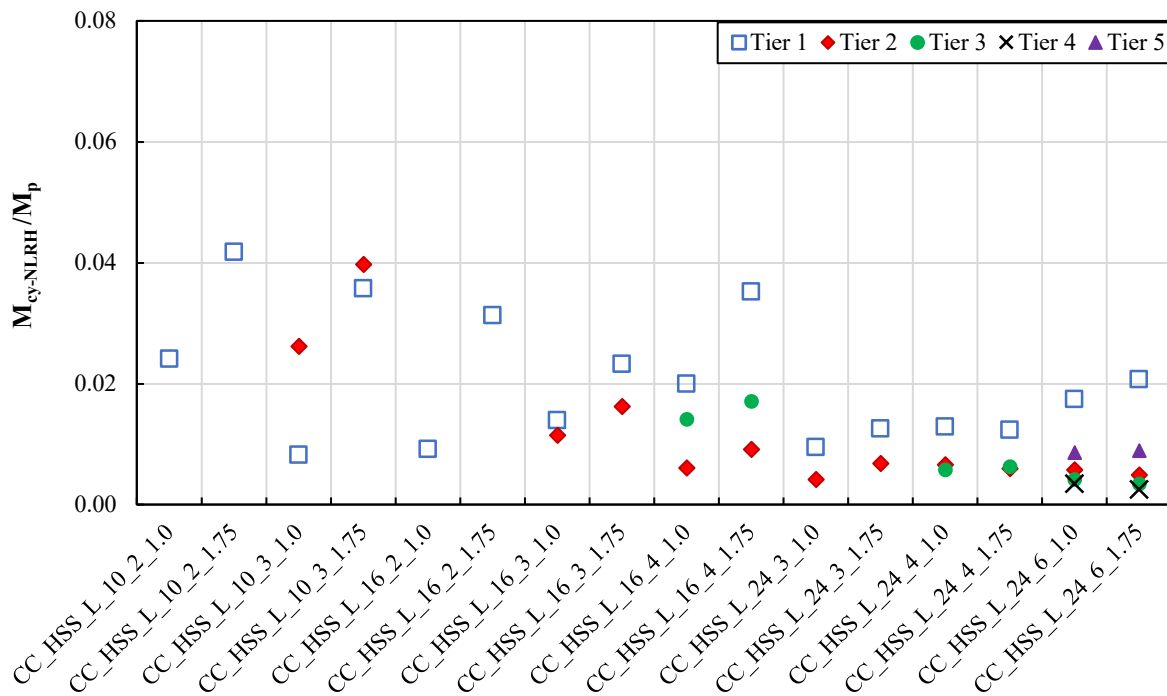
Figure 5.25. Statistics of normalized peak column in-plane moment demands for a) CC-HSS-2L frames, and b) CC-HSS-L frames.

a)
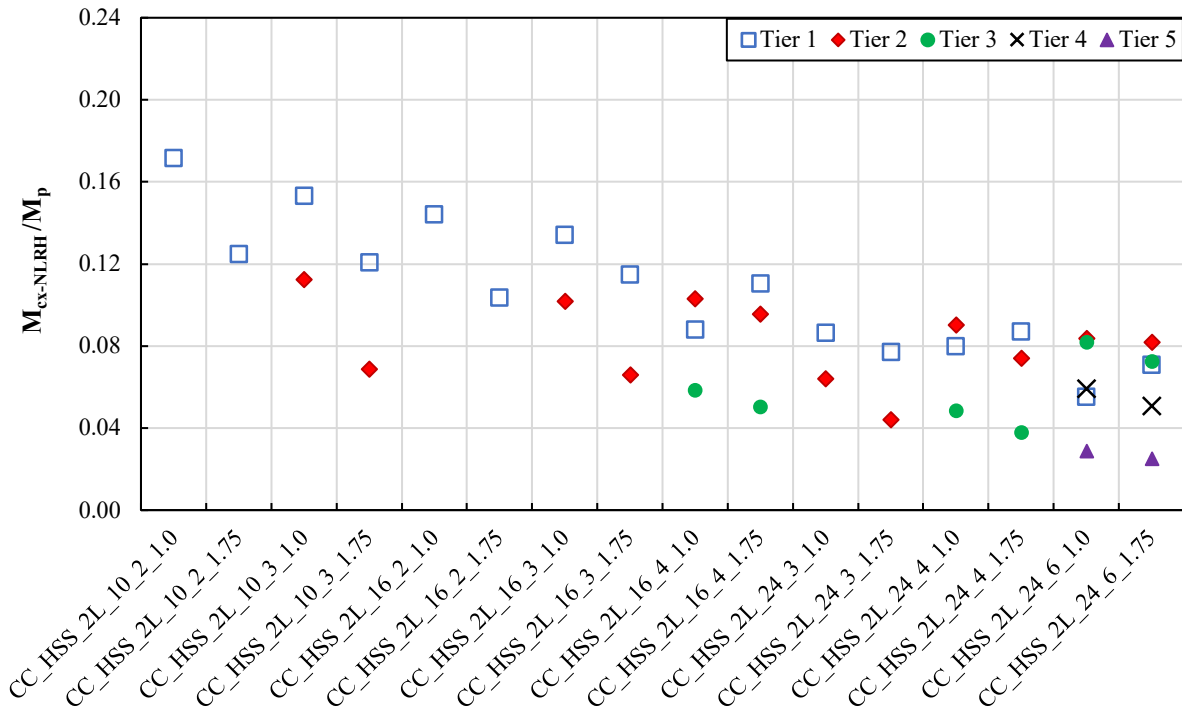
b)
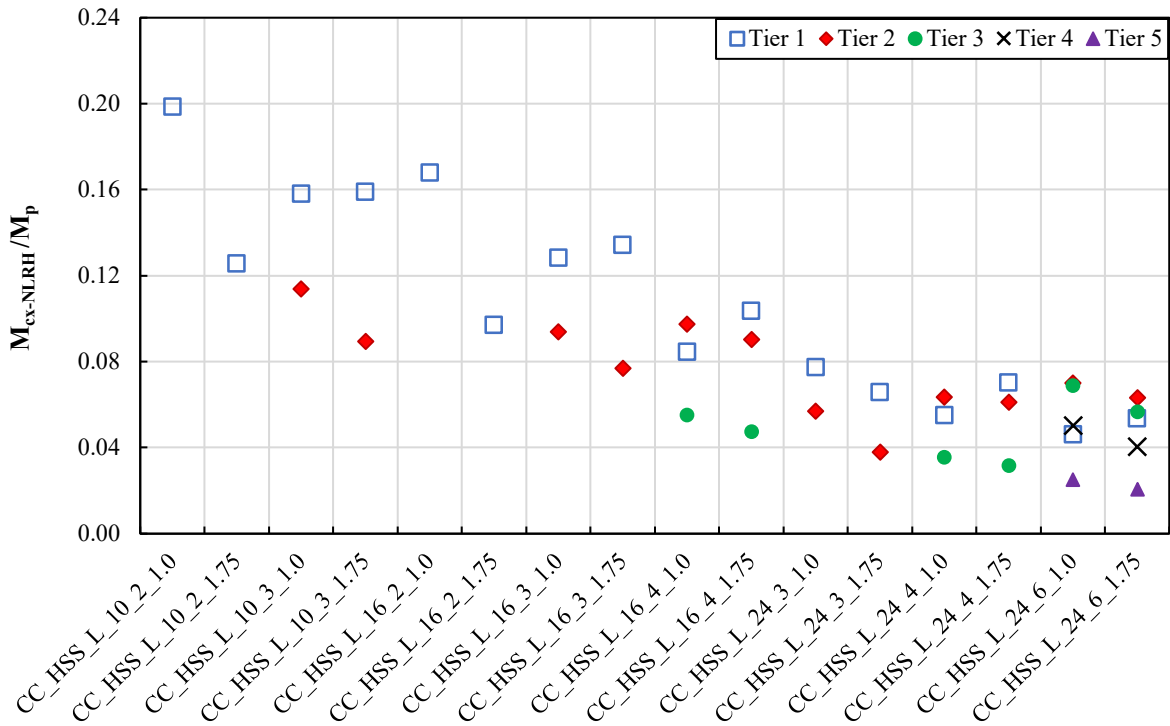
Figure 5.26. Statistics of normalized peak column out-of-plane moment demands for a) CC-HSS-2L frames, and b) CC-HSS-L frames.

Chapter 6: Design Recommendations

This chapter presents enhanced and yet simplified seismic design recommendations for the design of low-ductile MT-CBFs in low-to-moderate seismicity regions of Canada. The recommendations are made based on the results obtained from NLRH analyses, as provided in Chapter 5. Design recommendations for Type LD MT-CBFs are first discussed, followed by design recommendations for Type CC MT-CBFs.

6.1 Type LD Frames

6.1.1 Frame configuration

Results of NLRH analyses performed on the selected six-tiered CBFs exceeding the CSA S16-14 tier limit (five) indicate a satisfactory seismic response with no column buckling or frame collapse (Table 5.1). It is therefore recommended to extend the limit on the number of tiers to six.

6.1.2 Drift Requirements

Peak tier drifts for the selected Type LD frames range from 0.36% to 0.60%. As shown in past studies (Tremblay et al. 2003, Yang and Mahin 2005, Uriz et al. 2008, Fell et al. 2009, Roeder et al. 2011a, Hsiao et al. 2013, 2014), low-cycle fatigue fracture of commonly-used HSS braces is likely to happen at an inter-storey drift (or tier drift in the multi-tiered arrangement) between 2.0% and 2.5%. The tier drifts observed in the selected Type LD frames are significantly lower than the value that can cause low-cycle fatigue fracture. It is therefore recommended that the drift check in Type LD MT-CBFs be limited to storey drift specified in 2015 NBCC.

6.1.3 Column Design Forces

Column Axial Compression Demand

Peak column axial compression forces normalized to the respective axial compression resistances with a resistance factor of $\phi = 1.0$ as obtained from NLRH analysis range from 0.71 to 0.97. For the design purpose, the axial force ratios were modified to represent as a function of the column axial compression resistance with $\phi = 0.9$, which results in $0.79 - 1.08$. Although the maximum ratio slightly exceeds 1.0, due to relatively conservative design moments proposed here, the column design axial force is suggested to be set equal to the gravity load plus the maximum of the forces obtained using two loading conditions due to brace probable resistances as shown in Section 2.5.1. The additional brace loading condition as prescribed by CSA S16-14 special requirements for MT-CBFs can be waived.

Column In-plane Moment Demand

Peak in-plane moment demands normalized to the respective plastic moments as obtained from NLRH analyses range from 0.01 to 0.06 with the maximum value of $0.06M_{py}$. In lieu of in-plane bending moments computed using the special analysis case (Section 2.5.1) prescribed by CSA S16-14 for MT-CBFs, it is recommended in this study to use an in-plane bending moment equal to 10% of the plastic moment of the column section in the direction of the braced bay. A slightly higher value for the in-plane moment is chosen first to maintain consistency between all low-ductile frames studied here; secondly, although an extensive numerical simulation covering a wide range of frame configurations were covered in this study, a higher in-plane moment is intended to include a safety margin for potential cases not investigated in this study (see Section 7.3). It is worth noting that the in-plane moment arising from the special requirements of CSA S16-14 for

Type LD MT-CBFs was neglected in the design of columns of the select frames here. Therefore, those requirements are recommended to be replaced by the in-plane moment demand recommended in this study.

Column Out-of-plane Moment Demand

Peak column out-of-plane moments normalized to the respective plastic moments as obtained from NLRH analyses range from 0.02 to 0.08. To maintain the consistency between the CSA S16-14 special design requirements (see Section 2.5.1), a notional load approach is used to obtain the column out-of-plane moment. The moment is induced by an out-of-plane transverse Notional Load (NL) at each strut level with an amplitude equal to a fraction of the factored axial compression load in the column segments below the strut. To obtain the out-of-plane transverse NL at each strut level, the difference between column internal shear forces (in the out-of-plane direction) in adjacent tiers is computed using the results obtained from NLRH analyses of Type LD frames. The statistics of peak notional loads (the maximum of means over each earthquake ensemble of the peak response parameter) are presented in Table 6.1 as well as in Figure 6.1 as a fraction of the maximum axial compression load in the column segments below the strut. Column shear forces used to determine the notional loads were obtained at a ground motion time step where the maximum out-of-plane moment occurred. As shown, the maximum notional load among all of the selected Type LD MT-CBFs is 0.36%. The design notional load at each strut level is recommended to be taken equal to 1% of the factored axial compression load in the column below the strut. The increase in the notional load is to retain consistency among all low-ductile frames studied here, and to achieve a sufficient safety margin for potential cases not considered here. It is worth noting that CSA S16-14 requires an out-of-plane transverse notional load at each strut level equal to 2% of the factored axial compression load in the column segments below the strut.

Table 6.1. Statistics of peak notional load factors for Type LD frames.

Parameter	LD_W_HSS_10_2_1.0	LD_W_HSS_10_2_1.75	LD_W_HSS_10_3_1.0	LD_W_HSS_10_3_1.75	LD_W_HSS_16_2_1.0	LD_W_HSS_16_2_1.75	LD_W_HSS_16_3_1.0	LD_W_HSS_16_3_1.75	LD_W_HSS_16_4_1.0	LD_W_HSS_16_4_1.75	LD_W_HSS_24_3_1.0	LD_W_HSS_24_3_1.75	LD_W_HSS_24_4_1.0	LD_W_HSS_24_4_1.75	LD_W_HSS_24_6_1.0	LD_W_HSS_24_6_1.75
NL_1 (%)	0.33	0.29	0.20	0.26	0.36	0.13	0.24	0.20	0.14	0.16	0.27	0.09	0.20	0.16	0.10	0.07
NL_2 (%)			0.12	0.15			0.06	0.07	0.11	0.07	0.06	0.06	0.15	0.05	0.10	0.05
NL_3 (%)									0.01	0.05			0.13	0.10	0.07	0.03
NL_4 (%)															0.03	0.02
NL_5 (%)															0.12	0.04

Figure 6.1. Statistics of peak notional load factors for Type LD frames.

6.2 Type CC Frames

Identical design recommendations are proposed for all Type CC MT-CBFs studied here, including Type CC frames with T/C HSS braces (CC-W-HSS), with T/O double-angle braces (CC-HSS-2L), and with T/O single-angle braces (CC-HSS-L).

6.2.1 Frame Configuration

The results of the NLRH analyses of the prototype Type CC frames showed that the response of all frames with six tiers was satisfactory with no column instability. It is recommended to limit the number of braced tiers to six. Future studies should investigate the frames with a larger number of tiers.

6.2.2 Drift Requirements

The maximum tier drifts for CC-W-HSS, CC-HSS-2L, and CC-HSS-L frames are 0.59%, 0.50%, and 0.42%, respectively. The peak trier drifts are significantly smaller than the drift corresponding to low-cycle fatigue fracture of commonly used HSS and angle braces. Thus, a drift check for Type CC MT-CBFs is recommended to be limited to the storey drift only as specified by 2015 NBCC.

6.2.3 Struts

Horizontal components of peak axial forces in tension- and compression-acting braces (Table 5.5 and Table 5.6 for Type CC with T/C braces and Table 5.10 and Table 5.11 for Type CC with T/O double-angle braces, Table 5.12 and Table 5.13 for Type CC with T/O single-angle braces) in two adjacent tiers were found to be unequal. The difference between the horizontal component of brace axial forces is more pronounced in the frames with T/O braces because of the less contribution from slender compression-acting braces. The differential brace force causes an unbalanced horizontal force in intermediate brace-to-column joints, which can be resisted by horizontal intermediate struts in Type CC frames. However, if the frame was designed without intermediate struts, as shown in Figure 1.2b, the unbalanced brace forces would have produced additional in-plane bending moments on the columns because of the unsatisfactory K-brace response. Thus, it

is recommended in this study to add intermediate horizontal struts between adjacent braced tiers designed to the combination of the nodal bracing force required to brace the column against in-plane instability and a fraction of the brace design axial force that is 20% in T/C bracing systems and 60% in T/O bracing systems, respectively. The proposed design forces represent the average value of the horizontal components of the brace force differences between tiers obtained from NLRH analyses.

6.2.4   Column Design Forces

Column Axial Compression Demand

The recommendations for Type CC column's axial force follow the approach adopted by CSA S16-14 for frames taller than 15 m in moderate and high seismic regions to first increase the factored seismic forces by 2% per meter of height above 15 m, and second, amplify the column design force by 1.3 (see Section 0); however, the 16 m-tall frames are treated as 15-m tall frames because the increase in the frame seismic forces as a result of the first amplification factor is negligible and do not affect the member sizes. Maximum column axial compression forces obtained from NLRH analysis normalized to the respective column compression resistances with $\phi = 1.0$, range from 0.97 to 1.28 for CC-W-HSS frames, from 0.96 to 1.16 for CC-HSS-2L frames, and from 0.94 to 1.12 for CC-HSS-L frames. Similar to Type LD, for the design purpose, column demand, $C_{c\text{-}NLRH}$, was normalized to column compression resistance with $\phi = 0.9$, C_r. Table 6.2 shows a summary of the peak NLRH results of $C_{c\text{-}NLRH}/C_r$ for Type CC frames, as well as the proposed values. To account for the first amplification factor for 24 m-tall frames, first, the frame design base shear was recalculated considering the increase of 18% (2% per meter of height above 15 m) and the column design force corresponding to the new seismic forces was recalculated, $C_{f,2\%}$.

Then, the ratio $C_{f,2\%}/C_r$ was subtracted from the NLRH results for the column forces to determine the required second amplification factor for 24-m tall Type CC MT-CBFs. As shown, the second amplification factors vary from 1.24 to 1.42. An amplification factor of 1.4 is proposed for all Type CC MT-CBFs. Although the peak value for CC-HSS-2L/L frames with 10 m- and 16 m-tall frames is 1.24, an identical column compression force amplification factor is recommended here to maintain consistency between frames. Additionally, the slightly higher peak values (i.e. 1.42) compared to the proposed amplification factor in other frames is believed to be negligible due to the presence of column biaxial design moments as recommended in the subsequent sections.

Table 6.2. Proposed amplification factors for the column design force of Type CC MT-CBFs.

Frame Height m	Frame	Peak NLRH C_f/C_r	Proposed amplification factor	Seismic force incðrease for frames taller than 15m
10, 16	CC-W-HSS	1.42	1.40	-
	CC-HSS-2L/L	1.24	1.40	
24	CC-W-HSS	1.42	1.40	To be increased by 2% per meter of height above 15 m
	CC-HSS-2L/L	1.41	1.40	

Column In-plane Moment Demand

The maximum in-plane moments obtained from NLRH analysis of CC-W-HSS, CC-HSS-2L, CC-HSS-L frames normalized to the respective plastic moments are 0.08, 0.06, and 0.04, respectively. A design in-plane moment is recommended to be taken equal to 10% of the plastic moment of the column section in the direction of the braced bay. This slightly higher moment than the observed moments is recommended first to maintain consistency among all low-ductile frames studied here, and second to consider a safety margin for cases not studied here (see Section 7.3).

Column Out-of-plane Moment Demand

Maximum out-of-plane moments obtained from NLRH analyses normalized to the respective plastic moments are 0.28, 0.17, and 0.20 for CC-W-HSS, CC-HSS-2L, and CC-HSS-L frames, respectively. The notional load approach, as described for Type LD MT-CBFs (Section 6.1.3), is employed here for Type CC MT-CBFs. It is worth noting that this approach is consistent with the CSA S16-14 method for determining the design out-of-plane moment of columns in Type CC MT-CBFs. The statistics of peak Notional Loads at each strut level obtained from NLRH analyses divided by the respective peak axial compression load in the column below the strut are presented in Table 6.3 and Figure 6.2, Table 6.4 and Figure 6.3, Table 6.5 and Figure 6.4 for CC-W-HSS, CC-HSS-2L, and CC-HSS-L frames, respectively. As shown, the maximum notional loads at each strut normalized to the peak axial compression load in the column below the strut are 0.87%, 0.48%, and 0.48%, respectively. An identical out-of-plane notional load of 1.0% times the axial compression load carried by the column below the strut is proposed to be applied at each strut level.

Table 6.3. Statistics of peak notional loads divided by the peak axial compression load in the column below the strut for CC-W-HSS frames.

Parameter	CC_W_HSS_10_2_1.0	CC_W_HSS_10_2_1.75	CC_W_HSS_10_3_1.0	CC_W_HSS_10_3_1.75	CC_W_HSS_16_2_1.0	CC_W_HSS_16_2_1.75	CC_W_HSS_16_3_1.0	CC_W_HSS_16_3_1.75	CC_W_HSS_16_4_1.0	CC_W_HSS_16_4_1.75	CC_W_HSS_24_3_1.0	CC_W_HSS_24_3_1.75	CC_W_HSS_24_4_1.0	CC_W_HSS_24_4_1.75	CC_W_HSS_24_6_1.0	CC_W_HSS_24_6_1.75
NL_1 (%)	0.57	0.27	0.27	0.43	0.87	0.37	0.33	0.61	0.35	0.47	0.63	0.62	0.37	0.54	0.22	0.33
NL_2 (%)			0.12	0.08			0.09	0.28	0.32	0.21	0.14	0.69	0.29	0.10	0.26	0.24
NL_3 (%)									0.14	0.32			0.25	0.51	0.19	0.12
NL_4 (%)															0.05	0.12
NL_5 (%)															0.40	0.47

Figure 6.2. Statistics of peak notional load factors for CC-W-HSS frames.

Table 6.4. Statistics of peak notional loads divided by the peak axial compression load in the column below the strut for CC-HSS-2L frames.

Parameter	CC_HSS_2L_10_2_1.0	CC_HSS_2L_10_2_1.75	CC_HSS_2L_10_3_1.0	CC_HSS_2L_10_3_1.75	CC_HSS_2L_16_2_1.0	CC_HSS_2L_16_2_1.75	CC_HSS_2L_16_3_1.0	CC_HSS_2L_16_3_1.75	CC_HSS_2L_16_4_1.0	CC_HSS_2L_16_4_1.75	CC_HSS_2L_24_3_1.0	CC_HSS_2L_24_3_1.75	CC_HSS_2L_24_4_1.0	CC_HSS_2L_24_4_1.75	CC_HSS_2L_24_6_1.0	CC_HSS_2L_24_6_1.75
NL_1 (%)	0.39	0.23	0.48	0.18	0.30	0.38	0.41	0.21	0.25	0.27	0.20	0.14	0.21	0.17	0.17	0.18
NL_2 (%)			0.19	0.27			0.27	0.33	0.13	0.16	0.31	0.33	0.13	0.16	0.12	0.07
NL_3 (%)									0.29	0.30			0.37	0.31	0.10	0.08
NL_4 (%)															0.20	0.18
NL_5 (%)															0.31	0.26

Figure 6.3. Statistics of peak notional load factors for CC-HSS-2L frames.

182

Table 6.5. Statistics of peak notional loads divided by the peak axial compression load in the column below the strut for CC-HSS-L frames.

Parameter	CC_HSS_L_10_2_1.0	CC_HSS_L_10_2_1.75	CC_HSS_L_10_3_1.0	CC_HSS_L_10_3_1.75	CC_HSS_L_16_2_1.0	CC_HSS_L_16_2_1.75	CC_HSS_L_16_3_1.0	CC_HSS_L_16_3_1.75	CC_HSS_L_16_4_1.0	CC_HSS_L_16_4_1.75	CC_HSS_L_24_3_1.0	CC_HSS_L_24_3_1.75	CC_HSS_L_24_4_1.0	CC_HSS_L_24_4_1.75	CC_HSS_L_24_6_1.0	CC_HSS_L_24_6_1.75
Frame																
NL_1 (%)	0.35	0.32	0.48	0.31	0.21	0.38	0.31	0.18	0.24	0.21	0.18	0.11	0.14	0.13	0.15	0.14
NL_2 (%)			0.21	0.28			0.31	0.35	0.11	0.17	0.31	0.31	0.11	0.16	0.10	0.08
NL_3 (%)									0.29	0.31			0.30	0.30	0.10	0.11
NL_4 (%)															0.18	0.17
NL_5 (%)															0.26	0.23

Figure 6.4. Statistics of peak notional load factors for CC-HSS-L frames.

6.3 Summary of the Proposed Design Requirments

A summary of the seismic design recommendations proposed based on the findings of this study is presented in Table 6.6.

Table 6.6. Proposed seismic design requirements for Type LD and Type CCMT-CBFs.

Frame	Column Design Forces			Seismic force increase for frames taller than 15m	Maximum Number of Tiers	Drift Check	Strut
	C_f / C_r	M_{fy} / M_{py}	NL				
Type LD	1.0*	10.0%	1.0%	-	6	Only Storey Drift Check	Required
Type CC (h ≤ 15 m)	1.4	10.0%	1.0%	-	6	Only Storey Drift Check	Required
Type CC (h > 15 m)	1.4	10.0%	1.0%	To be increased by 2% per meter of height above 15 m.	6	Only Storey Drift Check	Required

* Column axial force obtained from two loading conditions due to brace probable resistances.

6.4 Case Study

To validate the proposed design requirements for Type LD and CC MT-CBFs, six prototype frames were chosen from the parametric study matrix (see Section 3.3) as case study frames, including frames LD_W_HSS_10_2_1.0, LD_W_HSS_24_3_1.0, CC_W_HSS_16_3_1.0, CC_W_HSS_24_4_1.0, CC_HSS_2L_24_3_1.0, and CC_HSS_L_24_3_1.0. The improved design requirements of this chapter (referred to as to the proposed method in this section) were then applied to redesign these frames. The member sizes obtained in Chapter 3 using the design method excluding CSA S16-14 special seismic design requirements for Type LD MT-CBF columns and design requirements for Type CC frames taller than 15 m (referred as to CSA S16-Ex in this section) were also presented here to allow comparison between the frame designs obtained using various methods. The selected frames were also redesigned according to CSA S16-14 provisions including the special seismic design requirements for Type LD MT-CBFs and design requirements for Type CC frames taller than 15 m (referred to as CSA

S16 in this section). The seismic performance of the frames designed to the proposed requirements was then evaluated using the NLRH analysis procedure described in Chapter 4.

6.4.1 Design of Type LD Case Study Frames

Summary of the design of the selected Type LD frames according to CSA S16 and CSA S16-Ex, and the proposed method is presented in Table 6.7. As shown, the seismic design forces for braces of the case study frames are identical to as described in Chapter 3; therefore, the brace sizes are the same for all three design methods. Design forces of the roof beam and struts arise from the probable resistances of braces, the sizes of those members are also identical between all three methods. The main difference between the three design methods is the determination of the column design forces, which is described for CSA S16 and proposed method. It should be noted that the design of the case study frames as per CSA S16-Ex was described in Chapter 3.

Column Design in accordance with CSA S16

The columns must resist the simultaneous effects of gravity loads, out-of-plane bending moments due to a series pf out-of-plane transverse point loads at each strut level equal to 2% of the factored axial compression load in the columns below the strut, and axial loads and in-plane bending moments induced when the frame reaches the design storey drift assuming that yielding develops in the tension-acting bracing members located at any one level along the height of the storey where the tension-acting brace in the critical tier reaches its probable resistance, T_u, the compression-acting brace in that tier reaches its probable buckled resistance, C'_u, and the compression braces in the other tiers reach their probable compressive resistances, C_u. The in-plane and axial force demands can be obtained using a nonlinear static analysis or a linear analysis where yielded, and buckled braces are replaced with their corresponding probable forces. Additionally, the analysis

must be repeated for all plausible critical tiers in case of frames with uniform tiers. The second analysis method, as recommended by Imanpour and Tremblay (2016c), was used here. The key design steps (Table 6.7) for the columns of frame LD_W_HSS_24_3_1.0 summarized as follows:

1) The probable resistances of braces were calculated using $R_yF_y = 460$ MPa: equal to $T_u = 865$ kN, $C_u = 223$ kN, and $C'_u = 169$ kN.

2) Three analyses are required to obtain the most critical combination of column axial force and in-plane bending moment as the frame has three identical tiers, and any of these three tiers can be critical. However, the frame storey shear resistance as obtained using the probable brace resistances ($V_u = 653$ kN) was larger than the base shear corresponding to $R_dR_o = 1.3$ ($V_{1.3} = 331$ kN). $V_u > V_{1.3}$ indicates that the tension-acting braces in the frame will remain elastic. Consequently, the number of analyses required by CSA S16-14 is reduced to one, where only the compression braces are replaced in the braced tiers with their probable compressive resistances, and tension braces remain unchanged. In any case, the column design axial force should be lesser than the axial force calculated under the gravity load plus seismic forces corresponding to $V_{1.3}$. The latter was obtained by replacing compression brace forces with C_u and a tension brace force back-calculated using $V_{1.3}$ and C_u, which resulted in T = 329 kN < T_u = 865 kN. The column design axial force was, therefore, equal to 1353 kN.

3) Two linear elastic models of the braced frame were created in SAP2000 (CSI 2009):

   a) The first model that consists of the elastic components of the frame was used to obtain the elastic storey displacement, δ_e, under the design seismic base shear plus gravity loads (Figure 6.5a), which was then used to compute the anticipated storey displacement including inelastic deformations, $R_dR_o\delta_e$. $\delta_e = 28.5$ mm and $R_dR_o\delta_e = 74$ mm.

b) The second elastic model was created where the compression braces (assuming the frame was being deformed laterally to the right) were removed and replaced by their respective probable compressive resistances (Figure 6.5c). The frame was then analyzed under gravity loads plus a roof displacement corresponding to the design storey drift as calculated in Step 2 using a linear static analysis method to obtain column design forces. This displacement-based linear analysis was used instead of the more complex pushover analysis of the frame.

4) Maximum column axial force in Tier 1 was obtained from Step 3b $C_f = 1507$ kN. However, it is larger than the column axial force corresponding to $V_{1.3}$ calculated in Step 2. Therefore, the column design axial force was taken as $C_f = 1353$ kN.

5) Maximum in-plane moment of the column in Tier 1 was obtained using the model of Step 3b $M_{fx} = 3$ kN.m.

6) The maximum design out-of-plane moment was obtained by applying two out-of-plane transverse notional loads (NL) to the column at strut levels. The magnitude of each load is equal to 2% of the axial load in the column below the strut: $NL_1 = 0.02 \times 1354 = 27$ kN and $NL_2 = 0.02 \times 912 = 18$ kN. The maximum out-of-plane induced in the column under the notional loads was 213 kN.m in Tier 1 and 187 kN.m in Tier 2.

7) The column was designed under the design axial load and biaxial moments obtained above, using the axial force-biaxial moment (P-M-M) interaction equation in Clause 13.8 of CSA S16-14. All of the required parameters in the equation calculated for frame LD_W_HSS_24_3_1.0 are given in Table 6.7.

Similar steps were followed to redesign frame LD-W-HSS-10-2-1.0 column. A summary of the column design is given in Table 6.7.

Table 6.7. Summary of the column design for LD-W-HSS case study frames using CSA S16 special provisions and the proposed method.

Parameter	LD_W_HSS_10_2_1.0			LD_W_HSS_24_3_1.0		
	CSA S16-Ex	CSA S16	Proposed Method	CSA S16-Ex	CSA S16	Proposed Method
$V_{E/Frame}$ (kN)	351	351	351	171	171	171
Brace Section (HSS)	88.9×88.9×6.4	88.9×88.9×6.4	88.9×88.9×6.4	88.9×88.9×6.4	88.9×88.9×6.4	88.9×88.9×6.4
Critical Segment	Tier 1	Tier 1	Tier 1	Tier 1	Tier 1	Tier 1
C_f (kN)	1144	1144	1144	1353	1353	1353
M_{fx} (kN.m)	-	61	29	-	213	82
M_{fy} (kN.m)	-	3	16	-	3	34
Column Section (W)	250×67	310×79	310×79	460×113	530×150	460×158
$(KL/r)_x$	91	75	75	122	105	121
$(KL/r)_y$	98	79	79	121	109	118
$b_f/2t_f$	6.5	8.7	8.7	8.1	7.7	6.0
$(b_f/2t_f)_{limit}$	9.2	9.2	9.2	9.2	9.2	9.2
h_w/t_w	22.5	28.1	28.1	37.8	37.5	27.2
$(h_w/t_w)_{limit}$	28.3	71.2	28.3	83.0	78.8	28.3
ω_{1x}	-	0.85	0.85	-	1.00	1.00
ω_{1y}	-	0.61	0.60	-	0.61	0.60
U_{1x}	-	1.26	1.26	-	1.64	1.99
U_{1y}	-	0.97	0.95	-	1.07	1.15
C_r (kN)	1175	1779	1779	1423	2263	2034
M_{rx} (kN.m)	-	397	397	-	1174	1171
M_{ry} (kN.m)	-	148	148	-	314	308
P-M-M Interaction Ratio	1.0	0.8	0.9	1.0	0.9	0.9
Governing Limit State (LS)	LS 2	LS 2 & LS 3	LS 2 & LS 3	LS 2	LS 3	LS 2
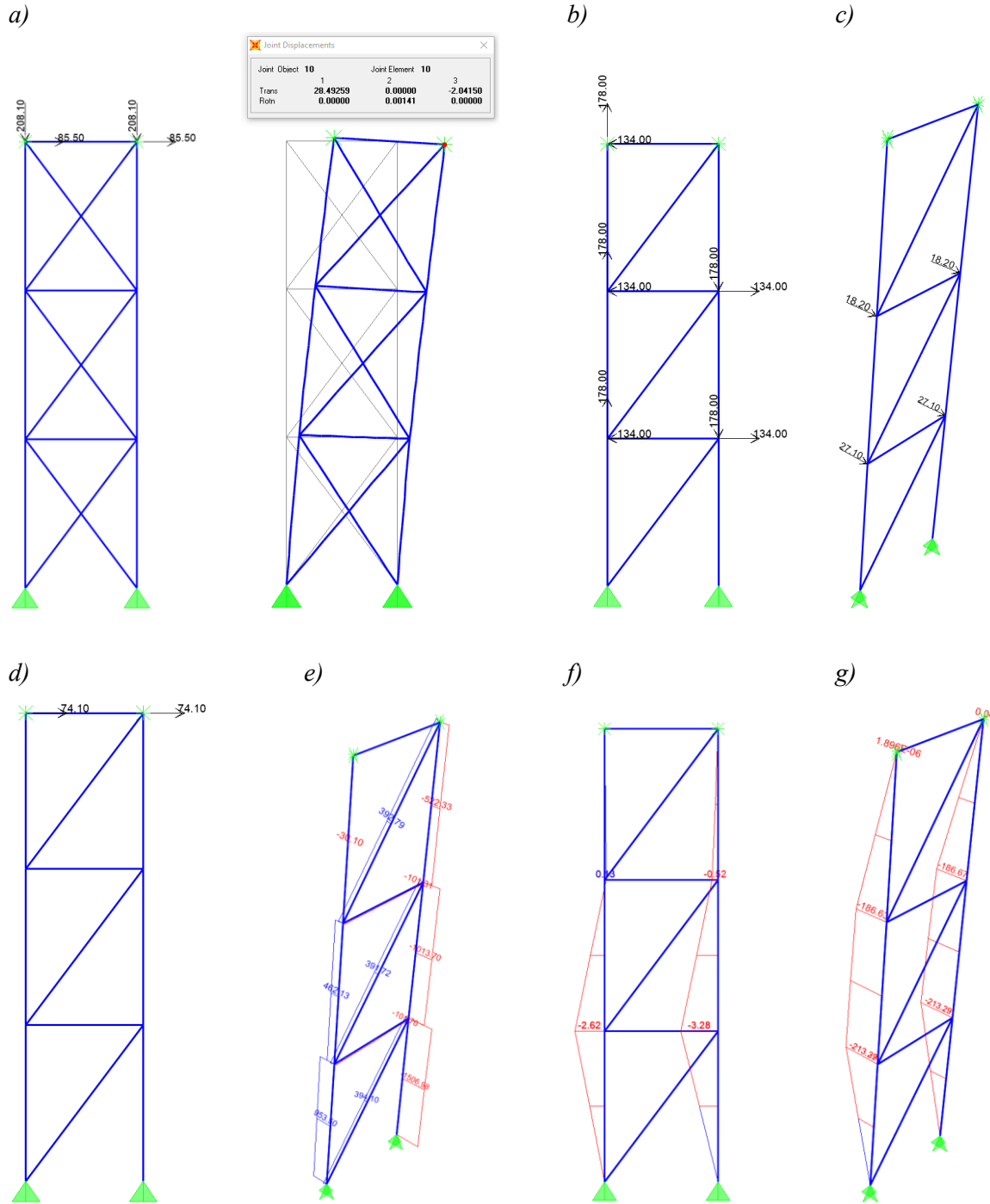
Figure 6.5. Design of frame LD-W-HSS-24-3-1.0 following CSA S16: a) frame analysis under the design seismic force and gravity (kN) to obtain roof displacement (mm); b) updated model by removing braces that buckle or yield; c) out-of-plane transverse notional loads (kN) at each strut level; d) frame analysis under gravity loads and displacement corresponding to design storey drift (mm) at the roof level to obtain column demands (gravity loads not shown); e) column axial force (kN) diagram at design storey drift; f) column in-plane moment diagram (kN.m) at design storey drift; g) column out-of-plane moment diagram (kN.m) under out-of-plane transverse notional loads.

Column Design Per the Proposed Method

The design of the frame LD_W_HSS_24_3_1.0 following the proposed method is summarized here. Since column design forces need not be computed at the roof displacement corresponding to the design storey drift, the pushover analysis or equivalent linear displacement-controlled analysis (e.g. using SAP 2000) is not required, and the column design forces can be obtained using a design spreadsheet.

1) Probable resistances of braces were computed: T_u = 865 kN, C_u = 223 kN, and C'_u = 169 kN.

2) Column design axial force is directly calculated under the gravity load plus the maximum of the two loading conditions due to brace probable resistances as described in Section 2.5.1. The calculated force must not exceed the force corresponding to $V_{1.3}$. V_u = 653 kN > $V_{1.3}$ = 331 kN. Thus, the column design axial force was obtained using the lateral seismic force corresponding to $V_{1.3}$ that gives C_f = 1353 kN.

3) Column design in-plane moment is taken equal to 10% of the weak-axis plastic moment of the column section as the columns are oriented such that in-plane response produces weak-axis moment in the column section. This moment is equal to 34 kN.m.

4) Column design out-of-plane moment was obtained under the out-of-plane transverse notional loads applied at each strut with an amplitude equal to 1% times the axial compression load in the column below the strut, which gives 82 kN.m.

5) Column was redesigned under the design axial load and bi-axial moments obtained above, using the axial force-biaxial moment (P-M-M) interaction equation in Clause 13.8 of CSA S16-14. The key design parameters are given in Table 6.7.

The design of the column of frame LD-W-HSS-10-2-1.0 follows the same steps described above and is summarized in Table 6.7.

As shown in Table 6.7, for the Type LD case study frames, the column sections designed according to the proposed method resulted in identical or close sections as CSA S16 method. Although the selected columns for Type LD frames did not reduce the steel tonnage, the proposed method provides the structural design engineers with a simpler and more efficient approach while preventing unsatisfactory limit states as described in Section 6.4.3. It is worth noting that the 5% increase in the column section of LD_W_HSS_24_3_1.0 is because of the web local buckling check (more stringent web width-to-thickness ratio is imposed by CSA S16-14 when a wide-flange is under biaxial moment) and not the need for additional strength.

6.4.2   Design of Type CC Case Study Frames

The design details of Type CC case study frames with T/C braces and those with T/O braces are summarized in Table 6.8 and Table 6.9, respectively. As shown, larger base shears were obtained for the case study frames when designing in accordance with CSA S16 and the proposed method, as they are taller than 15 m, and their base shear needs to be increased by 2% per meter of height above 15 m (Table 6.6). The braces were redesigned to carry the increased seismic forces. The brace sections for all designs are shown in Table 6.8 and Table 6.9 for CC-W-HSS and CC-HSS-2L/L frames, respectively. As shown, the brace sections were increased for the 24 m-tall case study frames. The roof beam and strut sections remained unchanged, and the sections designed in Chapter 3 were used.

The key differences between the column design approach using the proposed method and that prescribed by CSA S16 are summarized as follows:

1) CSA S16 requires the columns to be designed under an axial force and only an out-of-plane moment. Whereas, the column is sized under an axial force in combination with a bi-axial moment.

2) In accordance with the CSA S16 method, the column axial force needs to be amplified by 1.3 in frames taller than 15 m. The proposed method, however, uses an amplification factor of 1.4 for all MT-CBFs.

3) In both methods, the out-of-plane moment is calculated using the notional load approach. The notional load applied at each strut needs to be equal to 10% times the axial compression load in the column below the strut in CSA S16 method, while the proposed method requires a notional load of 1.0% times the axial compression load in the column below.

Columns were redesigned using the P-M-M interaction equation as per Clause 13.8 of CSA S16-14. The key design parameters for the columns are provided in Table 6.8 and Table 6.9 CC-W-HSS and CC-HSS-2L/L frames, respectively.

As shown in Table 6.8 and Table 6.9, the proposed design requirements for Type CC frames resulted in more economical designs when compared to CSA S16-14 approach. The reduction in the column size of the proposed design is predominantly because of the significantly lower out-of-plane bending moment requirement proposed here.

Table 6.8. Summary of the column design for CC-W-HSS case study frames using CSA S16 special provisions and the proposed method.

Parameter	CC_W_HSS_16_3_1.0			CC_W_HSS_24_4_1.0		
	CSA S16 (1)	CSA S16 (2)	Proposed Method	CSA S16 (1)	CSA S16 (2)	Proposed Method
$V_{E/Frame}$ (kN)	336	343	336	224	265	265
Brace Section (HSS)	101.6×101.6×4.8	101.6×101.6×4.8	101.6×101.6×4.8	88.9×88.9×4.8	101.6×101.6×4.8	101.6×101.6×4.8
Critical Segments	Tier 1	Tier 1	Tier 1	Tier 1	Tier 1	Tier 2	Tier 1
C_f (kN)	955	1199	1253	993	1423	1076	1507
M_{fx} (kN.m)	-	587	74	-	1109	1336	148
M_{fy} (kN.m)	-	0	23	-	0	0	39
Column Section (W)	360×64	760×134	360×110	410×100	840×193	840×193	460×177
$(KL/r)_x$	108	54	105	136	72	72	119
$(KL/r)_y$	111	100	85	96	99	99	88
$b_f/2t_f$	7.5	8.5	6.4	7.7	6.7	6.7	5.3
$(b_f/2t_f)_{limit}$	9.2	9.2	9.2	9.2	9.2	9.2	9.2
h_w/t_w	37.4	57.5	25.4	35.9	51.7	51.7	24.5
$(h_w/t_w)_{limit}$	65.0	78.8	28.3	71.2	81.2	83.7	28.3
ω_{1x}	-	1.0	1.00	-	1.00	1.00	1.00
ω_{1y}	-	-	0.60	-	-	-	0.60
U_{1x}	-	1.12	1.97	-	1.17	1.13	1.93
U_{1y}	-	-	0.89	-	-	-	0.81
C_r (kN)	932	2248	1763	1057	3338	3338	2323
M_{rx} (kN.m)	-	1339	640	-	2230	1925	1332
M_{ry} (kN.m)	-	-	206	-	-	-	351
P-M-M Interaction Ratio	1.0	1.0	1.0	0.9	0.9	1.0	0.9
Governing Limit State (LS)	LS 2	LS 3	LS 2	LS 2	LS 3	LS 3	LS 2

Table 6.9. Summary of the column design for CC-HSS-2L and CC-HSS-L case study frames using CSA S16 special provisions and the proposed method.

Parameter	CSA S16 (1)	CSA S16 (2)	Proposed Method
	CC_HSS_2L_24_3_1.0 and CC_HSS_L_24_3_1.0		
$V_{E/Frame}$ (kN)	224	265	265
Brace Section (2L)	76×51×7.9-12 LLBB	76×64×7.9-12 LLBB	76×64×7.9-12 LLBB
Brace Section (L)	76×76×12.7	89×89×12.7	89×89×12.7
Critical Segment	Tier 1	Tier 1	Tier 1
C_f (kN)	1105	1584	1690
M_{fx} (kN.m)	-	1145	122
M_{fy} (kN.m)	-	0	171
Column Section (HSS)	355.6×355.6×19	558.2×558.2×22.2	457.2×457.2×19
$(KL/r)_x$	175	110	135
$(KL/r)_y$	58	37	45
b_{el}/t	17.0	24.1	22.8
$(b_{el}/t)_{limit}$	28.3	28.3	28.3
ω_{1x}	-	1.00	1.00
ω_{1y}	-	-	0.60
U_{1x}	-	1.29	2.04
U_{1y}	-	-	0.64
C_r (kN)	1246	5041	2573
M_{rx} (kN.m)	-	2698	1537
M_{ry} (kN.m)	-	-	1537
P-M-M Interaction Ratio	0.9	0.9	0.9
Governing Limit State (LS)	LS 2	LS 2	LS 2

6.4.3 NLRH Analysis of the Case Studies

Seismic performance of the selected case study frames designed in accordance with the proposed design requirements was examined using the NLRH analysis method as described in Chapter 4. The statistics of peak response parameters were then calculated using the procedure described in Section 5.3.1. The summary of these parameters, including storey drift, tier drifts, DCF, column axial force, in-plane and out-of-plane moments, are presented in Table 6.10.

Table 6.10. Statistics of peak response parameters for case study frames designed to the proposed design method.

Parameter	LD_W_HSS_10_2_1.0	LD_W_HSS_24_3_1.0	CC_W_HSS_16_3_1.0	CC_W_HSS_24_4_1.0	CC_HSS_2L_24_3_1.0	CC_HSS_L_24_3_1.0
Frame						
Instability	—	—	—	—	—	—
δ_{St}/h (%)	0.39	0.33	0.34	0.30	0.32	0.33
$\dfrac{\delta_{St}/h}{R_d R_o \delta_e}$	0.97	1.08	1.01	1.02	0.54	0.56
δ_1/h_1 (%)	0.37	0.27	0.30	0.24	0.29	0.30
δ_2/h_2 (%)	0.41	0.35	0.36	0.30	0.32	0.34
δ_3/h_3 (%)		0.37	0.36	0.33	0.34	0.35
δ_4/h_4 (%)				0.34		
DCF	1.06	1.16	1.13	1.18	1.11	1.11
$C_{c\text{-}NRLH}/C_{r,\phi=1}$	0.59	0.68	0.74	0.65	0.53	0.54
$(M_{cy\text{-}NLRH}/M_{py})_1$	0.01	0.01	0.01	0.01	0.01	0.01
$(M_{cy\text{-}NLRH}/M_{py})_2$		0.01	0.01	0.01	0.00	0.00
$(M_{cy\text{-}NLRH}/M_{py})_3$				0.01		
$(M_{cx\text{-}NLRH}/M_{px})_1$	0.03	0.04	0.05	0.03	0.04	0.04
$(M_{cx\text{-}NLRH}/M_{px})_2$		0.03	0.04	0.03	0.03	0.03
$(M_{cx\text{-}NLRH}/M_{px})_3$				0.03		

Neither column instability nor frame collapse was observed when the proposed design method was applied. Frames LD_W_HSS_24_3_1.0, CC_W_HSS_16_3_1.0, and CC_W_HSS_24_4_1.0, in particular, which experienced column buckling under 2, 10, and 5 ground motion records, respectively when designed initially without the consideration of CSA S16-14 special provisions, exhibited a stable and satisfactory response when redesigned following the requirements proposed in this chapter. The storey drift for all of the case study frames is considerably smaller than the

2.5% limit of 2015 NBCC. The tier drifts are also noticeably smaller than the drift corresponding to low-cycle fatigue failure in HSS or L-shaped braces. Smaller drift concentration was observed for all of the case studies, compared to those recorded for frames designed without CSA S16-14 special provisions. Column forces and, in particular, in-plane and out-of-plane moments did not exceed the proposed design forces.

Chapter 7: Conclusions and Recommendations for Future Research

7.1   Summary

Multi-Tiered Concentrically Braced Frames (MT-CBFs) consist of two or more concentric braced panels that are stacked between two adjacent floor levels in multi-storey structures or between ground and roof levels in single-storey structures. Steel MT-CBFs are commonly used in North America in tall single-storey buildings, such as sports facilities, shopping centres, airplane hangers, warehouses, or industrial buildings. Multi-tiered configuration offers a favourable design option for such buildings as this configuration leads to shorter and smaller braces, practical connection sizes, and columns with shorter in-plane unbraced lengths. Furthermore, when used to resist seismic forces, stringent seismic design requirements for braces, including global slenderness and local buckling limits, can be easily satisfied given the shorter length of braces in multi-tiered configuration. Moreover, the design forces of other frame components arising from the capacity of the braces are expected to alleviate in such bracing systems due to smaller brace sizes.

 A large proportion of steel MT-CBF structures in North America is located in regions of low-to-moderate seismicity, where low-ductile systems are often desirable to avoid using complicated structural details and strict requirements prescribed for high-ductile systems and the lower seismic ductility demand expected in such regions.

In Canada, two categories of low-ductile steel concentrically braced frame systems can be designed according to CSA S16-14 seismic provisions, Limited-ductility (Type LD) braced frames

and braced frames of Conventional Construction (Type CC) category. Type LD MT-CBFs must be designed and detailed following the capacity design principle. In addition, special seismic design requirements prescribed for multi-tiered configuration with a focus on the column design forces must be met. As per these special requirements, intermediate struts must be provided between braced tiers, and a set of nonlinear analyses must be conducted, assuming that when the frame reaches the design storey drift, brace tensile yielding occurs in one of the tiers while compression braces in all tiers buckle. Alternatively, the column design forces can be computed using a series of linear analyses when the frame reaches the design storey drift, assuming that the tension-acting brace in one tier reaches its probable resistance, T_u, the compression-acting brace in that tier reaches its probable buckled resistance, C'_u, and the compression braces in the other tiers reach their probable compressive resistances, C_u. The linear or nonlinear analyses must be repeated, assuming that, for each analysis, brace tensile yielding takes place in any one of the other tiers. Additionally, the columns of Type LD MT-CBFs must resist a concomitant out-of-plane bending moment arising from out-of-plane transverse loads applied at each strut level equal to 2% times the axial compression load in the column below the strut.

For Type CC frames, CSA S16-14 does not require capacity design. The frame components in Type CC braced frames must be designed to carry the design seismic base shear. A set of safety measures are prescribed for Type CC structures taller than 15 m located in moderate and high seismic regions. The key requirements include an increase in the factored seismic force by 2% per meter of height above 15 m and an amplification factor of 1.3 to be applied to the factored design force of the columns. In addition to the increase in the axial compression force, columns that are intersected by bracing members at an unbraced location (e.g. multi-tiered configuration) must resist a concomitant out-of-plane bending moment due to out-of-plane transverse forces at every

brace-to-column intersection equal to 10% of the axial compression load carried by the column below the intersection points.

Limited past studies showed that low-ductile MT-CBFs might not experience severe inelastic response as opposed to their moderate or ductile counterparts. Additionally, it has been demonstrated that the application of the CSA S16 special design provisions, which may necessitate using a nonlinear static (pushover) analysis or a set of linear static analyses, can become tedious, in particular, when the frame consists of more than two tiers. Furthermore, despite the significant improvement of CSA S16 for Type MD and LD MT-CBFs over the past decade, the standard is silent for the design of Type CC MT-CBFs. This study, therefore, aimed to assess the seismic behaviour of Type LD and Type CC MT-CBFs designed to CSA S16-14 in low-to-moderate seismicity regions, propose a simplified seismic analysis and design method for Type LD MT-CBFs, and develop a new seismic design procedure for Type CC MT-CBFs. Furthermore, the nonlinear response history analyses data generated in this research provides a valuable database for future studies in steel concentrically braced frames.

A parametric study matrix of 64 low-ductile steel MT-CBFs was first developed by varying various parameters, including frame ductility level (Type LD and Conventional Construction category), number of tiers (2, 3, 4, and 6), frame height (10 m, 16 m, and 24 m), first tier to second tier height ratio (1.0 and 1.75), brace section (Square HSS, single-angle, and double-angle), bracing system (tension-compression and tension-only), and column section (Square HSS and W-shape). The selected frames were then designed to CSA S16-14 provisions. To verify the need for the key requirements of the special seismic design provisions for Type LD MT-CBF, including column design forces and the limit on the number of tiers, these requirements were excluded in design. For Type CC frames, the amplification factors in frames taller than 15 m, as well as the

special requirements for columns that are intersected by bracing members at an unbraced location, were excluded in the design to assess the need for such requirements.

The fibre-based nonlinear numerical models of the selected frames capable of simulating the buckling response of braces and columns were developed using the *OpenSees* software framework. Two nonlinear static (Pushover) analyses were performed to examine the lateral performance of MT-CBFs and verify the capability of the model in reproducing the brace inelastic buckling response and column instability. The Nonlinear Response History (NLRH) analysis was performed on the prototype frames under 30 ground motion accelerations. The seismic performance of the frames was then evaluated using the results obtained from NLRH analyses. The results were used to propose improved and yet simplified seismic design methods for the design of MT-CBFs of Type LD and Type CC category. The adequacy of the proposed methods was finally examined by applying the new requirements on six case study frames.

7.2 Conclusions

The key findings of this study are summarized as follows:

➢ Fibre-based numerical models of MT-CBFs were developed in *OpenSees*. The critical components of the models were validated using past experimental test data. The models are capable of reproducing nonlinear buckling response of braces and columns for the various cross-sections used in this study.

➢ The maximum storey drift of the frames was noticeably lesser than the 2.5% limit of 2015 NBCC. Although the brace fracture was not explicitly included in the numerical model, a maximum tier drift of 0.6% in braced tiers indicates that premature brace fracture is less likely

to happen in the low-ductile MT-CBFs studied here. Additionally, limited drift concentration was observed in the majority of the frames.

➢ In the majority of the frames, brace tensile yielding did not occur, while the compression braces buckled with an insignificant post-buckling response due to the elastic response of tension braces.

➢ Results of the NLRH analyses for Type LD frames designed to CSA S16-14, excluding the special requirements for MT-CBFs can be summarized as follows:

➢ Column buckling was observed for one of the 24 m-tall frames, under two ground motion records (out of 30). The column buckling occurred as a result of the combined effects of a large axial compression force arising from gravity loads and brace axial forces, in-plane moments due to the non-uniform distribution of frame lateral deformation, and out-of-plane bending moments due to brace out-of-plane buckling and P-Delta effects in the column, the latter was more pronounced.

➢ Non-uniform distribution of frame lateral deformations induced limited in-plane moments in the columns with a maximum of 0.06 times the respective column plastic moments.

➢ Maximum of the out-of-plane transverse notional loads at strut levels corresponding to the out-of-plane moments of the columns was 0.36% times the compression load of the column below the strut.

➢ Results of the NLRH analyses for Type CC frames designed to CSA S16-14, excluding the amplification factors for frames taller than 15 m and special requirements for multi-tiered systems, can be summarized as follows:

- No column instability was observed in frames with T/O braces. However, several cases of column buckling were observed in 16 m- and 24 m-tall frames with T/C braces.

- On average, columns experienced axial compression forces higher than the respective column axial compression resistances.

- In-plane moments were induced in the columns due to the limited non-uniformity of lateral deformations with a peak of 0.08 times the respective column in-plane plastic moment.

- Maximum of the out-of-plane transverse notional loads at the strut levels corresponding to the out-of-plane moments of the columns was 0.87% times the compression load in the column below the strut which is significantly lower than the demand specified in CSA S16-14.

➢ Enhanced and yet simplified seismic design requirements were proposed for Type LD and Type CC MT-CBFs in the framework of CSA S16, which improve efficiency in design while maintaining structural safety under seismic loading.

➢ Proposed seismic design recommendations for Type LD MT-CBFs are as follows:

- The number of braced tiers is recommended to be increased to six.

- A tier drift check is not required in design, provided that the 2015 NBCC storey drift check is met.

- Columns are recommended to be designed under gravity loads plus:
  a) the maximum axial compression force obtained from the brace loading scenarios when they reach their probable resistances as prescribed for CBFs,

b) an in-plane bending moment equal to 10% of the plastic moment of the column in the direction of the braced bay, and

c) an out-of-plane bending moment due to a series of out-of-plane transverse notional loads applied at each strut level with an amplitude of 1.0% times the force in the column below the strut.

➤ Proposed new seismic design recommendations for MT-CBFs of Conventional Construction (Type CC) category are as follows:

o MT-CBFs with a maximum of six braced tiers can be designed using the requirements proposed here.

o A tier drift check is not required in design provided that the 2015 NBCC storey drift check is met.

o Intermediate horizontal struts between adjacent braced tiers must be used. The design force is equal to the nodal bracing force required to brace the column against in-plane instability plus a fraction of brace design axial force that is 20% in T/C bracing systems and 60% in T/O bracing systems.

o Lateral seismic forces for the frames taller than 15 m should be increased by 2% of height above 15 m as prescribed by CSA S16-14 for Type CC frames. There is no need to amplify seismic forces of MT-CBFs shorter than 15 m.

o Columns are designed to resist
   a) an axial compression force due to the effects of gravity loads combined with 1.4 times the member factored axial compression force under seismic loads,

b) an in-plane moment equal to 10% of the plastic moment of the column in the direction of the braced bay, and

c) an out-of-plane moment resulting from a series of out-of-plane transverse notional loads at each strut level equal to 1% of the axial compression load carried by the column below the strut.

➤ Column instability was not observed in any of the case study frames redesigned to the proposed methods.

➤ The proposed seismic design requirements resulted in nearly similar column sections for Type LD case study frames and significantly lighter (up to 30%) sections for Type CC case study frames when compared to columns designed to the CSA S16-14 seismic provisions.

➤ The special seismic design requirements prescribed by CSA S16-14 to determine the column design forces in Type LD MT-CBFs can be waived in regions of low to moderate seismicity when applying the proposed design method.

7.3   Limitations of this Study

The limitations of this study are as follows:

➤ One concentric bracing configuration (i.e. X-bracing) was studied.

➤ The selected building was a single-storey industrial building.

➤ Type LD frames with W-shape columns and tension-compression Square HSS braces were assessed.

➢ Three sets of Type CC frames were studied, including frames with W-shape columns and T/C Square HSS braces, Square HSS columns with T/O single-angle braces, and Square HSS columns with T/O double-angle braces.

➢ Number of tiers studied were 2, 3, 4, and 6.

➢ Brace low-cycle fatigue fracture and local buckling were not simulated in the numerical model.

7.4 Recommendations for Future Studies

➢ Full-scale experimental tests should be performed on low-ductile MT-CBFs to evaluate the frame response, column buckling modes observed in NLRH and validate the proposed design methods.

➢ Other bracing configurations such as chevron bracing, structures having more than one braced bay in width, and braced frames with tension-compression double-angle braces should be studied.

➢ Braced frames with the number of tiers larger than six should be investigated.

➢ Seismic behaviour of multi-tiered concentrically braced frames in multi-storey buildings needs to be studied.

➢ Similar research study for Type LD and Type CC MT-CBFs in high seismic regions needs to be performed.

➢ Seismic performance of existing MT-CBFs should be investigated, and retrofit solutions are to be recommended if required.

➢ Given the extensive use of steel MT-CBFs in industrial buildings, where overhead cranes are present, the effects of the loads arising from the cranes on the seismic response of MT-CBF need to be investigated.

➢ Reliability analysis needs to be conducted to determine the reliability index of the proposed method.

Bibliography

1) Adluri, S.M.R., and Madugula, M.K.S. 1996. Flexural buckling of steel angles: experimental investigation. Journal of structural engineering, **122**(3): 309–317. American Society of Civil Engineers.

2) Agarwal, A., and Fahnestock, L.A. 2017. Seismic stability of multi-tiered ordinary concentrically-braced frames. *In* Annual Stability Conference Structural Stability Research Council 2017.

3) Agarwal, A., and Fahnestock, L.A. 2018. Seismic performance assessment of steel multi-tiered ordinary concentrically-braced frames. *In* Structural Stability Research Council Annual Stability Conference 2018.

4) Aguero, A., Izvernari, C., and Tremblay, R. 2006. Modelling of the seismic response of concentrically braced steel frames using the OpenSees analysis environment. International Journal of Advanced Steel Construction, **2**(3): 242–274.

5) AISC. 2016. ANSI/AISC 341-16, Seismic Provisions for Structural Steel Buildings. American Institute of Steel Construction, Chicago, IL.

6) Ancheta, T.D., Darragh, R.B., Stewart, J.P., Seyhan, E., Silva, W.J., Chiou, B.S.-J., Wooddell, K.E., Graves, R.W., Kottke, A.R., and Boore, D.M. 2014. NGA-West2 database. Earthquake Spectra, **30**(3): 989–1005. Earthquake Engineering Research Institute.

7) Ashrafi, A., and Imanpour, A. 2019. Seismic Response of Steel Multi-Tiered Eccentrically Braced Frames. *In* 12th Canadian conference on earthquake engineering. Quebec City.

8) Astaneh-Asl, A., and Goel, S.C. 1984. Cyclic in-plane buckling of double angle bracing. Journal of Structural Engineering, **110**(9): 2036–2055. American Society of Civil Engineers.

9) Astaneh-Asl, A., Goel, S.C., and Hanson, R.D. 1985. Cyclic out-of-plane buckling of double-angle bracing. Journal of structural Engineering, **111**(5): 1135–1153. American Society of Civil Engineers.

10) ASTM. 2015a. ASTM A500/A500M Standard Specification For Cold-Formed Welded And Seamless Carbon Steel Structural Tubing In Rounds And Shapes. ASTM International, West Conshohocken, PA.

11) ASTM. 2015b. A992/A992M-11 Standard Specification for Structural Steel Shapes. ASTM International, West Conshohocken, PA.

12) ASTM. 2015c. A1085/A1085M-15 Standard Specification for Cold-Formed Welded Carbon Steel Hollow Structural Sections (HSS). ASTM International, West Conshohocken, PA.

13) Atkinson, G.M. 2009. Earthquake time histories compatible with the 2005 National building code of Canada uniform hazard spectrum. Canadian Journal of Civil Engineering, **36**(6): 991–1000. NRC Research Press.

14) Auger, K. 2017. Conception parasismique des contreventements concentriques en treillis à segments multiples combinés aux poteaux gravitaires. École Polytechnique de Montréal.

15) Balazadeh-Minouei, Y., Tremblay, R., and Koboevic, S. 2018. Seismic Retrofit of an Existing 10-Story Chevron-Braced Steel-Frame. Journal of Structural Engineering, **144**(10): 4018180. American Society of Civil Engineers.

16) Balazadeh Minouei, Y. 2017. Seismic Evaluation and Retrofit of Existing Concentrically Braced Steel Frames in Canada. École Polytechnique de Montréal.

17) Bernal, D. 1994. Viscous damping in inelastic structural response. Journal of Structural Engineering, **120**(4): 1240–1254. American Society of Civil Engineers.

18) Black, R.G., Wenger, W.A., and Popov, E.P. 1980. Inelastic buckling of steel struts under cyclic load reversals. Earthquake Engineering Research Center, University of California Berkeley.

19) Bradley, C., Sizemore, J., Nelson, J., Tremblay, R., Hines, E.M., and Fahnestock, L.A. 2014. Large-scale testing of low-ductility, concentrically-braced frames. *In* Structures Congress 2014. pp. 2417–2428.

20) Bradley, C.R., Fahnestock, L.A., Hines, E.M., and Sizemore, J.G. 2017. Full-scale cyclic testing of low-ductility concentrically braced frames. Journal of Structural Engineering, **143**(6): 4017029. American Society of Civil Engineers.

21) Callister, J.T., and Pekelnicky, R.G. 2011. Seismic evaluation of an existing low ductility braced frame building in California. *In* Structures Congress 2011. pp. 2756–2767.

22) Cano, P.A. 2019. Evaluation of the Seismic Design Methods for Steel Multi-Tiered Concentrically Braced Frames.

23) Charney, F.A. 2008. Unintended consequences of modeling damping in structures. Journal of structural engineering, **134**(4): 581–592. American Society of Civil Engineers.

24) Choi, K.-S., Park, J.-Y., and Kim, H.-J. 2017. Numerical investigation on design requirements for steel ordinary braced frames. Engineering Structures, **137**: 296–309. Elsevier.

25) Chopra, A.K. 2005. Earthquake dynamics of structures. *In* University of California, Berkeley. Earthquake Engineering Research Institute.

26) CSA. 2014. CAN/CSA S16-14, Design of Steel Structures. Canadian Standard Association, Mississauga, ON, Canada.

27) CSI. 2009. SAP2000 - INTERGRATED SOFTWARE FOR STRUCTURAL ANALYSIS & DESIGN, Version 14 (Computer Program). Computer & Structures INC., Berkeley, CA.

28) D'Aniello, M., Ambrosino, G.L.M., Portioli, F., and Landolfo, R. 2013. Modelling aspects of the seismic response of steel concentric braced frames. Steel and Composite Structures, **15**(5): 539–566. Techno-Press.

29) Dalal, S.T. 1969. Some non-conventional cases of column design. Engineering J, Am Inst Steel Constr,.

30) Davaran, A. 2019. Stability analysis and design of double shear lap bolted connections in steel x-bracing systems. Journal of Constructional Steel Research, **153**: 31–41. Elsevier.

31) Decaen, S. 2015. Amélioration du comportement sismique des assemblages à cisaillement simple des contreventements concentriques en X en acier de construction conventionnelle (type CC). École Polytechnique de Montréal.

32) Dehghani, M., Tremblay, R., and Leclerc, M. 2017. Fatigue failure of 350WT steel under large-strain seismic loading at room and subfreezing temperatures. Construction and Building Materials, **145**: 602–618. Elsevier.

33) Fahnestock, L.A., Hines, E.M., Tremblay, R., Bradley, C., Nelson, J., Beland, T., Davaran, A., and Sizemore, J. 2014. Reserve capacity and implications for seismic collapse prevention for low-ductility braced frames in moderate seismic regions. *In* Proceedings of the 10th US National Conference on Earthquake Engineering: Frontiers of Earthquake Engineering, Anchorage, AK.

34) Fell, B. V, Kanvinde, A.M., Deierlein, G.G., and Myers, A.T. 2009. Experimental investigation of inelastic cyclic buckling and fracture of steel braces. Journal of structural engineering, **135**(1): 19–32. American Society of Civil Engineers.

35) Gélinas, A., Tremblay, R., and Davaran, A. 2012. Seismic behavior of steel HSS X-bracing of the conventional construction category. *In* Structures Congress 2012. pp. 1649–1660.

36) Goel, S.C., and El-Tayem, A.A. 1986. Cyclic load behavior of angle X-bracing. Journal of Structural Engineering, **112**(11): 2528–2539. American Society of Civil Engineers.

37) Goggins, J.M., Broderick, B.M., Elghazouli, A.Y., and Lucas, A.S. 2006. Behaviour of tubular steel members under cyclic axial loading. Journal of Constructional Steel Research, **62**(1–2): 121–131. Elsevier. doi:10.1016/J.JCSR.2005.04.012.

38) Halchuk, S., and Adams, J. 2004. Deaggregation of seismic hazard for selected Canadian cities. *In* Proceedings of the 13th World Conference on Earthquake Engineering, Vancouver, Canada. Paper.

39) Hall, J.F. 2006. Problems encountered from the use (or misuse) of Rayleigh damping. Earthquake engineering & structural dynamics, **35**(5): 525–545. Wiley Online Library.

40) Hsiao, P.-C., Lehman, D.E., Berman, J.W., Roeder, C.W., and Powell, J. 2014. Seismic vulnerability of older braced frames. Journal of Performance of Constructed Facilities, **28**(1): 108–120. American Society of Civil Engineers.

41) Hsiao, P., Lehman, D.E., and Roeder, C.W. 2013. A model to simulate special concentrically braced frames beyond brace fracture. Earthquake engineering & structural dynamics, **42**(2): 183–200. Wiley Online Library.

42) Imanpour, A. 2015. Seismic response and design of steel multi-tiered concentrically braced frames. École Polytechnique de Montréal.

43) Imanpour, A., Auger, K., and Tremblay, R. 2016a. Seismic design and performance of multi-tiered steel braced frames including the contribution from gravity columns under in-plane seismic demand. Advances in Engineering Software, **101**: 106–122. Elsevier. doi:10.1016/J.ADVENGSOFT.2016.01.021.

44) Imanpour, A., Stoakes, C., Tremblay, R., Fahnestock, L., and Davaran, A. 2013. Seismic stability response of columns in multi-tiered braced steel frames for industrial applications. *In* Structures Congress 2013: Bridging Your Passion with Your Profession. pp. 2650–2661.

45) Imanpour, A., and Tremblay, R. 2014. Seismic design of steel multi-tiered braced frames. *In* EUROSTEEL 2014.

46) Imanpour, A., and Tremblay, R. 2016a. Analysis methods for the design of special concentrically braced frames with three or more tiers for in-plane seismic demand. Journal of Structural Engineering, **143**(4): 4016213. American Society of Civil Engineers.

47) Imanpour, A., and Tremblay, R. 2016b. Seismic design procedure for steel multi-tiered concentrically braced frames beyond CSA S16 limit. *In* Proceedings, Annual Conference - Canadian Society for Civil Engineering.

48) Imanpour, A., and Tremblay, R. 2016c. Seismic design and response of steel multi-tiered concentrically braced frames in Canada. Canadian Journal of Civil Engineering,. doi:10.1139/cjce-2015-0399.

49) Imanpour, A., and Tremblay, R. 2017. Analysis Methods for the Design of Special Concentrically Braced Frames with Three or More Tiers for In-Plane Seismic Demand. Journal of Structural Engineering (United States),. doi:10.1061/(ASCE)ST.1943-541X.0001696.

50) Imanpour, A., Tremblay, R., and Davaran, A. (n.d.). Seismic Evaluation of Multi-Panel Steel Concentrically braced frames Paper Title Line.

51) Imanpour, A., Tremblay, R., Davaran, A., Stoakes, C., and Fahnestock, L.A. 2016b. Seismic performance assessment of multitiered steel concentrically braced frames designed in accordance with the 2010 AISC seismic provisions. Journal of Structural Engineering, **142**(12): 4016135. American Society of Civil Engineers.

52) Imanpour, A., Tremblay, R., Fahnestock, L.A., and Stoakes, C. 2016c. Analysis and Design of Two-Tiered Steel Braced Frames under In-Plane Seismic Demand. Journal of Structural Engineering (United States),. doi:10.1061/(ASCE)ST.1943-541X.0001568.

53) Jain, A.K., Hanson, R.D., and Goel, S.C. 1980. Hysteretic cycles of axially loaded steel members. Journal of the Structural Division, **106**(8): 1777–1795. ASCE.

54) Jiang, Y. 2013. Numerical and experimental seismic assessment and retrofit of steel tension-only double angle braced frames designed before the implementation of detailing provisions for ductile seismic response. École Polytechnique de Montréal.

55) Jiang, Y. 2019. Personal Communication.

56) Jiang, Y., Tremblay, R., and Tirca, L. 2012. Seismic assessment of deficient steel braced frames with built-up back-to-back double angle brace sections using OpenSees modeling. 15 conferrence WCEE. Proceedings of the 15WCEE,.

57) Karamanci, E., and Lignos, D.G. 2013. Collapse assessment and performance-based evaluation techniques for concentrically braced frames designed in seismic regions. McGill University Libraries.

58) Karamanci, E., and Lignos, D.G. 2014. Computational approach for collapse assessment of concentrically braced frames in seismic regions. Journal of Structural Engineering, **140**(8): A4014019. American Society of Civil Engineers.

59) Kazemzadeh Azad, S., Topkaya, C., and Bybordiani, M. 2018. Dynamic buckling of braces in concentrically braced frames. Earthquake Engineering & Structural Dynamics, **47**(3): 613–633. Wiley Online Library.

60) Lamarche, C.-P., and Tremblay, R. 2011. Seismically induced cyclic buckling of steel columns including residual-stress and strain-rate effects. Journal of Constructional Steel Research, **67**(9): 1401–1410. doi:https://doi.org/10.1016/j.jcsr.2010.10.008.

61) Lee, S., and Goel, S.C. 1987. Seismic behaviour of hollow and concrete-filled square tubular bracing members. Report No. UMCE87-11, Department of Civil Engineering, The University of Michigan. Ann Arbor, Michigan,.

62) Li, G., and Fahnestock, L.A. 2013. Seismic response of single-degree-of-freedom systems representing low-ductility steel concentrically braced frames with reserve capacity. Journal of Structural Engineering, **139**(2): 199–211. American Society of Civil Engineers.

63) Mazzoni, S., McKenna, F., Scott, M.H., and Fenves, G.L. 2006. Open System for Earthquake Engineering Simulation (OpenSEES) User Command-Language Manual. Pacific Earthquake Engineering Research Center,.

64) McKenna, F., Fenves, G.L., and Scott, M.H. 1997. Open system for earthquake engineering simulation. University of California, Berkeley, CA,.

65) Medina, R.A., and Krawinkler, H. 2004. Seismic demands for nondeteriorating frame structures and their dependence on ground motions. Pacific Earthquake Engineering Research Center.

66) Naeim, F. 1989. The seismic design handbook. Springer Science & Business Media.

67) Newell, J.D., and Uang, C.-M. 2008. Cyclic behavior of steel wide-flange columns subjected to large drift. Journal of structural engineering, **134**(8): 1334–1342. American Society of Civil Engineers.

68) NRC_Commentaries. 2015. User's Guide – NBC 2015 Structural Commentaries (Part 4 of Division B). Associate Committee on the National Building Code, Ottawa, ON.

69) NRC. 2015. National Building Code of Canada (NBCC). Associate Committee on the National Building Code, Ottawa, ON.

70) Popov, E.P., Mahin, S.A., and Zayas, V.A. 1979. Cyclic inelastic buckling of thin tubular columns. Journal of the Structural Division, **105**(11): 2261–2277. ASCE.

71) Roeder, C.W., Lehman, D.E., Clark, K., Powell, J., Yoo, J., Tsai, K., Lin, C., and Wei, C. 2011a. Influence of gusset plate connections and braces on the seismic performance of X-braced frames. Earthquake engineering & structural dynamics, **40**(4): 355–374. Wiley Online Library.

72) Roeder, C.W., Lumpkin, E.J., and Lehman, D.E. 2011b. A balanced design procedure for special concentrically braced frame connections. Journal of Constructional Steel Research, **67**(11): 1760–1772. Elsevier.

73) Schmidt, B.J., and Bartlett, F.M. 2002. Review of resistance factor for steel: data collection. Canadian Journal of Civil Engineering, **29**(1): 98–108. NRC Research Press.

74) Sizemore, J.G., Fahnestock, L.A., Hines, E.M., and Bradley, C.R. 2015. Full-scale cyclic testing of a low-ductility concentrically-braced frame. *In* Proc., 8th Int. Conf. on Behavior of Steel Structures in Seismic Areas (STESSA 2015). pp. 168–177.

75) Sizemore, J.G., Fahnestock, L.A., Hines, E.M., and Bradley, C.R. 2017. Parametric study of low-ductility concentrically braced frames under cyclic static loading. Journal of Structural Engineering, **143**(6): 4017032. American Society of Civil Engineers.

76) St-Onge, E. 2019. Personal Communication.

77) Tang, X., and Goel, S.C. 1987. Seismic Analysis and Design Considerations of Braced Steel Structures Report UMCE 87-4, The University of Michigan Department of Civil and Environmental Engineering. Ann Arbor, MI,.

78) Toutant, G. 2016. Stabilité des colonnes dans les contreventements concentriques en acier sous les efforts combinés axiaux et de flexion induits par les séismes. École Polytechnique de Montréal.

79) Tremblay, R. 2001. Seismic behavior and design of concentrically braced steel frames. Engineering Journal, **38**(3): 148–160.

80) Tremblay, R. 2002. Inelastic seismic response of steel bracing members. Journal of Constructional Steel Research, **58**(5–8): 665–701. Elsevier. doi:10.1016/S0143-974X(01)00104-3.

81) Tremblay, R. 2003. Achieving a Stable Inelastic Seismic Response for Multi-Story Concentrically Braced Steel Frames. Engineering Journal ASC,: 111–129.

82) Tremblay, R., Archambault, M.-H., and Filiatrault, A. 2003. Seismic response of concentrically braced steel frames made with rectangular hollow bracing members. Journal of Structural Engineering, **129**(12): 1626–1636. American Society of Civil Engineers.

83) Tremblay, R., Atkinson, G.M., Bouaanani, N., Daneshvar, P., Léger, P., and Koboevic, S. 2015. Selection and scaling of ground motion time histories for seismic analysis using NBCC 2015. *In* Proceeding 11th Canadian Conference on Earthquake Engineering, Victoria, BC, Canada, Paper no.

84) Tremblay, R., Bruneau, M., Driver, R., Metten, A., Montgomery, C.J., and Rogers, C. 2010. Seismic Design of Steel Structures in accordance with CSA-S16-09. *In* Proceedings of the 9th US National and 10th Canadian Conference on Earthquake Engineering.

85) Tremblay, R., Castonguay, P.X., Guilini-Charette, K., and Koboevic, S. 2009. Seismic performance of conventional construction braced steel frames designed according to Canadian seismic provisions. *In* Structures Congress 2009: Don't Mess with Structural Engineers: Expanding Our Role. pp. 1–10.

86) Tremblay, R., Filiatrault, A., Bruneau, M., Nakashima, M., Prion, H.G.L., and DeVall, R. 1996. Seismic design of steel buildings: lessons from the 1995 Hyogo-ken Nanbu earthquake. Canadian Journal of Civil Engineering, **23**(3): 727–756. NRC Research Press.

87) Tremblay, R., and Stiemer, S.F. 1994. Back-up stiffness for improving the stability of multi-storey braced frames under seismic loading. Proceedings of the 1994 SSRC Annual Technical Session, Bethlehem, Pa,: 311–325.

88) Uriz, P., Filippou, F.C., and Mahin, S.A. 2008. Model for cyclic inelastic buckling of steel braces. Journal of structural engineering, **134**(4): 619–628. American Society of Civil Engineers.

89) Uriz, P., and Mahin, S.A. 2004. Seismic vulnerability assessment of concentrically braced steel frames. International Journal of Steel Structures, **4**(4): 239–248. 한국강구조학회.

90) Yang, F., and Mahin, S. 2005. Limiting net section fracture in slotted tube braces. Steel TIPS Report,.

91) Zareian, F., and Medina, R.A. 2010. A practical method for proper modeling of structural damping in inelastic plane structural systems. Computers & structures, **88**(1–2): 45–53. Elsevier.